2020

MULTISCALE MODELING OF CARBON FIBERS/GRAPHENE NANOPLATELETS/EPOXY HYBRID COMPOSITES FOR AEROSPACE APPLICATIONS

Hashim Al Mahmud
Michigan Technological University, hnalmahm@mtu.edu

MULTISCALE MODELING OF CARBON FIBERS/GRAPHENE NANOPLATELETS/EPOXY HYBRID COMPOSITES FOR AEROSPACE APPLICATIONS

By

Hashim Naji Azooz Al Mahmud

A DISSERTATION

Submitted in partial fulfillment of the requirements for the degree of

DOCTOR OF PHILOSOPHY

In Mechanical Engineering–Engineering Mechanics

MICHIGAN TECHNOLOGICAL UNIVERSITY

2020

This dissertation has been approved in partial fulfillment of the requirements for the Degree of DOCTOR OF PHILOSOPHY in Mechanical Engineering–Engineering Mechanics.

Department of Mechanical Engineering–Engineering Mechanics

Dissertation Advisor:	*Dr. Gregory Odegard*
Committee Member:	*Dr. Ranjit Pati*
Committee Member:	*Dr. Trisha Sain*
Committee Member:	*Dr. Gowtham S*
Department Chair:	*Dr. William Predebon*

To My Parents and My Family

TABLE OF CONTENTS

LIST OF FIGURES

LIST OF TABLES

PREFACE

The work outlined in this dissertation was performed under the supervision of Dr. Gregory M. Odegard in the department of Mechanical Engineering-Engineering Mechanics at Michigan Technological University over the period of November 2015 to May 2020. The outcomes including the writing in this dissertation were performed along with the constant directions, suggestions, and revisions provided by Dr. Gregory M. Odegard. During this project, Matthew Radue, Ph.D., provided me with his valuable instructions and help in learning the fundamentals of Molecular Dynamics. Most of the training materials and example input scripts in molecular dynamics, micromechanics modeling, and post-processing calculations were prepared and conducted along with his support. My colleagues, Sorayot Chinkanjanarot, Ph.D., and William Pisani, Ph.D., have also contributed to this work through sharing their experience in modeling and scripting with me. The valuable revisions and comments provided by William Pisani have helped me to improve the writing of this dissertation.

ACKNOWLEDGMENTS

This research work was funded by the scholarship granted to me by the University of Kufa in Najaf, Ministry of Higher Education, Iraq; represented by the Cultural Office, Embassy of the Republic of Iraq in Washington D.C., USA, and by the Richard and Elizabeth Henes Endowment at Michigan Technological University. SUPERIOR, a high-performance computing infrastructure at Michigan Technological University, was used in performing all the molecular dynamics simulations and obtaining the results presented in this work.

I would like to express my sincere thanks and gratitude to my esteemed advisor Dr. Gregory M. Odegard for having me in his scientific research team, the Computational Mechanics and Materials Research Laboratory (CMMR Lab). His highly ranked academic and research reputation has inspired me to be one of his Ph.D. students. He has provided me with the opportunity and support to afford the challenge of performing this work. He has been awesome in mentoring me through my Ph.D. degree studies. He has provided me with his valuable instructions and advice in a timely manner. My research ethics and writing experience have been significantly improved by his valuable comments, suggestions, and revisions.

Many thanks to my colleague, Matthew Radue, Ph.D., who helped me to be on the right track when I first joined Dr. Odegard's scientific research team. I appreciate the time and effort he dedicated to me in learning the fundamentals of molecular dynamics and micromechanics. His keen thoughts and motivation have encouraged me to undertake the challenge of completing my Ph.D. degree. I also would like to thank my colleagues, Sorayot Chinkanjanarot, Ph.D, and William Pisani, Ph.D., for their help, input, and positive discussion during my Ph.D. degree. For their positive discussion and feedback during our weekly research group meetings, thanks to my colleagues: Prathamesh Deshpande, Oladeji Fadayomi, Sagar Patil, Khatereh Kashmari, Swapnil Bamane, Prashik Gaikwad, Ivan Gallegos, and Joshua Kemppainen. For sharing their research experience, I would also like to thank: Dr. Trisha Sain and her Ph.D. students Muhammed Imam and Shabnam Konica; Dr. Susanta Ghosh and his Ph.D. student Upendra Yadav. I really enjoyed the company and the research work with such wonderful people. Thanks also to Dr. Evan Pineda from NASA Glenn Research Center for his input in using MAC/GMC 4.0 code for micromechanics analysis.

For serving on my advisory committee, thanks to Dr. Ranjit Pati, Dr. Trisha Sain, and Dr. Gowtham. Many thanks to Dr. Gowtham for his input in high-performance computing. I would also like to thank the faculty and staff members at Michigan Tech and the friendly people and community in Houghton who have made my career life easy and pleasant. In particular, but not limited to, thanks to Dr. Reza Yassar, Dr. Ibrahim Miskioglu, Dr. Beatrice Smith, Ms. Anne Stander, Dr. Silke Feltz, Dr. Sara Amani, Ms. Frann Grossman, Mrs. Noor Miskioglu, Miss Kathleen Burke, Miss Cori VanOstran, and Ms. Janey Pindral. I appreciate the on-campus dissertation formatting and submission process sessions given by Dr. Debra Charlesworth from the Graduate School at Michigan Tech. For their encouragement and advice, thanks to my friends: Shubber Falah, Basim Al Shubber, Wahaab Mousa, Mohanad Al Abedi, and Khairullah Al Mahmud.

Thankful and sincere gratitude always to my father and my mother (mercy and peace upon their souls) for inspiring and supporting me in this life, without which I would not be who I am. Many thanks for the help and support from my elder brother, Aziz Al Mahmud, and from my amiable six sisters. I would also like to recognize the substantial role that my wife, Maryam, has played by supporting and encouraging me over my career life. My beloved and wonderful kids: Ahmed, Noora, Ameer, and Nabaa, thank you very much guys for sharing the experience with me. I believe and testify that this study would not have been possible without the help and support from those wonderful people.

Above all, Thank God, Allah, the most gracious and merciful, for the kindness and blessings. Thank God Almighty for providing me with the uncountable gifts and the infinite grace including the wonderful people that have helped me in performing this work. I sincerely believe and am totally confident that my energy and determination has been enabled and sustained by Him Almighty.

"My success can only come from Allah. In Him I trust, and unto Him I return."
Qur'an 11:88 (translated)

ABSTRACT

Significant research effort has been dedicated for decades to improve the mechanical properties of aerospace polymer-based composite materials. Lightweight epoxy-based composite materials have increasingly replaced the comparatively heavy and expensive metal alloys used in aeronautical and aerospace structural components. In particular, carbon fibers (CF)/graphene nanoplatelets (GNP)/epoxy hybrid composites can be used for this purpose owing to their high specific stiffness and strength. Therefore, this work has been completed to design, predict, and optimize the effective mechanical properties of CF/GNP/epoxy composite materials at different length scales using a multiscale modeling approach. The work-flow of modeling involves a first step of using molecular dynamics (MD) with a reactive force field (ReaxFF) to predict the structure and mechanical behavior of the GNP/epoxy materials at the molecular level. A micromechanics approach is then used to model and predict the mechanical properties of the CF/GNP/epoxy hybrid composite at the bulk level. One of the major findings of this study refers to an alignment behavior of phenyl rings in epoxy with the planar GNP surface at the interphase region. This alignment plays an important role to drive the molecular density of epoxy at the interphase and promote the GNP-epoxy interfacial adhesion. The results also validate the use of ReaxFF in MD modeling of such nanocomposites as the predicted properties compare well with experiment.

The impact on the mechanical properties of aerospace epoxy materials reinforced with pristine GNP, highly concentrated Graphene Oxide (GO), and Functionalized Graphene Oxide (FGO) has also been investigated in this study. A systematic computational approach to simulate the reinforcing nanoplatelets and probe their influence on the mechanical response of the epoxy matrix at both nanoscale and bulk levels. The nanoscale outcomes indicate a significant degradation in the in-plane elastic and shear moduli of the nanocomposite when introducing large amounts of oxygen and functional groups to the robust sp^2 structure of the GNP. However, the wrinkled and rough topology of GO and FGO promotes the nanoplatelet-matrix interlocking mechanism which produces a significant improvement in the out-of-plane shear modulus. In addition, surface functionalization of GNP promotes the nanoplatelet-epoxy interfacial interaction/adhesion significantly which is important for the material toughness. Using micromechanics analysis, the influence of the nanoplatelets content and aspect ratio on the mechanical response of the proposed nanocomposites has also been predicted and validated with experimental data available from the literature. Generally, there is an improvement in the predicted mechanical response of the bulk nanocomposite materials with increasing nanoplatelets content and aspect ratio.

The predicted mechanical properties of the nanoplatelet/epoxy nanocomposites are then used to generate hybrid composite models reinforced with unidirectional CF. The micromechanics predictions are used to analyze the reinforcing effect of the proposed nanoplatelets on the unidirectional CF/nanoplatelet/epoxy hybrid composites. Three laminated hybrid composite panels are also modeled and analyzed to address the reinforcing effect of the proposed nanoplatelets on the laminated hybrid composite panels. The predicted mechanical properties of the laminated hybrid composite panels are important in assessing the mechanical performance of in-service structural components.

Chapter 1

INTRODUCTION

1.1 Motivation

Over the last several decades the aerospace industry has pursued the improvement of aircraft fuel efficiency, which in turn has driven the development of high-performance, lightweight structural composite materials [1-5]. Many major structural components in the passenger aircraft, Airbus 380, have been made from carbon fibre (CF) composites. About 25% of the entire weight of the Airbus 380 (~280 tons as the typical operating empty weight) is made from composite materials. Interestingly, about 50% of the entire structural mass in Boeing 787 and Airbus A350 is built using carbon fiber–epoxy composite materials. With respect to the use of composite materials in military aircraft, about 35% of the entire structural weight in the US fifth-generation combat aircraft F-35 Lightning II and 40% of the entire structural weight in the Eurofighter Typhoon was made from epoxy-based composites reinforced with carbon fibers [6]. Although traditional carbon fiber composites are now well-established for use in structural components such as fuselages and wings (Figure 1.1), the development of a new generation of hybrid composites that incorporates nanoparticles (e.g. carbon nanotubes and graphene nanoplatelets) could result in composites with improved properties [7-10]. Such hybrid composite materials are promising for aeronautical and aerospace structural applications. Thus, persistent research effort is necessary towards achieving the goal of synthesizing lightweight and ultra-strength composite materials.

Figure 1.1: Production of a fuselage composite panel using automated fiber placement (AFP) technology (Courtesy of Electroimpact, Inc. See Appendix C.1 for copyright agreement).

The success of using epoxy-based nanocomposite materials as the alternative for some traditional metallic alloys represents a great milestone in the aerospace industry [5, 11, 12]. The exceptional mechanical, thermal, and electromagnetic properties of graphene nanoplatelets, along with their relatively low cost concerning other nanofillers make them ideal candidates for strengthening epoxy matrices [13]. Additionally, the decent and natural affinity between graphene and epoxy monomers can be chemically improved to promote their adhesion [14, 15]. The chemical integrity of such carbon allotrope nanofillers and their content, shape, size, orientation, dispersion, and interfacial interaction with polymers play an important role in establishing a robust load transfer network in the nanocomposite [16, 17]. Therefore, the key point for optimizing the mechanical properties of nanocomposite materials is governed by these factors, which are referred to as the key processing parameters.

There is some difficulty in dealing with the wide range of factors that can affect the structure of epoxy-based composite material. This can be manifested by the additional effort that is required to manipulate and control the mutual effect of these factors on the mechanical response of a nanocomposite. For example, increasing the content of graphene in a polymer matrix can significantly improve the mechanical response of the nanocomposite. Yet, a detrimental effect can occur due to graphene agglomeration (low dispersion). Also, an increase in the matrix viscosity could arise at high levels of graphene content. These two undesirable features can lead to a significant degradation in material mechanical properties. Despite the possibility of the trade-off impact of the key processing parameters on the mechanical properties of nanocomposite material, these factors altogether keep the door open to improving the composite properties.

Experimental studies have contributed significantly to the development of polymer-based composite materials reinforced with carbon allotropes. However, experimental work can be expensive and practically limited to handling the effect of a few numbers of the key processing parameters mentioned above. Thus, the development of these materials can be greatly facilitated with efficient and accurate computational simulation techniques. Given the advances in computational tools and high-performance computing (HPC) infrastructures, polymer-based composite materials could be extensively investigated to acquire a deep physical insight starting at the molecular level up to the bulk level.

1.2 Background

This section involves background on key topics used in performing this work.

1.2.1 Computational Tools versus Experiments

Experimental studies of polymer-based composite materials require the use of sophisticated apparatus', tools, and microscopies which allows users to probe the molecular structure of the material. X-ray diffraction (XRD), Fourier transform infrared spectroscopy (FT-IR), Raman spectroscopy, X-ray photoelectron spectroscopy (XPS), UV-vis diffuse reflectance spectroscopy (DRS), photoluminescence spectroscopy (PL), transmission electron microscopy (TEM), scanning electron microscopy (SEM), atomic force

microscopy (AFM), EDX elemental mapping, photo-electrochemical measurements, and thermal-gravimetric analysis (TGA) are necessary for surface analysis, imaging, characterizing, and investigating nanocomposite materials. Even though these tools are crucial and provide fundamental information in the field of studying such materials, there is still a need to know more. For example, the degree of polymerization of a polymer or its crosslinking density, density distribution, and the molecular structure at the interphase region of the nanocomposite constituents cannot be fully resolved with the available experimental tools. For these reasons, computational tools have been developed and widely used to complement experiments to provide a complete understanding of composite structures at both molecular and bulk levels.

1.2.2 Molecular Mechanics

From the computational perspective, molecular mechanics (MM) employs classical physics to simulate the molecular geometry and predict the potential energy surface of a molecular system. The term molecular mechanics was initially established in the 1970s to clarify that classical mechanics is applicable to determine the equilibrium state in a molecular structure. In that context, the process of MM has also been referred to as "Molecular Minimization". For a molecular system, several assumptions need to be considered with MM:

- The entity of an atom is treated as an individual sphere.
- The chemical environment of an atom defines its type, e.g. carbon atom in Methane (CH_4) is different than carbon atoms in graphene.
- Classic spring force representation is used to model covalent bonds between atoms.
- Noncovalent interactions need to be considered in the energy function formulations.
- Accurate experimental parameters of intermolecular forces and pair potentials are fundamental for the potential energy functions of the molecular system.
- Individual potential energy functions are compiled together to produce the overall potential energy function or magnitude of the molecular system.

The computational approach with MM requires parameter sets which are known as force fields. The parameter sets in a force field are essential for the potential energy functions used to determine the potential energy of a molecular system at different configurations. Because MM is not applicable for electronic properties, molecular modeling with MM requires less computational effort than quantum mechanical methods and conserves the required accuracy. Furthermore, MM can be implemented to model large molecules such as polymers and proteins. Further details about intermolecular forces and potential energy formulations can be found in "Molecular Modelling for Beginners" by Alan Hinchliffe [18].

1.2.3 Molecular Dynamics

While MM is used to predict the local minima of molecular potential energy surfaces, molecular dynamics (MD) is used to model and study the time evolution of infinitesimal molecular systems. MD uses computer simulations to study the local vibrations, rotations, and translations of interacting particles within a physical domain. These particles can be a set of atoms or molecules. Generally, MD simulation processes are computationally expensive (see Appendix A.2). Thus, atoms and molecules are only allowed to interact for a very limited period of time in the range of a few nanoseconds (ns). The computational approach with MD involves applying Newton's equations of motion on the interacting particles and solving them numerically to determine their trajectories at every time step of the simulation. These equations of motion utilize the intermolecular forces and pair potentials that are already established with MM.

MD simulations can be performed using LAMMPS[1] [19, 20], an open-source software package which has been primarily developed by researchers at Sandia National Labs and Temple University. LAMMPS is a powerful computational tool that has been utilized in simulating solid materials and soft matter in a liquid or gaseous state. LAMMPS uses Newton's equations of motion for a specified group of interacting particles. LAMMPS can be used to simulate two-dimensional and three-dimensional material systems. Depending on the computational resources, the number of particles in the system domain can range from several particles to billions of them. For more information about simulation principles, features, computational equations, and the usage of LAMMPS commands, an MD user can refer to the LAMMPS official documentation website[2].

Polymers and their nanocomposites have been extensively investigated with LAMMPS to provide deep physical insight into the material molecular structure under different circumstances of loadings and physical or chemical effects [10, 21-23]. It is noteworthy that MD simulations with LAMMPS are mainly dependent on the selection of the force field which is used in representing the interatomic potentials of the simulated molecular system. In other words, more accurate MD simulation outcomes can be obtained using an appropriate and efficient force field.

1.2.4 Force Fields

Given the background in molecular modeling [18], a force field involves the parameter sets and functional forms which can be applied to an atomistic system domain using MM and MD to compute or predict its potential energy. These energy functions or interatomic potentials are formulated to be implicitly used for molecular mechanics and molecular dynamics simulations. The parameter sets of a force field can be derived from either experiments or quantum mechanics calculations, such as using Density Functional Theory (DFT) simulations. A combined approach for deriving the parameter sets is also possible. Generally, there are two types of force field; fixed-bonding (valance) force fields and

[1] LAMMPS stands for Large-scale Atomic/Molecular Massively Parallel Simulator
[2] https://lammps.sandia.gov

reactive force fields. An intermediate or hybrid force field between the two types is also available.

A fixed-bonding force field uses only chemical terms (e.g. bond lengths, bond angles, dihedral angles) to describe pair interactions between atoms in the molecular system. In this type of force field, the chemical bonding configurations in the molecular system can be stretched and deformed but cannot be broken. A simple mathematical expression for the bond potential energy (U) between two bonded atoms using a fixed-bonding force field can be represented by the following Harmonic potential equation:

$$U = k\,(r - r_e)^2 \tag{1.1}$$

where k is a constant that refers to the bond stiffness, r is the distance between atoms, and r_e is the equilibrium distance between atoms.

In a reactive force field, however, the parameter sets contain additional terms used to define the bond strength order. That is, the bond strength (pair potential) can be modified to simulate bonds scission and formation. The mathematical expression for such reactive bond can be represented by the following Morse potential equation:

$$U = D_e\left[1 - \exp\left(-\alpha(r - r_e)\right)\right]^2 \tag{1.2}$$

where D_e is the depth of the potential energy well (i.e. the thermodynamic dissociation energy of the bond), and α controls the width of the potential energy well. Figure 1.2 illustrates the difference between the Harmonic and Morse potential energy profiles according to Equations 1.1 and 1.2. Clearly, Morse potential is more realistic than the Harmonic potential when the bond is significantly stretched. This is because the Harmonic potential continues to increase as the distance between atoms increases, which is unrealistic. However, the increment in Morse potential settles at the dissociation energy value which indicates the bond has broken.

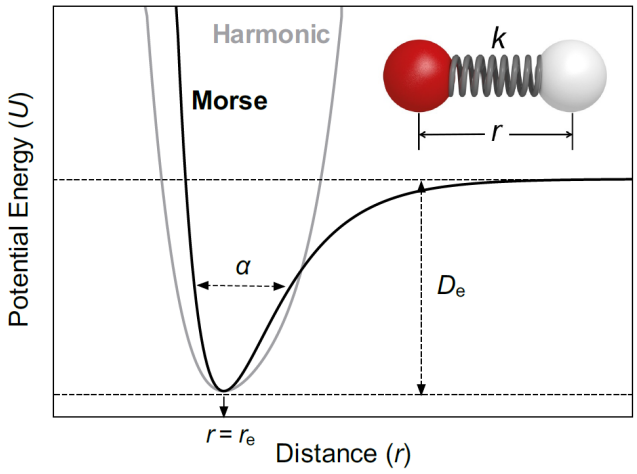

Figure 1.2: Harmonic and Morse potential energy profile.

The Lennard-Jones (LJ) potential is used to describe the van der Waals (vdW) interaction energy between any two neighboring atoms in the system domain. The total potential energy of the molecular system is obtained by adding the contributions from other energy terms, such as valence angle, torsion, conjugation, charge, and Coulomb energy. There are many different types of force fields, and the parameter sets in each have been derived and modified to perform specific simulation tasks depending on the molecular characteristics of the material. Thus, the selection of an appropriate force field is essential for MD simulations. That is, the successful and accurate outcome of MD simulations is highly governed by the force field parameter sets used to describe the molecular system configurations and its potential energy terms. In this work, two different types of force fields were used to perform the MD simulations. The All-Atom fixed-bond Optimized Potentials for Liquid Simulations (OPLS-AA) force field [24, 25] has been used to initially create, crosslink, and stabilize the molecular structure of the nanocomposite MD systems. A reactive force field (ReaxFF) with the parameter sets developed by Liu et al. [26] has been used to predict the mechanical response of the nanocomposite MD systems. Further information and details about force field parameter sets and types, the mathematical derivation of force and energy numerical equations, molecular mechanics, and molecular dynamics modeling can be found in "Molecular Modelling for Beginners" by Alan Hinchliffe [18], "The Art of Molecular Dynamics Simulation" by D. C. Rapaport [27], "Computer Simulation of Liquids" by Michael P. Allen and Dominic J. Tildesley [28], or any other relevant source.

1.2.5 Micromechanics

The micromechanics predictions in this work were performed using MAC/GMC[1] 4.0, a computer code developed at NASA Glenn Research Center. The computational approach in this code is based on the High-Fidelity Generalized Method of Cells (HFGMC) micromechanics theory [29-32]. HFGMC is more accurate and efficient in predicting the local stress and strain fields relative to the standard GMC. This improvement is essential to provide accurate predictions and more detailed analysis for composite materials. Specifically, the availability of accurate local stress and strain fields is critical to deal with the interphase transition between composite constituents. This is necessary to analyze composite material damage and failure such as matrix inelasticity and fiber-matrix debonding. In this micromechanics approach, the microscale architecture of materials, including composites, is characterized using a doubly and triply periodic repeating unit cell (RUC) to model the mechanical behavior and response. The RUC comprises of a number of subcells. Each subcell can be used to represent a single phase in heterogeneous or composite materials. Thus, the code can be used to analyze a wide range of material constitutive models. The constitutive model of the material could be isotropic, transversely isotropic, and completely anisotropic. Furthermore, subroutines of user-defined constitutive models can be also included in the code. The preference of using MAC/GMC 4.0 rather than other micromechanics approaches is attributed to the attractive advantages of HFGMC over other micromechanics theories in addition to the capabilities and

[1] MAC/GMC stands for Micromechanical Analysis Code based on the Generalized Method of Cells.

flexibility of MAC/GMC 4.0 code. The HFGMC advantages and the MAC/GMC 4.0 capabilities and features can be summarized as follows:

- HFGMC involves a fully multiaxial formulation technique.
- Accurate local stress and strain fields are provided by HFGMC, that is, it has the capability to analyze local fiber damage and interface failure between composite constituents.
- MAC/GMC 4.0 is efficient, fast, and provides accurate predictions.
- The code includes a convenient built-in constitutive model library in addition to the ability of creating new models.
- Smart composites and laminates can be efficiently analyzed using MAC/GMC 4.0.
- The temperature and electromagnetic effect on the mechanical behavior of the material can be considered in the predictions.
- Capable of predicting both elastic and inelastic behavior of the material.
- Capable of performing static failure analysis, fatigue damage analysis, maximum stress, maximum strain, and Tsai-Hill criteria.
- MAC/GMC 4.0 can interface with commercial finite element software packages.

For more information and details about features, capabilities, and usage of the code, refer to MAC/GMC 4.0 User's Manual-Keywords Manual [33], and MAC/GMC 4.0 User's Manual- Example Problem Manual [34].

1.3 Literature Review

This section reviews experimental and computational research studies which have been performed on developing polymer-based composite materials. Different approaches to prepare and evaluate GNP-reinforced polymer nanocomposites are briefly cited in this section. Although CF/polymer composites are well-established in the literature, some new synthesizing or modeling techniques have also been included herein to establish the idea of developing the new generation of CF/GNP-reinforced polymer hybrid composites.

The competitive engineering properties of epoxy matrices relative to traditional structural materials have attracted the attention of engineers and manufacturers to be used in aerospace composite structural components, in addition to many other engineering applications. These thermoset polymer materials are highly processable and possess lightweight, high specific stiffness, high specific strength, and excellent corrosion resistance. Furthermore, their chemical compatibility with carbon allotropes, which are used as reinforcing fillers, has been utilized to produce nanocomposites with improved toughness and strength. These carbon additives can also improve the poor thermal and electrical conductivities of epoxy matrices.

Monolayer defect-free sheets of graphene have been reported as the strongest tested material [35, 36]. They have attracted the attention of scientists and researchers to be utilized in many engineering applications. Their exceptional strength, high specific surface area, unique graphitized plane structure, and the high charge mobility have been harnessed in improving the mechanical, thermal, and electrical properties of polymer matrices. Unlike

the reinforcing effect of CF which is restricted with its longitudinal direction, a global or three-dimensional reinforcing effect of well-dispersed GNP within the hosting matrix can be typically obtained.

Among the early experimental studies that have been performed in synthesizing graphene/polymer nanocomposites, a general approach was presented by Stankovitch et al. [37]. Their bottom-up chemical approach involved the preparation of highly dispersed chemically modified graphene sheets in organic polymers. Treating exfoliated graphene oxide sheets by organic isocyanate was found to help in reducing their hydrophilic character and allow for a stable dispersion in polar aprotic solvents. Incorporating about 0.1 volume percent (vol%) of the modified graphene sheets into polystyrene resulted in about 0.1 S m^{-1} electrical conductivity. The claimed low percolation threshold of graphene (~0.1 vol%) is beneficial for a wide range of electrical applications of polymer-based composites at room temperature.

Ramanathan et al. [38] observed an increase in the elastic modulus by 80% and 20% improvement in the tensile strength owing to the inclusion of 1.0 weight percent (wt%) of high-surface-area functionalized graphene sheets (FGS) in poly(methyl methacrylate) (PMMA). The FGS were prepared using a fast-thermal expansion of an entirely oxidized graphite. The incorporation of the highly-dispersed FGS in PMMA resulted in a composite with mechanical and thermal properties outperforming that resulted from incorporating traditional expanded graphite (EG) nanoparticles and even single-walled carbon nanotubes (SWNTs) in PMMA. The remarkable improvement in the thermal and mechanical properties of FGS-PMMA composite were attributed to three factors: the homogeneous dispersion of FGS in PMMA, the large surface area of FGS which allows for stronger interfacial interaction with PMMA due to the formation of hydrogen bonds between hydroxyl groups in FGS and carbonyl groups in PMMA, and the mechanical interlocking mechanism that is triggered by the nanoscale wrinkled topology of FGS. As a result, a co-continuous network between FGS nanoparticles and PMMA chains was shaped, which introduced a fundamental modification to the polymer matrix.

Later, Shen et al. [39] examined the mechanical properties of graphene reinforced epoxy nanocomposite. They noticed that the inclusion of 0.5 wt% of graphene flakes, resulted in an increase in the Young's modulus from 2.0 to 3.1 GPa when tested at room temperature, and from 5.9 GPa to 7.4 GPa when tested at cryogenic temperature of 77 K. In part of their study, King et al. [40] investigated the effect of GNP content on the tensile modulus of the epoxy-based nanocomposite. They observed an increase in the tensile modulus by ~23.5% at 6.0 wt% (3.7 vol%) of GNP content.

Rafiee et al. [41] showed that GNP-based nanocomposites can surpass the properties of carbon nanotubes (CNT)-based nanocomposites. Adding a small amount of GNP (0.1 wt%) can significantly improve the overall mechanical response of an epoxy matrix. The improvement in mechanical properties for pure epoxy indicates that GNP/epoxy out-performs the single/multi-walled CNT/epoxy by: Young's modulus ~31% for GNP versus ~3% for single-walled CNT, tensile strength ~40% for GNP versus ~14% for multi-walled CNT, and mode I fracture toughness ~53% for GNP versus ~20% for multi-walled CNT. In their article, they attributed the substantial improvement in mechanical response of GNP/epoxy over CNT/epoxy to the strong nanofiller-matrix adhesion arises due to the high

specific surface area of GNP. Also, the wrinkled topology of GNP has enhanced the interlocking mechanism with the epoxy matrix.

Given their high tensile strength, stiffness, and low weight, carbon fibers have been used for decades to reinforce polymer matrices and produce structural composite panels. Providing the adhesion property of epoxy polymers, unidirectional carbon fibers can be held together in a thin composite laminate. The major improvement in the properties of the produced composite laminate is mostly restricted or limited to the longitudinal direction of the CF. Therefore, a large number of thin laminates with different orientations of CF are stacked together to produce high performance laminated composite panels. Recent studies on CF/polymer composites have been focused on resolving specific issues such as improving the fiber-matrix adhesion and interlaminar shear strength. Zhang et al. [42] showed that the fiber-matrix interfacial adhesion plays an important role in addressing the mechanical performance of CF/epoxy composites. They observed that the sizing agent used in CF surface coating can increase the CF-epoxy interfacial shear strength by ~36.3%. Furthermore, adding 5.0 wt% of graphene oxide (GO) to modify the sizing agent can increase the fiber-matrix interfacial shear strength by 70.9% relative to that observed for virgin CF reinforced epoxy. The CF coated with GO-modified sizing agent was also found to enhance the interlaminar shear strength of the laminated composite by ~12.7% relative to that observed for CF coated with commercial (unmodified) sizing agents. Later, Pathak et al. [43] observed an increase in the mechanical response of CF reinforced epoxy composites as 0.3 wt% of GO was introduced to the matrix. The flexural strength, flexural modulus, and interlaminar shear strength of the hybrid composite were increased by 66%, 72%, and 25%, respectively. This substantial improvement in the mechanical properties was attributed to the additional reinforcing effect of GO. The large surface area of GO nanosheets maximizes interfacial interaction with the hosting matrix in addition to the toughening and interlocking mechanism features of GO. Recently, Liu et al. [44] noticed that CF coated with sizing agents can increase the interfacial adhesion with the epoxy matrix by ~10%, where the interfacial strength increased from 48 MPa to 53 MPa. Grafting a CNT layer on the CF surface could further increase the interfacial strength by 3.64% to measure 55 MPa. An additional improvement of ~5.2% in the interfacial strength was obtained when grafting an oxidized-CNT layer on the CF surface to measure 58 MPa.

Despite the fundamental role of experiments in studying and developing polymer-based composite materials, many predictive computational approaches have been adopted to speed up the development wheel of composite materials at minimal cost and effort. Shiu et al. [45] performed MD modeling simulations to characterize the thermal and mechanical properties of graphene flakes (a chunk comprised of eight graphene sheets stacked together), and intercalated GNP and GO each comprised of three individual (dispersed) sheets incorporated in epoxy matrix. A general observation in this study indicates that intercalated GNP or GO allows for larger surface contact with the epoxy. That is, more interphase regions of dense epoxy at the intercalated GNP or GO surfaces which improves the load transfer within the nanocomposite. As a result, an improvement in the Young's modulus of intercalated GNP and GO nanocomposite MD models relative to graphene flakes-epoxy model. The best reinforcing efficiency was observed in the case of intercalated GO/epoxy MD model since it involved the highest interfacial interaction between the constituents.

To capture the effect of the molecular structure at the bulk behavior of nanocomposites, different micromechanics approaches have been employed [9, 22, 23, 46, 47]. Shokrieh et al. [48] conducted a combined molecular dynamics-micromechanics procedure to estimate the stiffness of randomly dispersed graphene sheets in epoxy matrix. The predicted elastic moduli from MD simulations for different sizes of graphene sheets embedded in epoxy were extrapolated to capture the actual values of the principal moduli. Then, an empirical equation was used to randomize the moduli and obtain an approximated effective stiffness of the nanocomposite at the microscale level.

Using a numerical analysis methodology based on XFEM (eXtended Finite Element Method), Bienias et al. [49] investigated the damage mechanism and failure in CF/epoxy composites under static tension. The micromechanics modeling approach involved the use of Cohesive Zone Method (CZM) to capture the cohesive behavior at the CF-matrix interface. The conclusion from this study referred to the fact that the material damage is most likely to be initiated and developed at the CF-matrix contact layer. The microstructure analysis and XFEM simulations indicated that the failure scenario started with material damage and CF-matrix interfacial deboning which then evolved to an intralaminar cracking.

Tomasi et al. [50] performed a computationally-driven study to construct a new CF/GNP/epoxy hybrid composite which can be used for the NASA space launch system composite exploration upper stage forward skirt structure. The computational approach used in this study was based on the Integrated Computational Materials Engineering (ICME). The designing scheme started at the molecular level to predict the localized mechanical properties of GNP/epoxy interphase region using MD modeling. The next step involved the use of MAC/GMC 4.0 for the micromechanics analysis and predictions toward constructing a laminated hybrid composite panel. The last step involved using FEM to design the space structure component in its full-scale. The material design was optimized using both multiscale modeling and experiments to control the key processing parameters and acquire better mechanical performance. The multiscale ICME workflow used in this study provides a powerful computational approach to model and optimize the properties of composite material structures for aerospace applications.

1.4 Objectives

The purpose of this work is to develop an efficient multiscale computational approach to model and predict the mechanical properties of CF/GNP/epoxy hybrid composites. The approach considers the fundamental role of the key processing parameters at different levels of the modeling scheme to optimize the material structure and its mechanical behavior. Below are the main objective points which are considered in this approach towards achieving the main goal:

- Perform MD simulations using an efficient reactive force field to acquire deep physical insight into the molecular structure at the GNP-epoxy interphase region, such as the molecular mass density distribution and interfacial adhesion.
- Assess the performance of the reactive force field used to achieve this purpose.

- The MD simulations are also intended to predict the molecular structure and the localized mechanical properties of the interphase region using different GNP configurations.
- Investigate the GNP agglomeration effect on the predicted mechanical properties of the nanocomposite using two certain levels of GNP dispersion degree.
- Investigate the chemical functionalization influence on the GNP structural integrity and its reinforcing function, the molecular structure of the matrix at the interphase region, the interfacial interaction and adhesion, and the local mechanical response of the interphase region under this consideration.
- Use micromechanics analysis to transmit the impact of the nanoscale key processing parameters mentioned above to the bulk level of the nanocomposite.
- Use micromechanics analysis to inspect the influence of the GNP content and aspect ratio on the mechanical response of the bulk nanocomposite.
- Evaluate the mechanical performance the CF/GNP/epoxy hybrid composite with four different configurations: hybrid composite laminate reinforced with unidirectional CF, and three different configurations of laminated composite panel.
- Consider all the nanoscale key processing parameters in addition the influence of CF volume fraction in the predictions of the CF/GNP/epoxy hybrid composite configurations.

The computational approach in this study provides a step-by-step systematic modeling scheme supported by detailed descriptions and illustrative graphs. Detailed information about the adopted MD simulations and micromechanics calculations with figures and plots for the obtained results are also provided. The predicted results were discussed and verified with experimental data available from the literature.

1.5 Roadmap

This section briefly addresses the roadmap of this work. Chapter 1 was written to attract the reader's attention to the importance of research studies on developing polymer-based composite materials for the future of the aerospace industry. The brief motivation and background were intended to prepare the reader for this topic. The basic definitions, information, and resources given in the background and the literature review were also intended to help interested readers and beginners to acquire basic knowledge and be aware of research tools needed for such research studies.

The next chapters address the roadmap to achieve the objectives of this study. Chapter 2 provides a computational case study to model GNP/epoxy nanocomposite with a certain level of GNP dispersion. A detailed modeling scheme to create the GNP crystal and the epoxy matrix monomers is provided. Subsequent steps of combining the nanocomposite constituents, densifying the model, crosslinking (curing) the epoxy monomers, and equilibrating the MD model are also included. The MD simulations are utilized to assess the performance of the selected reactive force field in predicting the molecular structure and its mechanical response at the nanoscale level. The predicted mechanical properties at

the nanoscale level are processed using a micromechanics approach to predict the mechanical response of the composite at the bulk level.

Chapter 3 discusses the functionalization effect on the GNP structure, GNP-matrix interfacial interaction, and overall mechanical behavior of the nanocomposite. For the first time, functionalized GNP MD models are established based on elemental data analysis of the functional groups reported for a real case study of functionalized GNP. This modeling process involves taking into account the chemical composition of functional groups and their chemical concentration on the GNP surface. The modeling scheme in this chapter includes illustrative figures and plots supported by a detailed description, analysis, results and discussion, and validation.

Chapter 4 focuses on the micromechanics analysis of CF/GNP/epoxy hybrid composites. Several models of the hybrid composite are constructed based on the predictions obtained in Chapters 2 and 3 for the GNP/epoxy nanocomposites. In other words, the micromechanics analysis of the hybrid composites involves a comparison study of the reinforcing effect of the different GNP configurations which are modeled in the preceding chapters. The multiscale modeling approach considers the nano/micro/macro key processing parameters in optimizing the mechanical behavior and properties of the composite material.

Chapter 5 involves some important suggestions and recommendations for future work which can be used to extend the scope of this study. The next section includes the references used in preparing this work which are listed based on the in-text citation numbers appear in the main text. Additional supporting information, technical resources, and the copyright agreement documentation used in this work are provided in the appendices.

Chapter 2

MULTISCALE MODELING OF CF/GNP/EPOXY HYBRID COMPOSITE USING A REACTIVE FORCE FIELD

This chapter focuses on predicting the local molecular structure and mechanical properties at the interphase region of the GNP/epoxy nanocomposite using MD modeling with a reactive force field. The multiscale computational approach involves using MAC/GMC 4.0 to predict the mechanical properties of the nanocomposite at the bulk level. The nanocomposite mechanical properties are then implicitly used in the predictions of the unidirectional CF/GNP/epoxy hybrid composite at the bulk level. The nanoscale outcome provides evidence of an alignment behavior of phenyl rings in epoxy with the planar GNP surface at the interphase region. The results also indicate the validity of using a reactive force field, as they compare well with experiment [51, 52][1].

2.1 Introduction

This chapter is intended to provide deep insight into the molecular structure and the mechanical performance of GNP/epoxy nanocomposites. Such computational studies are essential for driving the development of the new generation of polymer-based hybrid composites reinforced with CF and carbon nanofillers. Hadden et al. [46] performed a detailed multiscale computational study validated with experimental work to investigate the effect of GNP content and the degree of dispersion on the elastic properties of CF/GNP/epoxy hybrid composites. An improvement in elastic properties was observed with increasing levels of GNP dispersion and volume fraction. The multiscale modeling approach involved MD simulations for the prediction of the material mechanical response at the molecular level. The MD simulations utilized the united-atom fixed-bond Optimized Potentials for Liquid Simulations (OPLS) force field [24, 25]. LAMMPS implementation of OPLS is rather pioneer and it was foremost used for MD modeling of liquids and proteins. Its parameter set overestimates energy calculations as it was originally derived utilizing the approximated assumptions of the Hartree-Fock theory in quantum mechanics. Energy calculation is particularly crucial for the quality of the torsion angles description. For this reason, even simple polymers such as longer hydrocarbons failed in the framework of the original OPLS. Despite the aforementioned limitations in OPLS, this force field has been recently shown to predict accurate mechanical properties of polymer-based composite materials within the elastic limit [46].

At relatively high mechanical strains, the material response can be more accurately predicted using the reactive force field (ReaxFF) which was initially developed by van Duin et al. [53]. Odegard et al. [10] utilized the ReaxFF parameter set developed by Liu et

[1] Most of the material contained in this chapter has been previously published in the ASCE-2018 Earth & Space conference proceedings (See Appendix C.2 for copyright agreement). The work was then modified and published as a journal article in Composites Part B: Engineering, © Elsevier Ltd (See Appendix C.3 for copyright agreement).

al. [26] to predict Young's modulus and yield strength of a crosslinked epoxy system. Due to the computational expense, MD simulations are restricted to a few nanoseconds. Therefore, deformation simulations must be performed at high strain rates beyond what is experimentally feasible. Owing to the high strain rate used in the MD simulation and the viscoelastic nature of epoxy, an overestimation trend was observed in the predicted mechanical response compared to experiments. Despite the substantial strain rate effect, the predicted mechanical properties of the MD model were mathematically correlated with experiments considering the large time-scale difference. Under these circumstances, the extrapolated experimental results for higher strain rates were within the standard deviation of the predicted values. Radue and Odegard [9] utilized ReaxFF in their MD modeling to investigate the mechanical behavior of three different epoxy systems reinforced with an embedded carbon nanotube (CNT). This work introduced a computational approach to assess the mechanical performance of CNT-based nanocomposites depending on the epoxy functionality. To minimize the strain rate effect, the predicted elastic modulus for each nanocomposite was normalized by its matrix modulus as a convenient baseline. Accordingly, a good agreement with experiments was observed as the strain rate effect was somewhat mitigated with this approach.

It is unknown if ReaxFF can be reliably used for simulating polymer-based nanocomposites reinforced with GNP. Thus, the objective of this chapter is focused on assessing the performance of using ReaxFF in predicting the localized effective mechanical properties of GNP/epoxy within the elastic limit. This assessment could open the door for future computational research to utilize the reactive features in ReaxFF involving bond formation and scission. In this work, a multiscale modeling study was performed to predict the effective mechanical properties of CF/GNP/epoxy hybrid composites using ReaxFF. First, a unit cell of GNP/epoxy nanocomposite was simulated, and the corresponding nanoscale mechanical properties were predicted. Second, these results were used as inputs into a micromechanical analysis of a CF/GNP/epoxy hybrid composite. The effective bulk mechanical properties were predicted for different volume fractions of GNP in the composite matrix. The results show good agreement with experimental values available in the literature, demonstrating the accuracy of ReaxFF for modeling hybrid composite systems.

2.2 Multiscale Modeling Approach

The step-by-step methodology for developing the multiscale model is described in this section. A description of the MD modeling and subsequent micromechanics analysis steps for predicting the mechanical properties of hybrid composite is included.

2.2.1 Molecular Modeling (Nanoscale)

All MD simulations were carried out with the LAMMPS software package with 3D periodic boundary conditions to account for the bulk material behavior. The Lennard-Jones cutoff distance was set to 10 Å. All post-processing visual snapshots were rendered utilizing the OVITO software package [54].

2.2.1.1 Creating GNP-epoxy unit cell

The MD modeling procedure adopted in this study is based on those found in the literature [8-10, 22, 23, 46, 55-57]. In most of these modeling studies, the fixed-bond force field OPLS was used to initially create epoxy monomer solutions and perform the crosslinking reactions using a wide range of approaches. Using a fixed bond force field during this modeling step enables the creation of the epoxy crosslinked network via the "fix bond/create" LAMMPS command. The presence of physical bonding connectivity between atoms allows the user to track and update the topology of the molecular structure using a python script.

Figure 2.1 shows the EPON 862 (diglycidyl ether of bisphenol F, DGEBF) molecule, which has 43 atoms, and the EPIKURE curing Agent W (diethyltoluenediamine, DETDA) molecule, with 31 atoms, were separately created using the ChemDraw Professional software package, version: 15.0.0.106, PerkinElmer Informatics, Inc. The OPLS-All Atom (OPLS-AA) force field was initially used to build the molecular structures. The stoichiometric mixture 2:1 of the epoxy system (two EPON 862 molecules to one DETDA molecule) was created in a periodic MD simulation box comprising 117 atoms (Figure 2.2.a). This mixture was replicated 16 times to form a larger system that contained 48 monomers with 1872 atoms (Figure 2.2.b). This system was subjected to 1 ns of MD simulation using the NVT ensemble (constant number of atoms, volume, and temperature) at 300 K followed by a molecular minimization simulation to establish a thermodynamically equilibrated structure. The epoxy molecules at this point had a low mass density and were clustered together due to vdW interaction (Figure 2.2.c). The epoxy cluster was replicated in the z-direction, leaving a space to insert a GNP sheet in the subsequent simulation step (Figure 2.2.d). At this point, the epoxy system included 3744 atoms forming 96 molecules (64:32 monomer ratio).

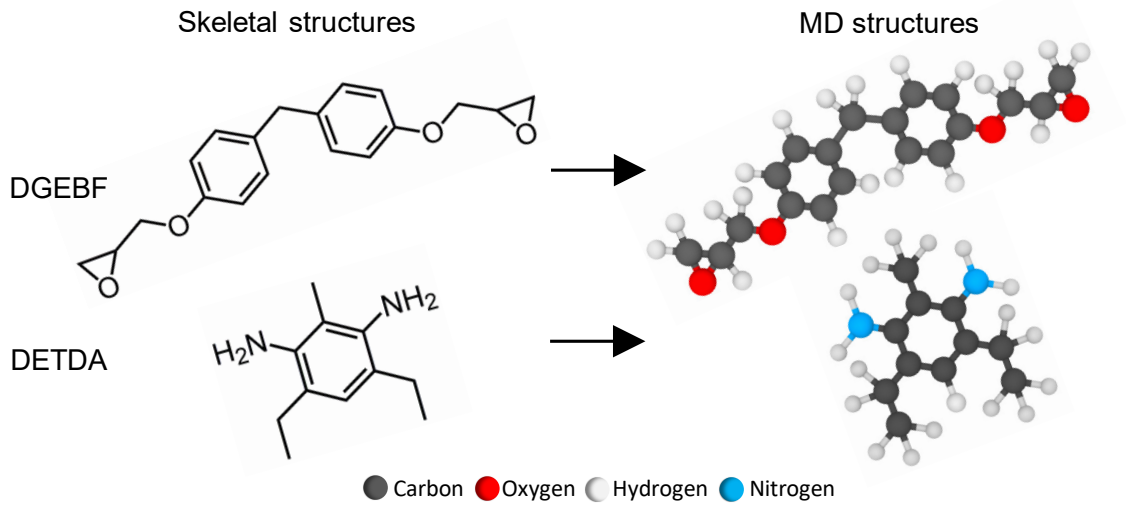

Figure 2.1: Molecular structures of epoxy monomers (EPON 862/DETDA).

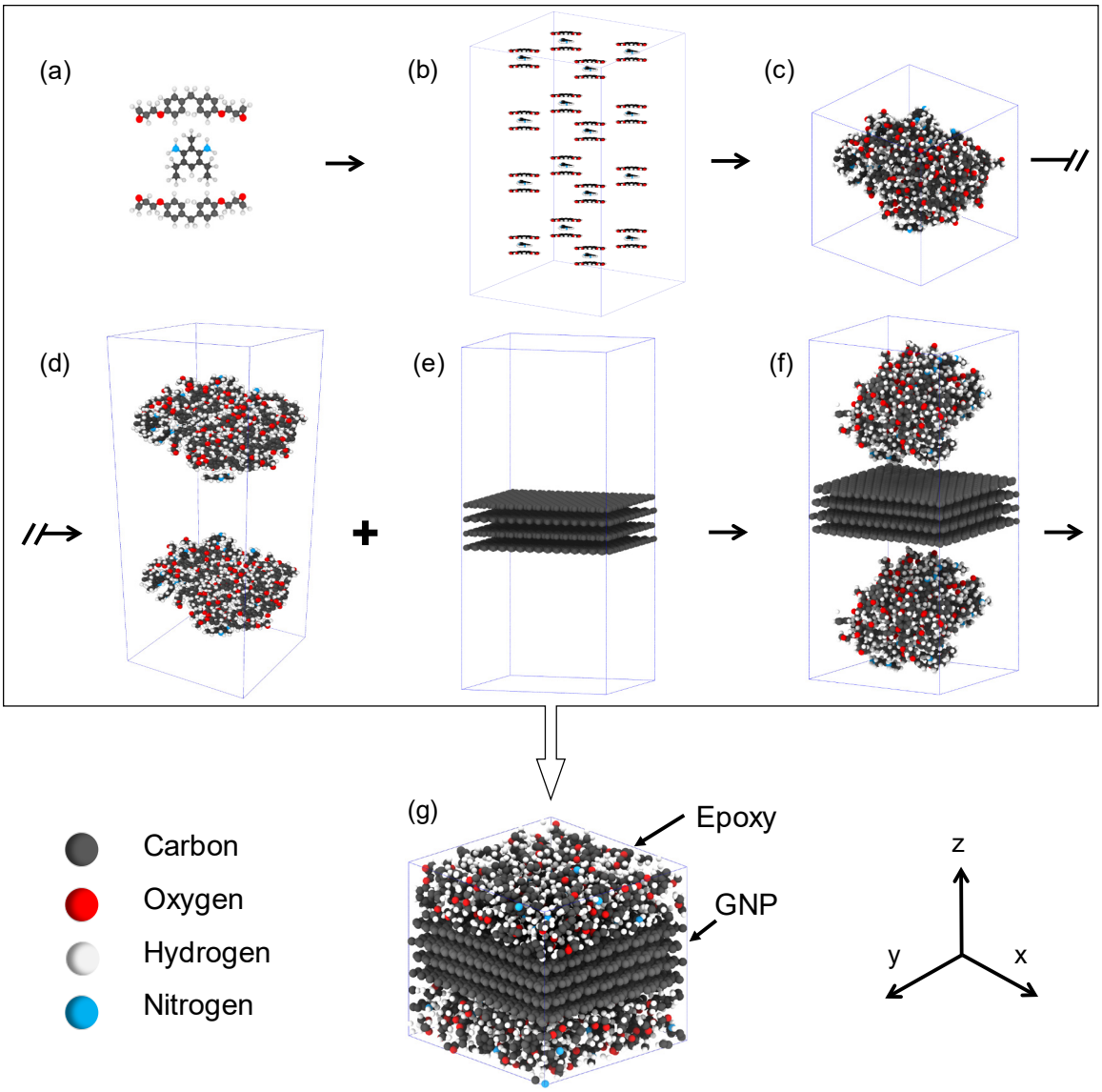

Figure 2.2: The MD modeling scheme to create the 4-layer GNP/epoxy unit cell.

A LAMMPS script utilizing the "lattice" command was used to generate a crystal structure of the 4-layer GNP. The lattice parameters for the planar structure of graphene and the crystal structure of graphite were taken from Gray et al. [58]. To account for graphene agglomeration, a procedure similar to that used by Hadden et al. [46] was implemented in which the generated GNP molecule was comprised of four graphene sheets/layers, where each layer included 576 carbon atoms (Figure 2.2.e). Hence, the 4-layer GNP included 2304 carbon atoms. Both MD data files from epoxy and the GNP were combined into one MD data file which represented the unit cell of the nanocomposite (Figure 2.2.f). The assembled unit cell (simulation box) of the 4-layer GNP/epoxy nanocomposite had 6048 atoms. It was subjected to several steps of size reduction along the *z*-axis to densify the epoxy monomers to the expected bulk level (Figure 2.2.g). A

constant temperature of 300 K was maintained with the Nose/Hoover thermostat while the simulation box size was gradually decreased to reach the target density. It is important to note that the simulation box is relatively small due to the high computational cost of using ReaxFF. Thus, five replicates of the MD model were developed for statistical sampling. This approach provided the appropriate uncertainty in the predicted mechanical properties, which is critical for discrete molecular structures of this size.

The targeted mass density of the epoxy system from the densification process was approximately 1.2 g/cm^3, which is the observed mass density for this system [56]. Figure 2.3 (left) shows a representative volume element (RVE) of the 4-layer GNP/epoxy nanocomposite unit cell after the densification process (not yet crosslinked). The simulation box size measured 40×39×37 Å along the x-, y-, and z-axis, respectively. It is important to note that the lateral size of the MD simulation box is governed by the lateral size of the GNP crystal. Also, the z-axis length of the RVE was selected to completely encompass the ~10 Å interphase region [8]. The wt% of the GNP in the RVE was about 52%, and the spatial mass density distribution along the z-axis is illustrated in Figure 2.3 (right). The four mass density spikes in the middle represent the four layers of the GNP. The next smaller spikes represent the epoxy mass density concentration in the interphase region. These results are consistent with those reported previously [8, 46], which employed a fixed-bond potential.

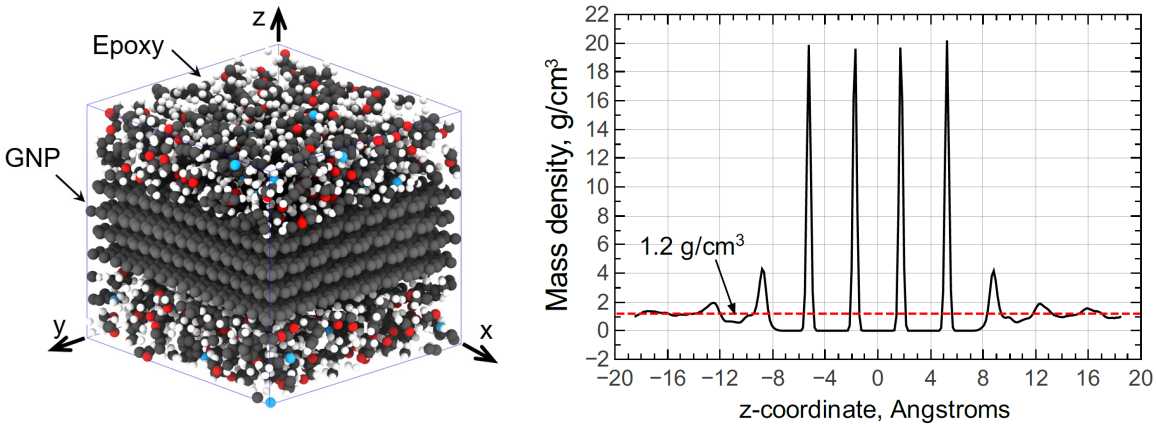

Figure 2.3: MD modeling; (left) Representative volume element for 4-layer GNP/epoxy, (right) Spatial density distribution along z-axis.

2.2.1.2 Epoxy curing (crosslink algorithm)

A dynamic crosslinking approach was used to perform the curing reactions between epoxy monomers. It is based on the approach used by Varshney et al. [55]. Generally, all C (carbon) atoms in the epoxide groups in the EPON 862 monomers have the same probability to react only once and form a covalent bond with a N (nitrogen) atom from the amine groups in the DETDA monomers. Each N atom can react twice and form two covalent bonds with two different C atoms in the epoxide groups (Figure 2.4). The “fix bond/create” LAMMPS command was used to create the N-C bonds. A Python script was

developed to complete the crosslink reaction and update the topological information of the epoxy system.

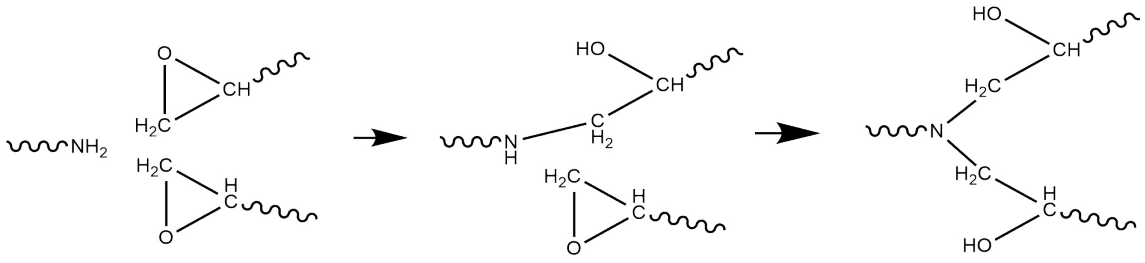

Figure 2.4: Epoxy curing reaction.

The crosslinking process was performed using a BASH (Bourne-Again SHell) script to run LAMMPS and Python scripts iteratively until a crosslink density of 80% was achieved (Figure 2.5), which was shown by Hadden et al. [46] to be sufficient for accurate prediction of bulk mechanical properties of CF/GNP/epoxy hybrid composites. The MD models were equilibrated for 1 ns using the NPT ensemble (constant number of atoms, pressure, and temperature) at 300 K. The Nose/Hoover anisotropic barostat was implemented during the simulation to stabilize the molecular structure and minimize the overall residual stresses in the MD cell. Such internal residual stresses are likely to be produced during the epoxy crosslinking reactions.

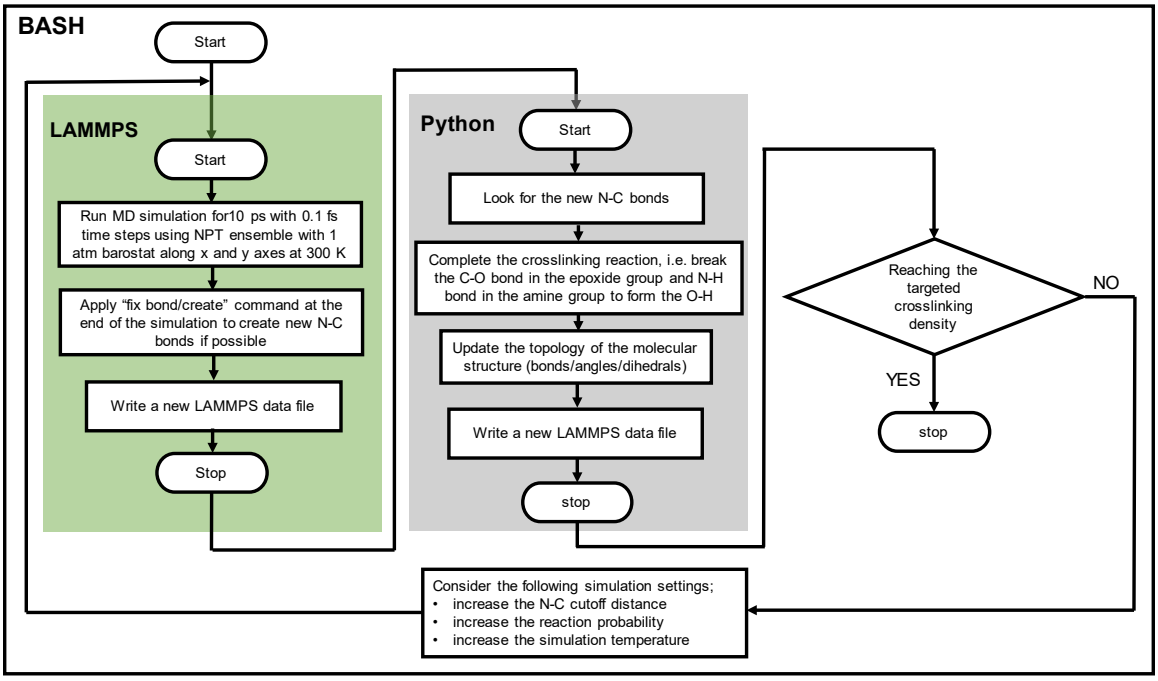

Figure 2.5: Crosslinking flowchart.

2.2.1.3 Import into ReaxFF

The main objective of this work was to assess the validity of using ReaxFF in analyzing the mechanical response of CF/GNP/epoxy hybrid composites. Therefore, once the five MD replicates were well equilibrated using OPLS, a transition to ReaxFF with the parameterization of Liu et al. [26] was performed. First, the transition process was performed slowly using a time step of 0.1 fs with 1 ns of MD simulation. In order to sustain the molecular structure integrity, the simulation temperature was gradually increased from 1 K to 300 K. This helped to constrain the atomic natural vibrations and velocities during the early steps of the transition process. After completing the transition into ReaxFF, the MD models were further equilibrated for 1 ns of MD simulation using the NPT ensemble at 300 K with the anisotropic Nose/Hoover barostat. Eventually, each of the five relaxed MD models had a simulation box size of 40×39×36 Å with a GNP volume fraction of ~36%.

2.2.1.4 Interphase region of GNP-epoxy

The structural integrity and mechanical performance of nanocomposites are highly governed by the interphase region [46]. The pi-stacking interaction between phenyl rings in polymers and hexagonal surfaces of GNP is the primary driver for the formation of the interphase region [59-61]. It is important to note that the MD modeling herein does not explicitly account for the interaction of pi-orbitals. In spite of this, some features are moderately captured by a simple non-bonded potential, such as the potential energy variations along graphitic surfaces [62]. Interesting visual results were obtained from the equilibrated MD models by utilizing the "slice" tool in OVITO. Figure 2.6 shows the top views of 2 Å thick slices that were taken from a representative MD simulation box at different distances from the GNP. Clearly, most of phenyl rings at the interphase region are aligned with the GNP surface, which corresponds to the mass density spike around z = 8.5 Å. However, the alignment decreases with distance from the GNP, which can be clearly observed in the slices far from the GNP surface. Thus, a typical epoxy mass density (~1.2 g/cm^3) was observed beyond a distance of ~10 Å from the GNP surface.

To examine this issue further, a Python script was written to calculate the angle between the normal to each phenyl ring in the epoxy molecules and the normal to the GNP surface or the *xy*-plane. The results are shown in Figure 2.7 for various points along the z-axis. The data confirms the stacking interaction at the interphase region, where most of phenyl rings are aligned with the GNP within the range of 8-10 Å. Yang et al. [61] asserts that such alignment can help to increase the interfacial binding between the two constituents. Another finding in the current work was that the GNP/epoxy interfacial interaction decreases with the increase of epoxy molecular weight. This is because the extension of the epoxy network during the crosslinking process limits the orientation of epoxy phenyl rings with respect to the GNP. Figure 2.8 illustrates how the epoxy mass density slightly decreased at the interphase region as the crosslink density reached 80% for both OPLS and ReaxFF force fields.

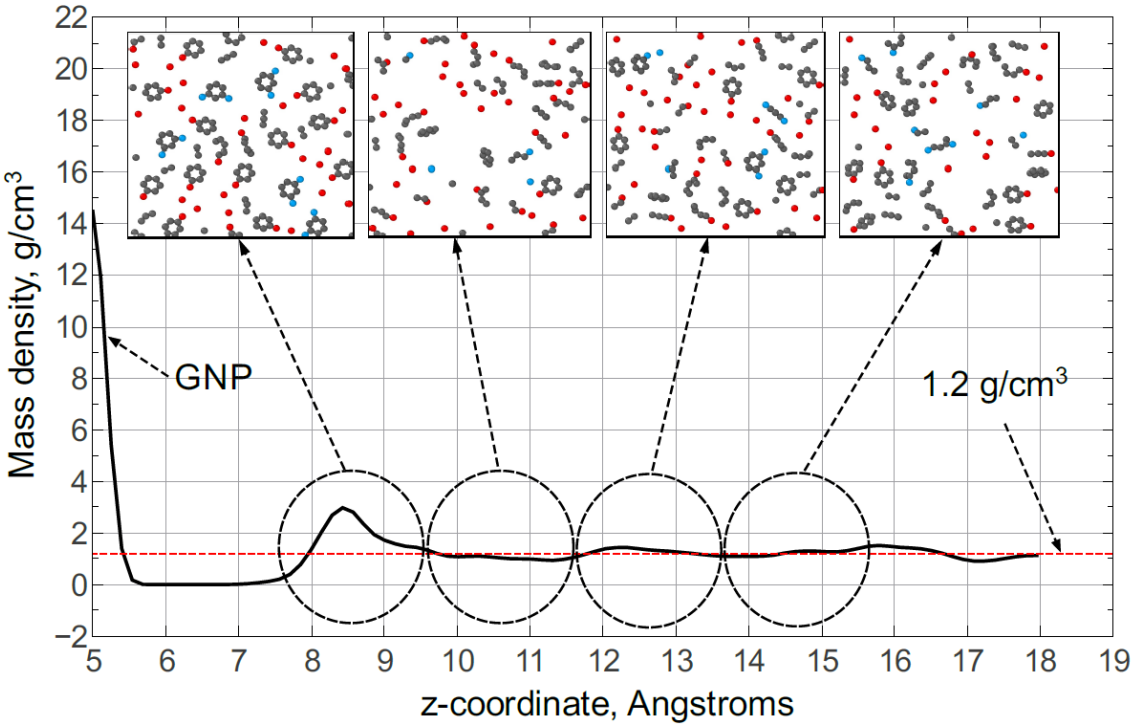

Figure 2.6: Alignment of phenyl rings in epoxy near the GNP surface.

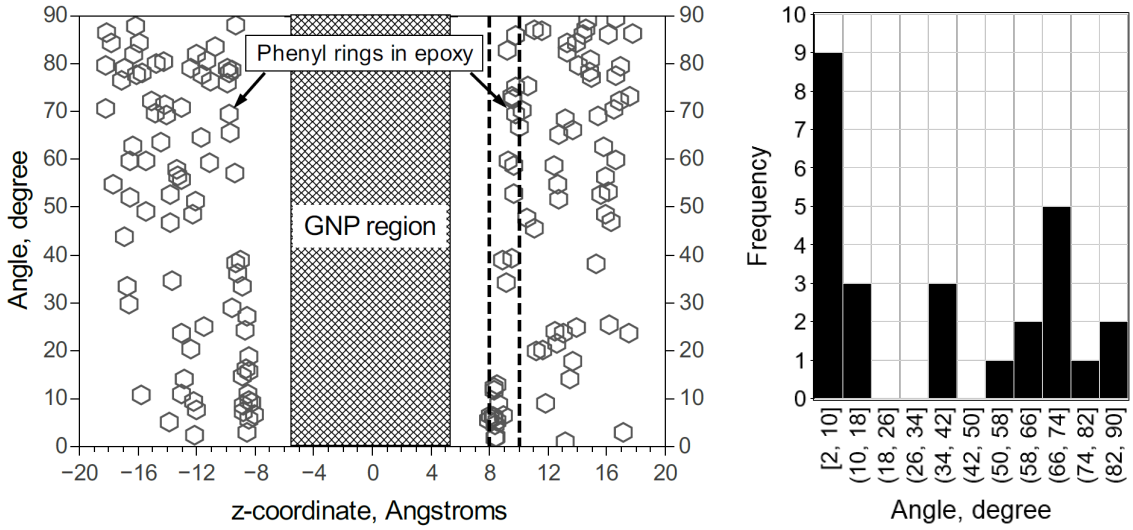

Figure 2.7: The angle between the normal to each phenyl ring in the epoxy molecules and the normal to the GNP surface: (left) angle distribution along z-coordinate, (right) histogram of region (8-10) Å

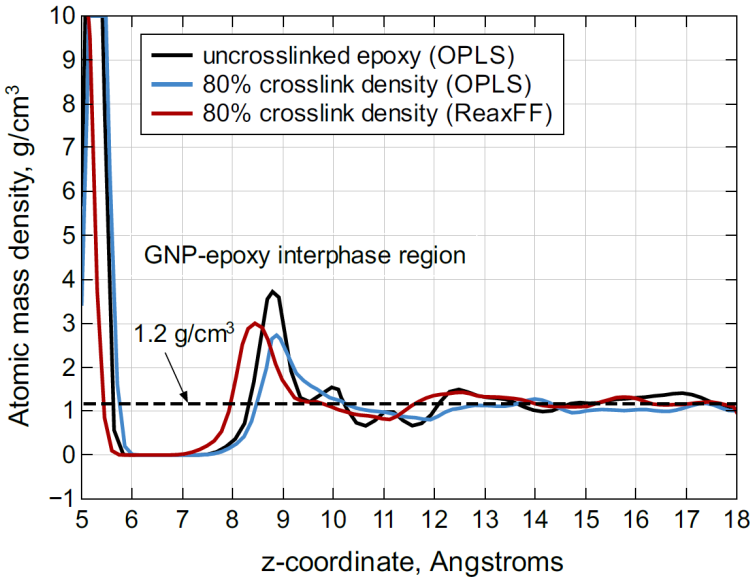

Figure 2.8: Crosslink effect on mass density distribution

Figure 2.9 shows the interfacial interaction energy (IIE) averaged over the five MD replicates. The IIE was calculated to assess the interfacial adhesion between GNP and epoxy. The calculation process involved subtracting the isolated potential energy of the GNP (PE_{GNP}) and epoxy (PE_{epoxy}) from the total potential energy of the entire model (PE_{MD}) [9]:

$$IIE = PE_{MD} - PE_{GNP} - PE_{epoxy} \tag{2.1}$$

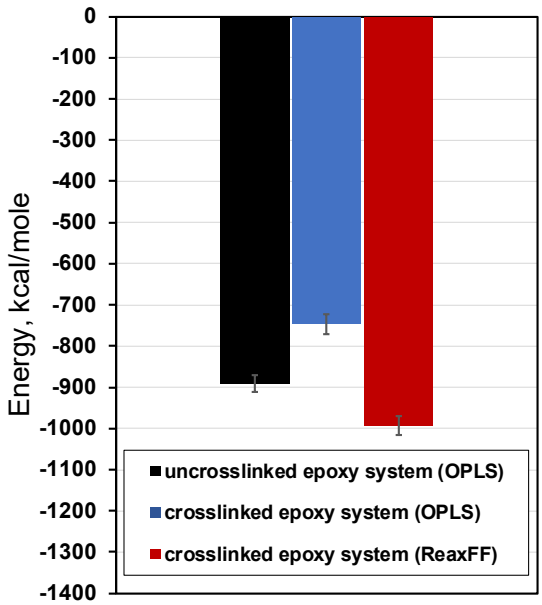

Figure 2.9: Interfacial Interaction Energy

The more negative the *IIE* is, the stronger the GNP/epoxy attraction. With the OPLS force field, the *IIE* decreased by ~16% after crosslinking. This behavior indicates the reduction in the GNP/epoxy interfacial adhesion which can be attributed to the change in the epoxy network after crosslinking. In other words, the increase in the molecular weight of epoxy network resulted in a lower mass density of the epoxy matrix at the interphase and lower *IIE* with GNP. A similar trend was observed by Radue and Odegard [9] in their CNT/epoxy MD models. They demonstrated that the CNT/epoxy interaction is directly governed by the matrix mass density at the interphase. With ReaxFF, the *IIE* settled to a much higher value than that for the crosslinked epoxy with OPLS (~33% increase). This extra amount of *IIE* is attributed to the Coulomb and charge equilibration energy contributions in the potential energy with ReaxFF. In fact, the potential energy vector evaluated using the "pair-style reax" command includes 14 energy terms. Thus, a more comprehensive representation of the molecular interaction can be obtained with ReaxFF relative to OPLS. Moreover, OPLS is derived for simulations of liquids and does not provide parameters for graphene. As a result, ReaxFF is expected to perform better than OPLS in predicting the mechanical response of GNP/epoxy MD models under applied mechanical loads.

2.2.1.5 Mechanical response (nanoscale)

Once the five GNP/epoxy MD models were well-equilibrated with ReaxFF, they were subjected to three simulated tensile strains along the *x*-, *y*-, and *z*-directions; and three shear strains in the *xy*-, *xz*-, and *yz*-planes. In order to account for the Poisson contraction, the axial tensile strains were performed using NPT ensemble with the Nose/Hoover barostat in the lateral directions to maintain one-atmospheric pressure surfaces. The shear strain simulations were performed using the NVT ensemble, and the "triclinic" parameter was activated for the simulation boxes using the "change_box" command in LAMMPS. This step is necessary to increase the degrees of freedom of the simulation box from three (deformations along *x*, *y*, *z* axes) to six (deformations along *x*, *y*, *z* axes and tilts in the *xy*, *xz*, *yz* planes). Thus, both axial and shear deformations of the simulation box are possible.

All MD models were subjected to a maximum engineering strain of 5%. The mechanical deformation simulations were performed for the models constructed with both the OPLS and ReaxFF force fields. Each deformation simulation in OPLS was carried out gradually, at a strain rate of 0.5×10^{8} s^{-1}, over a total simulation time of 1 ns using 0.1 fs time steps. The simulations with the OPLS force field were used to estimate the elastic mechanical response and validate the current MD simulation procedure with Hadden et al. [46]. The deformations for each of the five equilibrated MD models using ReaxFF were carried out gradually, at a strain rate of 1×10^{8} s^{-1}, over a total simulation time of 0.5 ns using 0.1 fs time steps. It is important to note that due to the very high computational time cost for MD simulations with ReaxFF relative to OPLS, the deformation simulations with ReaxFF were accelerated by increasing the strain rate. It has been established that for strain rate values less than 22×10^{8} s^{-1} there was no effect observed on the predicted mechanical response for simulated carbon allotropes [63]. To verify that this is applicable to the current MD modeling, deformation simulations for one of the MD replicates were performed using

ReaxFF with a strain rate 0.5×10^{8} s^{-1}. The results indicated an identical mechanical response as the strain rate was increased from 0.5×10^{8} s^{-1} to 1×10^{8} s^{-1}. The predicted mechanical properties from MD models are listed in Table 2.1, along with the results from Hadden et al. [46]. Each specific property was averaged over the five MD models, and the uncertainty in the table represents the corresponding standard deviation.

At this point, it is important to highlight two important issues considered in this work. First, OPLS was not used for accuracy purposes. Its predictions were used as a baseline to compare the predicted properties from ReaxFF. OPLS was used in many legacy MD studies [8, 46, 56] which makes it a perfect candidate for benchmarking purposes. Second, the point of using ReaxFF herein is just to verify its advantage and accuracy in predicting the elastic properties and molecular structure of polymer nanocomposites, not to prove that the additional capabilities of ReaxFF are necessary for simulating polymer nanocomposites.

Table 2.1: The predicted mechanical properties for the 4-layer GNP/epoxy nanocomposite MD model, all moduli are given in (GPa).

Property	Present work (OPLS)[a]	Present work (ReaxFF)[b]	Hadden et al. (OPLS)[c] [46]
E_x	290.32±1.23	425.40±2.55	293.1
E_y	289.24±1.60	415.50±3.53	295.5
E_z	3.122±0.367	5.331±0.559	3.251
G_{xy}	104.92±0.79	102.00±1.03	72.50
G_{xz}	0.040±0.021	0.019±0.016	0.001
G_{yz}	0.044±0.022	0.020±0.013	0.001
v_{xy}	0.290±0.001	1.005±0.001	0.159
v_{yx}	0.294±0.002	0.980±0.002	0.156
v_{zx}	0.004±0.001	0.002±0.001	0.011
v_{zy}	0.005±0.001	0.002±0.001	0.009

[a] Present work: Average over five replicates of MD models, using OPLS-AA (All Atom) force field, 6048 atoms, 4-layer GNP/epoxy nanocomposite, 80% crosslink density, 36% GNP volume fraction (52.0 wt%), 0.5×10^{8} s^{-1} strain rate, 5% maximum engineering strain.

[b] Present work: Average over five replicates of MD models, using ReaxFF force field, 6048 atoms, 4-layer GNP/epoxy nanocomposite, 80% crosslink density, 36% GNP volume fraction (52.0 wt%), 1×10^{8} s^{-1} strain rate, 5% maximum engineering strain.

[c] Hadden et al. (2015): One MD model, using OPLS-UA (United Atom) force field, 37550 atoms, 4-layer GNP, 80% crosslink density, 33% GNP volume fraction, 0.5×10^{8} s^{-1} strain rate, 5% maximum engineering strain.

2.2.2 Micromechanics Modeling (Microscale)

Once the effective mechanical properties from the MD simulations were predicted within the elastic limit, their averaged values over the five MD models with ReaxFF were utilized in the next level of analysis (microscale). MAC/GMC 4.0 was used for these predictions by generating a RUC to represent the periodicity of material microstructure. The RUC is composed of a discrete number of subcells, where each subcell represents a single phase of the composite. For more information about MAC/GMC 4.0 and its usage, please refer to Chapter 1; subsection 1.2.5 Micromechanics. In this work, three sequential steps were adopted toward the ultimate prediction of the microscale mechanical properties of the hybrid composite. Figure 2.10 schematically illustrates the multiscale modeling workflow. Further details about the micromechanics analysis based on the three continuum-level steps are discussed in the following subsections.

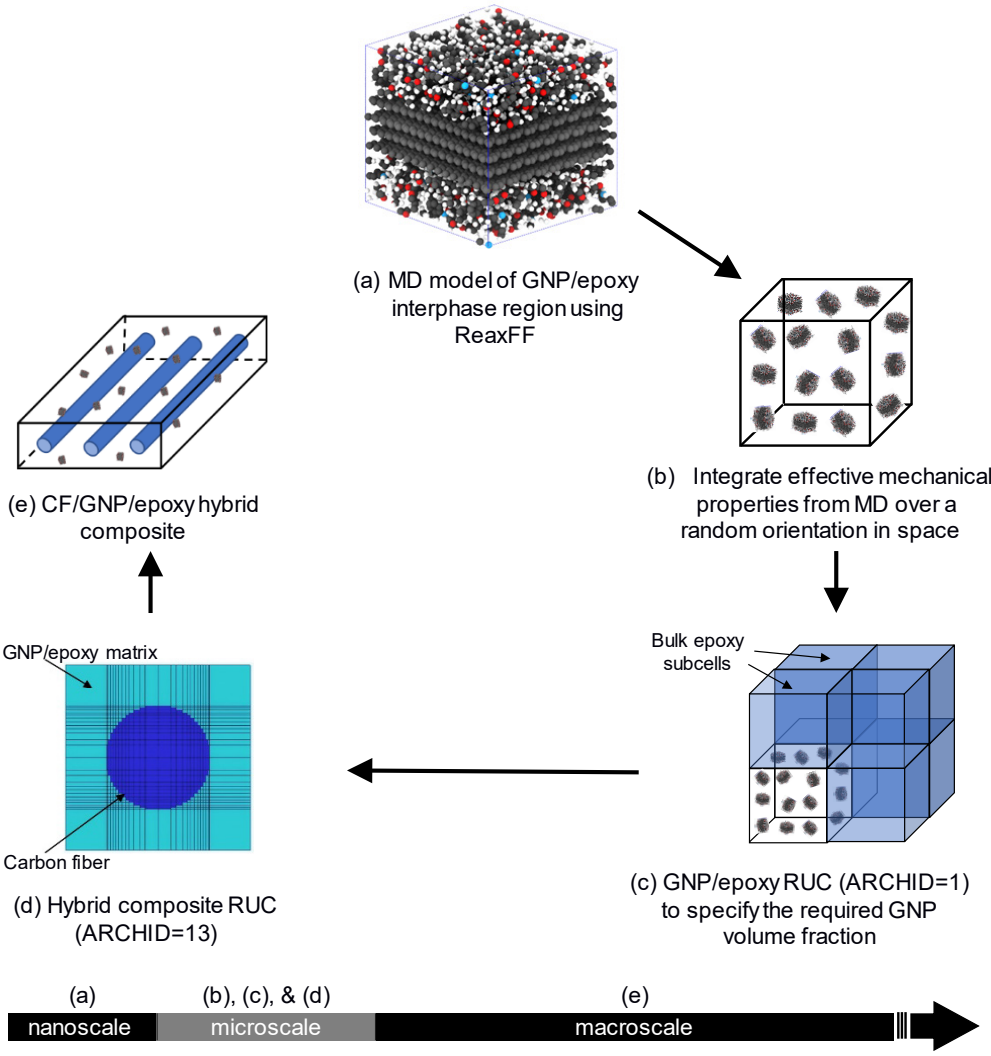

Figure 2.10: The multiscale modeling workflow of CF/GNP/epoxy composite.

2.2.2.1 GNP dispersion (randomization)

The 4-layer GNP/epoxy interphase region shown in Figure 2.10.a was implicitly captured within the MD-predicted effective mechanical properties. In order to model the arbitrary orientation of individual GNPs in the neat epoxy matrix, the effective mechanical properties of the molecular models using ReaxFF (Table 2.1) were further processed to predict the effective isotropic properties of the GNP/epoxy nanocomposite, as shown in Figure 2.10.b. The equations of Christensen and Waals [64] were used for this purpose.

2.2.2.2 The GNP volume fraction

The effective mechanical properties of the isotropic system shown in Figure 2.10.b were used as input to a MAC/GMC 4.0 script to generate a RUC of a GNP/epoxy nanocomposite. A built-in RUC (ARCHID=1) that contains 8 subcells was utilized to adjust the required GNP volume fraction in the neat epoxy matrix, as shown in Figure 2.10.c. In order to model a specific GNP volume fraction ($VF_{GNP/RUC}$) in the GNP/epoxy nanocomposite, it was necessary to adjust the size of the subcell that represents the effective mechanical properties of the randomly oriented GNP in epoxy with respect to the subcells of bulk epoxy ($VF_{MD/RUC}$). The GNP volume fraction within the simulated MD sample ($VF_{GNP/MD}$) was ~36%. Thus, the overall $VF_{GNP/RUC}$ can be determined from the direct product of $VF_{MD/RUC}$ and $VF_{GNP/MD}$ [9, 46]. According to this approach, it is feasible to choose the GNP volume fraction and acquire the mechanical properties of the nanocomposite without the need for new MD simulations.

2.2.2.3 Hybrid composite

A subsequent MAC/GMC 4.0 script was written to model the CF/GNP/epoxy hybrid composite. A built-in RUC (ARCHID=13) of a 26 × 26 circular array was selected to represent the carbon fiber architecture while the surrounding area represented the GNP/epoxy matrix, as shown in Figures 2.10.d,e. The homogenized properties that were calculated for randomly oriented GNP in epoxy for a specific value of $VF_{GNP/RUC}$ were used as the new matrix properties in the RUC for the hybrid composite. AS4 carbon fiber was modeled to reinforce the GNP/epoxy nanocomposite matrix, and its properties are given in Table 2.2.

Table 2.2: AS4 carbon fiber (HexTow®)

Property	value
Axial modulus, GPa	231
Transverse modulus, GPa	9.6
Shear modulus, GPa	112
Poisson's ratio	0.30
Fiber volume fraction	56%

2.3 Results and Discussion

The predicted properties of the 4-layer GNP/epoxy and CF/GNP/epoxy composites are described in this section. Comparison to literature values is provided for model validation.

2.3.1 GNP/Epoxy Nanocomposite

Hadden et al. [46] evaluated the effective mechanical properties for the same nanocomposite material using the fixed-bond OPLS force field. Despite the difference between the two MD models (namely; model size, force field, and GNP volume fraction), the effective mechanical properties that were predicted herein using OPLS provide a good indication regarding the validity of the present MD simulations (Table 2.1). However, there is a relative discrepancy in the predicted mechanical properties between OPLS and ReaxFF. Providing the discussion mentioned above concerning the parameter set of OPLS, the observed differences most likely originate from inaccuracy in bonding terms in OPLS. The discrepancy can be recognized in the in-plane Young's modulus E_{ip} which is the average of the two orthogonal moduli E_x and E_y, and it is essentially dominated by the in-plane elastic modulus of the GNP. A similar discrepancy is observed with the in-plane Poisson's ratio v_{ip}, which is the average of v_{xy} and v_{yx}. Using the experimental in-plane elastic modulus (1.06 $\pm$ 0.02 TPa) and in-plane Poisson's ratio (0.16 $\pm$ 0.06) of graphite [65], the experimental elastic modulus of epoxy (2.72 GPa) [40], and a GNP volume fraction of 36%, a simple estimation using the rule of mixtures results in an effective in-plane modulus for the GNP/epoxy nanocomposite of 413.5 GPa. This value is very close to what was predicted herein with MD modeling using ReaxFF, which indicates a more reliable prediction with ReaxFF.

Clearly, the out-of-plane Young's modulus (E_{op} or E_z) is much lower than the in-plane modulus because its magnitude is governed by the vdW interaction between GNP layers and interfacial interaction between GNP and epoxy. It is speculated that the inclusion of Coulomb and charge equilibration terms in the ReaxFF calculations caused the relative increase in the predicted modulus relative to the corresponding value calculated using OPLS. Regarding the predicted out-of-plane Poisson's ratio v_{op}, which is the average of v_{zx} and v_{zy}, a rather good agreement is observed in the predicted values using OPLS with those from Hadden et al. [46]. In contrast, the value of v_{op} predicted using ReaxFF was much lower than that predicted with OPLS, which can also be attributed to the atomic charge terms used with ReaxFF.

Interestingly, the values of the in-plane shear modulus G_{ip} or G_{xy} were in excellent agreement between the two force fields, but they are significantly greater than that reported by Hadden et al. [46] (Table 2.1). For a transversely isotropic material, the well-known relation derived by Hashin $G_{ip} = E_{ip}/\left[2\left(1 + v_{ip}\right)\right]$ [66] clearly implies the direct dependency of G_{ip} on E_{ip}, which in turn depends on the Young's modulus of GNP. For example, E_{ip} and v_{ip} can be calculated from the predicted properties in ReaxFF to be 420.5 GPa and 0.993, respectively. Applying Hashin's equation utilizing these values results in a G_{ip} value equals to 105.5 GPa, which is in excellent agreement with the predicted values

provided herein. The out-of-plane shear modulus G_{op}, which is the average of the two shear moduli G_{xz} and G_{yz}, is very low as its magnitude is governed by the vdW interaction between GNP layers and interfacial interaction between GNP and epoxy.

Figure 2.11 shows the elastic modulus of the GNP/epoxy nanocomposite as a function of the overall $VF_{GNP/RUC}$. It represents the response of the isotropic system achieved by randomly orienting the GNP in three-dimensional space. Two distinct points can be clearly recognized from the response curve shown in Figure 2.11. First, the response from the present work is relatively close the computational and experimental response reported by Hadden et al. [46]. Second, the isotropic elastic modulus is directly dependent on the GNP content in the epoxy matrix. The composite exhibits an increase of ~40% in the elastic modulus at an overall $VF_{GNP/RUC}$ of 5%. This represents a significant enhancement in the material stiffness despite the small amount of GNP content.

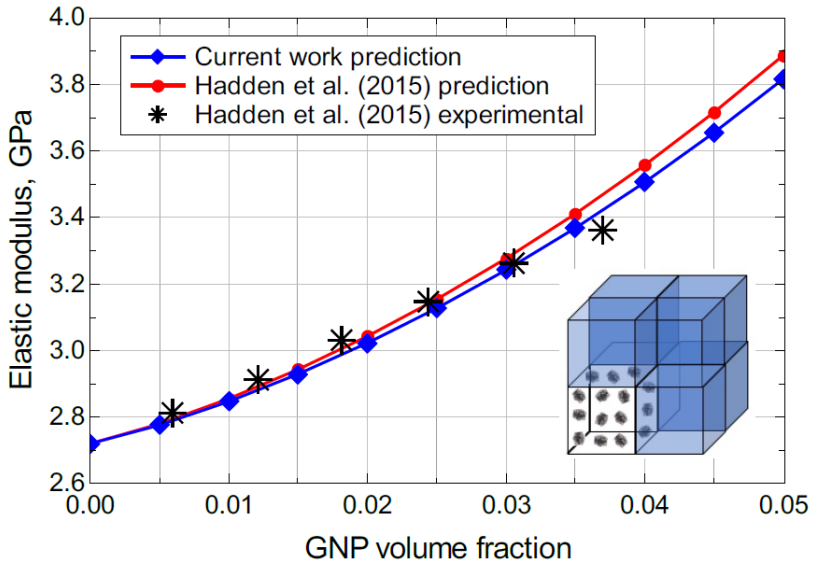

Figure 2.11: The elastic modulus of GNP/epoxy nanocomposite as a function of GNP volume fraction.

2.3.2 CF/GNP/Epoxy Hybrid Composite

The predicted properties of the GNP/epoxy nanocomposite were used as the matrix properties to generate a RUC of the CF/GNP/epoxy hybrid composite, as illustrated in Figures 2.10.d,e. Figure 2.12 shows a minor improvement in the axial elastic modulus of the hybrid composite with increases in $VF_{GNP/RUC}$. This is due to the domination of the carbon fibers on the axial modulus. However, a larger increase in the transverse elastic modulus of the hybrid composite is observed as the overall $VF_{GNP/RUC}$ increases, as shown in Figure 2.13. Generally, both the axial and the transverse elastic moduli predicted herein exhibit excellent agreement with the predictions from Hadden et al [46].

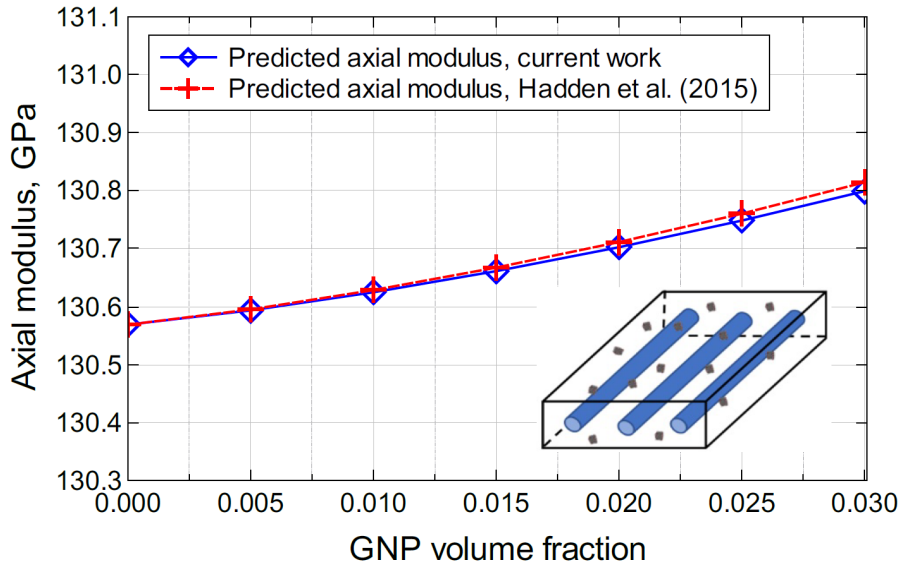

Figure 2.12: Predicted axial elastic modulus for the hybrid composite as a function of GNP volume fraction.

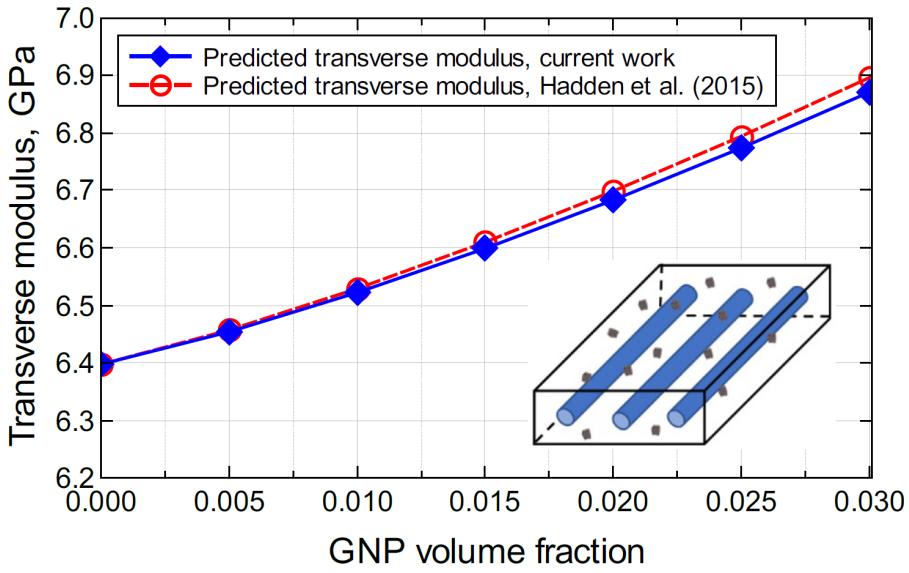

Figure 2.13: Predicted transverse elastic modulus for the hybrid composite as a function of GNP volume fraction.

Figure 2.14 shows a plot of the normalized axial and transverse moduli for the hybrid composite at different values of overall $VF_{GNP/RUC}$. Both normalized axial and transverse moduli predicted herein coincide with the computational results from Hadden et al. [46]. Even though the predicted axial modulus values fall beneath the mean values of the experimental results, they are still within the standard deviation. The predicted values indicate the insensitivity of the hybrid composite modulus to the GNP additives along the

axial direction due to the carbon fiber domination. However, the normalized transverse modulus exhibits greater sensitivity to the GNP content. The predicted transverse modulus is close to the experimental value at around 1% of the overall $VF_{GNP/RUC}$, however, it is slightly lower for the overall $VF_{GNP/RUC}$ above 1.5%.

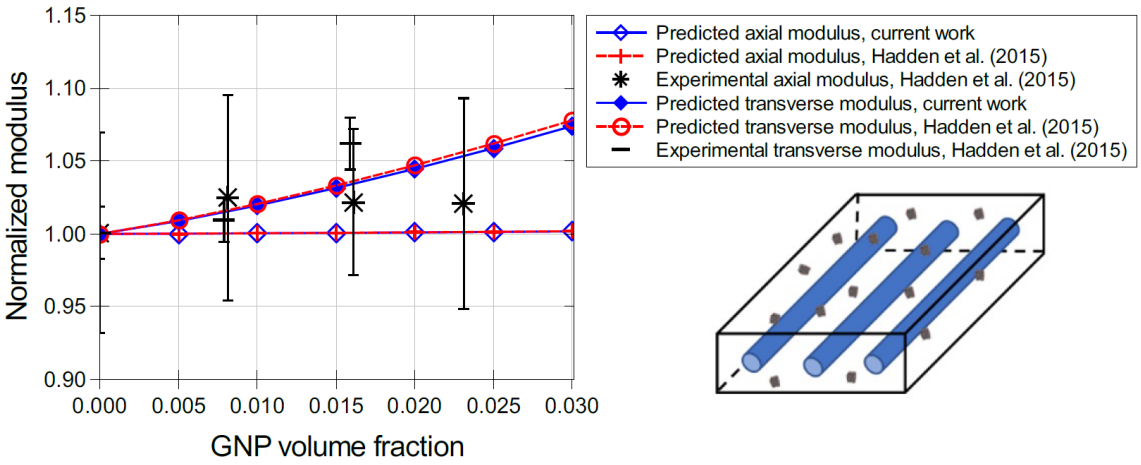

Figure 2.14: Normalized axial and transverse modulus for the hybrid composite as a function of GNP volume fraction.

2.4 Conclusions

This study has been mainly performed to address the potential for using ReaxFF with the Liu parameter set in MD modeling to predict the multiscale mechanical properties of GNP/epoxy nanocomposites and CF/GNP/epoxy hybrid composites. The results indicate that the predictions using ReaxFF agree with experiment. Also, it has been demonstrated that the GNP nanoparticle tends to attract the phenyl rings in the epoxy monomers, which results in alignment with the GNP surface due to noncovalent interaction. It has been demonstrated in this work that the agglomeration phenomenon of phenyl rings near the GNP surface can lead to an increase in the local mass density at the GNP/epoxy interface. Furthermore, the degree of noncovalent interaction decreases with increasing levels of crosslinking. Most importantly, it has been shown that MD modeling with a reactive force field (and an appropriate parameter set) can provide researchers with an accurate means to predict the mechanical behavior of hybrid and nanocomposite materials; and potentially be used in the future for predicting mechanical behavior under loading conditions that include large deformations and mechanical failure.

Chapter 3

THE INFLUENCE OF GNP SIZE AND SURFACE FUNCTIONALIZATION ON THE MECHANICAL PERFORMANCE OF THEIR COMPOSITES

This chapter proceeds to investigate the mechanical response of aerospace epoxy materials that are reinforced with different configurations of GNP. Particularly, the work in Chapter 3 focuses on studying the influence of GNP surface functionalization on the molecular structure and mechanical behavior of their nanocomposites using MD modeling with ReaxFF. As much as possible, realistic data of the chemical composition of the functional groups and their concentration are for the first time considered in this work to model the functionalized GNP nanoplatelets. Other paramount key processing parameters of such nanocomposites (namely the GNP dispersion, size, and content) are considered in the micromechanics analysis of the nanocomposite at the bulk level. A detailed description of the methodology used in modeling and predicting the mechanical properties of the nanocomposites is provided in this chapter. Results are compared with experiments to verify their validity and the performance of the multiscale modeling approach used in this study [67][1].

3.1 Introduction

GNP agglomeration, which is triggered by the noncovalent vdW forces and π-conjugation, is an undesirable phenomenon because it hinders GNP dispersion in polymer matrices [37, 68-71]. Poor GNP dispersion can significantly limit the reinforcing function of GNP by reducing the interfacial contact surface area and providing easy slip planes within the reinforcement [72]. To resolve the agglomeration problem, different methods of mixing and stirring techniques have been used in preparing polymer-based nanocomposites with the aid of adding liquid solvents and sonication to attain GNP dispersion. Also, the chemical modification of GNP surface (functionalization) has been widely used for improving the GNP dispersion and their adhesion with the polymer matrices [7, 37, 59].

Cha et al. [73] performed MD simulations to quantify the degree of dispersion of graphene nanosheets in ethylene glycol and water mediums. For pure graphene, there was a decrease in the degree of dispersion as the graphene content was increased. However, functionalized graphene additives maintained a higher degree of dispersion even for larger content within the hosting medium. That is, the presence of functional groups can effectively help to prevent the aggregation of graphene nanosheets within the hosting medium. In the same context, Karatasos and Kritikos [74] utilized MD simulations to characterize the molecular structure of graphene oxide (GO)/poly(acrylic acid)

[1] Part of the material contained in this chapter has been previously published in the proceedings of the American Society for Composites: Thirty-fourth Technical Conference, 2019. Lancaster, PA: DEStech Publications, Inc. See Appendix C.4 for copyright agreement.

nanocomposite at the melt state. The nanocomposite static and dynamic properties, hydrogen bonding (H-bonding) network formation, and its thermal behavior were characterized at a wide range of temperatures. The main findings in this study refer to a moderate increase in the glass transition temperature when adding the GO flakes to the polymer matrix. The GO flakes are found to form oligomeric clusters in addition to single GO nanosheets dispersed within the polymer matrix. The polymer chains mobility is governed by the intramolecular and intermolecular H-bonding network formation in the system which is highly affected by the presence of the GO flakes and temperature change. Interfacial hydrogen bonds formation is responsible for the adsorption of polymer chains onto the GO surface. This produces an improvement in the interfacial adhesion and polymer chains confinement within the GO clusters.

The method of Hummers (1958) [75] in preparing graphitic oxide has been widely used in the mass production of GNP in the form of graphene oxide (GO). In this method, the carbon-to-oxygen atomic ratio of the produced GO was reported to be within the range of 2.1-2.9. Introducing oxygen groups to the bulk material (graphite) increases the spacing distance (d-spacing) and weakens the stacking between graphene layers. Hence, it becomes easy to separate the layers from each other to produce a single to a few-stacked layer(s) of GO by either mild sonication in water or organic solvents. The GO layers can be subjected then to a series of post-processing or material treatment such as heating or chemical reduction stages to produce single layers of reduced graphene oxide (rGO) [76]. Attaching highly reactive chemical groups, in addition to the oxygen groups, onto the GO surface can be also performed to produce functionalized graphene oxide (FGO). Both oxygen and functional groups are found to attain better GNP dispersion and introduce covalent bonding with the hosting matrix. Adding a small amount of polymer functionalized graphene can substantially improve the mechanical, thermal, electrical, optical, and magnetic properties of the nanocomposite [71].

The mechanical performance of chemically modified GNP is highly dependent on the type, size, and amount of the chemical groups attached to the GNP surface. In the context of that, many research studies have claimed that improved engineering properties of polymer-based nanocomposites can be obtained when reinforced with certain types of functionalized GNP. Fang et al. [77] experimentally described a process of constructing functionalized GNP with a hierarchically-structured and long-chain of aromatic amines to improve the interphase in a high-performance tough and strong nanocomposites. The results revealed a convenient adjustment between load transfer and nanofillers mobility, which is governed by the introduced covalent links between the GNP and the epoxy matrix. In addition, reinforcing the epoxy matrix with 0.6 wt% of amine-functionalized GNP resulted in a substantial improvement in the mechanical properties of the nanocomposite as its Young's modulus increased by 95.6%, fracture toughness increased by 93.8%, and flexural strength increased by 91.5%. Su et al. [78] prepared aminated-reduced graphene oxide (NH_2-rGO) nanosheets using all aqueous self-assembly method. GO nanosheets were first treated with Diethylenetriamine (DETDA) and then integrated into poly(2-ethylhexyl acrylate) (P2EHA) to produce a highly stable colloid dispersion system of the nanocomposite. The produced functionalized graphene nanosheets exhibited a highly wrinkled structure. Also, there was an enhancement in the electrostatic interaction and improved adhesive property between the polymer matrix and the large functional aminated

groups. As a result, an improvement in the mechanical, thermal, and electrical properties of the nanocomposite was observed.

An important observation regarding functionalized GNP using ammonia radicals refers to the partial restoration of the conjugate structure by donating electron density to the distorted aromatic rings in the GO [79]. Xiao et al. [80] used a facile impregnation method to anchoring $H_3PW_{12}O_{40}$ on 3-aminopropyltriethoxysilane modified graphene oxide (GO-NH_2) which enhanced methyl orange (MO) absorption capacity onto the hybrid PW_{12}/GO-NH_2 nanoplatelets. The enhanced interaction between MO and the hybrid nanoplatelets was attributed to the electrostatic attraction and the hydrogen-bonding. In their article, during graphite oxidation process to produce GO and then functionalization of GO with NH_2 to produce NH_2-rGO, Navaee et al. [81] reported that the d-spacing was increased from 3.34 Å for graphite to 8.3 Å for GO and to 11.0 Å for NH_2-rGO. This has been attributed to the presence of oxygen and amine groups in addition to the trapped water molecules between the GNP layers. Furthermore, they found that NH_2-rGO has higher conductivity and more dispersibility than GO. Naebe et al. [82] performed an experimental study to prepare epoxy (EPON862)-based nanocomposites reinforced with thermally-rGO and with functionalized-rGO using organic carboxylic (-COOH) groups. The nanoscale surface roughness of the functionalized-rGO along with the attached organic (reactive) radicals provided a mechanical interlocking and interfacial covalent bonding which constrained polymer chains mobility. Furthermore, a uniform dispersion with a distinct interphase zone surrounding the functionalized-rGO nanoparticles was observed within the epoxy matrix. The reported results show that adding 0.1 wt% of the functionalized-rGO to the neat epoxy performs better than the thermally-rGO where the flexural strength increased by 22% versus 15% and the storage modulus increased by 18% versus 10%, respectively. Park et al. [83] reported a detailed experimental study to measure the influence of adding ammonia-treated GO on the mechanical properties of epoxy (EPON828)-based nanocomposite. Three different amounts of ammonia solution concentrations (14, 21, and 28%) were used in the treatment process. The prepared reinforcement particles were chemically analyzed using Raman spectroscopy and X-ray photoelectron spectroscopy (XPS). While the surface element analysis revealed the elemental contents for C, O, and N in atomic percent (at%), the XPS spectra provided information about functional groups (C-N-C, CONH, C-NH_2) formed by ammonia treatment. The Raman spectra for the structural integrity of GO and aminated-GO was also reported according to the measured D-band to G-band (I_D/I_G) peak ratio which indicates a slight increase in the aminated-GO particles. The reported mechanical properties of the prepared nanocomposite samples indicate a remarkable improvement in the mechanical response for aminated-GO/epoxy and GO/epoxy samples over neat epoxy. While the tensile strength indicates an increase of 59.4% for GO/epoxy, it indicates the best improvement by 120.4% for the 28% aminated-GO/epoxy. However, the tensile strain indicates a decrease by 10% for GO/epoxy over neat epoxy, while it indicates the best improvement by 15% for the 28% aminated-GO/epoxy. The tensile modulus indicates an increase of 70% for GO/epoxy over neat epoxy, while it indicates the best improvement by 100% for the 21% aminated-GO/epoxy over neat epoxy.

Despite that the overall mechanical performance of polymer matrices can be improved by adding surface-functionalized GNP, the functionalized GNP itself can exhibit weaker

structural performance. Pei et al. [84] performed MD simulations to investigate the effect of hydrogen content (H-coverage) on the mechanical properties of hydrogen functionalized graphene. The MD simulations indicate a dramatic deterioration in the mechanical properties of the graphene nanosheet as the H-coverage was increased up to a saturation value of ~30%, beyond which a stable mechanical response was predicted. The larger degradation was predicted in the tensile strength and fracture strain with a maximum drop of ~65%. However, ~30% maximum degradation in Young's modulus was predicted at the 30% of H-coverage. This dramatic drop in the mechanical properties was mainly attributed to the weak bonding structure of hydrogen functionalized graphene nanosheet. In other words, the chemical modification of graphene resulted in a local alteration of its strong sp^2 bonding structure into a weaker sp^3 bonding structure.

Among the several key processing parameters that can influence the mechanical response of polymer-based nanocomposites, Chong et al. [85] considered the nanofiller size and effective aspect ratio in their study. The use of different GNP configurations along with two different solvent agents in preparing the nanocomposites resulted in composite samples having a relatively wide range of GNP aspect ratio. The results referred to a general observation that GNPs with large aspect ratio exhibit better mechanical response, specifically, higher modulus and strain energy release rate during the fracture process. However, low fracture performance was observed for GNPs with sharp edges, even with a high aspect ratio. For samples with agglomerated nanofillers, there was a reduction in the effective aspect ratio of the GNPs due to the formation of graphene particulates. As a result, there was a reduction in the interfacial surface contact area and the stress transfer to the GNPs, which limited their stiffening effect. The fabrication of multifunctional polymer-based nanocomposites with engineered properties is a challenging task [86]. The excessive mixing process used to obtain a well-dispersed nanofillers in the polymer matrix can greatly reduce the size and the effective aspect ratio of nanofillers as they can be chopped by the stirring blades. On the other hand, inefficient mixing techniques can lead to agglomeration in the nanofiller additives which is another source of reducing the effective aspect ratio of the reinforcements and many other undesirable issues. According to the experimental observations of Karevan et al. [86], the aspect ratio of exfoliated graphite nanoplatelets (xGnP^{TM}) was decreased from 50 (as received xGnP) to 20 after incorporating xGnP in polypropylene (PP). Similarly, the aspect ratio for CNTs was also decreased from 800 to 200.

Using MD modeling and micromechanics analysis, Chinkanjanarot et al. [57] studied the effect of GNP content, dispersion, functionalization, and aspect ratio on the thermal conductivity of cycloaliphatic epoxy (CE) matrix. The increase in GNP aspect ratio was found to positively affect the thermal conductivity of GNP/CE composite. Specifically, at 4.0 wt% of single-layer GNP content, increasing the GNP aspect ratio from 50 to 1000 resulted in a 2.66-fold increment in the nanocomposite thermal conductivity relative to the pure CE matrix. A similar trend was observed for improving the transverse (and slightly the axial) thermal conductivity of CF/GNP/CE hybrid composite with increasing the GNP aspect ratio. In part of their work (micromechanics analysis), Radue and Odegard [9] studied the effect of CNT aspect ratio on the mechanical properties of epoxy-based nanocomposites. A general observation refers to an improvement in the reinforcing effect with increasing the CNT aspect ratio up to 10,000, at which a close effect of using infinitely

long CNT was observed. At 5.0 wt% of CNT perfectly dispersed in epoxy matrix, an improvement of about 12% in Young's modulus was observed as the aspect ratio increased from 100 to infinity.

The assortment of GNPs according to the attached functional groups in addition to their effective aspect ratio opens the door for more key processing parameters which can be used to tailoring the engineering properties of polymer-based composites. Consequently, additional effort is required to optimize the overall structural behavior of such composite materials. It is believed that computational tools, along with experiments, can play a paramount role in developing and optimizing the properties of these composite materials. Looking at the literature, previous computational studies have not comprehensively investigated the effect of functionalization and GNP aspect ratio on bulk mechanical properties of epoxy-based nanocomposites. Considering that, the aim of this study is to develop a computational approach to model functionalized GNP/epoxy nanocomposites. Three different forms of GNP are considered: pristine (GNP), highly concentrated graphene oxide (GO), and functionalized graphene oxide (FGO). The adopted approach involves a multiscale analysis to predict bulk-level mechanical properties of the nanocomposites. For the nanoscale level, MD modeling has been used to study the topology of the nanoplatelets before and after functionalization. It has also been used to generate the nanocomposite unit cells and characterize the interphase region between GNP/GO/FGO and epoxy. The mass density profile has been determined at the interphase region in addition to predicting the effective mechanical properties for the three proposed nanocomposites at the nanoscale level. For the microscale analysis, the influence of the nanoplatelet functionality, aspect ratio, and its content on the mechanical properties of the nanocomposites at the bulk level has been established. The predicted mechanical properties were compared with experimental data available from the literature to verify the validity of the computational approach used in this work.

3.2 Molecular Dynamics Modeling

For the nanoscale computational work, the MD modeling procedure adopted in this study is based on the previous modeling scheme used in Chapter 2. Additional modeling details used to establish and characterize the functionalized GNP and their interphase with the hosting matrix are described in this chapter.

3.2.1 Nanocomposite Constituents

Three unique nanocomposites were considered in this study to address the functionalization effect on the mechanical properties of the material. Simulated epoxy unit cells reinforced with GNP, GO, and FGO were created using LAMMPS. The size of each MD model was carefully assigned to capture the properties of nanoplatelet-epoxy interphase region and avoid the epoxy bulk effect [46]. Five MD replicates for each nanocomposite sample were created to explore the possible variation in the obtained mechanical properties from each case-study.

3.2.1.1 Epoxy monomers

The epoxy system EPON 828 (diglycidyl ether of bisphenol A, DGEBA) and the hardener EPIKURE curing Agent W (diethyltoluenediamine, DETDA) were modeled in this study. One EPON 828 molecule (49 atoms) and one DETDA molecule (31 atoms) were individually created (Figure 3.1) via the ChemDraw Professional software package, version: 15.0.0.106, PerkinElmer Informatics, Inc. The molecular structure was initially established using the OPLS-All Atom (OPLS-AA) force field [24] with a stoichiometric mixture ratio of two DGEBA molecules to one DETDA molecule. A single unit of the stoichiometric mixture (2:1) was simulated in a periodic MD box totaling 129 atoms. The mixture was then replicated 48 times to form a larger system comprising 144 monomers (96:48) with 6192 atoms.

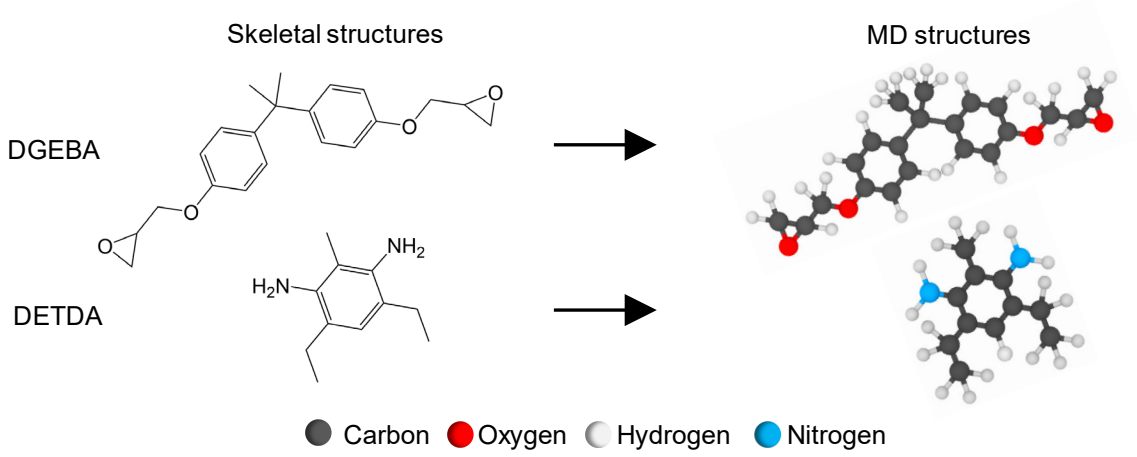

Figure 3.1: Molecular structures of epoxy monomers (EPON 828/DETDA).

3.2.1.2 Graphene nanoplatelets (GNP/GO/FGO)

The "lattice" command was used in a LAMMPS script to create a single layer of GNP. The lattice parameters for the hexagonal atomic structure of a pristine nanoplatelet of graphene were taken from Gray et al. [58]. A square-GNP-layer was created which includes 836 carbon atoms with lateral dimensions of ~47.5 Å along the *x*-axis and ~47.7 Å along *y*-axis, as shown in Figure 3.2.a. For the GO and FGO nanoplatelets, the functional groups were randomly attached (crosslinked) to the top and bottom surfaces of the GNP layer. The chemical composition and quantitative atomic data for GO and aminated GO or A21-GO (which is referred to as FGO herein) were taken from the surface element analysis results of X-ray photoelectron spectroscopy (XPS) performed by Park et al. [83]. Note that the A21-GO represents GO nanoplatelets treated with ammonia solution of 21% concentration as reported by Park et al. Table 3.1 includes the elemental contents (at%) from which the GNP and functional groups atomic data were derived and used to model GO and FGO nanoplatelets which are shown in Figures 3.2.b,c.

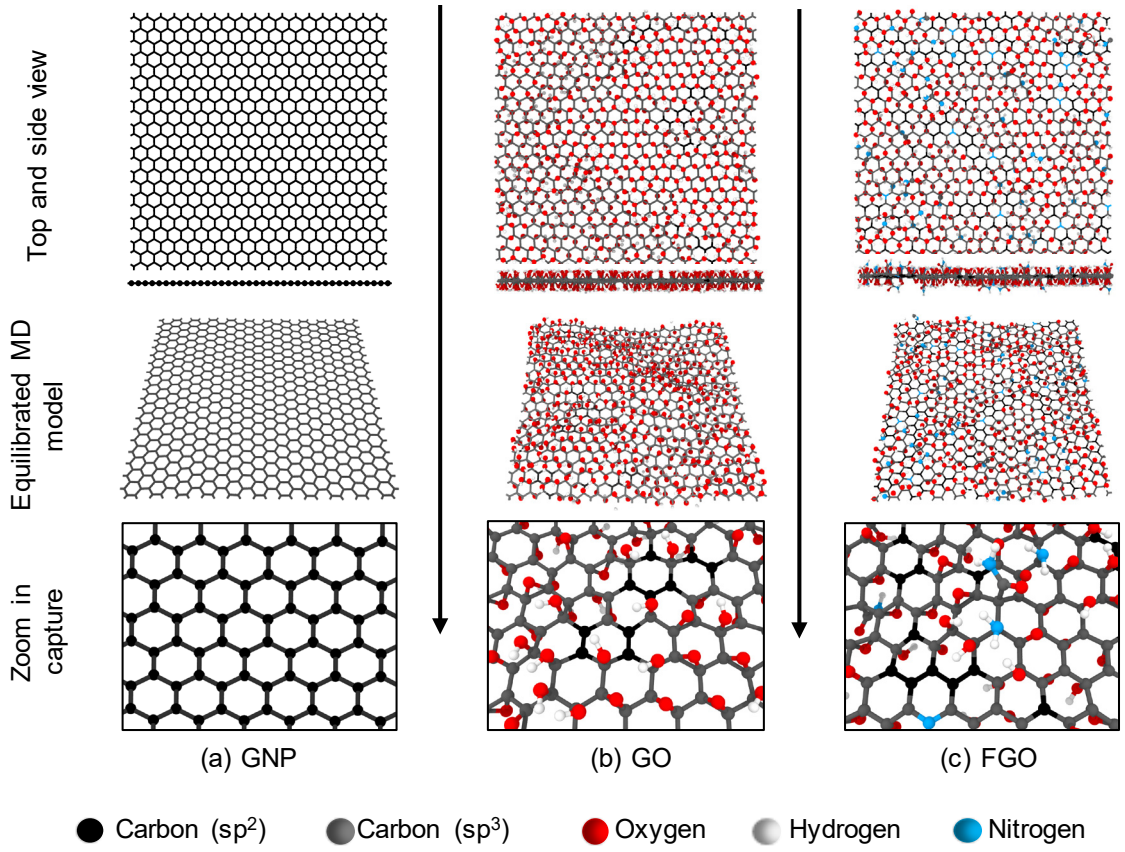

Figure 3.2: Representative MD models of GNP, GO, and FGO nanoplatelets.

Table 3.1: Elemental content (at%) and atomic data used to model GNP, GO, and FGO nanoplatelets.

Nanoplatelet			GNP	GO	FGO
Elemental contents (at%) [83]	core level spectra, Cls		---	60.65	63.98
	core level spectra, Ols		---	39.35	31.67
	core level spectra, Nls		---	---	4.35
Number of atoms used in MD modeling	C atoms in the GNP lattice		836	836	825
	Oxygen groups content	Epoxide: -O-	---	271×1	207×1
		Hydroxyl: -OH	---	271×2	207×2
	Nitrogen groups content	Amine: -NH_2	---	---	34×3
		Amide: -(O=C-NH_2)	---	---	12×5
		Graphitic Nitrogen: -N-	---	---	11×1
	Total number of atoms		836	1649	1619
	sp^3/sp^2 ratio for the GNP lattice		---	0.973	0.798
	C:O ratio in the nanoplatelet		---	1.542	1.936

The MD model of GO shown in Figure 3.2.b was created according to the data presented in Table 3.1 and based on Lerf-Klinowski GO model [87]. The core level spectra of the oxygen content (Ols = 39.35 at%, Table 3.1) was assumed to be existed as 50% of epoxide (-O-) and 50% of hydroxyl (-OH) functional groups, as there is no detailed information about the chemical composition of the oxygens in the reported data. It is important to note that each oxygen group has a different effect on the GNP structure, as each epoxide oxygen atom forms two covalent bonds with two carbon atoms in the GNP, while the hydroxyl oxygen atom forms only one covalent bond with GNP. This means that epoxide groups have a greater detrimental effect on the robust sp^2 structure of the GNP by turning it into a weak sp^3 structure. In other words, the sp^3/sp^2 carbons ratio in the GNP oxidized with a specific amount of epoxide groups is double of that if the oxygens were presented in the hydroxyl form. The variation in functional group types that can exist on the GNP surface is generally classified based on their chemical composition, size, and molecular configuration. This variation can produce different levels of interfacial interaction of the functionalized GNP with the hosting polymer matrix [88, 89].

For the FGO MD model shown in Figure 3.2.c, the core level spectra of the oxygen content (Ols = 31.67 at%, Table 3.1) was assumed to exist as 50% of epoxide (-O-) and 50% of hydroxyl (-OH) functional groups. The core level spectra of the nitrogen content (Nls = 4.35 at%, Table 3.1) was divided into; 59.1% of amine groups ($-NH_2$), 20.8% of amide groups ($O=C-NH_2$), and 20.1% of graphitic nitrogen (-N-). These values were taken from the curve fitting of the Nls spectra of aminated A21-GO performed by Park et al. [83]. For modeling simplicity, all the nitrogen content in the form (-N-) were assumed to exist as graphitic nitrogen which does not damage the hexagonal carbon rings in the GNP. The nitrogen doping process involved taking out 11 carbon atoms from the GNP lattice and replacing them with 11 nitrogen atoms. Both Pyrrolic-N and Pyridinic-N, as the other types of nitrogen-doped graphene, are found to cause structural defects (voids) in the graphene lattice. While Pyrrolic-N's are found to exist within pentagon rings in the graphene lattice [90], Pyrazole-N's are found to exist at the edges of the graphene lattice [91].

All the GNP nanoplatelets were simulated with continuous lateral edges (periodic boundary conditions) and free of defect graphene lattice. Thus, the presence of carboxyl and carbonyl as functional groups in GO and FGO was ignored because they are more likely to exist with low concentrations at the edges and defected regions (open rings or voids) in the GNP lattice [16, 37]. Nevertheless, the chemical concentrations of these functional groups were not reported in the experimental work from Park et al. [83]. Five MD replicates for each nanoplatelet of the GNP, GO, and FGO were simulated to account for the possible variation in the predicted properties. Each MD replicate of the GO and FGO had a unique random distribution of the attached functional groups. However, chemical concentration and content for functional groups were preserved for all GO and FGO MD replicates.

Both GO and FGO MD models shown in Figures 3.2.b,c exhibit a degree of wrinkling. This structural feature is mainly attributed to presence of the oxygen and functional groups on the GNP surface [38, 78]. Introducing oxygen/functional groups to the planar/unwrinkled structure of the graphene sheet can greatly disrupt its robust sp^2 structure. Functionalization degree can be used to specify the sp^3/sp^2 ratio, which is a

measure of the GNP purity (chemical integrity) and its structure robustness. Note that the lower the sp^3/sp^2 ratio, the more pristine and planar GNP can be obtained.

To determine the functionalization effect on the GNP structural integrity, one sample of the three nanoplatelet types was subjected to a simulated uniaxial tensile simulation. Figure 3.3 shows a representative stress-strain response of GNP, GO, and FGO. Clearly, GNP exhibits the best mechanical response with a predicted elastic modulus of 1,264 GPa. Both FGO and GO exhibit a weaker mechanical response with predicted elastic moduli of 386 and 119 GPa, respectively. Consequently, the nanoplatelets' stiffness can be arranged according to their elastic moduli in the order: GNP≫FGO>GO. That is, the lower the sp^3/sp^2 ratio, the stiffer the GNP can be obtained.

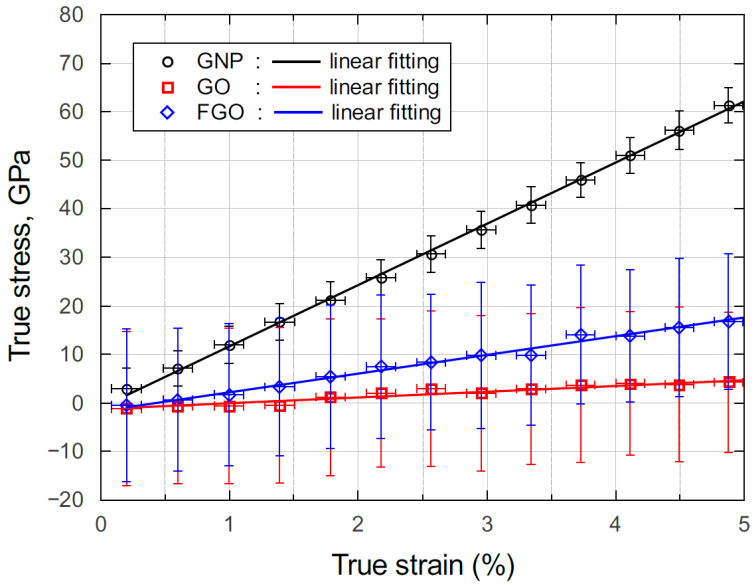

Figure 3.3: Representative uniaxial stress-strain response for GNP, GO, and FGO nanoplatelets.

3.2.2 Nanoplatelets Dispersion

The following MD simulations were performed in order to understand how the functional groups can help in improving the GNP dispersion. Three MD samples were modeled where each sample consists of five unique layers of GNP, GO, and FGO stacked together, respectively. Figure 3.4 shows the equilibrated MD models using ReaxFF with the size of the simulation box measures:

(a) for the 5-layer-GNP MD model; $(47.7)_x$ Å × $(47.8)_y$ Å × $(16.5)_z$ Å
(b) for the 5-layer-GO MD model; $(42.0)_x$ Å × $(42.5)_y$ Å × $(54.3)_z$ Å
(c) for the 5-layer-FGO MD model; $(42.2)_x$ Å × $(41.1)_y$ Å × $(57.0)_z$ Å

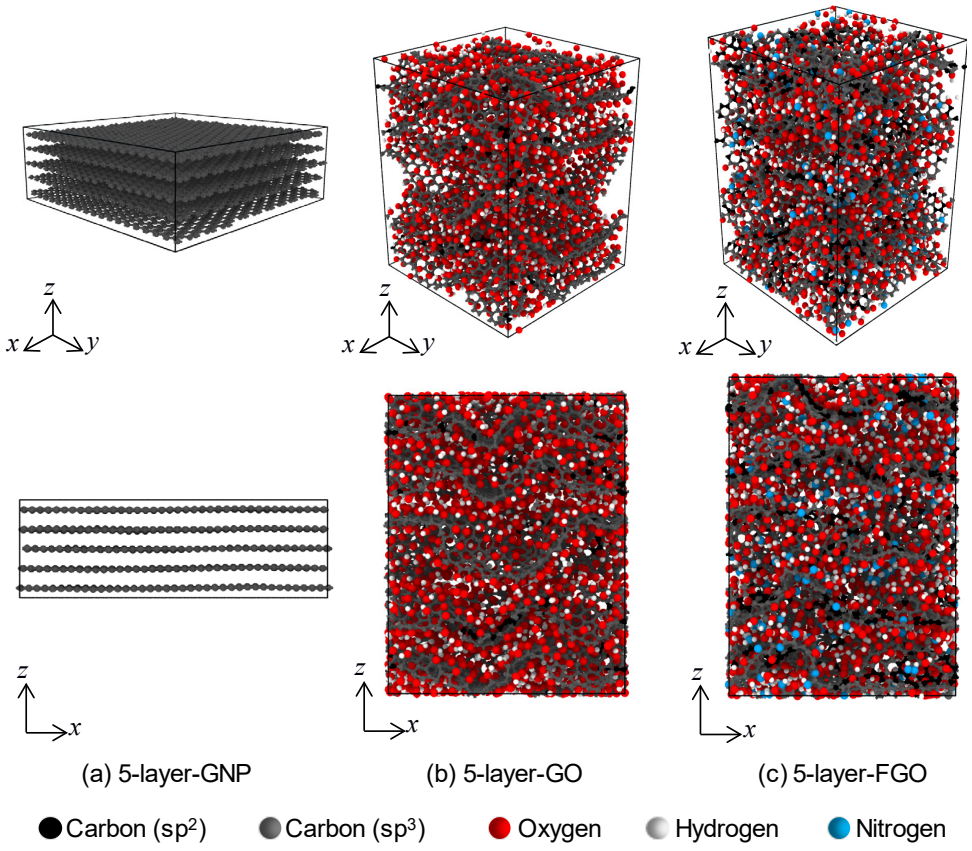

Figure 3.4: Equilibrated MD models of GNP, GO, and FGO 5-stacked nanoplatelets.

Clearly, introducing the oxygen and functional groups to the bulk GNP resulted in an increase in the overall simulation box volume by 157.6% and 162.8% for GO and FGO, respectively. This volume increment is totally attributed to the increase in the size along the z-axis which surpasses the reduction in the lateral size caused by the waviness in GO and FGO nanoplatelets.

Table 3.2 includes the predicted distance between individual platelets (d-spacing) compared with experimental observation values available from the literature. The predicted d-spacing was calculated using two approaches: first, by roughly dividing the MD simulation box length along the z-axis (l_z) by the number of the nanoplatelets (5 layers); and second, by obtaining the mean value of the measured distance between the center of mass for every two neighboring nanoplatelets. Generally, the predicted d-spacing values between GNP, GO, and FGO stacked nanoplatelets using both approaches indicate a good agreement with the experimental observations. The slight discrepancy in the predicted d-spacing for GO and FGO stacked nanoplatelets with the experimental observation values can be attributed to the amount of the oxygen and the other functional groups presented in each case. It has been reported that the d-spacing in graphite oxide increases as the humidity level increases, which results in various d-spacing values ranging from 6 to 12 Å between the carbon nanoplatelets [92].

Table 3.2: The distance between stacked platelets (d-spacing) in GNP, GO, and FGO.

d-spacing in (Å)			Reference
GNP	GO	FGO	
3.30	10.86	11.4	MD prediction using box size approach
3.31	9.50	9.56	MD prediction using center of mass approach
3.40	8.59	7.69	Experimental, by Park et al. (2017) [83]
3.40	---	8.20	Experimental, by Xiao et al. (2015) [80]
3.34	8.30	11.0	Experimental, by Navaee & Salimi (2015) [81]
---	6-12	---	Experimental, by Buchsteiner et al. (2006) [92]

The interaction energy between the stacked nanoplatelets was also investigated for the three MD samples. The interlayer interaction energy for each layer with the other four layers in the same sample was calculated by subtracting the isolated potential energy of the selected four layers from the overall potential energy including the fifth layer. Then, a mean value of the interlayer interaction energy was averaged over the five layers in each sample. It is important to note that the higher the negative value of the interlayer interaction energy, the stronger the attraction between the nanoplatelets. Figure 3.5 shows the level of the interlayer interaction energy for 1-layer with other 4-layers in the 5-layer-GNP, 5-layer-GO, and 5-layer-FGO MD samples. Clearly, the interlayer interaction energy decreases with introducing the oxygen groups the GNP by ~15%. However, replacing some of the oxygen groups with amine and amide functional groups restores ~7.5% out of the 15% loss in the interlayer interaction energy. This can be attributed to the change in the pi-stacking effect between GNP layers which depends on the sp^2 structure integrity (sp^3/sp^2 ratio), refer to Table 3.1. In addition, the variation in potential energy terms such as vdW, Coulomb, and charge equilibration energies produces different levels of interlayer interaction energy depending on the chemical composition of the stacked nanoplatelets.

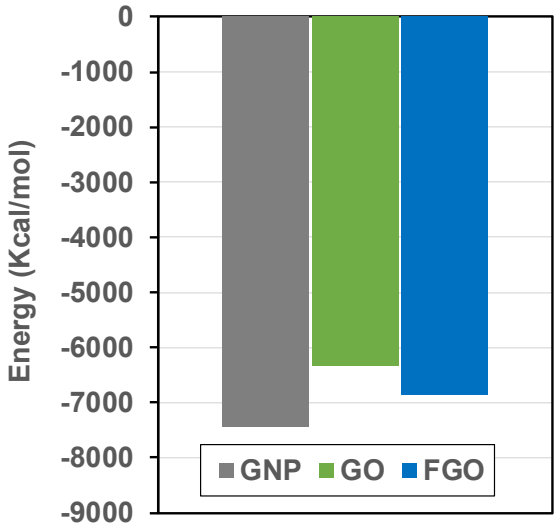

Figure 3.5: The interlayer interaction energy for the 5-layer-GNP, 5-layer-GO, and 5-layer-FGO MD samples.

Consequently, the increase in the d-spacing value with the relatively low interlayer interaction energy are two factors which can facilitate the separation between GO and FGO layers using mild sonication in water or organic solvent mediums. Practically, the process of preparing nanocomposites involves two essential actions: first, the mixing of the filler nanoplatelets with the polymer resin under the stirring action; and second, the constituents' interaction which involves the formation of covalent bonds between functional groups and the polymer resin. These two factors can effectively prevent or alleviate the agglomeration effect between the nanoplatelets. Thus, GO and FGO nanoplatelets can provide better dispersion levels in polymer matrices in comparison to GNP.

3.2.3 Nanocomposite MD Models

Independent MD data files of unpolymerized epoxy monomers were combined with GNP, GO, and FGO MD data files to form MD unit cells of the nanocomposites. As five unique MD replicates of each nanoplatelet were already created, five MD replicates of GNP/, GO/, and FGO/epoxy nanocomposite unit cells were consequently created. Note that each MD replicate had its unique MD simulation settings to maintain independent replicates of each nanocomposite. All MD models were subjected to slow densifying (size reduction) simulation steps for 2.5 ns along the normal axis to the plane of the nanoplatelets to densify the epoxy monomers to the bulk level density (~1.2 g/cm^3). To maintain a thermodynamically equilibrated molecular structure, the systems were subjected to 1 ns of MD simulation with the NVT (constant number of atoms, volume, and temperature) ensemble followed by a molecular minimization at every 1 fs of time step. The simulations involved the use of the Nose/Hoover thermostat with a temperature ramped down from 600 to 300 K. For the three nanocomposite types, the considered amount of the epoxy system (6192 atoms) was selected to be adequate to capture the interphase region (~10 Å) measured from the nanoplatelet surface.

The epoxy monomers in the nanocomposite MD models were subjected to a crosslinking simulation which was performed based on the approach presented in Chapter 2. The polymerization process of epoxy monomers in all MD models was stabilized at a saturation degree of ~80% out of the overall possible crosslinking density. For the FGO/epoxy MD models, the crosslinking process was first randomly performed between the epoxide reactive radicals in the DGEBA monomers and the amine/amide functional groups in the FGO nanoplatelet. The first step of the crosslinking simulation was stabilized at a saturation degree of ~20% out of the overall possible crosslinking density. The next step of the crosslinking simulation was performed for the epoxy monomers which was stabilized at a saturation degree of ~60% out of the overall possible crosslinking density.

Once the crosslinking simulations were completed, all MD models were equilibrated for 1 ns with 1 fs time steps. The equilibration simulations were performed using the NPT (constant number of atoms, pressure, and temperature) ensemble at 300 K with the Nose/Hoover anisotropic barostat to minimize residual stresses produced due the crosslinking process and to stabilize the molecular structure. Transition simulations from OPLS to a reactive force field (ReaxFF) with the parameterization of Liu et al. [26] were performed for the equilibrated MD models. This reactive force field has shown its validity

and potential in simulating epoxy systems and their nanocomposites [9, 10, 23]. The MD models were then equilibrated in ReaxFF for 1 ns using 0.1 fs time steps. The equilibration simulations involved the use of NPT ensemble at 300 K with the anisotropic Nose/Hoover barostat, followed by a molecular minimization at every 0.1 fs time step. It is important to note that all the nanoscale analysis and predictions were performed on the well equilibrated MD models with ReaxFF.

Figure 3.6 shows representative MD models of GNP/, GO/, and FGO/epoxy nanocomposites with the molecular mass density distribution along the z-axis for each nanocomposite. The total number of atoms and overall molecular mass density for each MD model are given in Table 3.3. The simulation box size for each nanocomposite averaged over its five MD replicates is:

(a) for the GNP/epoxy MD model; $(47.55\pm0.03)_x$ Å×$(47.67\pm0.04)_y$ Å×$(29.68\pm0.30)_z$ Å
(b) for the GO/epoxy MD model; $(42.38\pm1.97)_x$ Å×$(43.41\pm0.83)_y$ Å×$(38.42\pm2.35)_z$ Å
(c) for the FGO/epoxy MD model; $(43.39\pm1.16)_x$ Å×$(42.42\pm0.83)_y$ Å×$(38.51\pm1.16)_z$ Å

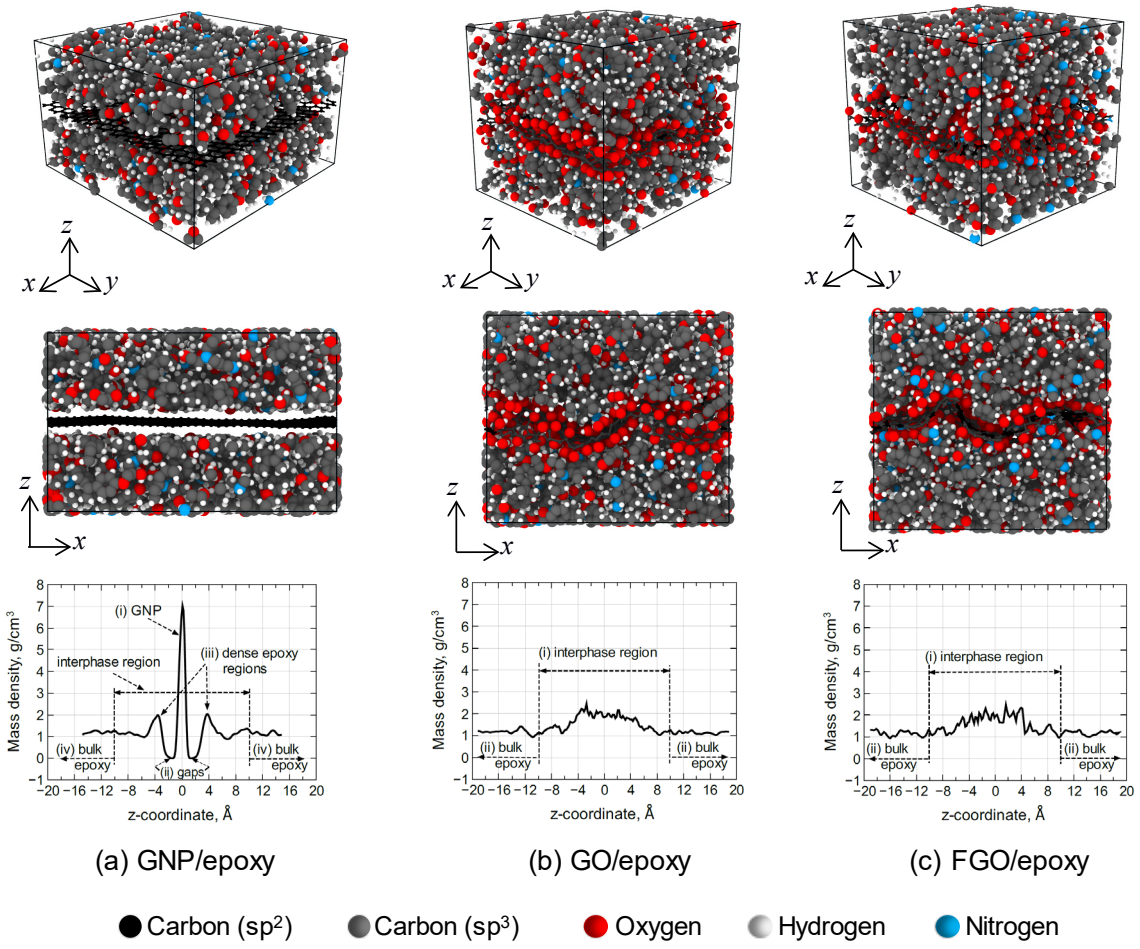

Figure 3.6: Representative MD models of the nanocomposites with their mass density distribution along z-coordinate.

Table 3.3: Details of the nanocomposite MD models.

MD model	GNP/epoxy	GO/epoxy	FGO/epoxy
Total number of atoms	7028	7841	7811
Mass density (ρ_{MD}), g/cm^3	1.27±0.01	1.42±0.01	1.38±0.01
Nanoplatelet content (wt%)	19.58±0.00	31.53±0.00	29.52±0.00
Nanoplatelet content (vol%)	11.36±0.09	19.16±0.24	18.15±0.17

It is noteworthy to mention that the lateral size of the simulation box is governed by the lateral size of the nanoplatelets. The wrinkled topology of GO and FGO nanoplatelets resulted in a decrease in the lateral dimensions of their composite simulation boxes in comparison to the flat GNP/epoxy composite.

The mass density distribution of the GNP/epoxy MD model exhibits a smooth profile reflected about z=0. There are four distinct regions that can be recognized from the mass density profile of the GNP/epoxy MD model: (i) the large spike at the center, which represents the molecular mass density of the flat GNP, (ii) the gap region between the GNP and epoxy which is caused by the repulsive portion of the vdW forces exerted by the GNP atoms on epoxy [9], (iii) the small spike next to the gap which represents a dense epoxy region (~2 g/cm^3 at 4 Å from the GNP) adjacent and highly affected by the GNP followed by a density drop to ~1 g/cm^3 and a gradual rise to the bulk density at ~10 Å from the center (it has been reported previously in Chapter 2 that most of the phenyl rings in the epoxy network were observed to be aligned with GNP surface at this region), and lastly (iv) the bulk epoxy region (~1.2 g/cm^3) in which the interfacial interaction between GNP and epoxy diminishes with distance from the GNP. On the other hand, both GO/epoxy and FGO/epoxy nanocomposite models exhibit a similar trend in their molecular mass density profiles. Two distinct regions can be recognized from their molecular mass density profiles: (i) the interphase region which includes the nanoplatelet (GO or FGO) and the adjacent highly interacted epoxy region with a density of ~2 g/cm^3 along z (-4:4) Å, which decreases with distance to the bulk density at ~10 Å from center, and (ii) the bulk epoxy region (~1.2 g/cm^3) in which the interfacial interaction between the nanoplatelet and epoxy diminishes with distance away from GO or FGO nanoplatelet.

According to the density profile of the MD models shown in Figure 3.6, it can be inferred that both the GO and FGO provide better adhesion with the epoxy matrix, as no gaps were observed at the interfacial region. In addition, the wrinkling and surface roughness in the GO and FGO are valuable to improve the interlocking mechanism with the epoxy matrix. The nanoplatelets content in wt% and vol% averaged over the five MD replicates of the proposed nanocomposite MD models are included in Table 3.3. As the elemental content (at%) of each nanocomposite sample was unchanged over the five MD replicates, the nanoplatelet wt% remained constant over the replicates. However, the different distribution of the oxygen and functional groups in addition to the unique MD simulation settings for each model resulted in a slight variation in the nanoplatelet vol% over the MD replicates. Note the volume fraction of each nanoplatelet (vol%) was calculated using the 3D Voronoi tessellation method which will be discussed later in this chapter.

3.2.4 Waviness Factor (WF)

In most experimental observations of GNP/polymer nanocomposites, GNPs exhibit a wrinkled or wavy morphology within polymer matrices. The GNPs morphology is governed by several factors. The production of GNPs in the form of a few layers of graphene nanosheets stacked together with a relatively large aspect ratio can exhibit a large amount of waviness. The low bending stiffness of the GNPs is another factor to induce its curled morphology. The integrity of the planar sp^2 structure of the GNPs can also be affected by the presence of vacancies, defects, and functional groups, which can promote the waviness degree [38, 93]. It has been reported that wrinkled GNP surface can provide better interlocking mechanism and strong interfacial interaction with the hosting matrix [41, 94]. Therefore, studying the GNPs morphology is of a great importance as it has been found to improve the mechanical properties of polymer-based nanocomposites.

The waviness (wrinkling) factor (WF) in GNP has been defined as the ratio of direct distance between the two ends of a wrinkled GNP (wrinkled length, L^w) to the original (actual) length of the unwrinkled GNP (actual length, L^a) [93]. In light of that, the WF of the graphene nanoplatelets within the epoxy matrix for all MD models simulated in this work were calculated. It is important to note that the original length of the GNP was considered to be as lateral length (47.60 Å along *x*-axis, and 47.65 Å along *y*-axis) of an equilibrated planar GNP morphology using ReaxFF. Table 3.4 includes the waviness factors along the *x*-axis (WF_x) and *y*-axis (WF_y) calculated for the graphene nanoplatelets in all replicates of GO/epoxy and FGO/epoxy MD models. The overall WF is calculated as the mean value of the averaged values over WF_x and WF_y. Noteworthy to mention that all GNPs exhibit an overall WF of ~1 which indicates the flat GNP morphology in the GNP/epoxy MD models, refer to Figure 3.6.a. However, both GO and FGO exhibit an overall WF of (~0.9) which indicates ~10% reduction in the lateral dimensions caused by the wrinkled morphology of the nanoplatelets, refer to Figures 3.6.b,c.

Table 3.4: Waviness factor of the nanoplatelets

Nanocomposite MD model	**Waviness Factor (WF)= L^w/L^a**			
	GO/epoxy		**FGO/epoxy**	
	WF_x	**WF_y**	**WF_x**	**WF_y**
Model_01	0.875	0.880	0.956	0.915
Model_02	0.954	0.913	0.902	0.874
Model_03	0.889	0.918	0.884	0.911
Model_04	0.896	0.900	0.918	0.874
Model_05	0.872	0.934	0.903	0.906
Average	0.897	0.909	0.912	0.896
Overall WF	0.903		0.904	

3.2.5 Weight and Volume Fraction of the Nanoplatelets

Practically, the properties of nanocomposites are evaluated based on the nanofiller content used to reinforce the polymer matrix. The nanofiller content can be represented by either its weight percentage (wt%) or its volume percentage (vol%) relative to the overall weight or volume of the nanocomposite, respectively. The vol% can also be referred to as the volume fraction (VF). The design criterion of nanocomposites stands on how much the material properties are improved with the lowest amount of the reinforcing nanofiller material. However, an excessive amount of the nanofiller material can produce a detrimental effect on the nanocomposite such as increasing its weight and viscosity. In addition, the reinforcing purpose can be highly restricted by the agglomeration tendency especially with large amounts of nanofillers. Thus, it is necessary to consider that when investigating the engineering properties of the nanocomposites.

In this work, both wt% and vol% were evaluated for the GNP, GO, and FGO nanoplatelets within their nanocomposite MD models. For the wt% evaluation, a simple LAMMPS script was performed on each MD model to obtain the ratio of the partial molecular weight of the nanoplatelet to the overall molecular weight of the nanocomposite MD model. The "group" command in LAMMPS was utilized to specify the atom types which are used to determine the partial weight for each nanoplatelet. For the vol% evaluation, the process is relatively complicated because of the overlapped volume between atoms, in addition to the possibility of voids presence in the nanocomposite molecular network. An acceptable estimation can be made for the GNP vol% (VF_{GNP}) utilizing the MD simulation box volume and its mass density distribution shown in Figure 3.6.a, as it is rather possible to estimate the planar GNP volume. However, this task is not applicable for the wrinkled GO and FGO nanoplatelets. Fortunately, the "compute voronoi/atom" LAMMPS command introduces an effective solution for estimating the vol% despite the atomic volume calculation process neglects the presence of voids. Practically, the voids vol% (VF_{void}) can be neglected as it is very small for a well processed and degassed sample. On the other hand, the visual snapshot of atoms in an MD model using OVITO is virtual and the actual physical volume of an atom is determined by its vdW radius. Mathematically, the 3D Voronoi tessellation method, which was originally proposed by Gregory Voronoi (1908) [95], is based on establishing a set of space vectors out of the position of each atom which is accounted for the nearest neighbor atoms. These vectors are used to generate a 3D polygon region which represents the atom volume within the atomic system.

Figure 3.7 shows representative samples of GNP/, GO/, and FGO/epoxy MD models analyzed using the 3D Voronoi tessellation. The atoms (white beads) and the red-wire-mesh were generated using the open source voro++ software library for the computation of the Voronoi tessellation [96], while the images were rendered using the POV-Ray (Persistence of Vision Raytracer) software package. Clearly, the overall volume mesh for each MD model is assembled out of the discretized volume cells of the atoms in the system. This method is powerful in assigning the nanoplatelet partial volume despite its wrinkled structure. The nanoplatelets wt% and vol% averaged over the five MD replicates of the proposed nanocomposites are given above in Table 3.3.

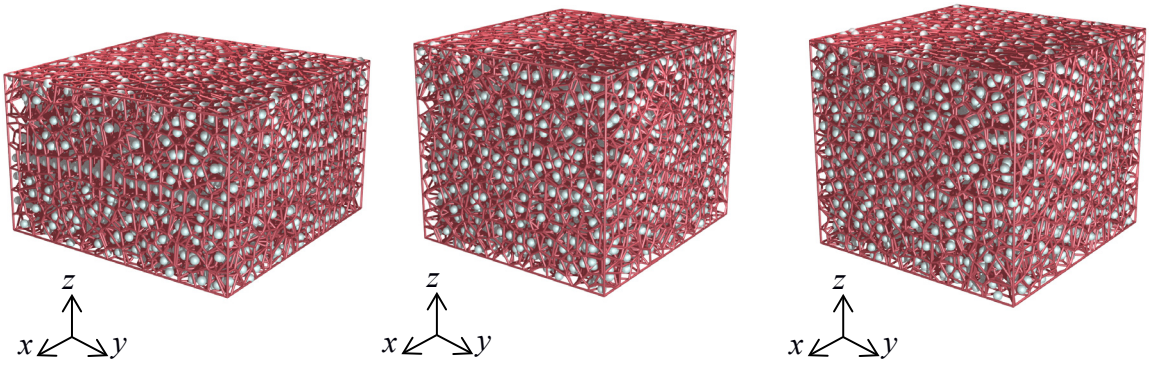

(a) GNP/epoxy (b) GO/epoxy (c) FGO/epoxy

Figure 3.7: The 3D Voronoi tessellation of GNP/, GO/, and FGO/epoxy nanocomposite MD models, the red line mesh represents the Voronoi cells generated for each atom (white beads).

3.2.6 Interfacial Interaction Energy (IIE)

Based on the concept of IIE, which is described in Chapter 2, the interfacial interaction between each of the GNP, GO, and FGO nanoplatelets and the hosting matrix were evaluated using Equation 2.1, which can be restated in the following general form:

$$IIE = PE_{MD} - PE_{NP} - PE_{epoxy} \tag{3.1}$$

Comparing Equation 3.1 with Equation 2.1, PE_{NP} is the isolated potential energy for any type of the reinforcing nanoplatelets. Figure 3.8 shows the IIE levels evaluated for the current GNP/, GO/, and FGO/epoxy MD models in addition to the IIE for the 4-layer GNP/epoxy (4GNP/epoxy) nanocomposite which is modeled previously in Chapter 2. The 4GNP/epoxy MD sample was modeled to account for the GNP agglomeration effect on the predicted mechanical properties of the nanocomposite. It is important to note that the IIE for each nanocomposite type was averaged over its five MD replicates which were well equilibrated with ReaxFF. In addition, the higher the negative IIE magnitude is, the stronger the nanoplatelet-epoxy interaction.

Clearly, the FGO/epoxy MD model with -9,356 kcal/mole exhibits the highest IIE among the other nanocomposites. The IIE of GO/epoxy MD model with -4,381 kcal/mole is in the second place. However, both GNP/epoxy and 4GNP/epoxy exhibit a much lower IIE of -1389 and -992 kcal/mole, respectively. Hence, the IIE of FGO/epoxy nanocomposite surpasses the GO/, GNP/, and 4GNP/epoxy nanocomposites by 113.6%, 573.6%, and 843.2%, respectively. However, the IIE of GO/epoxy nanocomposite surpasses the GNP/epoxy and 4GNP/epoxy nanocomposites by 215.4%, and 341.6%, respectively. Whereas, the IIE of GNP/epoxy nanocomposite exceeds the IIE of 4GNP/epoxy nanocomposite by 40%, which can be attributed to the additional epoxy-epoxy interaction energy term across the single layer of GNP.

Accordingly, the presence of functional and/or oxygen groups on the GNP surface resulted in a significant improvement in the IIE with the hosting matrix. That is, the attraction or adhesion between GNP and epoxy matrix can be greatly enhanced by introducing functional groups to the GNP surface. These functional groups provide a strong interfacial covalent bonding between the nanoplatelet and the epoxy matrix. The major contribution to IIE in FGO/epoxy can be attributed to the 20% of crosslinking density (covalent bonds) between the amine/amide functional groups and the epoxy matrix. Additional contribution to the IIE in FGO/epoxy can be attributed to the interfacial H-bonding and Coulomb energy. However, the H-bonding and Coulomb energy represent the major contribution to the IIE in GO/epoxy.

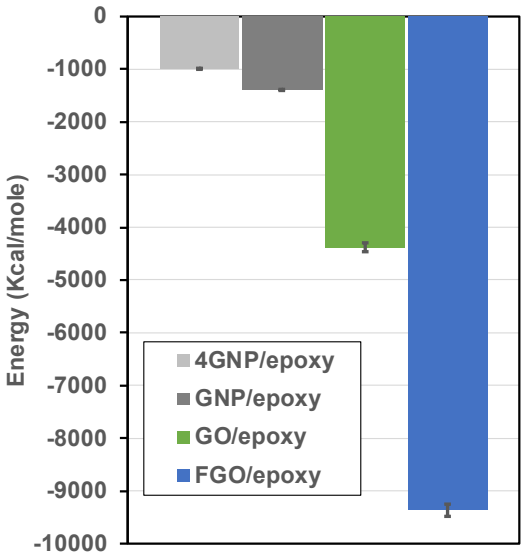

Figure 3.8: The interfacial interaction energy between epoxy matrix and 4GNP, GNP, GO, and FGO nanoplatelets.

3.2.7 The Effective Mechanical Properties (MD Prediction)

The MD modeling procedure used herein is based on that described in Chapter 2 to predict the effective mechanical properties of 4GNP/epoxy MD model. The well-equilibrated MD models in ReaxFF were subjected to six deformation MD simulations. Each of the five MD replicates of GNP/, GO/, and FGO/epoxy nanocomposites was subjected to two tensile strain simulations along the *x*- and *y*-directions to predict the in-plane elastic modulus $[E_{ip} = (E_x + E_y)/2]$ and Poisson's ratio$[\nu_{ip} = (\nu_{xy} + \nu_{yx})/2]$. However, the tensile strain simulations along the *z*-direction were used to predict the out-of-plane elastic modulus $[E_{op} = E_z]$ and Poisson's ratio $[\nu_{op} = (\nu_{zx} + \nu_{zy})/2]$. To predict the shear moduli, three shear strain simulations in the *xy*-, *xz*-, and *yz*-planes were performed on each MD sample. While the deformation simulations in *xy*-plane were used to predict the in-plane shear modulus $[G_{ip} = G_{xy}]$, the deformation simulations in *xz*- and

yz-plane were used to predict the out-of-plane shear modulus [$G_{op} = (G_{xz} + G_{yz})/2$]. Consequently, 30 MD deformation simulations were performed on the replicates of each nanocomposite which are totaled with 90 MD deformation simulations for the three nanocomposite types.

For the axial tensile strain simulations, the NPT ensemble at 300 K with the Nose/Hoover barostat was utilized to maintain the lateral surfaces at one-atmospheric pressure. These simulation settings were imposed to account for the Poisson contractions. However, the shear strain simulations were performed with the NVT ensemble at 300 K. Table 3.5 includes the predicted mechanical properties for the three nanocomposite MD models (localized interphase regions) simulated herein. The effective mechanical properties were averaged over the five MD replicates providing the corresponding standard deviations as the prediction uncertainties. All the deformation simulations were carried out over a total simulation time of 0.5 ns using 0.1 fs time steps and a strain rate of 1×10^{8} s^{-1} which resulted in a maximum engineering strain of 5%.

Table 3.5: The predicted effective mechanical properties of the GNP/, GO/, and FGO/epoxy nanocomposite MD models.

Mechanical properties	GNP/epoxy	GO/epoxy	FGO/epoxy
In-plane elastic modulus (E_{ip}), GPa	127.5±1.6	13.7±2.3	14.1±2.2
Out-of-plane elastic modulus (E_{op}), GPa	5.1±0.5	3.8±0.9	4.2±0.5
In-plane shear modulus (G_{ip}), GPa	30.1±0.9	7.7±1.1	8.3±0.8
Out-of-plane shear modulus (G_{op}), GPa	0.073±0.021	1.201±0.214	1.498±0.239
In-plane Poisson's ratio (ν_{ip})	0.964±0.003	0.080±0.021	0.071±0.043
Out-of-plane Poisson's ratio (ν_{op})	0.020±0.007	0.321±0.067	0.267±0.032

3.3 Micromechanics Modeling

The micromechanics modeling procedure used herein is based on that presented previously in Chapter 2 with some modification to account for the nanoplatelet aspect ratio. The multiscale modeling workflow is shown in Figure 3.9, which illustrates the continuum-level steps to predict the mechanical properties of the bulk nanocomposites. The MAC/GMC 4.0 RUC (ARCHID=1) shown in Figure 3.9.b contains 8 discretized subcells. One of the subcells was used to incorporate the predicted mechanical properties given in Table 3.5 for the MD model shown in Figure 3.9.a as the fiber subcell. However, bulk epoxy properties were incorporated in the other seven subcells. The bulk DGEBA-DETDA epoxy properties were taken from Qi et al. [97] in which the experimental elastic modulus was reported to be 2.71 ±0.11 GPa. Generating this RUC is essential to control the required nanoplatelet content (vol% or wt%) and its aspect ratio within the epoxy matrix [9, 57]. For the nanoplatelet content, it has been shown previously in Chapter 2 that the overall volume fraction of the nanoplatelet within epoxy matrix ($VF_{NP/RUC}$) can be evaluated using the following expression:

$$VF_{NP/RUC} = VF_{NP/MD} \times VF_{MD/RUC} \tag{3.2}$$

where $VF_{NP/MD}$ represents the GNP, GO, or FGO volume fraction within the MD model which is given as vol% in Table 3.3, and $VF_{MD/RUC}$ represents the volume fraction of the MD model within the RUC which can be adjusted in the MAC/GMC 4.0 script according to the required amount of the reinforcing nanoplatelets.

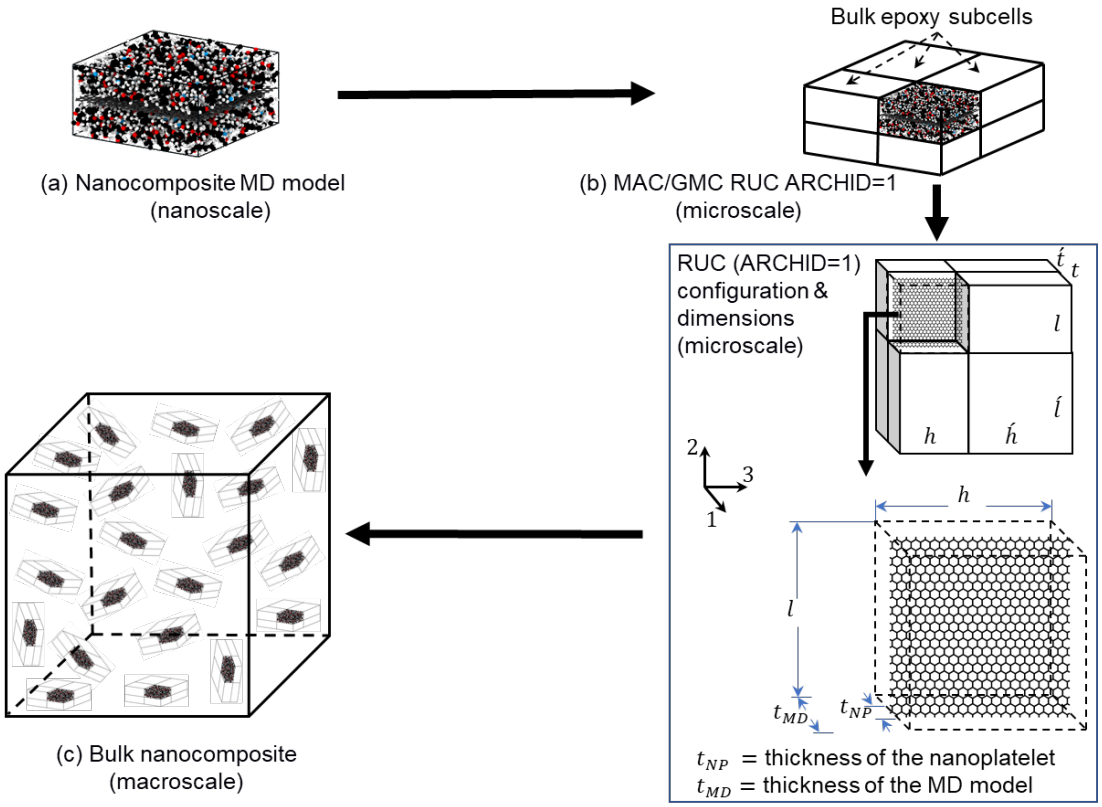

Figure 3.9: The multiscale modeling workflow of bulk nanoplatelet/epoxy nanocomposite.

A similar approach can be used to specify the nanoplatelet wt% within the epoxy matrix ($wt_{NP/RUC}$) according to the following expression:

$$wt_{NP/RUC}\% = wt_{NP/MD}\% \times wt_{MD/RUC}\% \tag{3.3}$$

where $wt_{NP/MD}\%$ represents the weight percentage of GNP, GO, or FGO within the MD model which is given as wt% in Table 3.3, and $wt_{MD/RUC}\%$ represents the weight percentage of the MD model within the RUC which can be evaluated using the following expression:

$$wt_{MD/RUC}\% = \frac{\rho_{MD} \times VF_{MD/RUC}}{\rho_{MD} \times VF_{MD/RUC} + \rho_B VF_{B/RUC}} \times 100\% \tag{3.4}$$

where ρ_{MD} and ρ_B are the molecular mass density of the MD model and bulk epoxy, respectively. The values of ρ_{MD} for MD models are given in Table 3.3, while the ρ_B is considered to be 1.2 g/cm^3 as the typical mass density of the bulk epoxy system used in this work. The bulk epoxy volume fraction within the RUC ($VF_{B/RUC}$) can be substituted as:

$$VF_{B/RUC} = 1 - VF_{MD/RUC} \tag{3.5}$$

With respect to the nanoplatelet aspect ratio (a_{NP}), it can be evaluated using the following expressions:

$$a_{NP} = l/t_{NP} \tag{3.6}$$

where l and t_{NP} are the length and the thickness of the nanoplatelet, respectively. For the fiber subcell in the RUC, the aspect ratio of the nanocomposite MD model as the fiber subcell (a_{MD}) can be calculated using the following expression;

$$a_{MD} = l/t_{MD} \tag{3.7}$$

where l and t_{MD} are the length and the thickness of the MD model, respectively. According to the RUC settings, the MD model length l is substituted as the fiber length while the MD model thickness t_{MD} is substituted as the fiber diameter. Rearranging Equation 3.6 for l, and substitute the value of l in Equation 3.7 results in the following expression for a_{MD}:

$$a_{MD} = \frac{a_{NP} \times t_{NP}}{t_{MD}} = a_{NP} \times \frac{t_{NP}}{t_{MD}} \tag{3.8}$$

given that;

$$VF_{NP/MD} = \frac{t_{NP} \times l \times h}{t_{MD} \times l \times h} = \frac{t_{NP}}{t_{MD}} \tag{3.9}$$

hence, Equation 3.8 can be rewritten as:

$$a_{MD} = a_{NP} \times VF_{NP/MD} \tag{3.10}$$

Equations 3.2-3.10 provide the flexibility to predict the effective mechanical properties of the nanocomposites at different nanoplatelets content and aspect ratio values without the need for running additional MD simulations. After running the MAC/GMC script, utilizing the RUC settings illustrated in Figure 3.9.b, the predicted mechanical properties of the nanocomposite were further processed using Christensen and Waals equations [64]. These equations were used to predict the effective homogenized/isotropic mechanical properties of the nanocomposites with randomly orientated and perfectly dispersed nanoplatelets in epoxy matrix, as shown in Figure 3.9.c. The predictions at this point represent the mechanical properties of the bulk nanoplatelet/epoxy nanocomposites.

3.4 Results and Discussions

The influence of the nanoplatelets dispersion, functionalization, content, and aspect ratio on the predicted mechanical properties of the nanocomposites at room temperature is described and discussed in this section. The nanoplatelet/epoxy nanocomposite predictions are divided into two levels; first, the localized interphase MD predictions (nanoscale), and second, the bulk nanocomposite predictions (microscale). The bulk nanocomposite predictions are validated with experiments from the literature.

3.4.1 Nanoplatelet/Epoxy MD Predictions (Nanoscale)

The effective mechanical properties of the localized interphase regions of nanoplatelet/epoxy MD models shown in Figure 3.6 were predicted and are given in Table 3.5. In general, introducing the functional and/or large amount of oxygen groups to the GNP structure produced a significant drop in the in-plane elastic (E_{ip}) and shear (G_{ip}) moduli. Particularly, GO/epoxy exhibits -89.25% and -74.42% reduction in the E_{ip} and G_{ip}, respectively. Whereas, FGO/epoxy exhibits -88.94% and -72.43% reduction in the E_{ip} and G_{ip}, respectively. A slight drop can be also observed in the out-of-plane elastic modulus (E_{op}) with -25.49% for the GO/epoxy and -17.65% for the FGO/epoxy.

The designated drop in E_{ip}, E_{op}, and G_{ip} is mainly attributed to the degradation in the robust sp^2 structure of the GNP due to the surface functionalization effect (refer to Figure 3.3). On the other hand, surface functionalization produced a tremendous improvement in the out-of-plane shear modulus (G_{op}) by 15.45 times for the GO/epoxy and by 19.52 times for the FGO/epoxy. This improvement in the G_{op} is mostly attributed to the rough and wrinkled surfaces of FGO and GO nanoplatelets (refer to Figure 3.2 and Figure 3.6) which triggered the interlocking mechanism with the hosting matrix. Better improvement in the interfacial adhesion can be particularly obtained in FGO/epoxy as the FGO is covalently bonded with the hosting matrix. However, the low G_{op} of GNP/epoxy is governed by the low noncovalent interfacial interaction between the planar GNP surface and epoxy.

For the Poisson contractions, the in-plane Poisson's ratio (ν_{ip}) value for the functionalized GNP/epoxy nanocomposites indicated a significant decrease. In contrast, the out-of-plane Poisson's ratio (ν_{op}) involved a large increase. This lateral contraction behavior can be attributed to the alteration in the GNP sp^3/sp^2 ratio and wrinkling effect. Generally, the FGO/epoxy exhibits a higher prediction of the localized moduli relative to the GO/epoxy nanocomposite. That is, the nanocomposite localized interphase stiffness is highly governed by the stiffness of the nanoplatelet which asserts the order GNP$\gg$FGO$>$GO.

3.4.2 Nanoplatelet/Epoxy Bulk Predictions (Microscale)

In fact, the process of comparing the predicted mechanical properties of nanocomposites with experiments involves some challenges. This is because of the wide range of factors that can affect the nanocomposite molecular structure and hence its

mechanical response. The size and number of layers in the GNP, integrity of the GNP lattice structure, the GNP surface functionalization, and the chemical composition of residual solvent solutions are the most important factors which can greatly affect the material response at both molecular and bulk scales. Tackling all of these factors requires significant modeling effort as the MD modeling can be used to simulate a particular case study of nanocomposites.

In this work, the bulk GNP/epoxy nanocomposite represents an ideal case of pristine and planar single layers of graphene perfectly dispersed in the epoxy matrix. However, GO/epoxy and FGO/epoxy involved introducing high levels of chemical elements to the GNP. In other words, GO and FGO nanocomposites involved changing the chemical composition of the GNP, yet keeping the same level of dispersion. The 4GNP/epoxy nanocomposite, which is modeled previously in Chapter 2, involved modelling the GNP with a certain level of dispersion/agglomeration. Fortunately, the modeling scheme and computational tools used in this study provide the ability to manipulate and control most of the aforementioned factors. The RUC settings shown in Figure 3.9.b tolerate the prediction of the mechanical properties for bulk nanocomposites at different nanoplatelets contents and aspect ratios. However, there are still some other important factors, such as the variation in the chemical composition of the functionalized GNP and the nanoplatelets dispersion levels, which can produce incomparable deviations with experiments. Hence, the aim of this section is to validate the current modeling approach under the consideration of the above discussion.

Figure 3.10 shows the predicted bulk elastic modulus for each nanocomposite type at different nanoplatelets content (wt%) at aspect ratio 6 (dashed lines), and 100 (sold lines). The unnormalized predicted moduli (Figure 3.10.a) are significantly higher than the experimental values from Park et al. [83] despite that the GO and FGO nanoplatelets were modeled according to the reported experimental data in their work (Table 3.1). The difference is attributed to the low magnitude of the epoxy matrix elastic modulus in the experiment which was reported as 1.0±0.4 GPa. This modulus value is much lower than the typical value of DGEBA-DETDA epoxy reported in the literature [85, 97]. In addition, the number of layers in the reinforcing nanoplatelets and their size (aspect ratio) is unreported in their work. However, the experimental elastic modulus of GNP-COOH/epoxy (and GNP-O_2/epoxy which is not reported herein as its mechanical properties are identical to the GNP-COOH/epoxy) from Chong et al. [85] indicates a good agreement with the current predictions.

The normalized composite elastic modulus (E_c) by the matrix elastic modulus (E_m) shown in Figures 3.10.b,c indicates excellent agreement between the current predictions and the experimental data provided by Chong et al. Note that the experimental aspect ratio of GNP-COOH nanoplatelet sample measured using field emission scanning electron microscopy (FESEM) was reported to be 85, while the manufacturer value is within 6-100. In general, all the predicted moduli fall within the standard deviation of the experimental modulus from Chong et al. at 1.0 wt% of the nanoplatelets content. However, the experimental mean value is slightly lower than the predicted moduli for GNP/epoxy nanocomposite which represents the ideal case using intact GNP structure with perfect dispersion in matrix. The experimental mean value of the modulus is also close the

predicted modulus values of 4GNP/, FGO/, and GO/epoxy nanocomposites with 100 aspect ratio, and slightly higher than those with 6 aspect ratio (Figure 3.10.c).

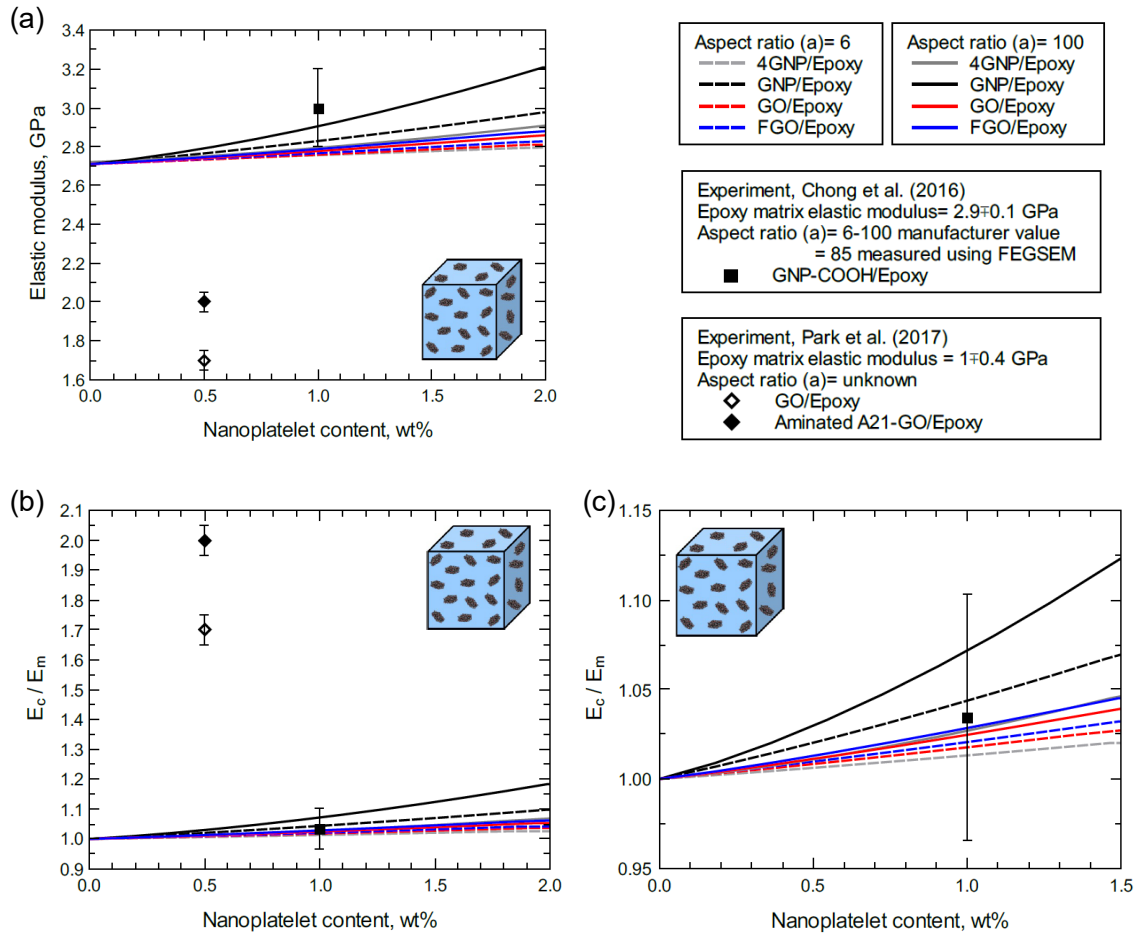

Figure 3.10: Elastic modulus predicted for various nanoplatelets content and compared with experiment, (a) unnormalized modulus, (b) normalized modulus, and (c) zoom in capture at the modulus data point of GNP-COOH/epoxy.

Zaman et al. [7] performed an experimental study to investigate the mechanical response of an epoxy matrix reinforced with graphene nanoplatelets (GP) and surface-modified graphene nanoplatelets (m-GP). The nanocomposites involved two levels of platelet-matrix interfacial strength. To prepare m-GP, GP suspensions were chemically modified using 4,4′-Methylene diphenyl diisocyanate (MDI). The chemical reaction between GP and MDI produced reactive functional groups (carbonyl and amine radicals) attached to the GP surfaces. These reactive functional groups were found to improve the m-GP dispersion and the interfacial strength via forming covalent bonds between the m-GP and the hosting matrix. Figure 3.11 shows the normalized elastic modulus (E_c/E_m) of GP/epoxy and m-GP/epoxy obtained for various wt% of nanoplatelets content. Clearly, the GP/epoxy samples involved higher elastic moduli relative to m-GP/epoxy samples as the

nanoplatelets content increased from 1.0-2.5 wt%. This is not the case at 4.0 wt% of the nanoplatelets content as the stiffening effect of GP diminished due to the agglomeration effect. In contrast, the m-GP/epoxy maintained a steadily improvement up to 4.0 wt% of m-GP content. A slight deterioration in the obtained elastic modulus can be observed at 5.5 wt% of m-GP content.

Considering the adverse effect of agglomeration on the obtained elastic moduli at higher nanoplatelets contents, the predicted elastic moduli of the nanocomposites modeled herein are in a good agreement with the experimental moduli obtained by Zaman et al. Specifically, the predicted elastic moduli of the GNP/epoxy are in excellent agreement with the experimental values obtained at 1.0-2.5 wt% nanoplatelets content. The experimental elastic moduli of the m-GP/epoxy at 1.0-2.5 wt% of nanoplatelets content are also excellently captured by the predicted moduli of 4GNP/, GO/, and FGO/epoxy nanocomposite models. A close agreement can be observed between the predicted and experimental moduli at higher nanoplatelets content (4.0-5.5 wt%). It is important to note that all the moduli predicted herein are at 100 aspect ratio of the nanoplatelets while the cluster size of GP and m-GP at 4.0 wt% were reported to be 0.7±0.5 μm and 1.8±1.5 μm, respectively. The weak mechanical performance of the m-GP/epoxy relative to the GP/epoxy at 1.0-2.5 wt% of nanoplatelets content supports the current predictions, as GO and FGO have weaker reinforcing effect relative to GNP. Practically, this trend does not apply at higher nanoplatelets content as the agglomeration effect becomes more predominant for unmodified nanoplatelets.

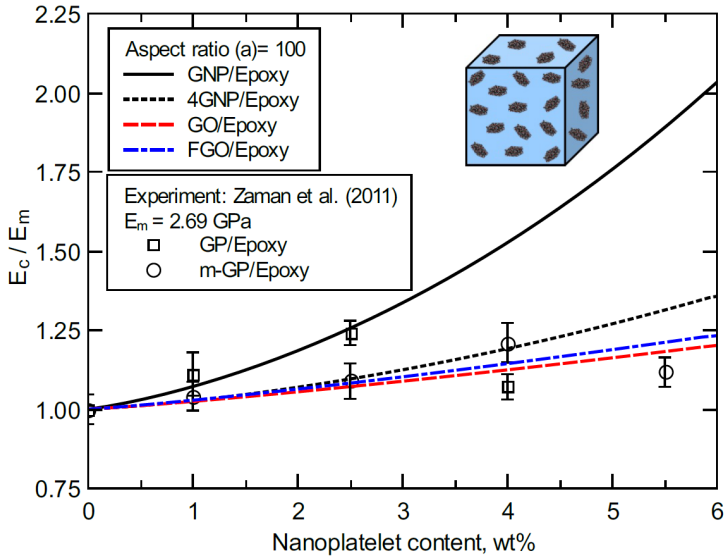

Figure 3.11: Normalized elastic modulus predicted at 100 aspect ratio for various nanoplatelets content and compared with experiment from Zaman et al. (2011).

Figure 3.12 shows the predicted elastic modulus of bulk GO/epoxy and FGO/epoxy nanocomposites (E_c) normalized by the matrix modulus (E_m). The moduli are predicted for various aspect ratio values at 1.0 wt% content of the nanoplatelets. The predictions are

in a good agreement with the experimental value of the GO/epoxy elastic modulus from Bortz et al. [14]. Even though the GO nanoplatelet dimensions were not identified in the experimental work, the variation in the measured modules spans a wide range (~10 to infinite) of possible aspect ratio values. Figure 3.12 also indicates an excellent agreement between the mean modulus value from experiment and the predicted modulus of GO/epoxy at aspect ratio span from ~10^3 to infinite. However, the mean modulus value from the experiment and the predicted modulus of FGO/epoxy are in excellent agreement at ~350 of aspect ratio.

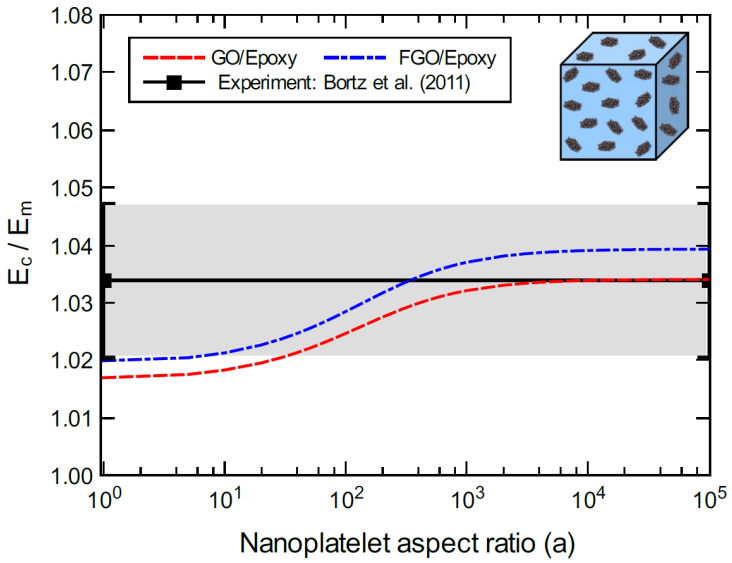

Figure 3.12: Normalized elastic modulus of GO/epoxy and FGO/epoxy predicted for various aspect ratio at 1.0 wt% of the nanoplatelets content. Experiment; epoxy matrix modulus= 2.99±0.15 GPa, GO content= 1.0 wt%.

Figure 3.13 shows the normalized elastic moduli of the proposed nanocomposites predicted for various aspect ratio values at 1.0 wt% of nanoplatelets content compared with experiment from Cho et al. [98]. The measured elastic modulus of the as-received graphite 100GNP/epoxy nanocomposite with 5 aspect ratio and 1.0 wt% of nanoplatelets content is in an excellent agreement with the predicted elastic moduli of 4GNP/, GO/, and FGO/epoxy. Also, the predicted modulus of GNP/epoxy is slightly higher than the mean value of the experimental modulus, yet still within the standard deviation. For the experimental modulus of the exfoliated graphite 100GNP/epoxy nanocomposite with 70 aspect ratio and 1.0 wt% of nanoplatelets content, its mean value is slightly higher than the predicted moduli. All the predicted moduli, however, are within the lower bound of the standard deviation. It is important to note that including GO/epoxy and FGO/epoxy nanocomposites in the comparison is to assess their performance, which is identical with 4GNP/epoxy for an aspect ratio less than 200. In general, the results indicate the validity of the current work predictions.

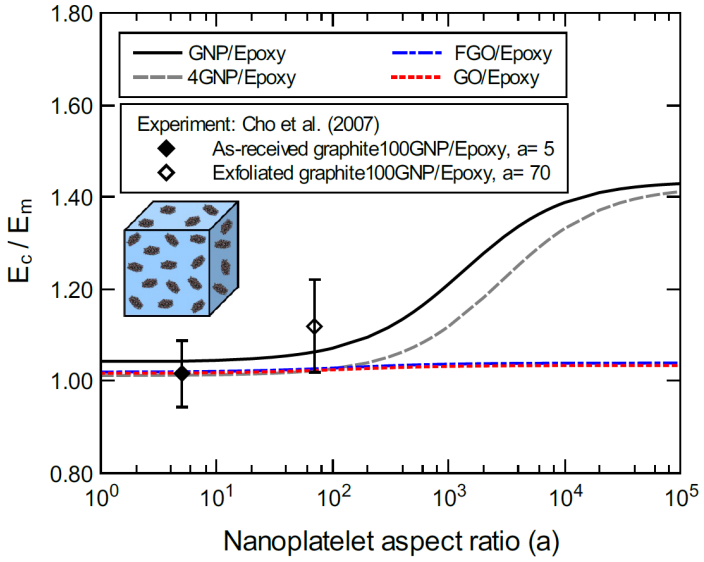

Figure 3.13: Normalized elastic modulus of 4GNP/, GNP/, GO/, and FGO/epoxy predicted for various aspect ratio values at 1.0 wt% of the nanoplatelets content. Experiment; epoxy matrix modulus= 3.27 GPa, nanoplatelets content= 1.0 wt%.

Karevan et al. [86] provided experimental mechanical properties of poly propylene (PP) reinforced with exfoliated graphite nanoplatelets (xGnP^{TM}). The chemical solvents used in the exfoliating process of graphite introduced some chemical elements to the xGnP lattice structure. In this particular case study, low amounts of oxygen, nitrogen, and sulfur are expected to exist as it is reported by the supplier. In addition, the xGnP aspect ratio was reported to be 50 as provided by the supplier, and 20 as measured after processing the nanocomposite material using the atomic force microscopy (AFM). Assuming pristine xGnP (that is, ignoring the effect of the residual chemical elements), the normalized experimental elastic moduli at 3.0, 5.0, and 10.0 wt% are comparable with the predicted normalized elastic moduli of 4GNP/epoxy and GNP/epoxy at the given nanoplatelets contents and aspect ratio span (Figure 3.14.a). Specifically, the experimental modulus value using 3.0 wt% of xGnP content is in an excellent agreement with predicted moduli of the perfectly dispersed GNP in matrix (GNP/epoxy). In addition, it is slightly higher than the predicted moduli at a certain agglomeration level from the 4GNP/epoxy. Due to the agglomeration effect at higher xGnP content, the experimental moduli at 5.0 and 10.0 wt% of xGnP content are deviated away from the predicted moduli of the perfectly dispersed GNP/epoxy nanocomposite toward the predictions of 4GNP/epoxy which are at lower dispersion level. On the other hand, all the experimental moduli are slightly higher than the predicted moduli using GO/epoxy and FGO/epoxy nanocomposites (Figure 3.14.b). This is mainly attributed to the detrimental effect of the large amount of oxygen and functional groups in the modeled composites relative to the experiment.

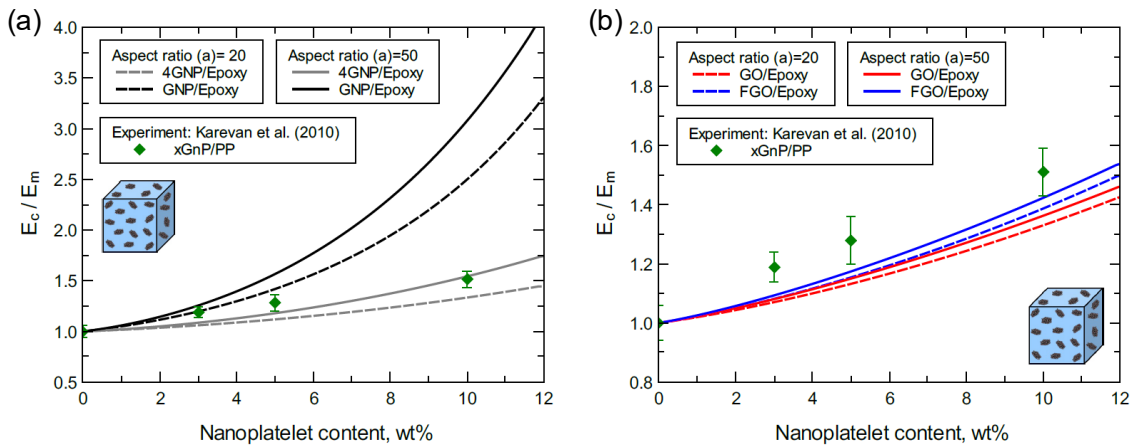

Figure 3.14: Normalized elastic moduli predicted for various nanoplatelets content, (a) GNP/epoxy and 4GNP/epoxy, (b) GO/epoxy and FGO/epoxy. Experiment; matrix modulus= 1.43±0.06 GPa, aspect ratio= 50 as provided by the supplier, 20 as measured using AFM.

Among the several types of nanoplatelets that were used to reinforce the epoxy matrix and experimentally tested by Chong et al. [85], the XG-C/epoxy and XG-M/epoxy are used herein for validating the predicted elastic moduli in this work. The manufacturing process used to prepare the nanocomposites involved using two different types of solvents to disperse the dry powder of GNP modifiers in matrix. They used ultrasonication with tetrahydrofuran (THF) or n-methyl-pyrrolidone (NMP) solvents that produced two different levels of GNP dispersion. Particularly, NMP solvent produced higher level of GNP dispersion relative to the THF. Therefore, the experimental moduli of the nanocomposites using NMP were higher relative to those using THF solvent. Residual solvents in the nanocomposites are expected to introduce chemical elements to the GNP. This affects the carbon lattice structure of GNP depending on the chemical elements' concentration. In addition, GNP exfoliation and the mixing technique used in preparing the nanocomposites can greatly affect the GNP aspect ratio.

The normalized elastic moduli predicted for GNP/epoxy and 4GNP/epoxy nanocomposites shown in Figure 3.15.a are generally in a good agreement with experimental normalized elastic moduli of XG-C-THF/epoxy and XG-C-NMP/epoxy. Practically, as agglomeration level increases with GNP content, the aspect ratio decreases. Hence, experimental values of the modulus at low GNP content (0.1 and 0.5 wt%) are in excellent agreement with the predicted moduli at large aspect ratio. However, experimental values of the modulus at higher GNP content (1.0 and 2.0 wt%) are deviated toward the predicted moduli at a lower aspect ratio. In both cases, the experimental moduli of XG-C-NMP/epoxy are close to the predictions of GNP/epoxy, while XG-C-THF/epoxy moduli are close to the predictions of 4GNP/epoxy. The experimental moduli were also compared with predicted moduli of GO/epoxy and FGO/epoxy (Figure 3.15.b). Considering the detrimental effect of the high concentration of oxygen in GO and FGO nanoplatelets, an acceptable agreement with experiment can be observed.

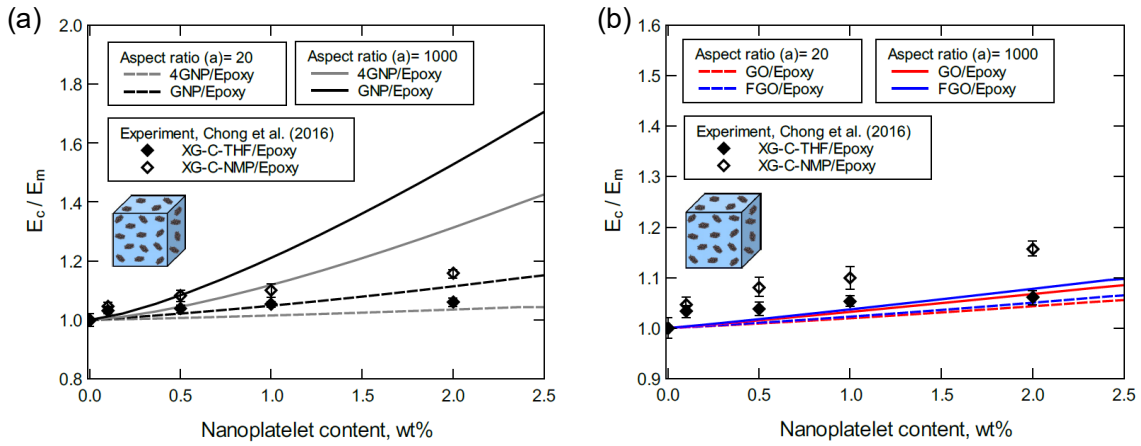

Figure 3.15: Normalized elastic modulus predicted for various nanoplatelets content, (a) GNP/epoxy and 4GNP/epoxy, (b) GO/epoxy and FGO/epoxy. Experiment; matrix modulus= 2.9±0.1 GPa, aspect ratio= 1000 as the manufacturer value, 19 as measured using FEGSEM.

To some extent, the judgment used in justifying the results shown in Figure 3.15 can also be feasible for the predicted moduli compared with experimental moduli of XG-M-THF/epoxy and XG-M-NMP/epoxy shown in Figure 3.16. However, the large deviation between predicted and experimental moduli at 2.0 wt% of GNP content can be attributed to the high agglomeration degree in the experimental value.

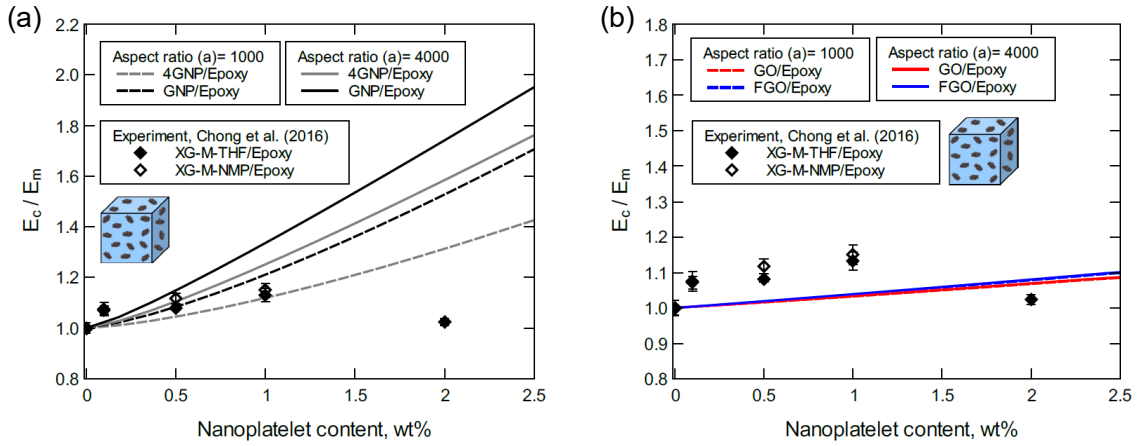

Figure 3.16: Normalized elastic modulus predicted for various nanoplatelets content, (a) GNP/epoxy and 4GNP/epoxy, (b) GO/epoxy and FGO/epoxy. Experiment; matrix modulus= 2.9±0.1 GPa, aspect ratio= 4167 as the manufacturer value, 1142 as measured using FEGSEM.

Most experimental results indicate a substantial increase in the mechanical response of nanocomposites at low nanoplatelets content. Yet limited and even unfavorable mechanical behavior could be observed at higher contents. Practically, pristine GNPs tend to agglomerate within the hosting matrix and form GNP particles having low aspect ratios,

which limits its reinforcing effect. At large GNP contents, the GNP agglomeration and the raised material viscosity become more destructive to the nanocomposite structure and in most cases causes a decline in the material mechanical response. Functionalization is an effective solution to prevent agglomeration and maintain the dispersibility even at large amounts of GNP content.

3.4.3 General Predictions of Bulk Nanocomposites Mechanical Response

This section provides generalized predictions of the elastic E_c and shear G_c moduli of the bulk nanocomposites supported by detailed discussions. These predictions can be utilized to better understand the influence of the nanoplatelets content, aspect ratio, functionalization, and dispersion on the mechanical response of the bulk nanocomposite. For the ideal case study with perfectly dispersed GNP in epoxy matrix, the normalized elastic and shear moduli of bulk GNP/epoxy were predicted and plotted for virous GNP content and aspect ratio values and are shown in Figure 3.17.

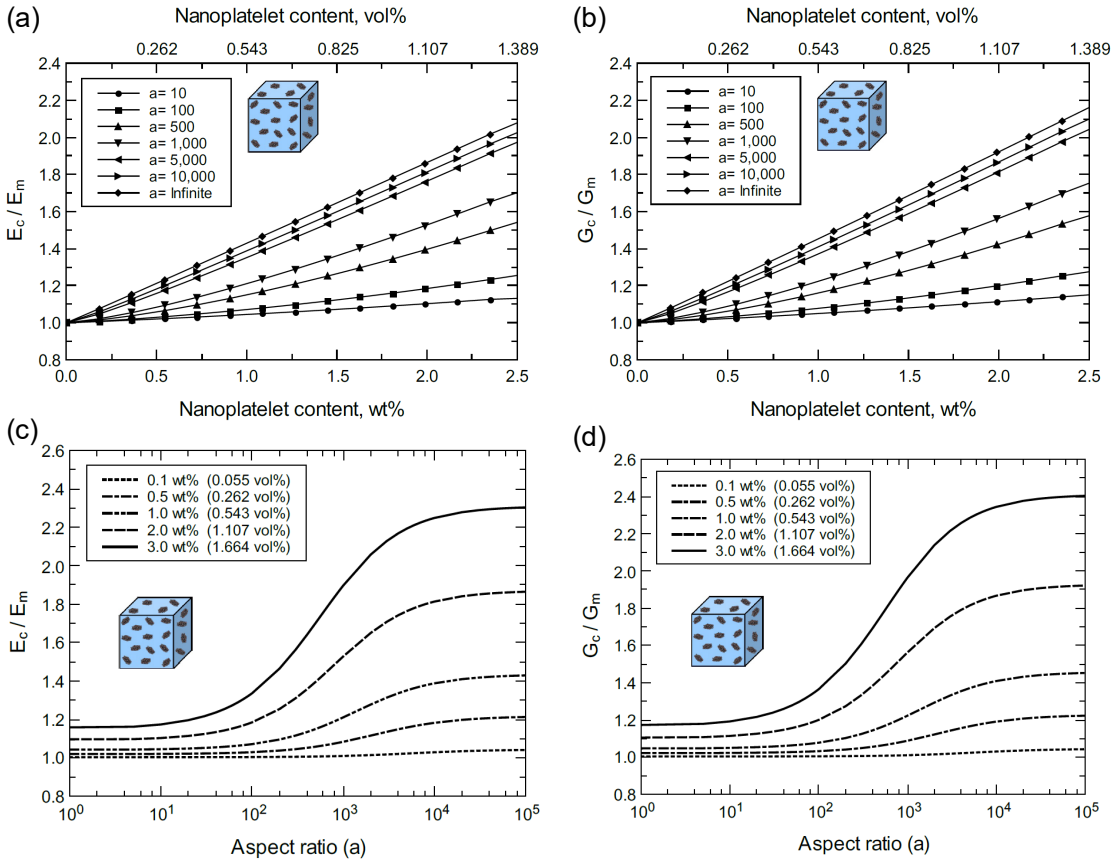

Figure 3.17: Normalized elastic and shear moduli of bulk GNP/epoxy predicted for various nanoplatelets content and aspect ratio values; (a) E_c/E_m vs GNP content at different aspect ratio values, (b) G_c/G_m vs GNP content at different aspect ratio values, (c) E_c/E_m vs aspect ratio at different GNP content, (d) G_c/G_m vs aspect ratio at different GNP content.

Figures 3.17.a,b show a consistent increase in E_c and G_c with GNP content and aspect ratio. The maximum improvement in E_c and G_c at 2.5 wt% (1.389 vol%) of GNP with infinitely aspect ratio is more than 100%. However, the reinforcing effect of GNP plateaus at aspect ratio values greater than 10^4, as shown in Figures 3.17.c,d. In addition, the reinforcing effect of GNP is limited for aspect ratio values below 10^2 and it becomes significant within 10^2-10^4 aspect ratio span. This trend can be clearly observed at high GNP contents.

At a certain lower level of GNP dispersion, the bulk 4GNP/epoxy nanocomposite response exhibits a similar trend to the bulk GNP/epoxy as shown in Figure 3.18. However, the reinforcement function of 4GNP is relatively less due to the agglomeration effect. In both nanocomposite types, the improvement in G_c is ~10% higher than E_c.

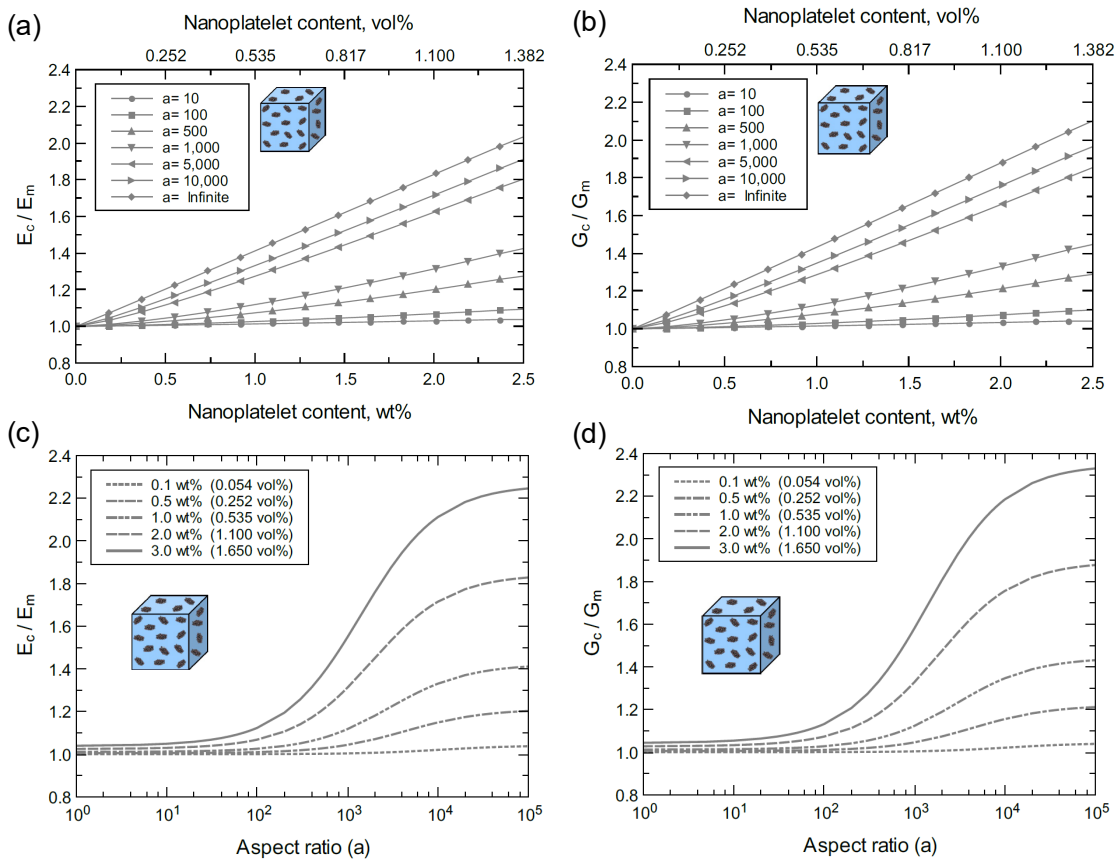

Figure 3.18: Normalized elastic and shear moduli of bulk 4GNP/epoxy predicted for various nanoplatelets content and aspect ratio values; (a) E_c/E_m vs 4GNP content at different aspect ratio values, (b) G_c/G_m vs 4GNP content at different aspect ratio values, (c) E_c/E_m vs aspect ratio at different 4GNP content, (d) G_c/G_m vs aspect ratio at different 4GNP content.

Figure 3.19 and Figure 3.20 show the mechanical response of bulk GO/epoxy and FGO/epoxy, respectively. The two nanocomposite types exhibit rather identical mechanical response with a slightly better reinforcing function when using FGO nanoplatelets. As discussed above in the previous section, both GO and FGO involved a weaker reinforcing effect in comparison to the GNP. Therefore, the mechanical properties of their nanocomposites at the bulk level involved limited improvement. Generally, there is an increase in E_c and G_c with increasing the GO or FGO content and aspect ratio. For the GO/epoxy mechanical response, the maximum improvement in E_c (Figure 3.19.a) and G_c (Figure 3.19.b) at 2.5 wt% (1.305 vol%) of GO with infinitely aspect ratio is ~9% and ~10%, respectively. For the FGO/epoxy mechanical response, however, the maximum improvement in E_c (Figure 3.20.a) and G_c (Figure 3.20.b) at 2.5 wt% (1.358 vol%) of FGO with infinitely aspect ratio is ~10% and ~11%, respectively. In both nanocomposites, the improvement in G_c is 1% higher than E_c.

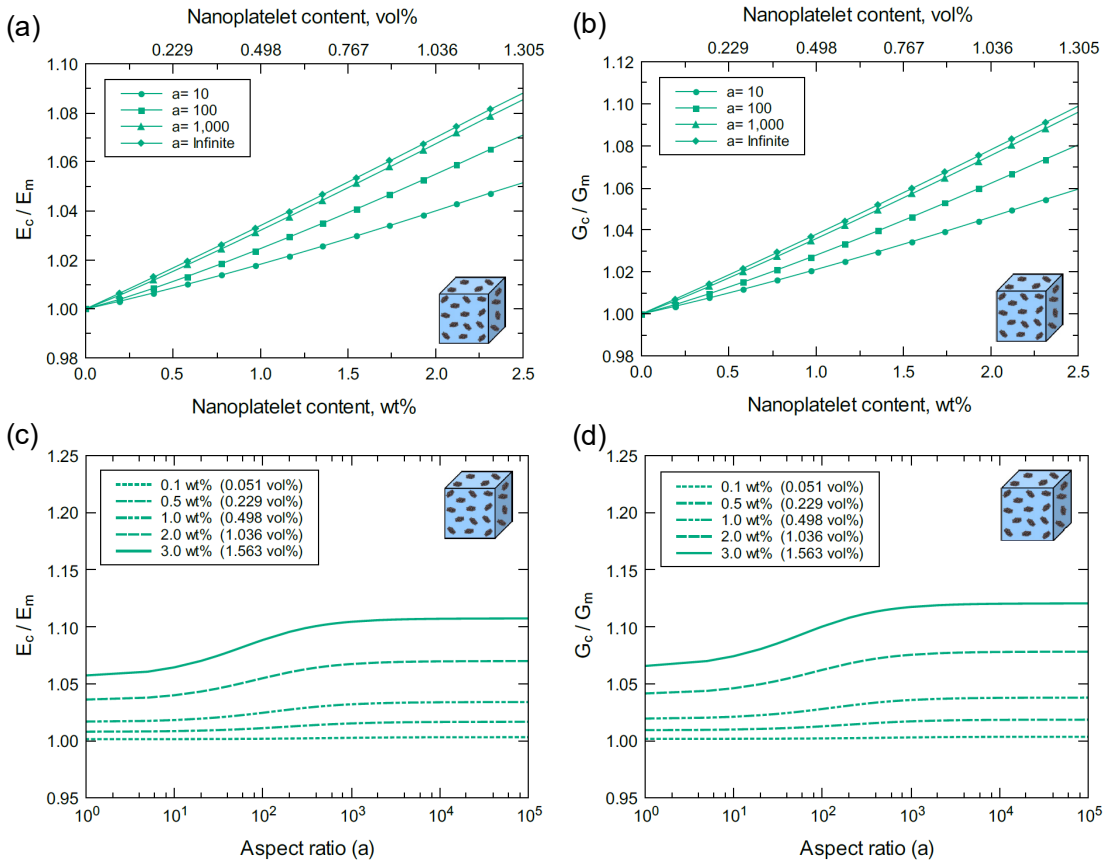

Figure 3.19: Normalized elastic and shear moduli of bulk GO/epoxy predicted for various nanoplatelets content and aspect ratio values; (a) E_c/E_m vs GO content at different aspect ratio values, (b) G_c/G_m vs GO content at different aspect ratio values, (c) E_c/E_m vs aspect ratio at different GO content, (d) G_c/G_m vs aspect ratio at different GO content.

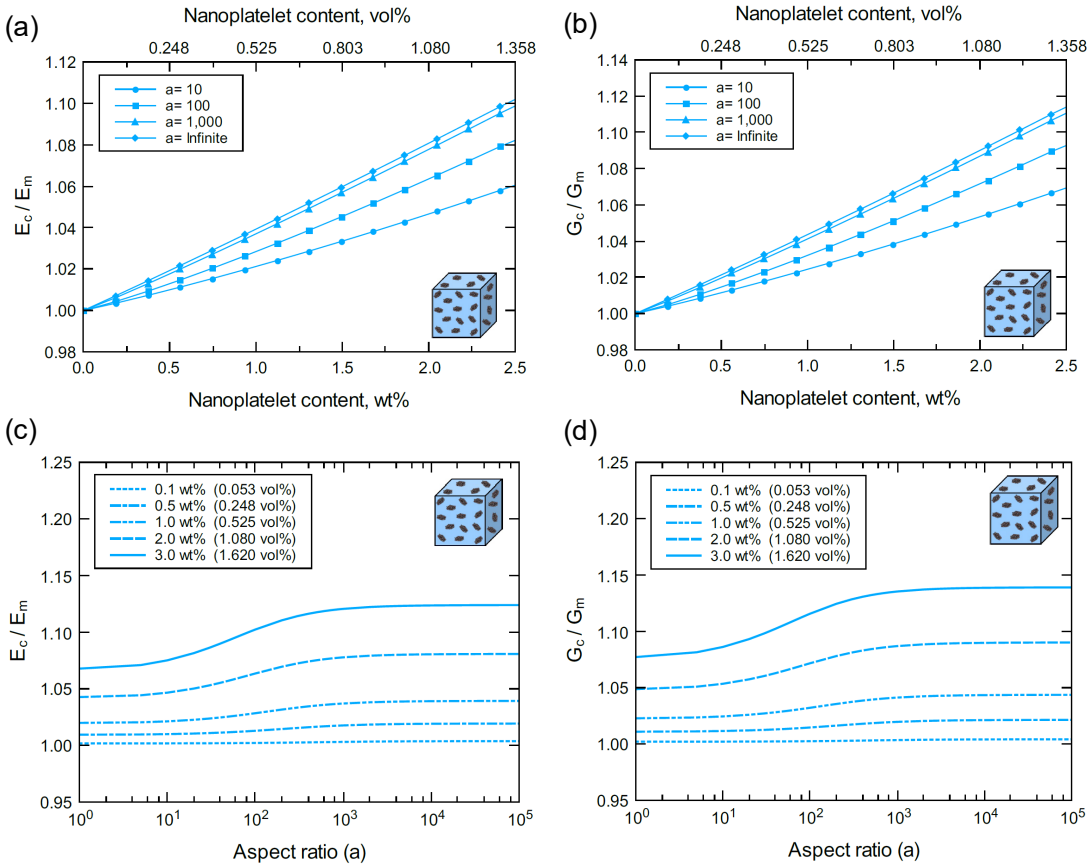

Figure 3.20: Normalized elastic and shear moduli of bulk FGO/epoxy predicted for various nanoplatelets content and aspect ratio values; (a) E_c/E_m vs FGO content at different aspect ratio values, (b) G_c/G_m vs FGO content at different aspect ratio values, (c) E_c/E_m vs aspect ratio at different FGO content, (d) G_c/G_m vs aspect ratio at different FGO content.

The reinforcing effect of GO (Figures 3.19.c,d) and FGO (Figures 3.20.c,d) plateaus at aspect ratio values greater than 10^3. In addition, it is limited for aspect ratio values below 10^1 and becomes slightly effective within 10^1-10^3 aspect ratio span. This trend can be clearly observed at high GO or FGO contents.

For comparison reason, the normalized elastic modulus (Figure 3.21.a) and normalized shear modulus (Figure 3.21.b) are plotted for bulk GNP/, 4GNP/, GO/, and FGO/epoxy together for various aspect ratio at 1.0 wt% of the nanoplatelets content. The volume fraction (vol%) for each nanoplatelet is also provided as there is a slight difference between them. The minor variation in the nanoplatelets volume fraction can be attributed to the number of atoms, chemical composition, and wrinkled morphology in each case. Clearly, the best response can be observed for the bulk GNP/epoxy nanocomposite which has the perfect dispersion of the intact GNP in matrix. The bulk 4GNP/epoxy exhibits a consistent lower response relative to the bulk GNP/epoxy which is attributed to the lower dispersion level with the 4GNP. However, the difference is likely to be decreased at aspect ratio values

larger than 10^4. Both FGO/epoxy and GO/epoxy bulks exhibit nearly identical response with FGO/epoxy in the lead. Increasing the aspect ratio involved approximately insignificant improvement in the mechanical response. This can be mainly attributed to the detrimental effect of the high concentration of oxygen introduced to the GNP as discussed previously. However, their mechanical response is comparable with the bulk 4GNP/epoxy response at aspect ratio values below 200. Considering the perfect dispersion of the current specific case studies, the GNP/epoxy composite response can be assumed as the ideal case or the upper bound of the mechanical response. However, the FGO/epoxy or GO/epoxy can be assumed as the lower bound of the mechanical response. That is, GO and FGO nanoplatelets with lower oxygen concentrations are expected to exhibit better mechanical response. Finally, a general indication that can be extracted from the current predictions refers to an improvement in the predicted elastic modulus with increasing the nanoplatelet content and its aspect ratio.

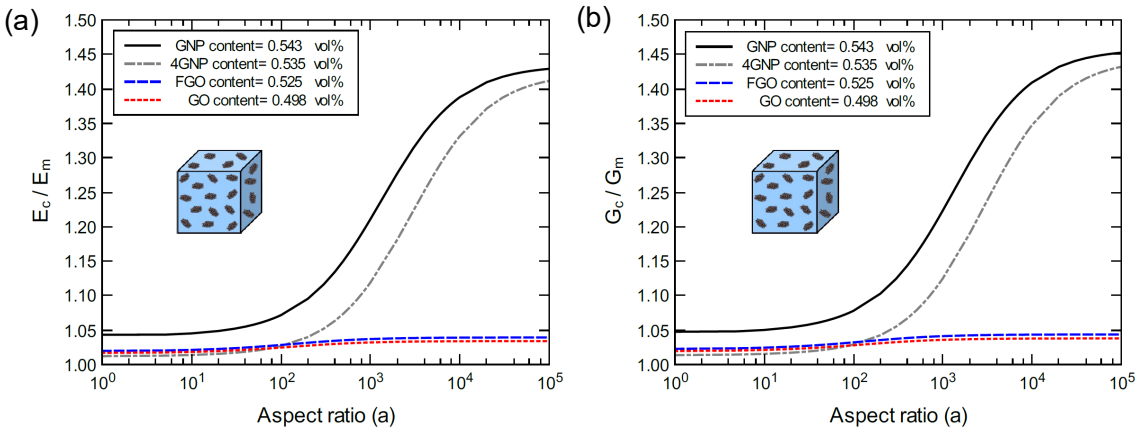

Figure 3.21: Normalized elastic modulus (a) and shear modulus (b) for bulk GNP/, 4GNP/, GO/, and FGO/epoxy for various aspect ratio values and at 1.0 wt% of the nanoplatelets content.

3.5 Summary and Conclusions

A multiscale computational approach has been performed to assess the mechanical performance of aerospace epoxy material reinforced with functionalized GNP. A single layer of GNP was initially modeled using MD to represent the pristine nanoplatelet of graphene and then modified to create a highly concentrated graphene oxide (GO) nanoplatelet and functionalized graphene oxide (FGO) nanoplatelet. For the first time, the functionalized GNP samples were modeled based on experimental measurements of which functional groups were presented and were experimentally informed. The three nanoplatelets were used to reinforce the epoxy matrix (DGEBA-DETDA epoxy system) and generate three MD models of nanoplatelet/epoxy nanocomposites. These MD models were used to predict the localized mechanical properties of the interphase region.

The outcome at the nanoscale level indicated a significant degradation in the reinforcing effect of the GO and FGO relative to the pristine GNP. The weakness in the mechanical performance of GO and FGO originated from the alteration in the carbon lattice structure of GNP from its robust sp^2 structure to a weak sp^3 structure. As a result, the FGO/epoxy and GO/epoxy MD models exhibited a significant weaker mechanical response relative to GNP/epoxy. For instance, introducing the large amount of oxygen groups to the GNP surface resulted in an in-plane elastic and shear moduli of GO/epoxy MD model less than that for GNP/epoxy MD model by -89.25% and -74.42%, respectively. On the other hand, the surface roughness and wrinkled morphology of GO and FGO were found to improve the interlocking mechanism with the hosting matrix which led to an improvement in the interfacial interaction/adhesion. As a result, the out-of-plane shear modulus involved a tremendous improvement which increased by 15.45 times for GO/epoxy and by 19.52 times for FGO/epoxy relative to the GNP/epoxy.

The predicted mechanical properties at the nanoscale level were then further processed using micromechanics to predict the mechanical response of the nanocomposites at the bulk level for various nanoplatelets content and aspect ratio values. The mechanical response of the 4-layer GNP/epoxy (4GNP/epoxy) bulk nanocomposite, which was modeled in Chapter 2, was included in the comparison study to represent a certain level of GNP dispersion. Despite the diversity in the factors which could potentially impact the mechanical response of the nanocomposites, such as; the nanoplatelets agglomeration, content, aspect ratio, and their chemical composition, the current work predictions were in a good agreement with the experimental results available from the literature. Providing the predicted mechanical properties at the bulk level, a remarkable observation refers to an improvement in the mechanical response of the nanocomposites with increasing the nanoplatelets content and aspect ratio.

The optimum mechanical response was observed for the bulk GNP/epoxy nanocomposite. This can be attributed to the perfect dispersion of the intact and strong graphene nanosheets within the hosting matrix. The mechanical response of the 4GNP/epoxy involved a similar trend relative to the GNP/epoxy, yet it was lower due to the agglomeration effect. In fact, increasing the number of graphene layers within the GNP crystal imitates higher agglomeration levels of GNP within the matrix. This reduces the effective aspect ratio of the GNP crystal and leads to more deterioration in the mechanical response of the nanocomposite. Considering the GNP surface functionalization influence, it has been found to preserve high levels of GNP dispersion within the epoxy matrix. Meanwhile, the high concentrations of oxygen groups resulted in a significant degradation in the reinforcing function of GO and FGO. According to the predictions of the particular case studies modeled in this work, the mechanical response of the pristine GNP/epoxy can be assumed as the upper bound limit. However, the mechanical response of GO/epoxy and FGO/epoxy can be assumed as the lower bound limit. Any other cases of GNP with oxygen concentration lower than that used herein is expected to register a mechanical response between the designated upper and lower bound limits.

The current work predictions indicate that the bulk GO/epoxy and FGO/epoxy can produce a comparable mechanical response to the bulk GNP/epoxy and 4GNP/epoxy at low nanoplatelets content and low nanoplatelets aspect ratio. At larger nanoplatelets content and aspect ratio values, however, the detrimental effect of the oxygen and

functional groups on the GNP strength predominates the overall mechanical response. Thus, performing such computational studies can be utilized to optimize the overall mechanical response of such nanocomposite materials through manipulating and adjusting the wide range of the controlling factors and key processing parameters.

Chapter 4

MICRO/MACRO MECHANICS ANALYSIS OF HYBRID COMPOSITE PLATES AND LAMINATED HYBRID COMPOSITE PANELS

This chapter focuses on the micro/macro mechanics analysis of CF/nanoplatelet/epoxy hybrid composites. The predicted mechanical properties are considered for unidirectional CF/nanoplatelet/epoxy hybrid composite plates and three different configurations of laminated CF/nanoplatelet/epoxy hybrid composite panels. The reinforcing effect of the four nanoplatelet types (4GNP, GNP, GO, FGO) is also considered in the predictions.

4.1 Introduction

Owing to their high strength and rigidity, in addition to the superior corrosion and fatigue resistance, CFs have been commonly used to reinforce the polymer-based composites. Such composites have been utilized in constructing strong and lightweight structural components for aerospace, automotive, marine, offshore, and civil infrastructure applications [42, 99, 100]. For composite materials to be used in aircraft structural components, the CF volume content can be more than 50%. The typical CF volume content is between 55% and 65%, however, 70% is the maximum possible content that can be achieved [6]. The reinforcing effect of unidirectional distribution/arrangement of CF in polymer composites is limited to the axial direction of the composite lamina. Therefore, adding carbon nanofillers (such as GNP and CNT) to the matrix are used to improve the mechanical performance of the lamina in the transverse direction [9, 46]. In light of that, this chapter involves developing a computational approach to model and predict the mechanical properties of unidirectional CF/nanoplatelet/epoxy hybrid composite plates and three different arrangements of laminated hybrid composite panels.

4.2 Micromechanics Modeling of Hybrid Composites

Figure 4.1 shows the modeling workflow used to generate different configurations of laminated hybrid composites. The hybrid composite modeling scheme utilized the ultimate predictions from the multiscale modeling workflow given in Chapter 3. Specifically, the nanoplatelet/epoxy homogenized mechanical properties predicted at the bulk level of the nanocomposite (Figure 3.9.c or Figure 4.1.a) were imposed as the matrix in a second MAC/GMC 4.0 script to generate the CF/nanoplatelet/epoxy hybrid composite. Figure 4.1.b shows the built-in RUC (ARCHID=13) of a 26 × 26 circular array which was selected to represent the CF architecture within the nanocomposite matrix. The mechanical properties of AS4 CF given in Table 2.2 were utilized to represent the fiber subcell in the RUC. Figure 4.1.c shows representative sketches of the unidirectional and cross-ply laminate hybrid composites.

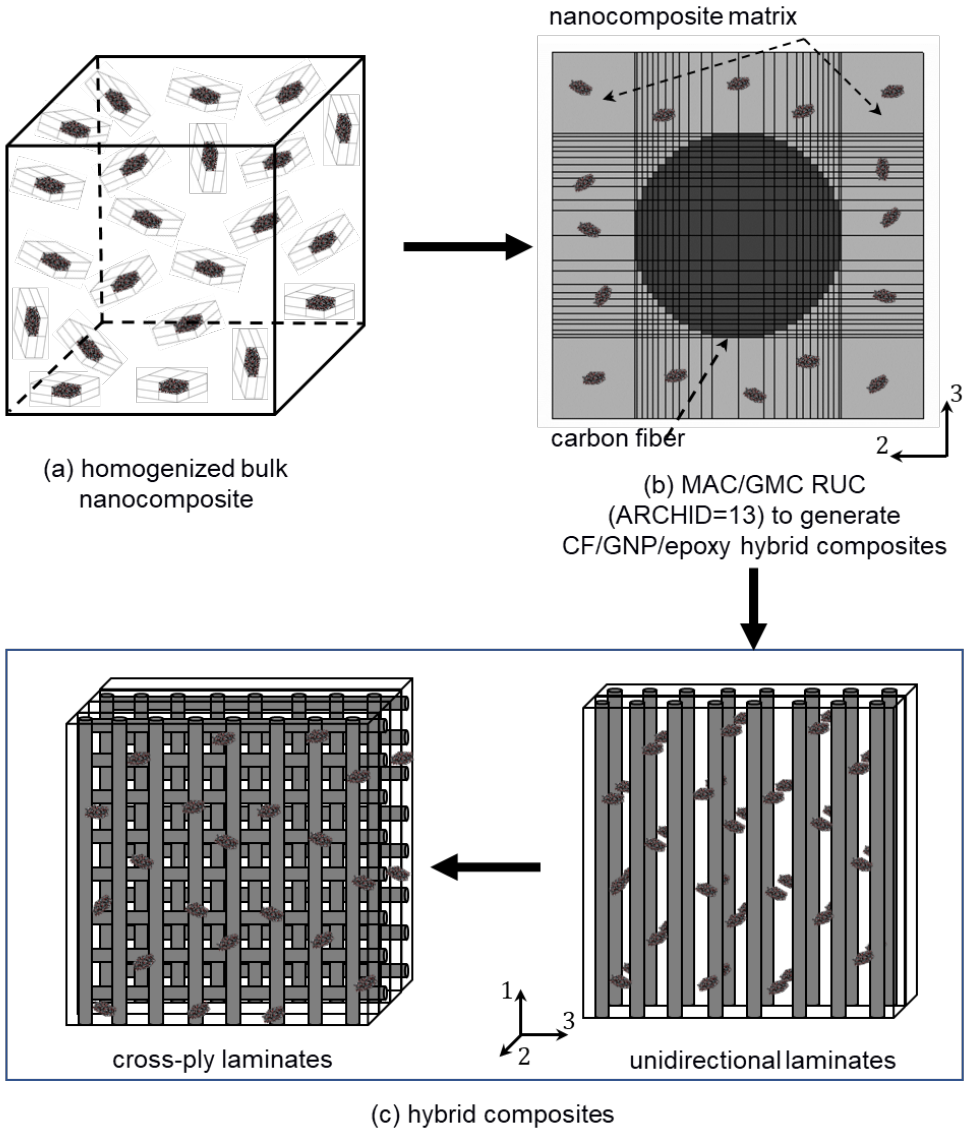

Figure 4.1: Modeling workflow of CF/nanoplatelet/epoxy hybrid composites (microscale/macroscale).

4.3 Results and Discussions

The modeling approach for hybrid composites has been applied and validated previously in Chapter 2 for the 4-layer GNP/epoxy nanocomposite reinforced with unidirectional CF. Accordingly, the predicted mechanical properties of the unidirectional CF/nanoplatelet/epoxy hybrid composites and three different configurations of laminated hybrid composite panels are described and discussed in this section. The reinforcing effect of CF based on its volume fraction (content), and of GNP based on the nanoplatelet content, dispersion, aspect ratio, and functionality are extensively explored in this section. Note that all the micromechanics modeling and predictions were performed at room temperature.

4.3.1 Unidirectional CF/Nanoplatelet/Epoxy Hybrid Composites

Figure 4.2 shows the predicted axial (E_{11}), transverse (E_{22}= E_{33}), and shear (G_{12}, G_{23}) moduli of unidirectional CF/GNP/Epoxy hybrid composite. Generally, there is an improvement in the mechanical response as either the GNP content or its aspect ratio was increased. The reinforcing degree, however, is governed by the direction of the measured mechanical property.

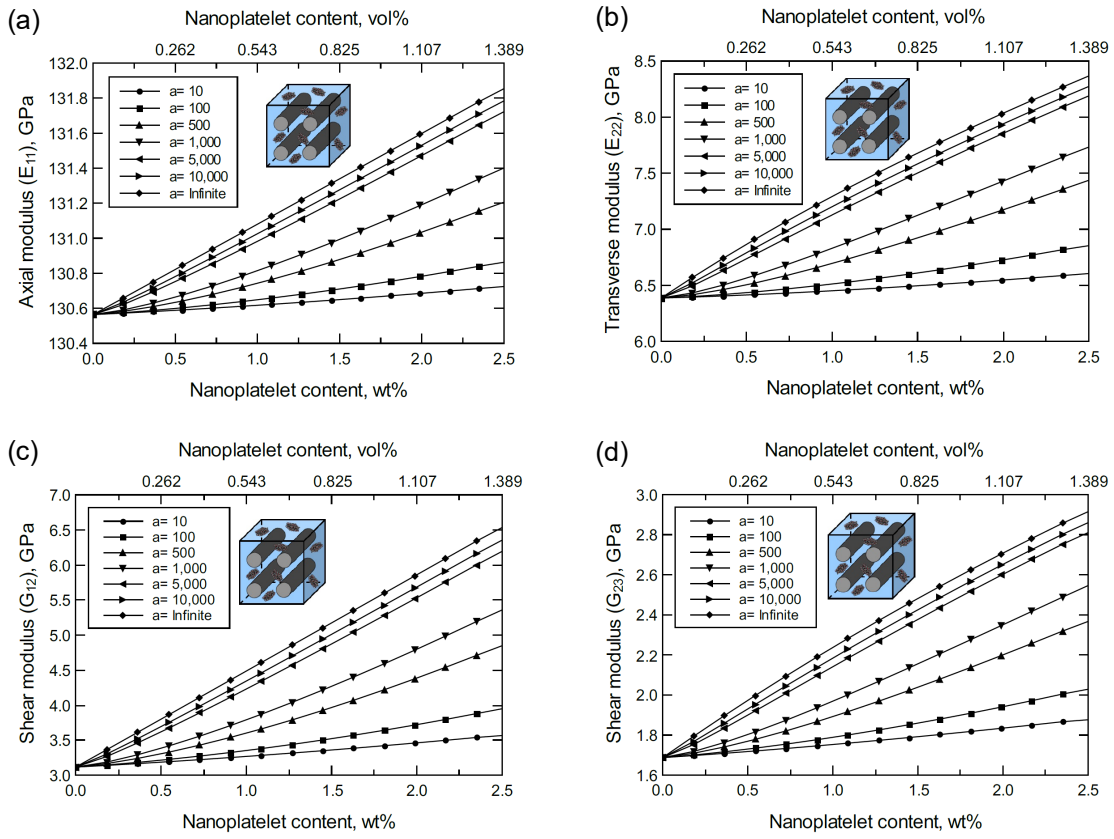

Figure 4.2: Predicted elastic and shear moduli of unidirectional CF/GNP/epoxy for various nanoplatelets content and aspect ratio values; (a) Axial elastic modulus E_{11}, (b) Transverse elastic modulus E_{22}, (c) Shear modulus G_{12}, (d) Shear modulus G_{23}. The volume fraction of CF is 56%.

To obtain the reinforcing effect of the GNP on each mechanical property of the hybrid composite, the mechanical properties were normalized and plotted together in one graph. For the reinforcing effect caused by increasing the GNP aspect ratio, Figure 4.3.a shows the normalized E_{11}, E_{22}, G_{12}, and G_{23} predicted at 1.0 wt% of GNP content. For the reinforcing effect caused by increasing the GNP content, Figure 4.3.b shows the normalized predicted mechanical properties at 10^3 GNP aspect ratio. Note that the mechanical properties in both cases were predicted at 56% of CF volume fraction. Clearly, the best improvement can be observed in the shear moduli with $G_{12} > G_{23}$. Meanwhile, E_{11}

involves trivial improvement relative to E_{22} due to the predomination of CF reinforcing effect along the axial direction. As a result, an overall order of the reinforcing effect of the GNP on the mechanical properties can be written as; the improvement in $G_{12} > G_{23} > E_{22} > E_{11}$.

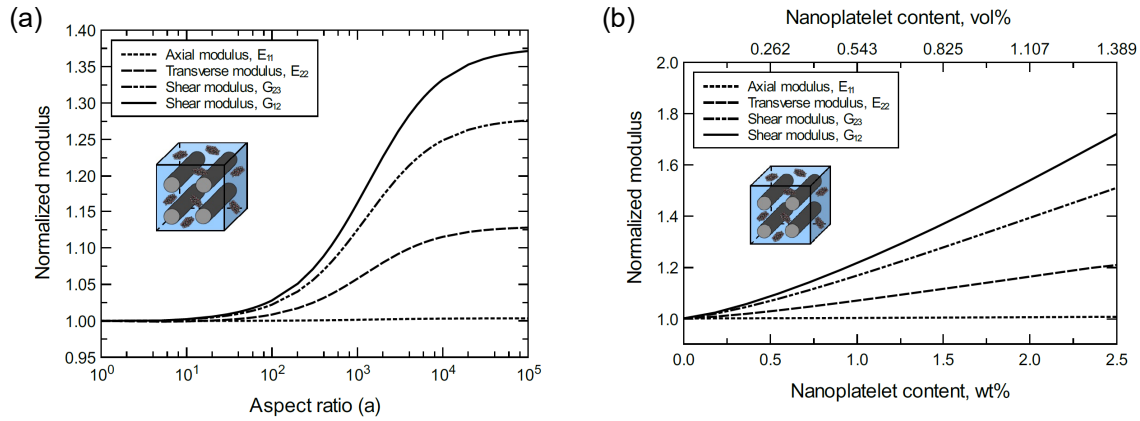

Figure 4.3: Normalized elastic and shear moduli for unidirectional CF/GNP/epoxy; (a) at 1.0 wt% of GNP content and various GNP aspect ratio, (b) at 10^3 GNP aspect ratio and various GNP content. The volume fraction of CF is 56%.

At a certain lower level of GNP dispersion, the mechanical response of unidirectional CF/4GNP/epoxy hybrid composite exhibits a similar trend to that observed for the unidirectional CF/GNP/epoxy. Figure 4.4 shows an improvement in the predicted E_{11}, E_{22}, G_{12}, and G_{23} moduli of the unidirectional CF/4GNP/Epoxy hybrid composite as either the 4GNP content or its aspect ratio was increased. The normalized mechanical properties predicted at 1.0 wt% of the 4GNP content and for various values of its aspect ratio are shown in Figure 4.5.a. Meanwhile, Figure 4.5.b exhibits the normalized mechanical properties predicted at 10^3 as the aspect ratio of the 4GNP and for various values of its content. Once again, the reinforcing effect of the 4GNP on G_{12} surpasses that on G_{23} while both exceed the observed reinforcing effect of 4GNP on E_{22}. However, the improvement in E_{22} is greater than that in E_{11} which involved insignificant (trivial) improvement as its value is dominated by the reinforcing effect of CF.

Figures 4.6-4.9 show the mechanical response of unidirectional CF/GO/epoxy and unidirectional CF/FGO/epoxy hybrid composites. Even though the FGO reinforced hybrid composite indicates slightly better mechanical response relative to the GO reinforced hybrid composite, both hybrid composites involved a limited improvement in the mechanical properties with increasing the nanoplatelet content and its aspect ratio. The improvement range for the hybrid composite reinforced with GO or FGO is very small in comparison to the hybrid composite reinforced with GNP or 4GNP. Yet, similar trends can be observed when comparing the reinforcing effect on each mechanical property. That is, the trend of reinforcing effect of GO or FGO on the mechanical properties is similar to that

observed for GNP or 4GNP, where the improvement in $G_{12} > G_{23} > E_{22} > E_{11}$ as shown in Figure 4.7 and Figure 4.9, respectively.

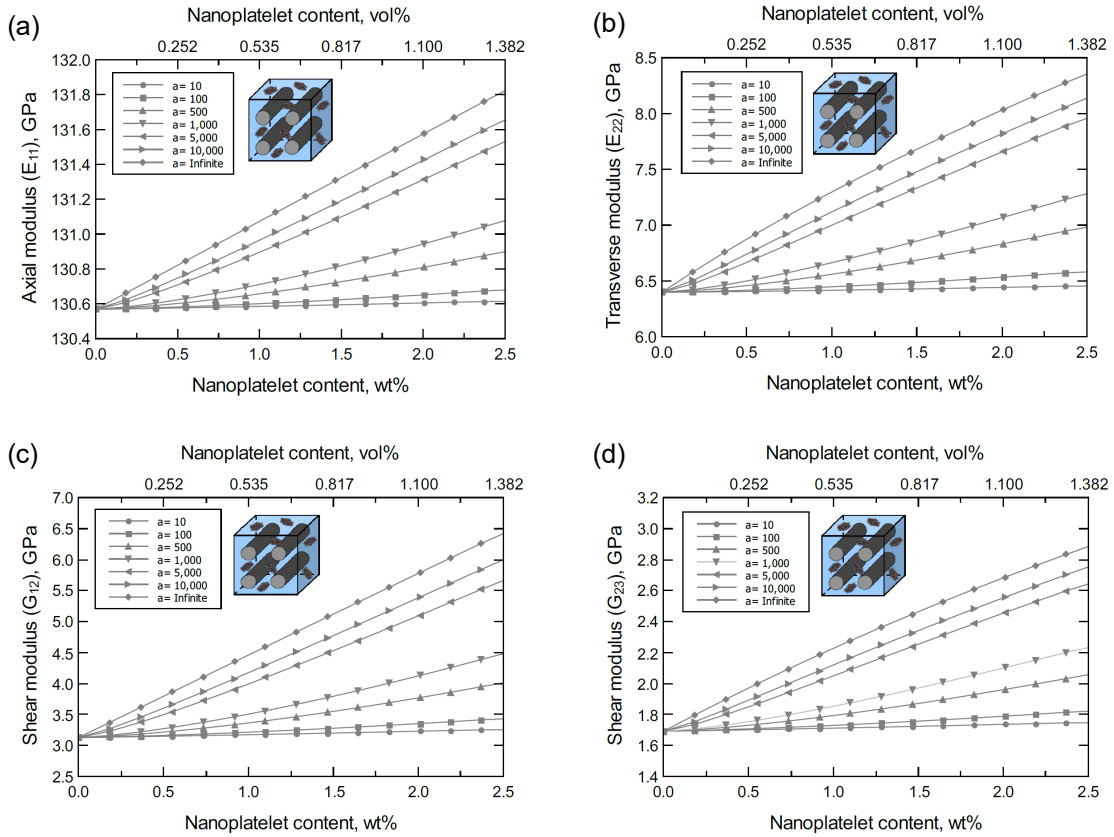

Figure 4.4: Predicted elastic and shear moduli of unidirectional CF/4GNP/epoxy for various nanoplatelets content and aspect ratio values; (a) Axial elastic modulus E_{11}, (b) Transverse elastic modulus E_{22}, (c) Shear modulus G_{12}, (d) Shear modulus G_{23}. The volume fraction of CF is 56%.

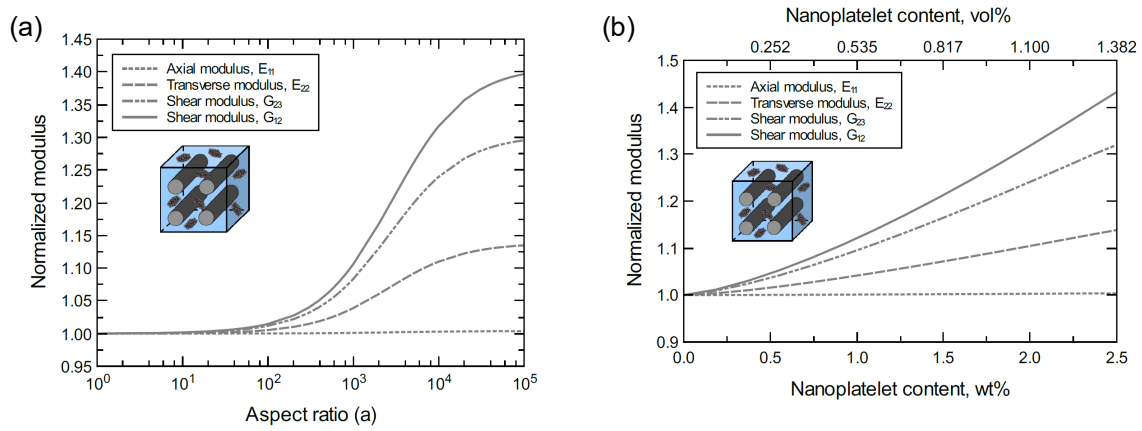

Figure 4.5: Normalized elastic and shear moduli for unidirectional CF/4GNP/epoxy; (a) at 1.0 wt% of 4GNP content and various 4GNP aspect ratio, (b) at 10^3 4GNP aspect ratio and various 4GNP content. The volume fraction of CF is 56%.

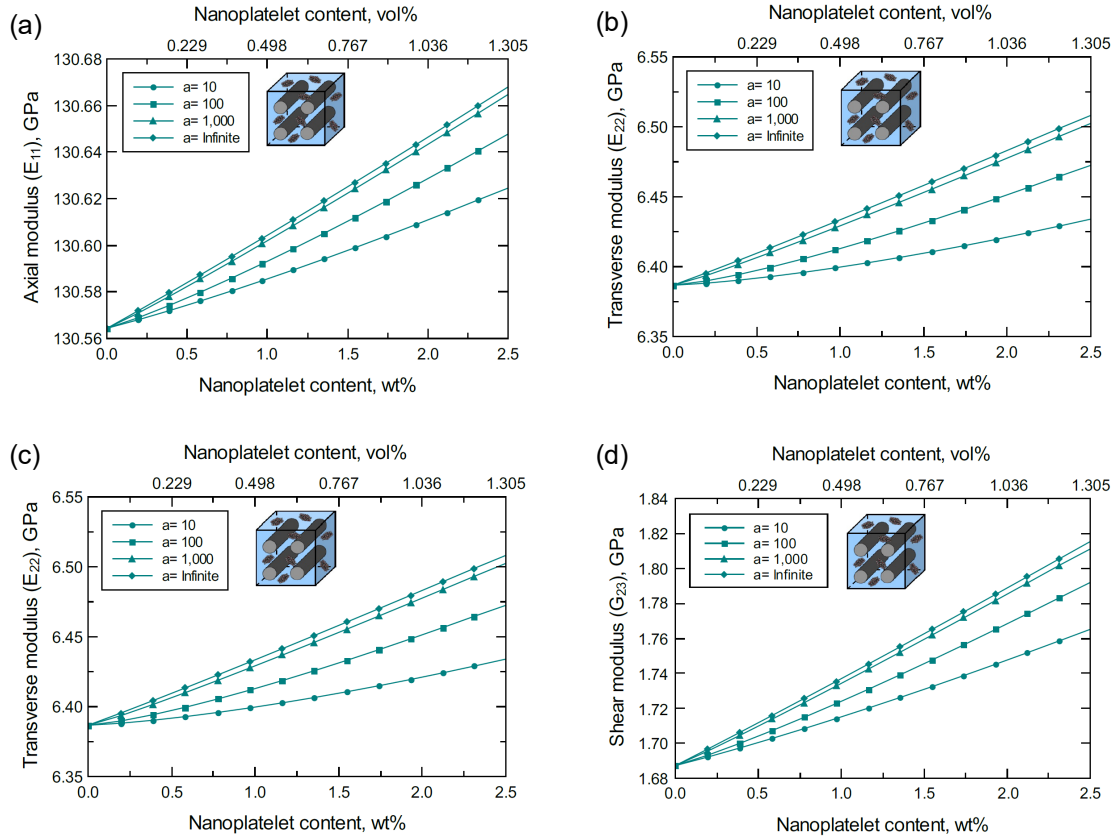

Figure 4.6: Predicted elastic and shear moduli of unidirectional CF/GO/epoxy for various nanoplatelets content and aspect ratio values; (a) Axial elastic modulus E_{11}, (b) Transverse elastic modulus E_{22}, (c) Shear modulus G_{12}, (d) Shear modulus G_{23}. The volume fraction of CF is 56%.

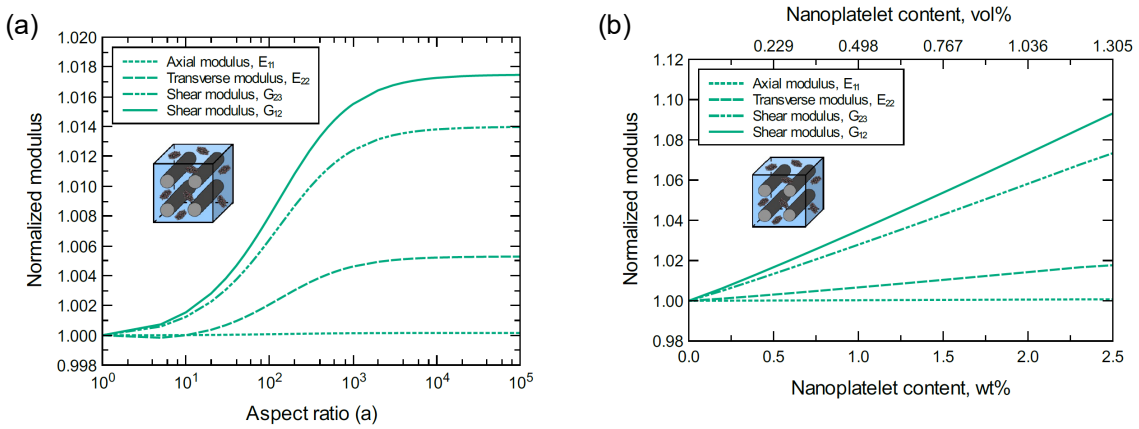

Figure 4.7: Normalized elastic and shear moduli for unidirectional CF/GO/epoxy; (a) at 1.0 wt% of GO content and various GO aspect ratio, (b) at 10^3 GO aspect ratio and various GO content. The volume fraction of CF is 56%.

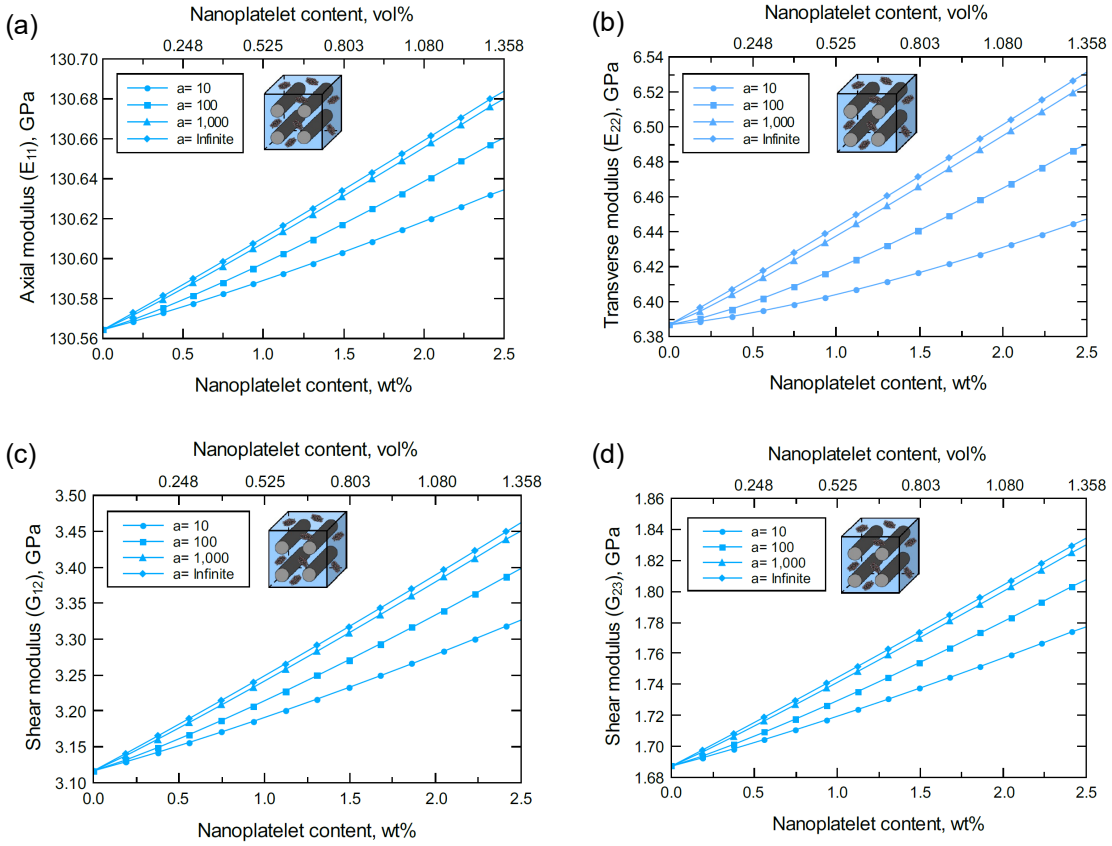

Figure 4.8: Predicted elastic and shear moduli of unidirectional CF/FGO/epoxy for various nanoplatelets content and aspect ratio values; (a) Axial elastic modulus E_{11}, (b) Transverse elastic modulus E_{22}, (c) Shear modulus G_{12}, (d) Shear modulus G_{23}. The volume fraction of CF is 56%.

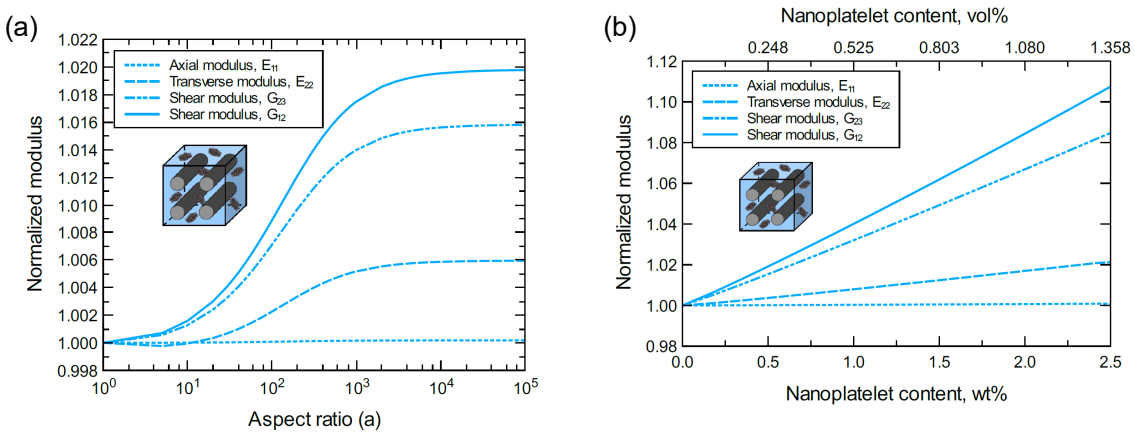

Figure 4.9: Normalized elastic and shear moduli for unidirectional CF/FGO/epoxy; (a) at 1.0 wt% of FGO content and various FGO aspect ratio, (b) at 10^3 FGO aspect ratio and various FGO content. The volume fraction of CF is 56%.

Figure 4.10 shows four sets of plots to separately compare the improvement in each mechanical property based on the hybrid composite type. These plots provide an evaluation of the reinforcing effect of the nanoplatelets on each mechanical property. Each set of plots provides the response of a specific mechanical property obtained at 1.0 wt% of the nanoplatelets content for various aspect ratio and at 10^3 aspect ratio for various nanoplatelets content. To emphasize the reinforcing effect, each predicted mechanical property was normalized by its initial magnitude. In general, the reinforcing effect of GNP is the highest among the other nanoplatelets. While the reinforcing effect of the 4GNP is slightly lower than that of GNP, FGO followed by GO have the lowest reinforcing effect. This is true for aspect ratio range 10^2-10^4. For aspect ratio values less than 10^2, which is most common to be observed in nanocomposites, all the nanoplatelet types involve a comparable reinforcing function. Interestingly, at very high aspect ratio (>10^4) the reinforcing effect of 4GNP can surpass that of GNP. That is, the larger the GNP aspect ratio, the lower the detrimental effect of agglomeration.

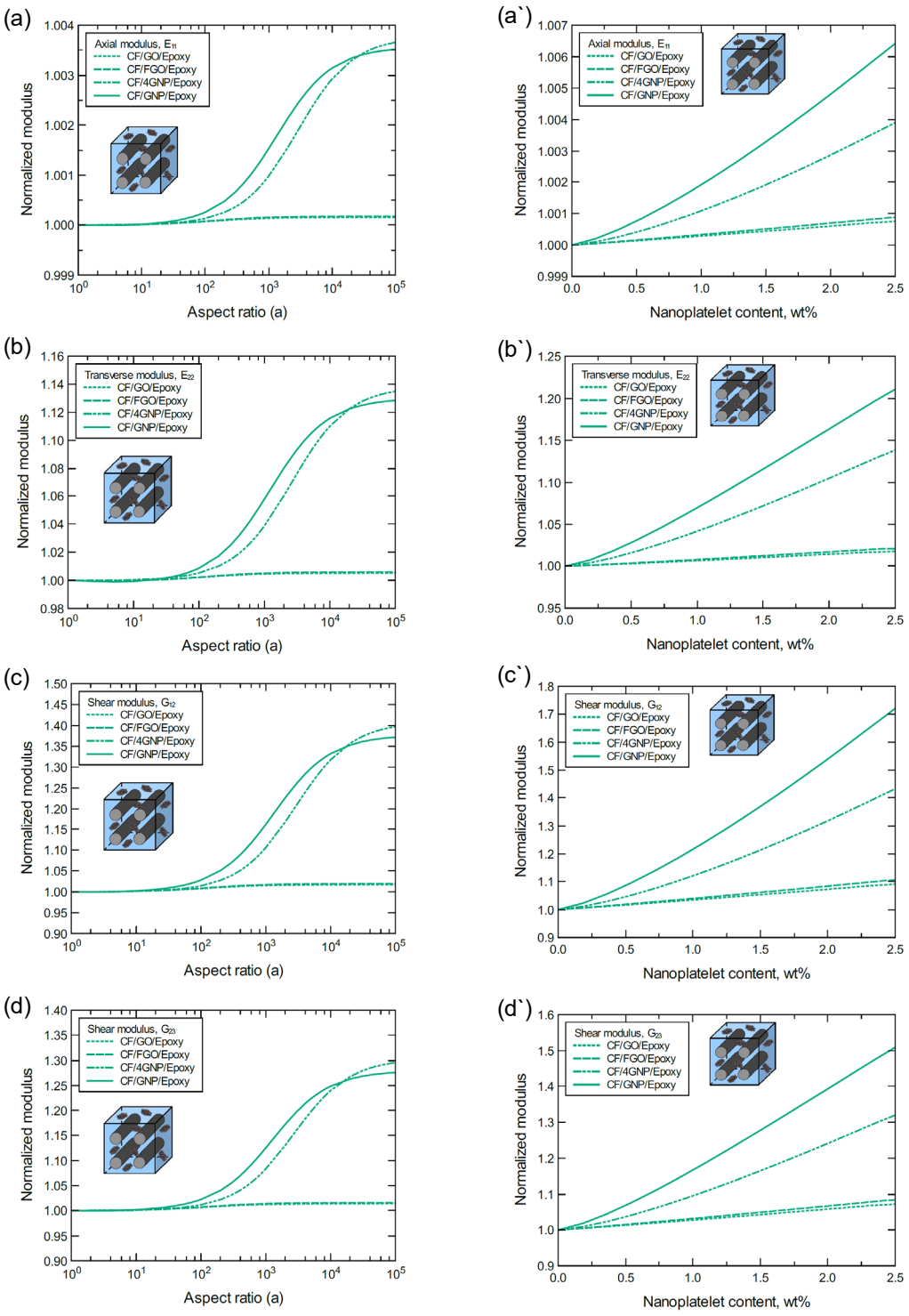

Figure 4.10: The reinforcing effect of nanoplatelets on the predicted mechanical properties for the hybrid composites; (a-d) at 1.0 wt% of the nanoplatelets content for various aspect ratio values, (a`-d`) at 10^3 aspect ratio of the nanoplatelet for various nanoplatelets content. The volume fraction of CF is 56%.

Figures 4.11-4.14 show design map plots of unidirectional CF/nanoplatelet/epoxy hybrid composites which can be used to optimize the axial and transverse moduli by controlling the CF volume fraction (vol%) and the nanoplatelets content (wt%). The design map graphs were also plotted for different values of nanoplatelet aspect ratio which represents an additional factor to optimize the mechanical response. Generally, the plots reveal that both CF and the nanoplatelets have a tremendous impact on the elastic response of the hybrid composite. More specifically, CF shows a direct impact on the axial modulus of the hybrid composite which significantly increases with increasing the CF vol%. A limited contribution to the improvement in the axial modulus can be attributed to the nanoplatelet content and its aspect ratio. Whereas, the improvement in the transverse modulus of the hybrid composite is largely dominated by the nanoplatelet content and its aspect ratio.

Due to the domination of CF on the axial modulus of the hybrid composite, the improvement trend in the axial modulus associated with the CF vol% is nearly determined across the four types of hybrid composites. However, different improvement levels in the transverse modulus can be observed in each case depending on the nanoplatelet type, content, and its aspect ratio. The best improvement levels in the transverse modulus are registered for the unidirectional CF/GNP/epoxy hybrid composite (Figure 4.11). This is attributed to the aforementioned ideal circumstances of modeling bulk GNP/epoxy nanocomposite. The agglomeration in 4GNP resulted in an implicitly negative effect on the nanoplatelets dispersion and their effective aspect ratio. Therefore, the unidirectional CF/4GNP/epoxy involved lower improvement levels in the transverse modulus (Figure 4.12) relative to the unidirectional CF/GNP/epoxy (Figure 4.11). Finally, the improvement levels in the transverse modulus of unidirectional CF/GO/epoxy (Figure 4.13) and CF/FGO/epoxy (Figure 4.14) are limited with the later hybrid composite being slightly in the lead. As discussed above, this is mainly attributed to the weak mechanical performance of GO and FGO nanoplatelets relative to the pristine GNP which is mainly attributed to the large oxygen content. Thus, the limited reinforcing effect of GO and FGO resulted in relatively short ranges of improvement in the transverse modulus of their hybrid composites as the nanoplatelets content and aspect ratio were increased.

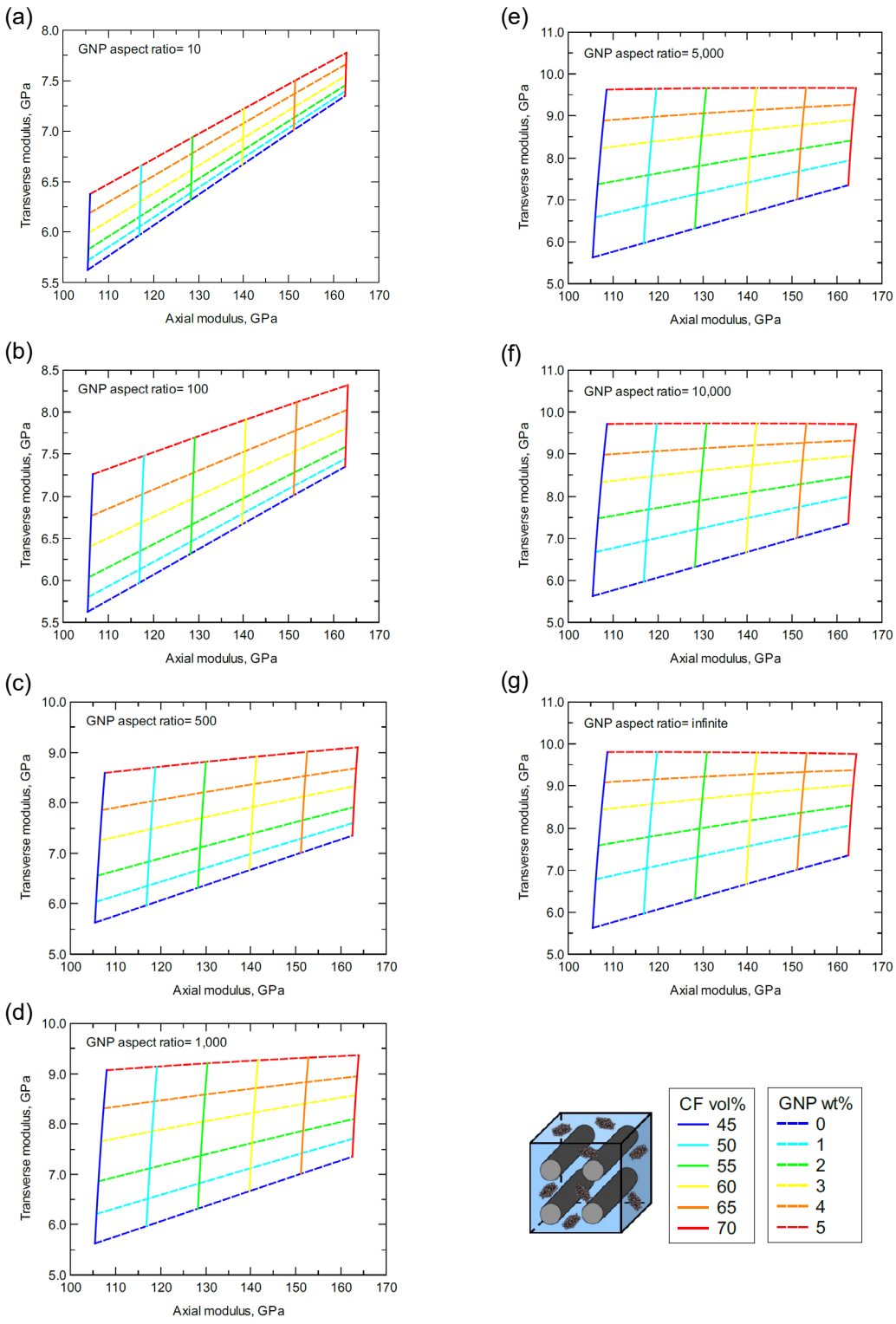

Figure 4.11: Predicted axial and transverse moduli of unidirectional CF/GNP/epoxy at different; CF volume fraction (vol%), GNP content (wt%), and GNP aspect ratio values.

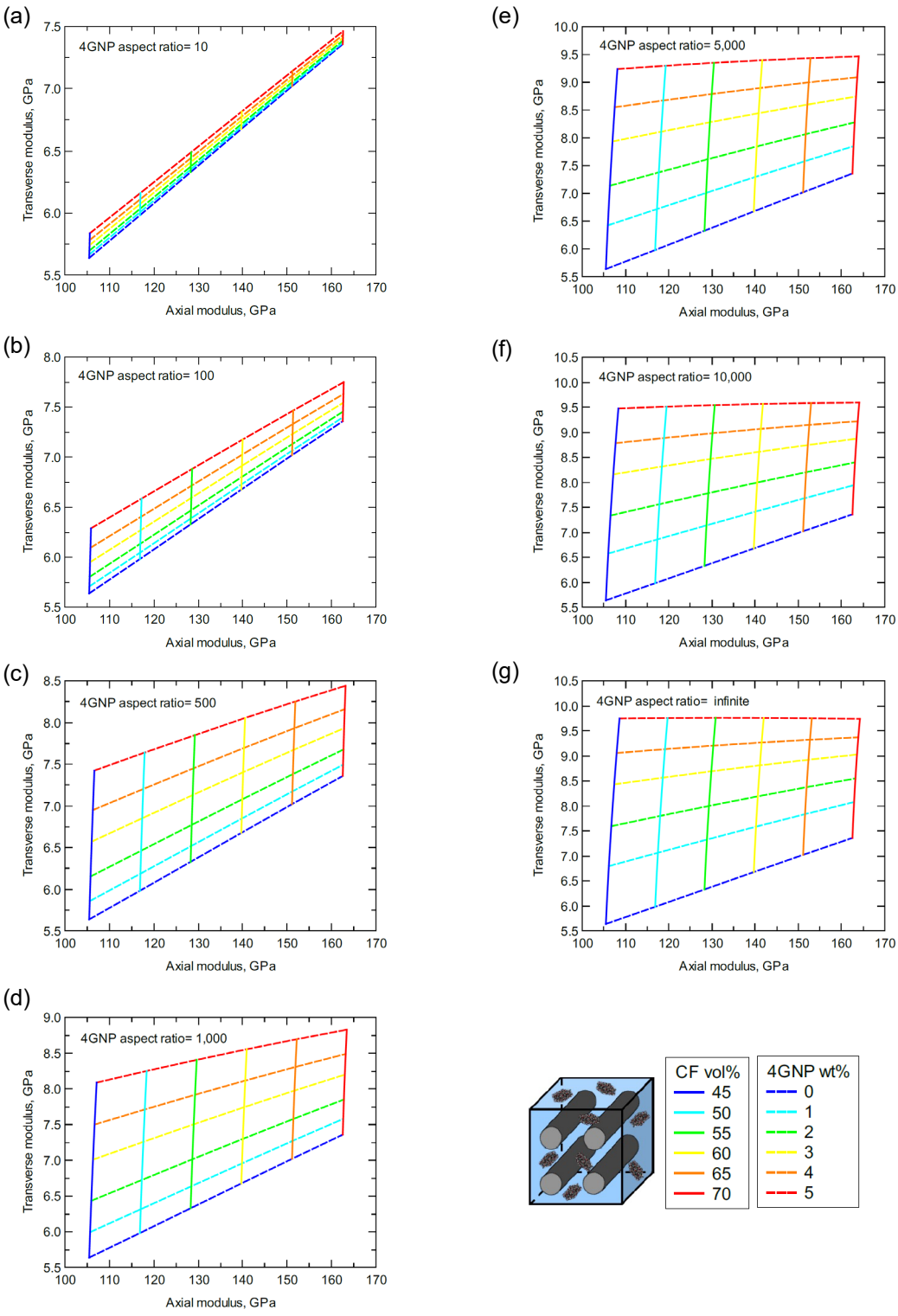

Figure 4.12: Predicted axial and transverse moduli of unidirectional CF/4GNP/epoxy at different; CF volume fraction (vol%), 4GNP content (wt%), and 4GNP aspect ratio values.

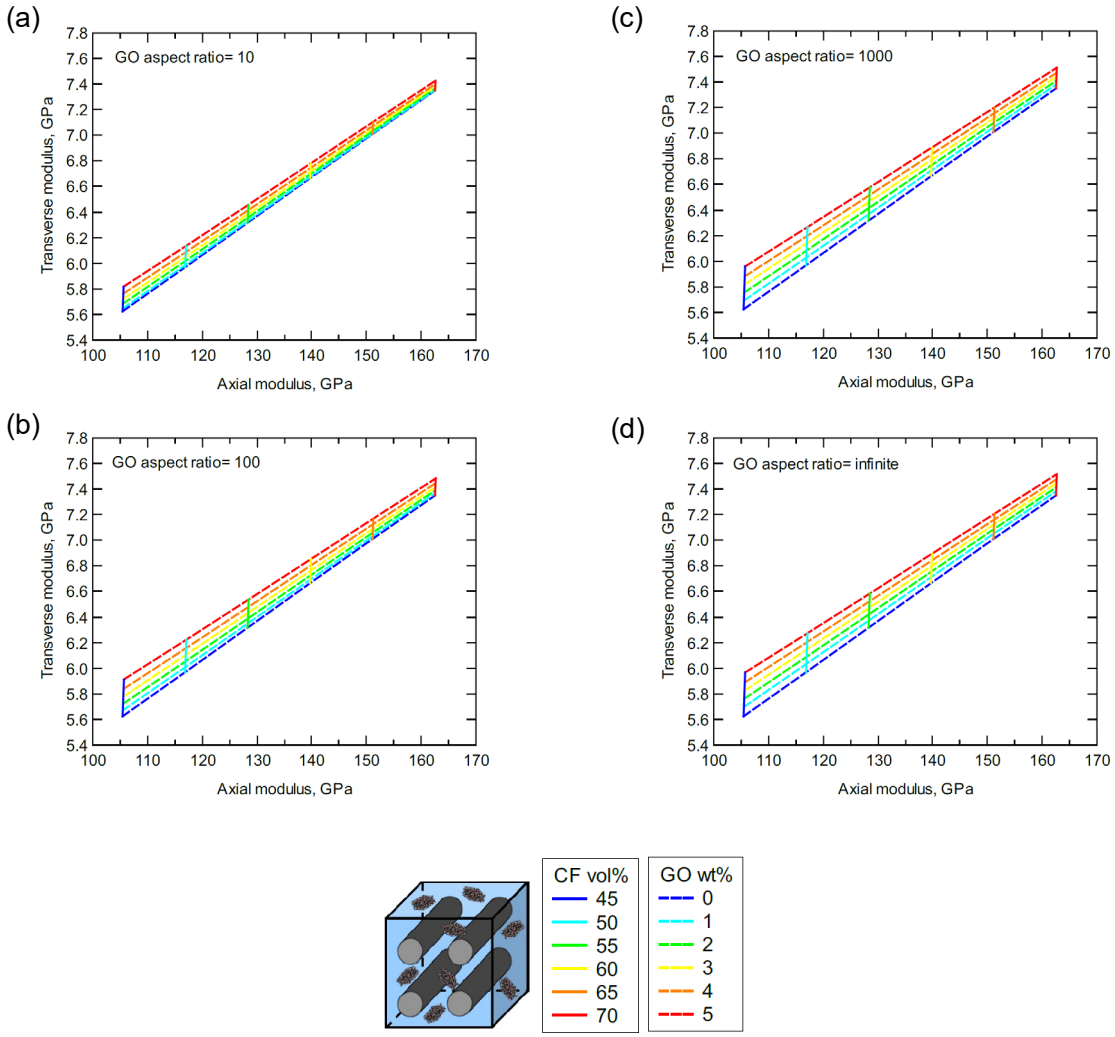

Figure 4.13: Predicted axial and transverse moduli of unidirectional CF/GO/epoxy at different; CF volume fraction (vol%), GO content (wt%), and GO aspect ratio values.

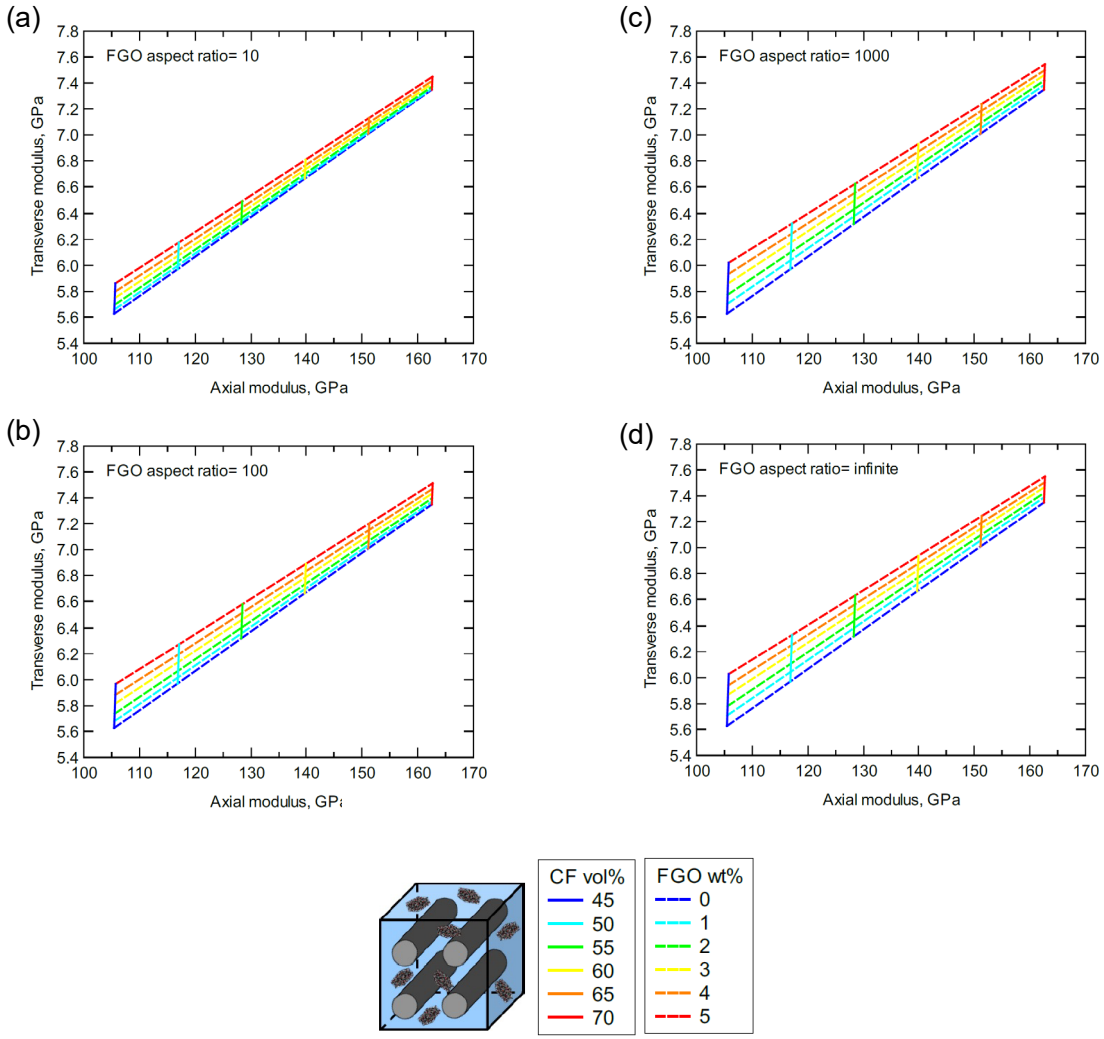

Figure 4.14: Predicted axial and transverse moduli of unidirectional CF/FGO/epoxy at different; CF volume fraction (vol%), FGO content (wt%), and FGO aspect ratio values

4.3.2 Laminated Hybrid Composite Panels

The mechanical response of three different stacking configurations of laminated CF/nanoplatelet/epoxy hybrid composite panels is explored. The stacking order for each laminated composite panel is given as;

- Symmetric balanced cross-ply laminated composite panel (8 layers)
  [0/90/0/90/90/0/90/0] ≡ [0/90/0/90]s ≡ CP-8
- Symmetric balanced angle-ply laminated composite panel (8 layers)
  [45/0/-45/90/90/-45/0/45] ≡ [45/0/-45/90]s ≡ AP-8
- Symmetric balanced angle-ply laminated composite panel (6 layers)
  [60/-60/0/0/-60/60] ≡ [60/-60/0]s ≡ AP-6

Note that each lamina in the laminated composite panel has a thickness of 0.25 mm, and the CF volume fraction is 56%. Figures 4.15-4.17 show the predicted mechanical properties of the three proposed laminated composite panels constructed using the CF/GNP/epoxy hybrid composite. Generally, there is an improvement in the mechanical response as the predicted mechanical properties exhibit an increase with increasing the GNP content and its aspect ratio. Note the coupling stiffness (B_{11}) for symmetric balanced laminated composite panels is always zero. Also, the in-plane elastic moduli E_{xx} and E_{yy} are identical due to the symmetry in laminating order. While the cross-ply composite panel exhibits a slight increase in its Poisson's ratio with GNP content and aspect ratio, both angle-ply composite panels show a slight decrease. In all cases, however, the variation in the laminated panel contraction is very limited and can be ignored. Likewise, the predicted mechanical properties of the laminated composite panels using the CF/4GNP/epoxy hybrid composite are shown in Figures 4.18-4.20. Due to the certain level of agglomeration in 4GNP relative to perfect dispersion in GNP (previously discussed), lower improvement levels in the mechanical properties can be observed for the laminated composite panels constructed using CF/4GNP/epoxy relative to that constructed using CF/GNP/epoxy. Both CF/GO/epoxy (Figures 4.21-4.23) and CF/FGO/epoxy (Figures 4.24-4.26) laminated composite panels exhibit nearly identical mechanical response. Referring to the low mechanical performance of functionalized nanoplatelets (previously discussed), the improvement in the predicted mechanical properties of the laminated composite panels constructed using functionalized GNP is limited in comparison to those constructed using pristine GNP.

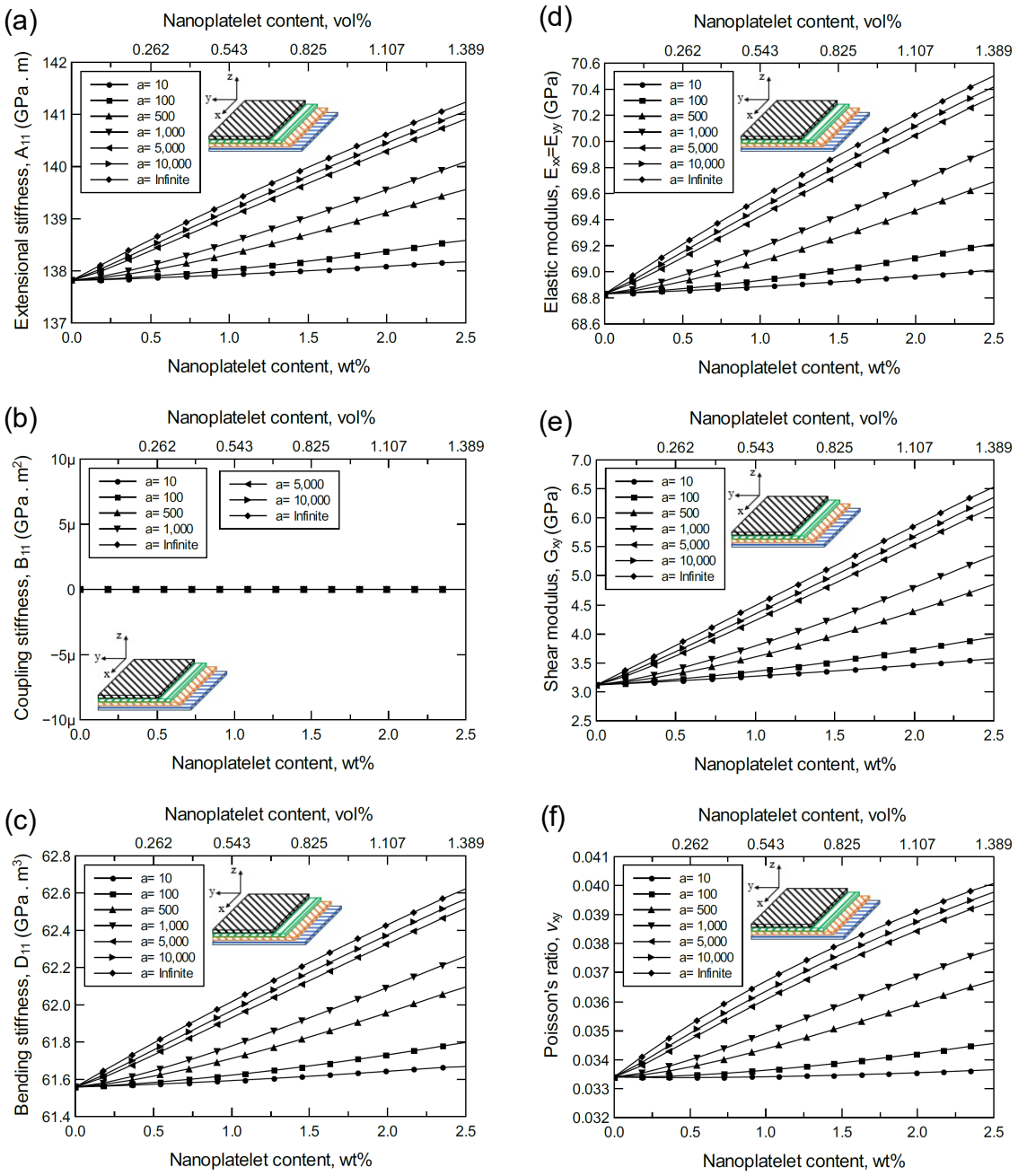

Figure 4.15: Predicted mechanical properties of laminated CF/GNP/epoxy, a symmetric balanced cross-ply laminated composite panel [0/90/0/90]s ≡ CP-8; (a) Extensional stiffness, A_{11}; (b) Coupling stiffness, B_{11}; (c) Bending stiffness, D_{11}; (d) Elastic modulus, $E_{xx}= E_{yy}$; (e) Shear modulus, G_{xy}; (f) Poisson's ratio, ν_{xy}. The volume fraction of CF is 56%.

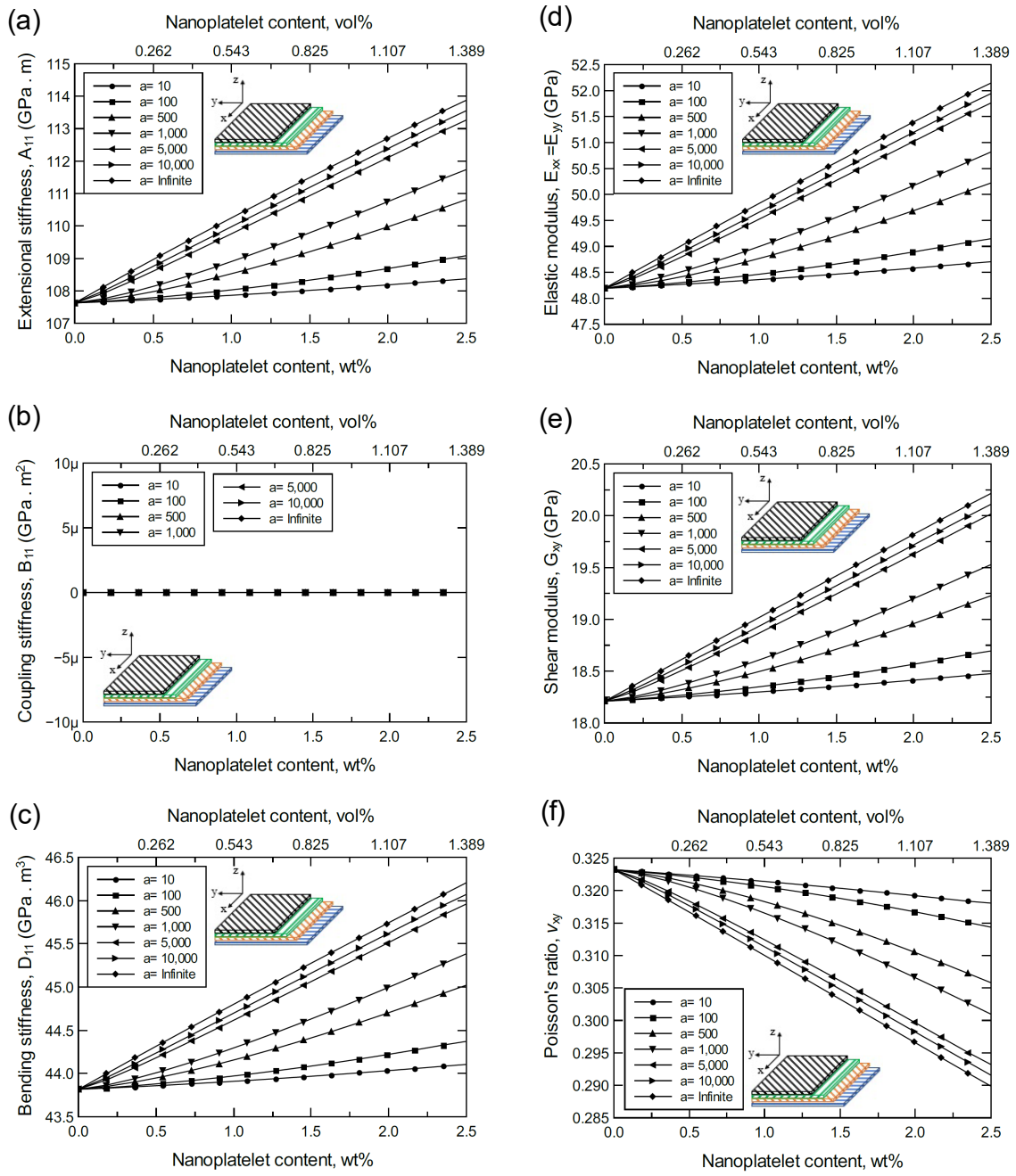

Figure 4.16: Predicted mechanical properties of laminated CF/GNP/epoxy, a symmetric balanced angle-ply laminated composite panel [45/0/-45/90]s ≡ AP-8; (a) Extensional stiffness, A_{11}; (b) Coupling stiffness, B_{11}; (c) Bending stiffness, D_{11}; (d) Elastic modulus, $E_{xx}= E_{yy}$; (e) Shear modulus, G_{xy}; (f) Poisson's ratio, ν_{xy}. The volume fraction of CF is 56%.

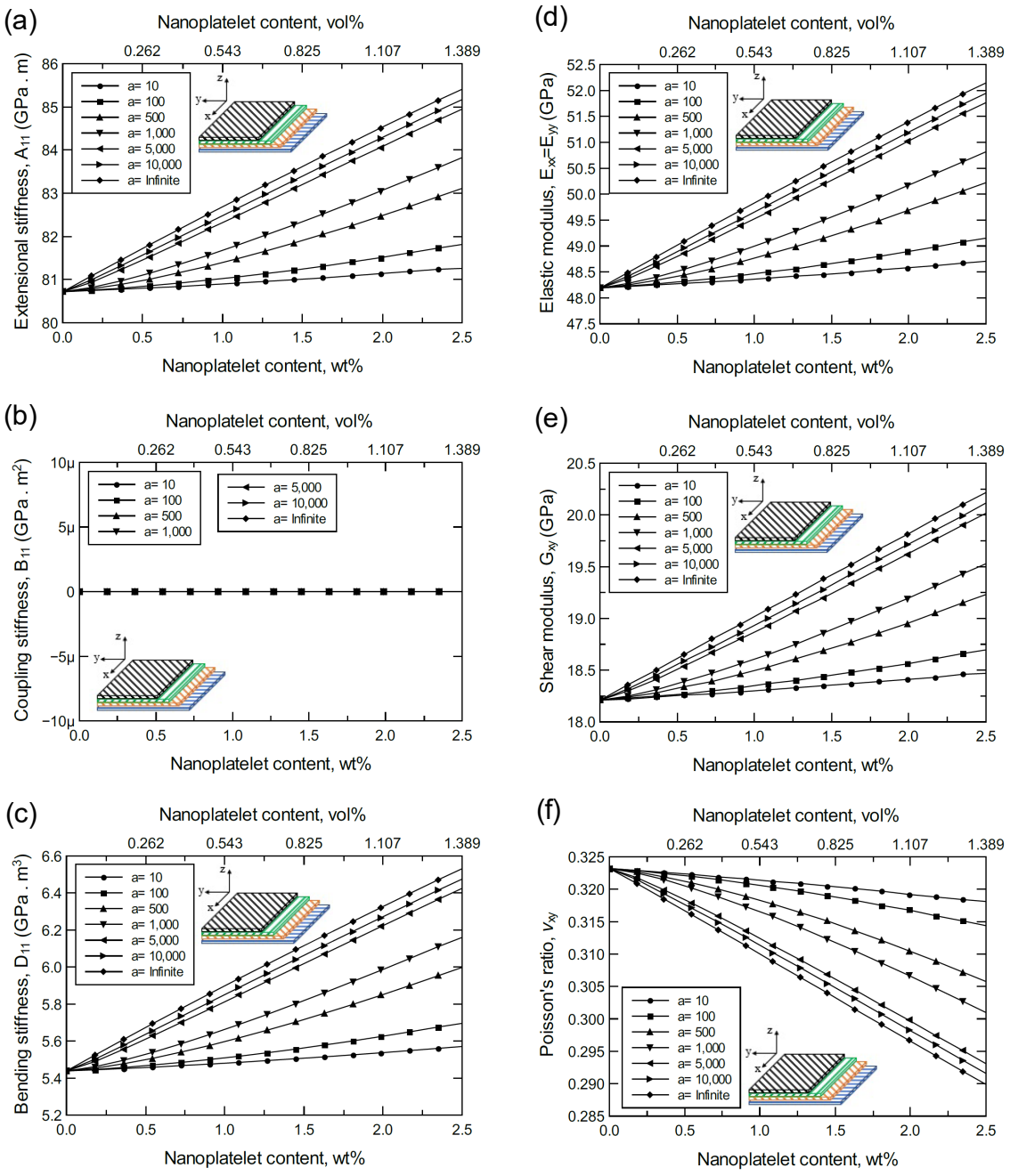

Figure 4.17: Predicted mechanical properties of laminated CF/GNP/epoxy, a symmetric balanced angle-ply laminated composite panel [60/-60/0]s ≡ AP-6; (a) Extensional stiffness, A_{11}; (b) Coupling stiffness, B_{11}; (c) Bending stiffness, D_{11}; (d) Elastic modulus, $E_{xx}= E_{yy}$; (e) Shear modulus, G_{xy}; (f) Poisson's ratio, ν_{xy}. The volume fraction of CF is 56%.

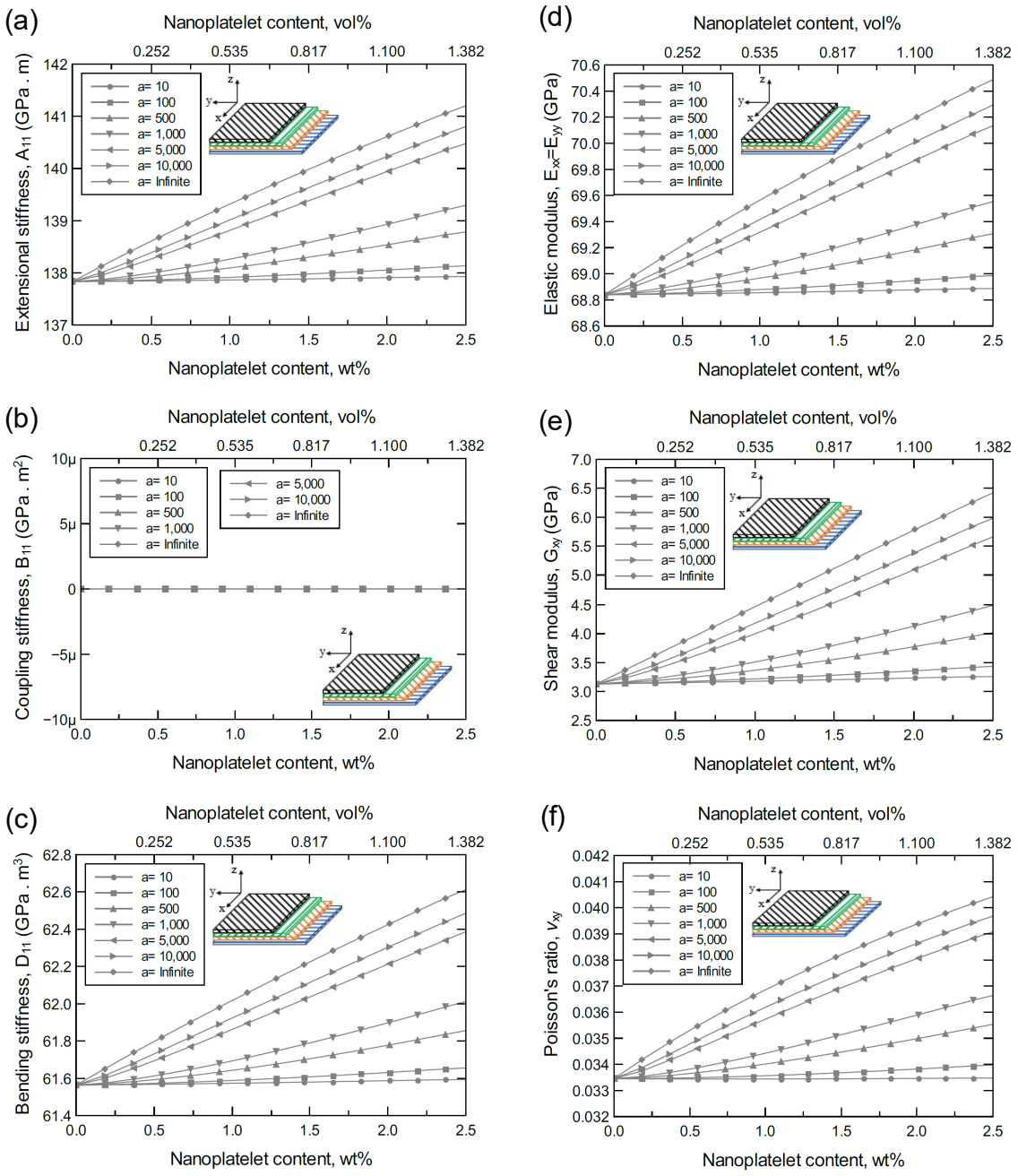

Figure 4.18: Predicted mechanical properties of laminated CF/4GNP/epoxy, a symmetric balanced cross-ply laminated composite panel [0/90/0/90]s ≡ CP-8; (a) Extensional stiffness, A_{11}; (b) Coupling stiffness, B_{11}; (c) Bending stiffness, D_{11}; (d) Elastic modulus, $E_{xx}= E_{yy}$; (e) Shear modulus, G_{xy}; (f) Poisson's ratio, ν_{xy}. The volume fraction of CF is 56%.

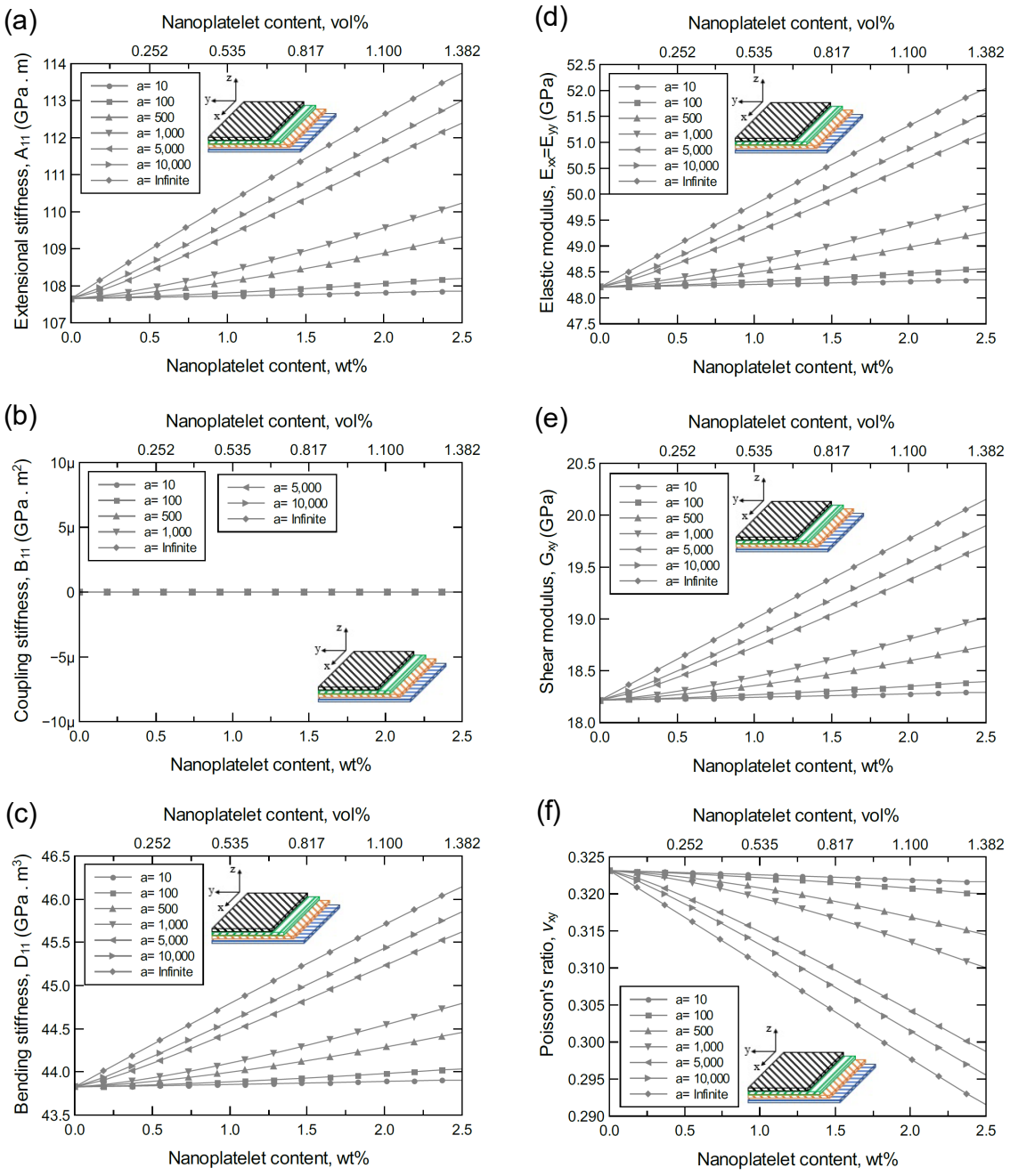

Figure 4.19: Predicted mechanical properties of laminated CF/4GNP/epoxy, a symmetric balanced angle-ply laminated composite panel [45/0/-45/90]s ≡ AP-8; (a) Extensional stiffness, A_{11}; (b) Coupling stiffness, B_{11}; (c) Bending stiffness, D_{11}; (d) Elastic modulus, $E_{xx}= E_{yy}$; (e) Shear modulus, G_{xy}; (f) Poisson's ratio, ν_{xy}. The volume fraction of CF is 56%.

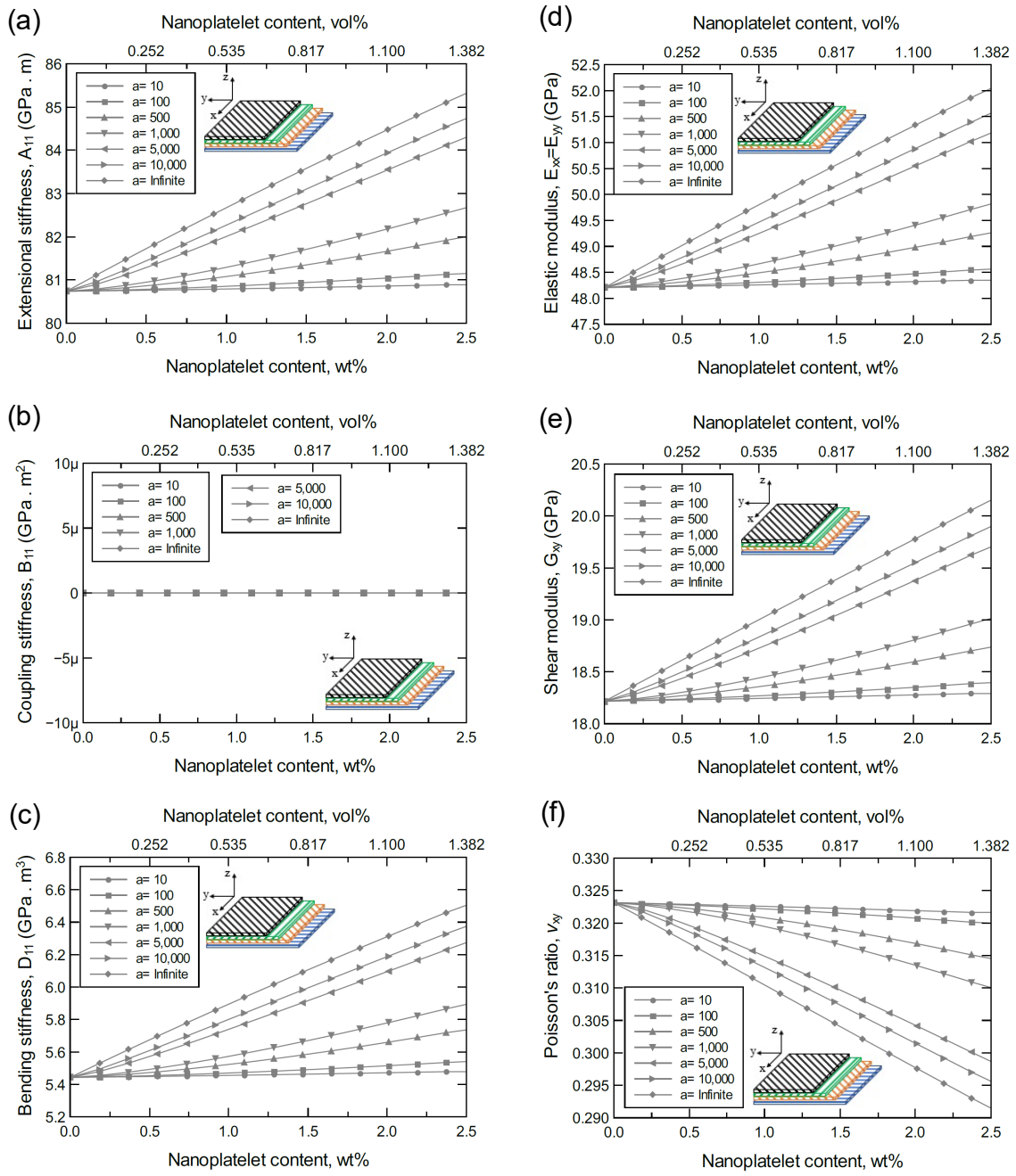

Figure 4.20: Predicted mechanical properties of laminated CF/4GNP/epoxy, a symmetric balanced angle-ply laminated composite panel [60/-60/0]s ≡ AP-6; (a) Extensional stiffness, A_{11}; (b) Coupling stiffness, B_{11}; (c) Bending stiffness, D_{11}; (d) Elastic modulus, $E_{xx}= E_{yy}$; (e) Shear modulus, G_{xy}; (f) Poisson's ratio, ν_{xy}. The volume fraction of CF is 56%.

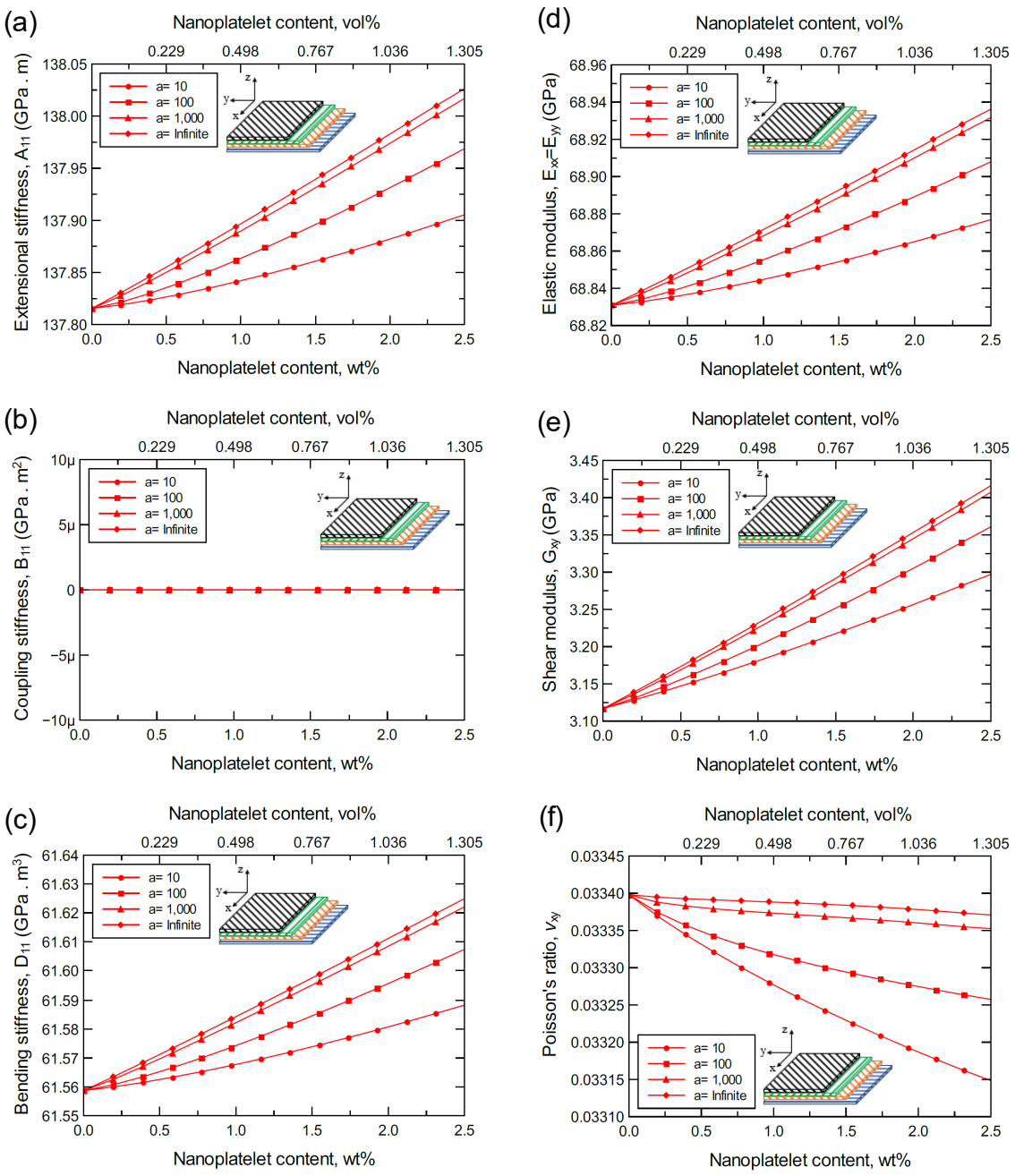

Figure 4.21: Predicted mechanical properties of laminated CF/GO/epoxy, a symmetric balanced cross-ply laminated composite panel [0/90/0/90]s ≡ CP-8; (a) Extensional stiffness, A_{11}; (b) Coupling stiffness, B_{11}; (c) Bending stiffness, D_{11}; (d) Elastic modulus, $E_{xx}= E_{yy}$; (e) Shear modulus, G_{xy}; (f) Poisson's ratio, ν_{xy}. The volume fraction of CF is 56%.

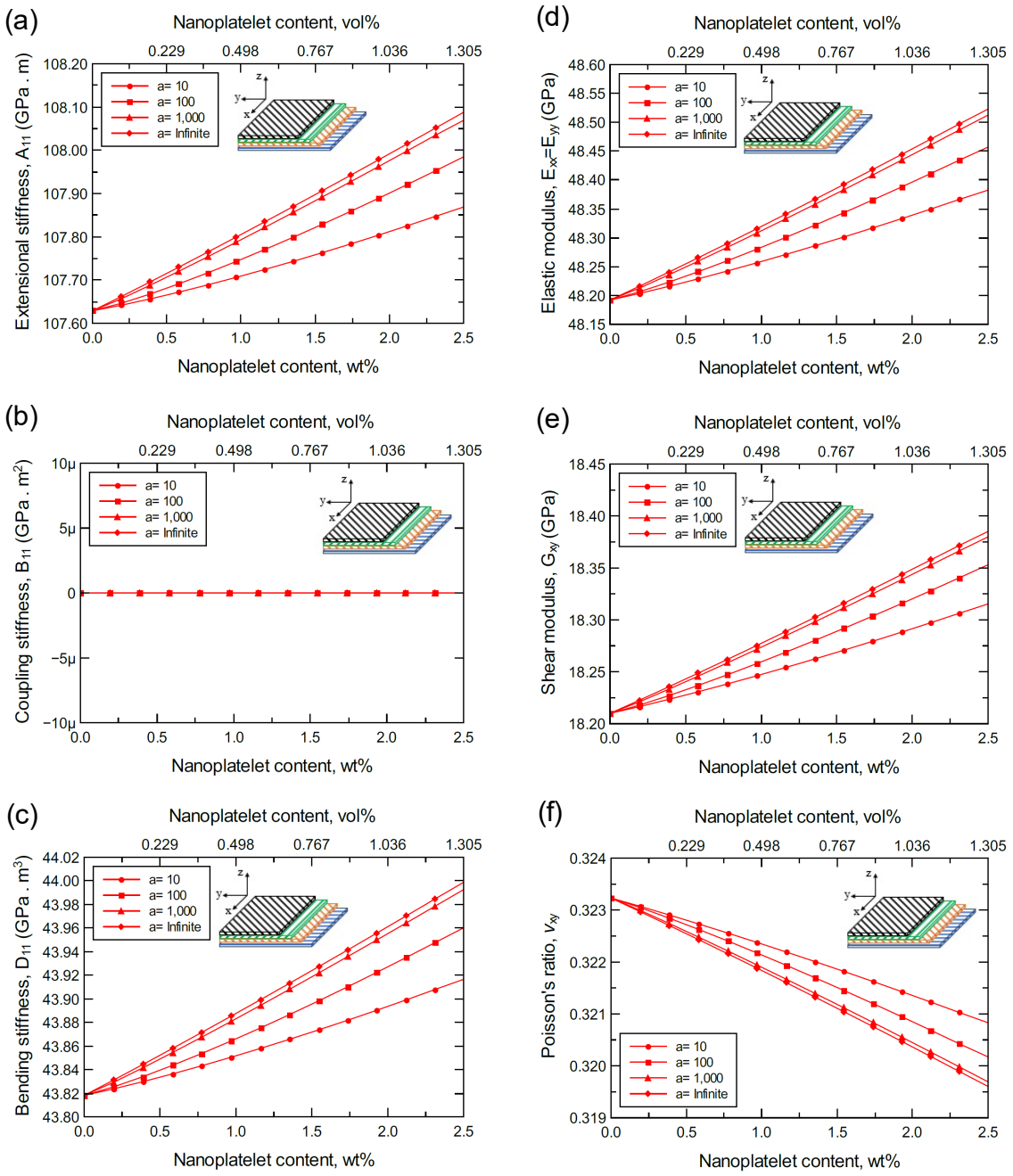

Figure 4.22: Predicted mechanical properties of laminated CF/GO/epoxy, a symmetric balanced angle-ply laminated composite panel [45/0/-45/90]s ≡ AP-8; (a) Extensional stiffness, A_{11}; (b) Coupling stiffness, B_{11}; (c) Bending stiffness, D_{11}; (d) Elastic modulus, $E_{xx}= E_{yy}$; (e) Shear modulus, G_{xy}; (f) Poisson's ratio, ν_{xy}. The volume fraction of CF is 56%.

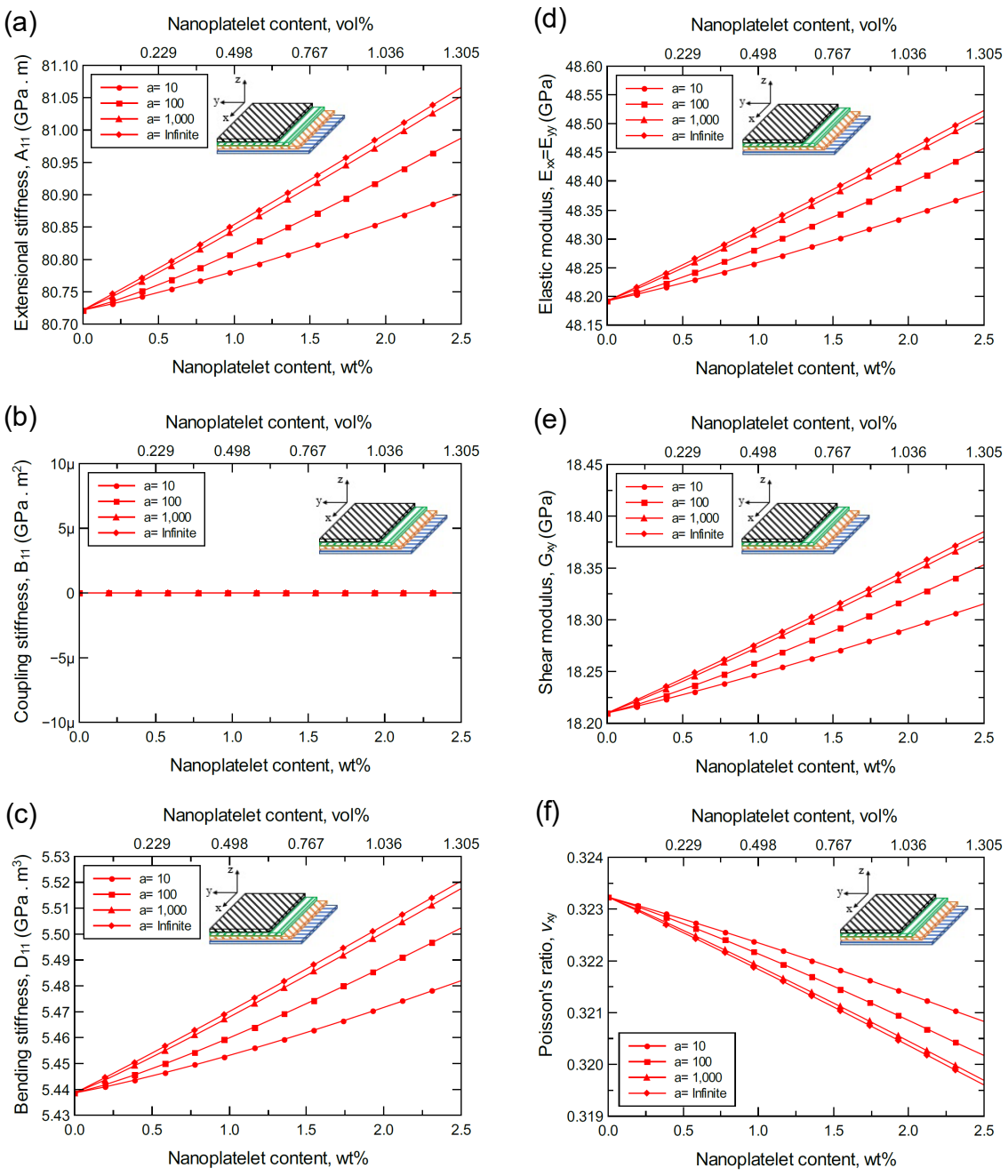

Figure 4.23: Predicted mechanical properties of laminated CF/GO/epoxy, a symmetric balanced angle-ply laminated composite panel [60/-60/0]s ≡ AP-6; (a) Extensional stiffness, A_{11}; (b) Coupling stiffness, B_{11}; (c) Bending stiffness, D_{11}; (d) Elastic modulus, $E_{xx}= E_{yy}$; (e) Shear modulus, G_{xy}; (f) Poisson's ratio, ν_{xy}. The volume fraction of CF is 56%.

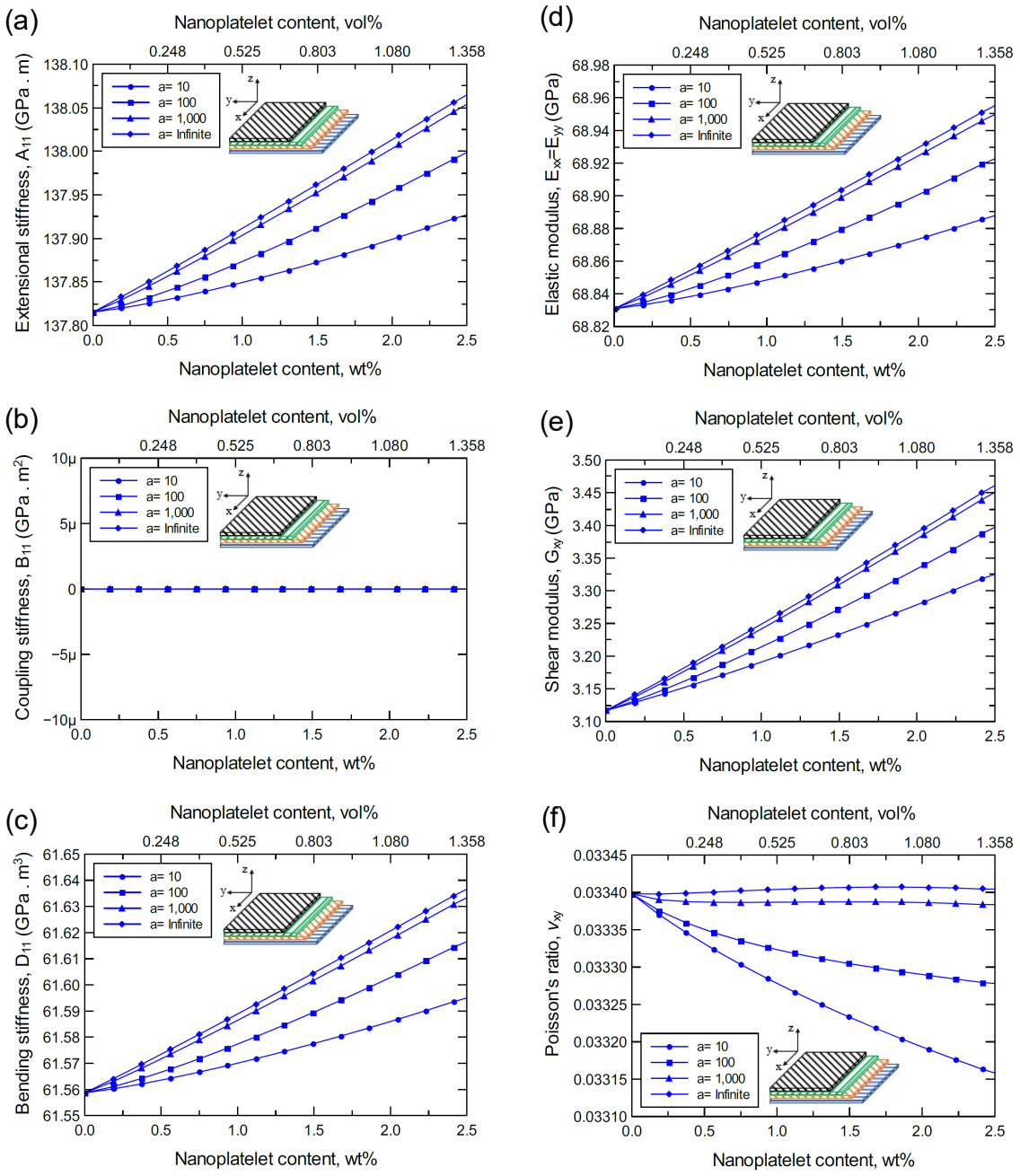

Figure 4.24: Predicted mechanical properties of laminated CF/FGO/epoxy, a symmetric balanced cross-ply laminated composite panel [0/90/0/90]s ≡ CP-8; (a) Extensional stiffness, A_{11}; (b) Coupling stiffness, B_{11}; (c) Bending stiffness, D_{11}; (d) Elastic modulus, $E_{xx}= E_{yy}$; (e) Shear modulus, G_{xy}; (f) Poisson's ratio, ν_{xy}. The volume fraction of CF is 56%.

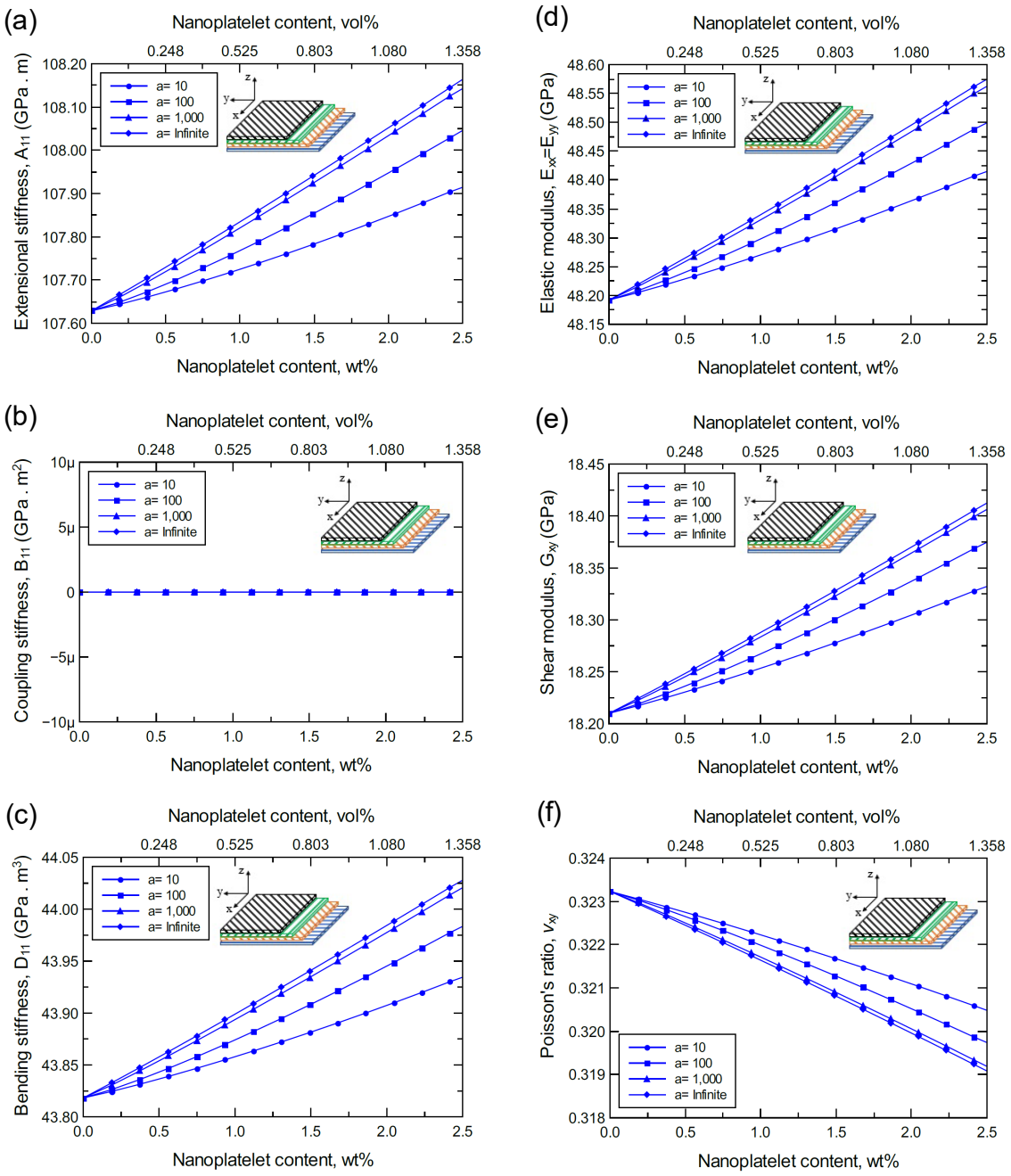

Figure 4.25: Predicted mechanical properties of laminated CF/FGO/epoxy, a symmetric balanced angle-ply laminated composite panel [45/0/-45/90]s ≡ AP-8; (a) Extensional stiffness, A_{11}; (b) Coupling stiffness, B_{11}; (c) Bending stiffness, D_{11}; (d) Elastic modulus, $E_{xx}= E_{yy}$; (e) Shear modulus, G_{xy}; (f) Poisson's ratio, ν_{xy}. The volume fraction of CF is 56%.

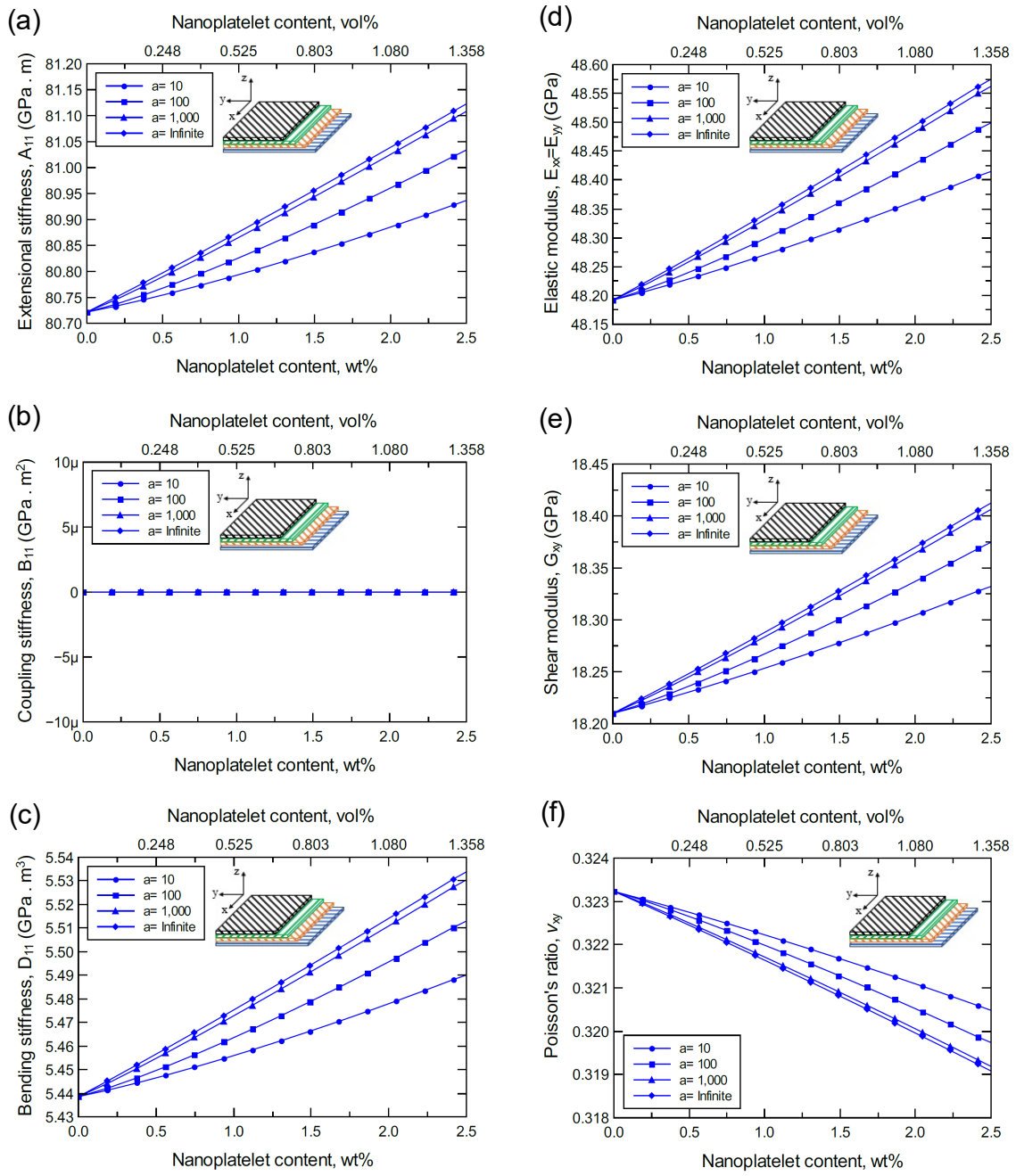

Figure 4.26: Predicted mechanical properties of laminated CF/GO/epoxy, a symmetric balanced angle-ply laminated composite panel [60/-60/0]s ≡ AP-6; (a) Extensional stiffness, A_{11}; (b) Coupling stiffness, B_{11}; (c) Bending stiffness, D_{11}; (d) Elastic modulus, $E_{xx}= E_{yy}$; (e) Shear modulus, G_{xy}; (f) Poisson's ratio, ν_{xy}. The volume fraction of CF is 56%.

Figures 4.27-4.31 show the predicted mechanical properties of the laminated hybrid composite panels at 100 aspect ratio and various nanoplatelets content. Each plot compares the predicted elastic mechanical properties based on the three proposed structure configurations of the hybrid composite panels for each nanoplatelet type. The plots of the normalized elastic properties compare the reinforcing effect of the nanoplatelets content on the mechanical response.

Considering Figure 4.27, the predicted extensional stiffness (A_{11}) for the cross-ply composite panel model (CP-8) is much higher than those predicted for angle-ply composite panel models (AP-8 and AP-6). As AP-8 exhibits intermediate values of A_{11}, the AP-6 exhibits the lowest A_{11} values. Nevertheless, the normalized A_{11} plots refer to an identical and larger reinforcing effect of the nanoplatelets content in AP-8 and AP-6 relative to CP-8. A similar trend in the improvement of the predicted response of A_{11} can be observed with increasing the nanoplatelets content.

Considering Figure 4.28, the predicted bending stiffness (D_{11}) for the angle-ply composite panel model (AP-6) is much lower than those predicted for cross-ply composite panel model (CP-8). The D_{11} values of AP-8 are also lower, yet closer to the D_{11} of CP-8. However, the normalized D_{11} plots refer to a larger reinforcing effect of the nanoplatelets content in AP-6 relative to CP-8. Furthermore, the reinforcing effect of the nanoplatelets content in AP-8 is slightly higher than that in CP-8. The improvement in D_{11} involved a similar trend in all plots with increasing the content of each of the four nanoplatelet types.

Considering Figure 4.29, the predicted in-plane elastic modulus (E_{xx}= E_{yy}) of CP-8 is higher relative to that in AP-8 and AP-6. Interestingly, both AP-6 and AP-8 show an identical in-plane elastic modulus despite the difference in the number of plies. They also show a better reinforcing effect when increasing the nanoplatelets content relative to that observed in CP-8. The improvement in the in-plane elastic modulus involved a similar trend in all plots when increasing the content of each of the four nanoplatelet types.

For the predicted in-plane shear modulus (G_{xy}) shown in Figure 4.30, the case is the opposite to that observed in the predicted in-plane elastic modulus. That is, G_{xy} of CP-8 is much lower than that observed for AP-8 and AP-6, which are showing an identical G_{xy} values. However, the reinforcing effect of the nanoplatelets content observed in the CP-8 is higher relative to that observed in AP-6 or AP-8. The improvement in the in-plane shear modulus involved a similar trend in all plots with increasing the content of each of the four nanoplatelet types.

The predicted in-plane Poisson's ratio values (ν_{xy}) for the laminated composite panels are shown in Figure 4.31. The CP-8 indicates a very low lateral contraction in comparison to that observed for both AP-6 and AP-8. In addition, the normalized plots show an increase in the lateral contraction for the CP-8 with increasing the GNP and 4GNP nanoplatelets content. In contrast, for hybrid composite panels reinforced with GO and FGO nanoplatelets and all AP-6 and AP-8 panels indicate a decrease in the lateral contraction with increasing the nanoplatelets content.

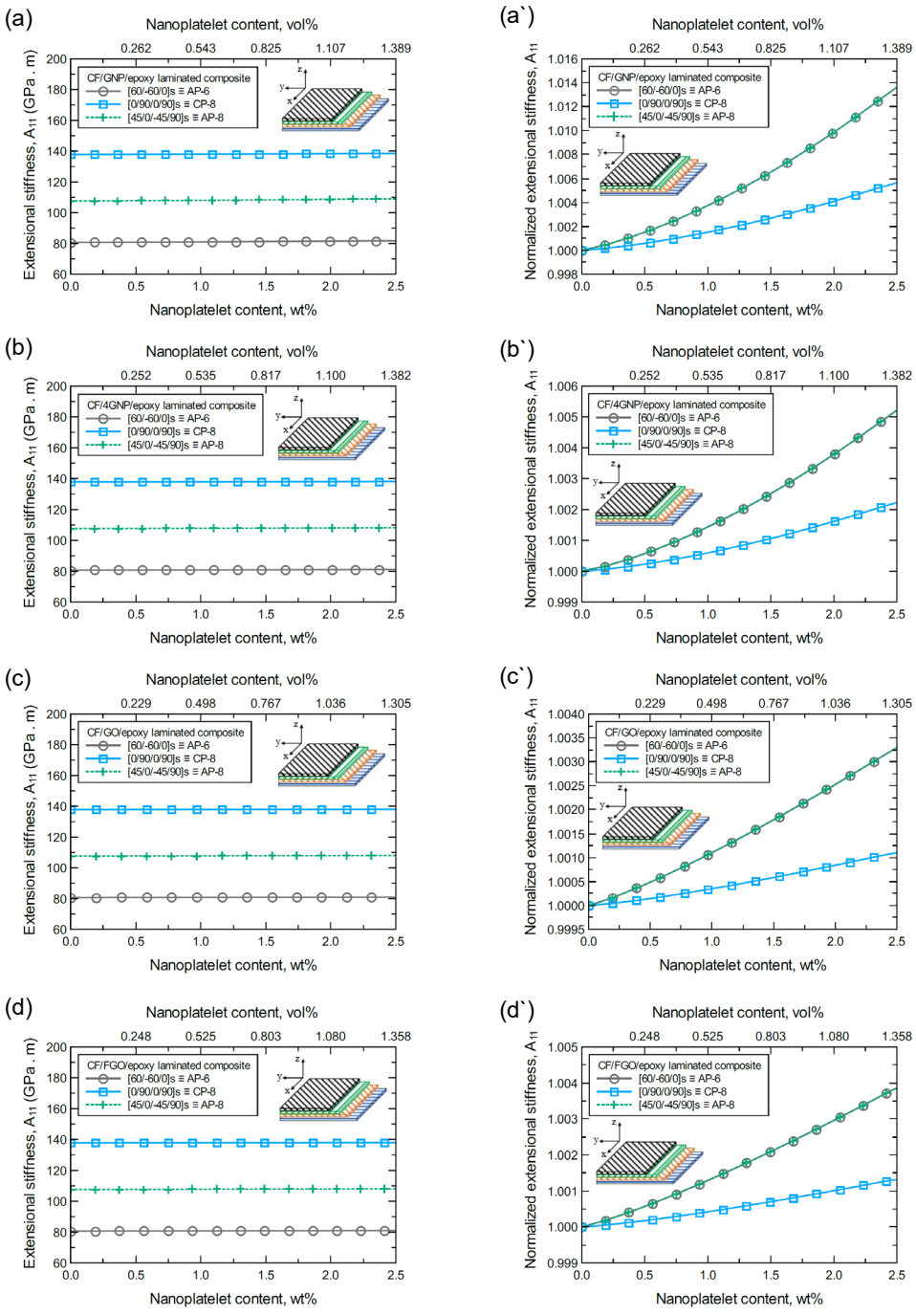

Figure 4.27: The predicted extensional stiffness (A_{11}) and its normalized value for laminated hybrid composites with 100 aspect ratio and various nanoplatelets content; (a) A_{11} of CF/GNP/epoxy laminated hybrid composite and its normalized value (a`); (b) $A_{11}$ of CF/4GNP/epoxy laminated hybrid composite and its normalized value (b`); (c) A_{11} of CF/GO/epoxy laminated hybrid composite and its normalized value (c`); (d) $A_{11}$ of CF/FGO/epoxy laminated hybrid composite and its normalized value (d`). The volume fraction of CF is 56%.

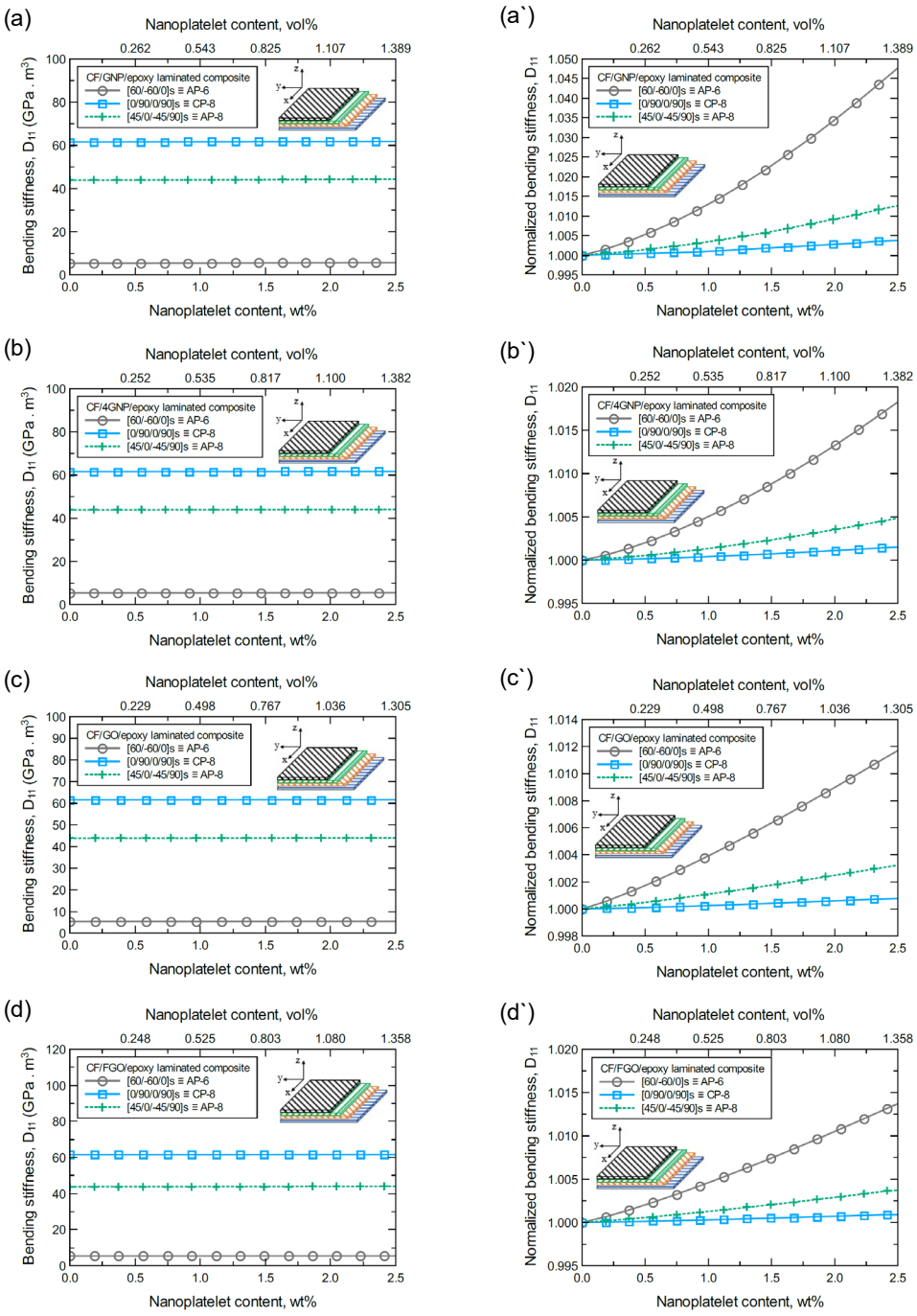

Figure 4.28: The predicted bending stiffness (D_{11}) and its normalized value for laminated hybrid composites with 100 aspect ratio and various nanoplatelets content; (a) D_{11} of CF/GNP/epoxy laminated hybrid composite and its normalized value (a`); (b) $D_{11}$ of CF/4GNP/epoxy laminated hybrid composite and its normalized value (b`); (c) D_{11} of CF/GO/epoxy laminated hybrid composite and its normalized value (c`); (d) $D_{11}$ of CF/FGO/epoxy laminated hybrid composite and its normalized value (d`). The volume fraction of CF is 56%.

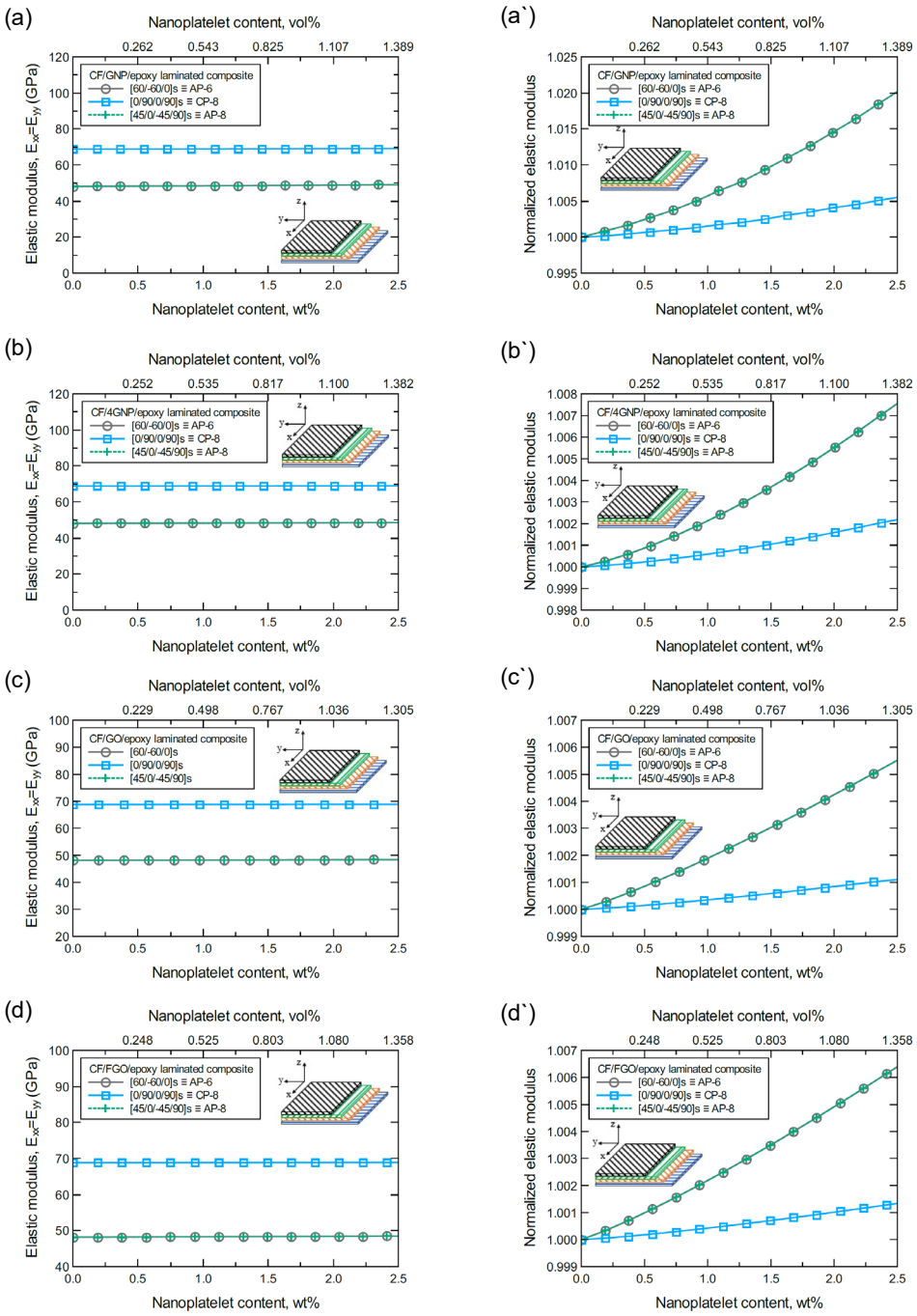

Figure 4.29: The predicted elastic modulus (E_{xx}= E_{yy}) and its normalized value for laminated hybrid composites with 100 aspect ratio and various nanoplatelets content; (a) E_{xx} of CF/GNP/epoxy laminated hybrid composite and its normalized value (a`); (b) $E_{xx}$ of CF/4GNP/epoxy laminated hybrid composite and its normalized value (b`); (c) E_{xx} of CF/GO/epoxy laminated hybrid composite and its normalized value (c`); (d) $E_{xx}$ of CF/FGO/epoxy laminated hybrid composite and its normalized values (d`). The volume fraction of CF is 56%.

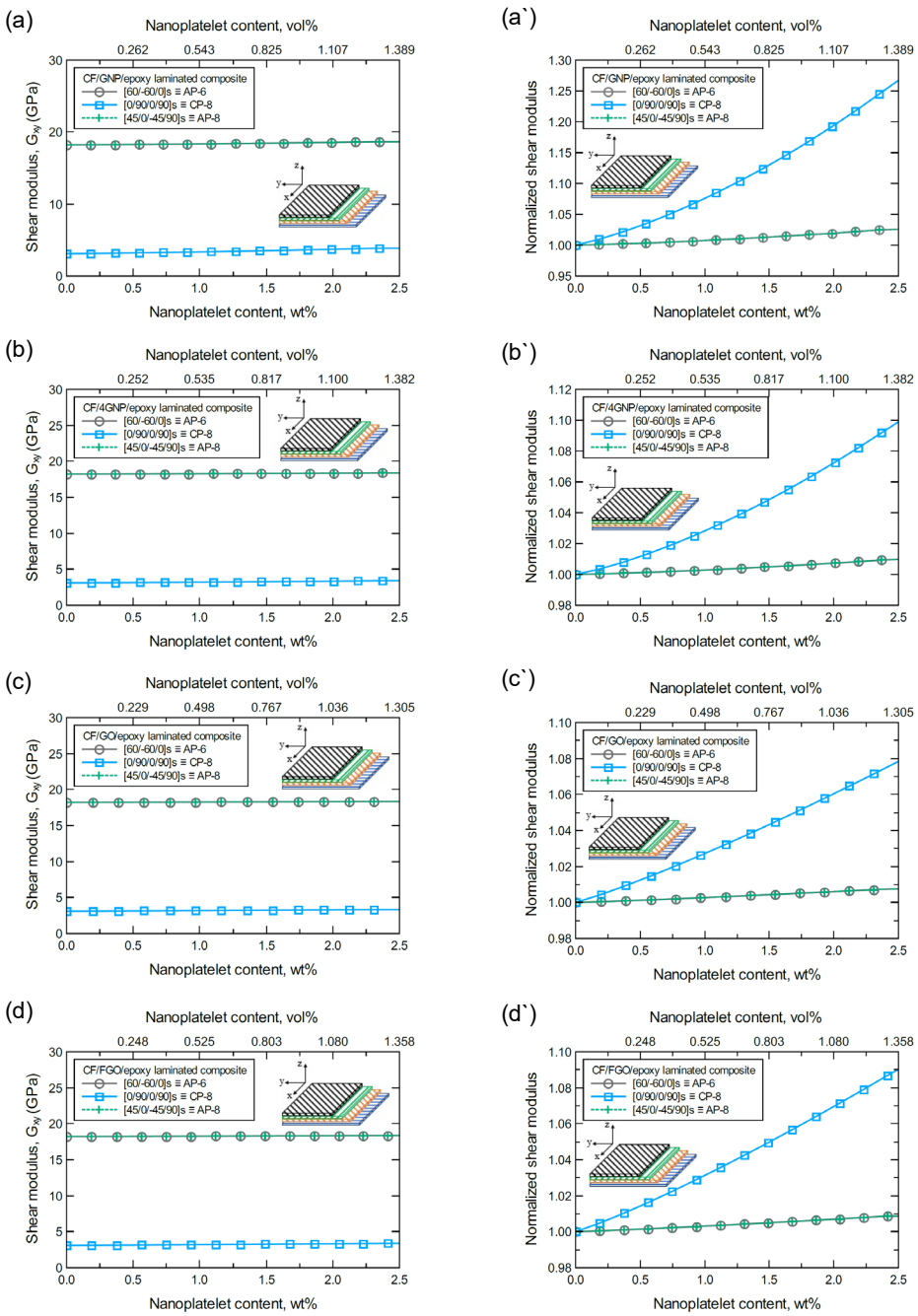

Figure 4.30: The predicted shear modulus (G_{xy}) and its normalized value for laminated hybrid composites with 100 aspect ratio and various nanoplatelets content; (a) G_{xy} of CF/GNP/epoxy laminated hybrid composite and its normalized value (a`); (b) $G_{xy}$ of CF/4GNP/epoxy laminated hybrid composite and its normalized value (b`); (c) G_{xy} of CF/GO/epoxy laminated hybrid composite and its normalized value (c`); (d) $G_{xy}$ of CF/FGO/epoxy laminated hybrid composite and its normalized values (d`). The volume fraction of CF is 56%.

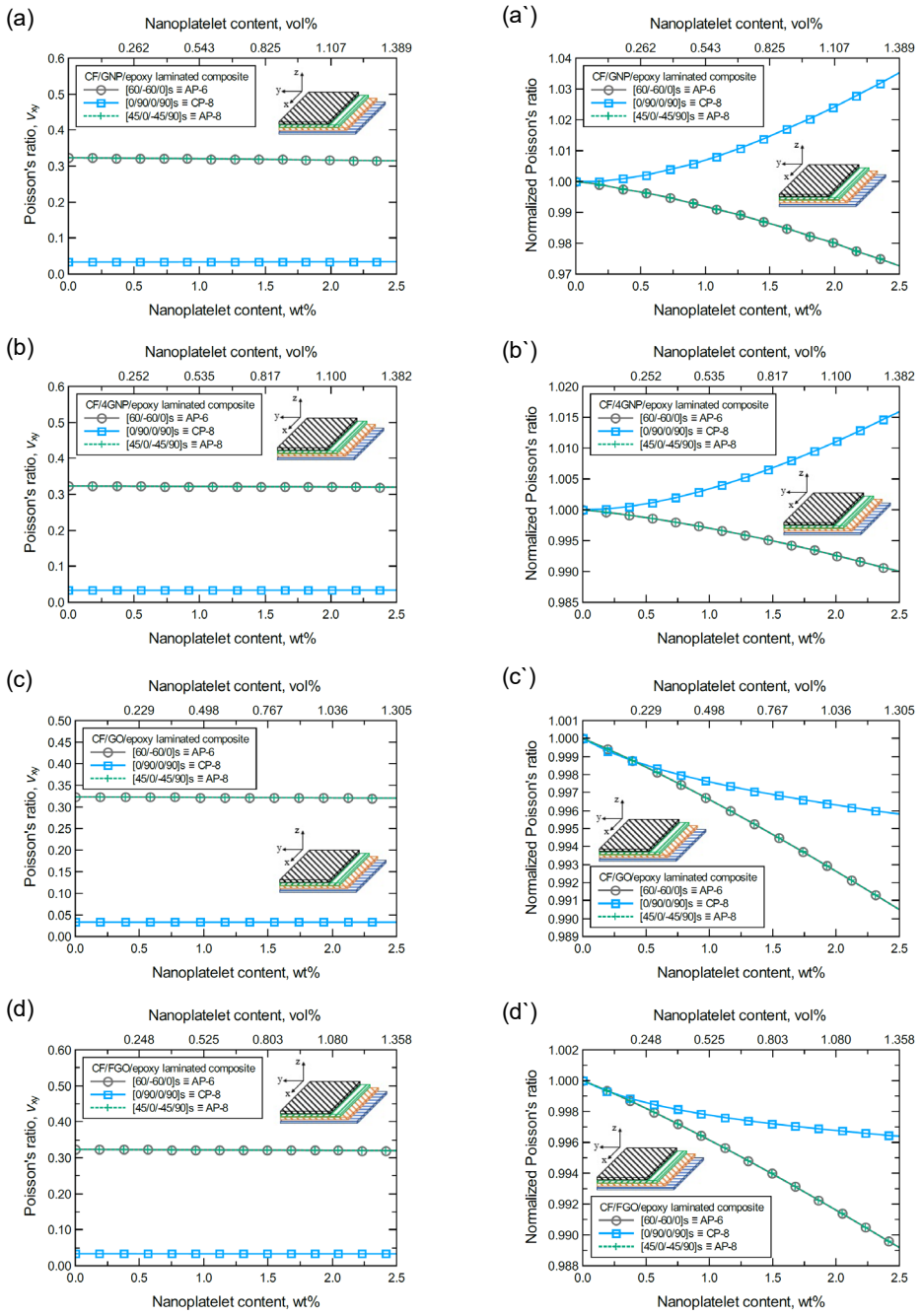

Figure 4.31: The predicted Poisson's ratio (ν_{xy}) and its normalized value for laminated hybrid composites with 100 aspect ratio and various nanoplatelets content; (a) ν_{xy} of CF/GNP/epoxy laminated hybrid composite and its normalized value (a`); (b) $\nu_{xy}$ of CF/4GNP/epoxy laminated hybrid composite and its normalized value (b`); (c) ν_{xy} of CF/GO/epoxy laminated hybrid composite and its normalized value (c`); (d) $\nu_{xy}$ of CF/FGO/epoxy laminated hybrid composite and its normalized value (d`). The volume fraction of CF is 56%.

To better understand the reinforcing effect of each of the four nanoplatelet types on the mechanical response of the laminated hybrid composite panels, Figures 4.32-4.46 compare the response of each of the predicted mechanical properties based on the nanoplatelet type, content, and its aspect ratio. The comparison analysis was performed for the three proposed structures of the laminated hybrid composite panels at CF volume fraction of 56%. It has been previously established that the reinforcing effect of the nanoplatelets is limited/minor along the longitudinal direction of the CF, yet it is more valuable for the transverse direction of each individual lamina. Thus, the stacking order (angle of orientation of each unidirectional lamina in the laminated composite panel) can increase the advantage of the reinforcing feature from both CF and nanoplatelets. This allows for redistributing the overall reinforcing effect of the CF and the nanoplatelets within the laminated hybrid composite panel. The number of laminas and their angle of rotation now represent additional factors that control the mechanical response of the laminated hybrid composite panel. For the nanoplatelets reinforcing effect, the discrepancy in the mechanical response is dependent on the nanoplatelet type, content, and aspect ratio. It can be generalized that the reinforcing effect of the nanoplatelets follows the order GNP > 4GNP > FGO ≥ GO.

Particularly, Figure 4.32.a shows the predicted extensional stiffness (A_{11}) values of CP-8 laminated hybrid composite panel along with their normalized values shown in Figure 4.32.a`. The comparison between A_{11} values is based on the nanoplatelet type whether being GNP, 4GNP, FGO, or GO with various nanoplatelets content and constant aspect ratio of 100. Accordingly, the hybrid composite panel reinforced with GNP exhibits the highest improvement in A_{11} with increasing the nanoplatelets content. Yet, hybrid composite panels reinforced with 4GNP, FGO, and GO exhibit lower improvement in the predicted A_{11} values which shows nearly identical mechanical response at nanoplatelets content less than 1.0 wt% and slightly diverge at higher nanoplatelets content. Meanwhile, a rather different scenario can be observed in the predicted mechanical response as the nanoplatelet aspect ratio is increased. Figure 4.32.b shows the predicted A_{11} values for the same laminated hybrid composite panel along with their normalized values shown in Figure 4.32.b`, which are predicted for various nanoplatelet aspect ratio values and constant nanoplatelets content of 1.0 wt%. Based on the predicted A_{11} values, the mechanical response for CP-8 panels reinforced with GNP, 4GNP, FGO, and GO is mostly insensitive to the increase in the nanoplatelet aspect ratio up to 100. A virtually identical reinforcing effect can be observed for the nanoplatelets with aspect ratio values less than 100. CP-8 panels reinforced with FGO or GO remain insensitive (very slight improvement in the predicted A_{11}) to the increase in the nanoplatelet aspect ratio up to 10^5. For CP-8 panels reinforced with GNP or 4GNP, however, rapid improvement in the predicted A_{11} as the nanoplatelet aspect ratio was increased up to 10^4, with CP-8 panels reinforced with GNP being slightly in the lead. However, the reinforcing effect of 4GNP slightly surpasses that of GNP at nanoplatelet aspect ratio values greater than 10^4 (Figure 4.32.b`). Similar trends can be observed for the predicted A_{11} values of AP-8 and AP-6 laminated hybrid composite panels shown in Figure 4.33 and Figure 4.34, respectively.

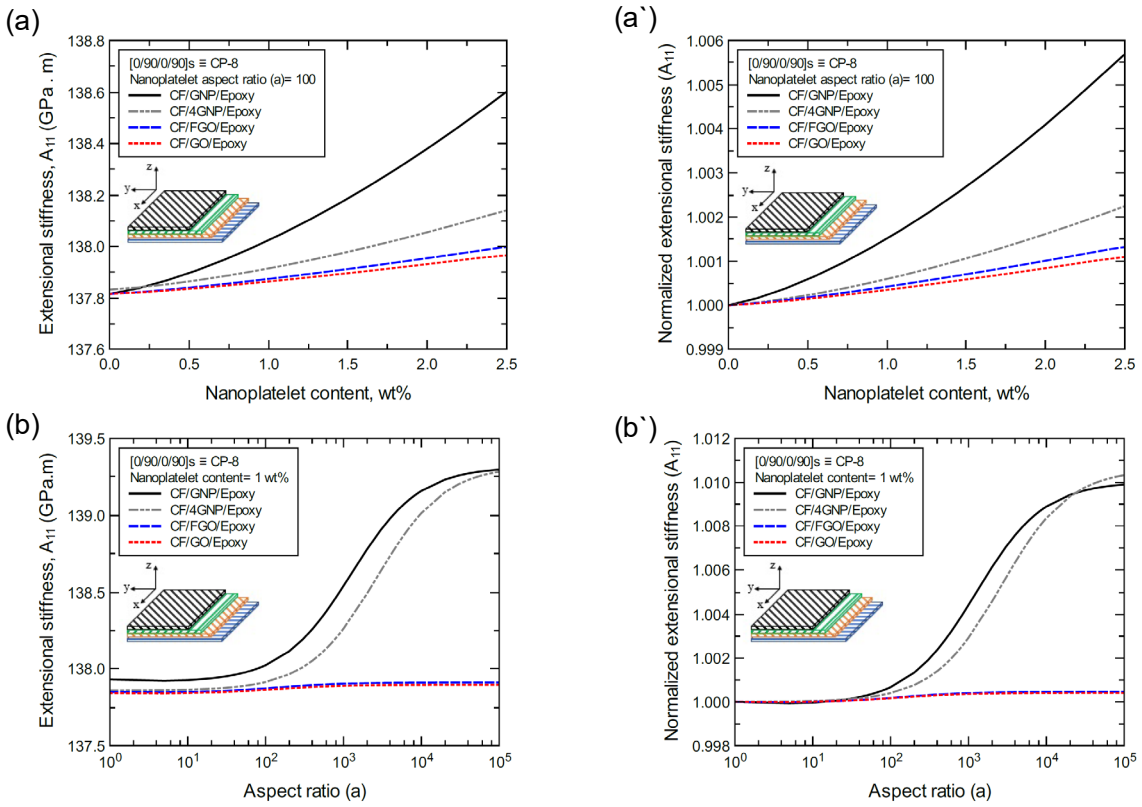

Figure 4.32: Comparison of the predicted extensional stiffness (A_{11}) for [0/90/0/90]s ≡ CP-8 laminated composite panels based on the nanoplatelet type, content, and aspect ratio; (a) predicted A_{11} for various nanoplatelets content at 100 aspect ratio, and the normalized response is shown in (a`); (b) predicted $A_{11}$ for various aspect ratio values at 1.0 wt% of the nanoplatelets content, and the normalized response is shown in (b`). The volume fraction of CF is 56%.

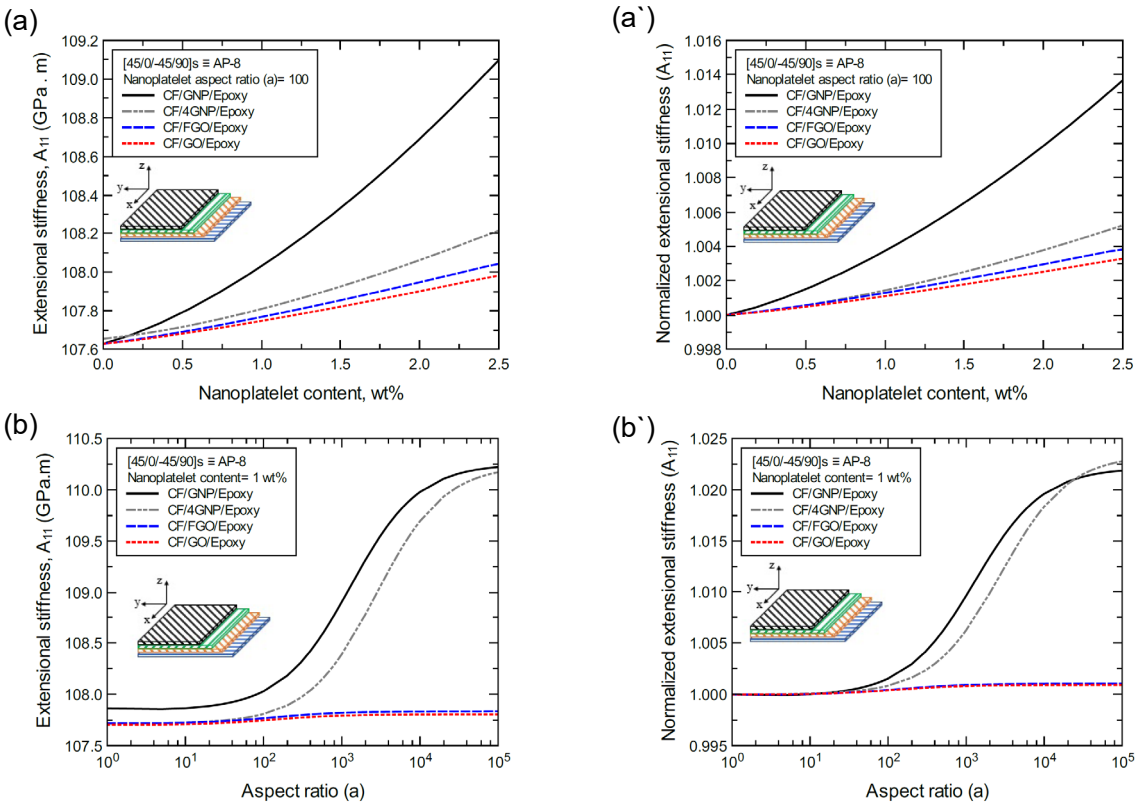

Figure 4.33: Comparison of the predicted extensional stiffness (A_{11}) for [45/0/-45/90]s ≡ AP-8 laminated composite panels based on the nanoplatelet type, content, and aspect ratio; (a) predicted A_{11} for various nanoplatelets content at 100 aspect ratio, and the normalized response is shown in (a`); (b) predicted $A_{11}$ for various aspect ratio values at 1.0 wt% of the nanoplatelets content, and the normalized response is shown in (b`). The volume fraction of CF is 56%.

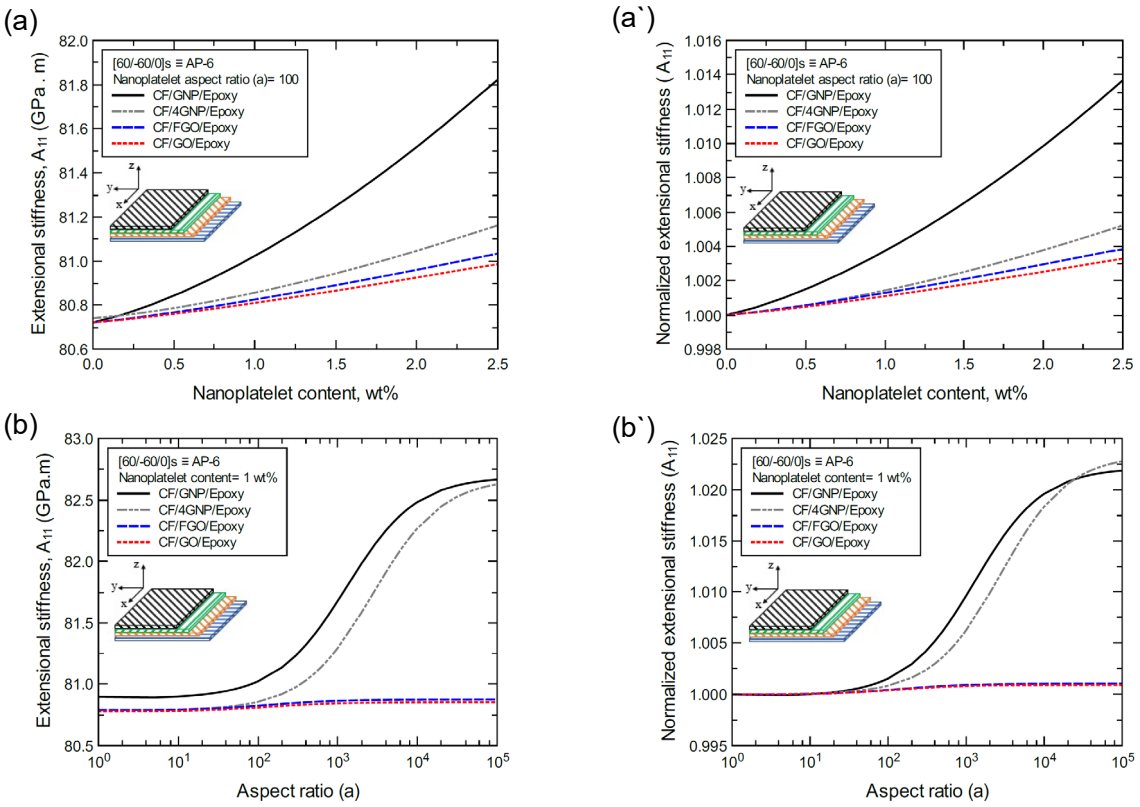

Figure 4.34: Comparison of the predicted extensional stiffness (A_{11}) for [60/-60/0]s ≡ AP-6 laminated composite panels based on the nanoplatelet type, content, and aspect ratio; (a) predicted A_{11} for various nanoplatelets content at 100 aspect ratio, and the normalized response is shown in (a`); (b) predicted $A_{11}$ for various aspect ratio values at 1.0 wt% of the nanoplatelets content, and the normalized response is shown in (b`). The volume fraction of CF is 56%.

In a similar manner, Figure 4.35.a shows the predicted bending stiffness (D_{11}) values of CP-8 laminated hybrid composite panel along with their normalized values shown in Figure 4.35.a`. The comparison between D_{11} values is based on the nanoplatelet type whether being GNP, 4GNP, FGO, or GO with various nanoplatelets content and constant aspect ratio of 100. However, Figure 4.35.b shows the D_{11} values for the same laminated hybrid composite panel along with their normalized values shown in Figure 4.35.b`, which are predicted for various nanoplatelet aspect ratio values and constant nanoplatelets content of 1.0 wt%. Considering the improvement trend observed in the predicted A_{11}, the CP-8 hybrid composite panel reinforced with GNP exhibits the highest improvement in D_{11} with increasing the nanoplatelets content. Yet, hybrid composite panels reinforced with 4GNP, FGO, and GO exhibit lower improvement in the predicted D_{11} values which shows nearly identical mechanical response at nanoplatelets content less than 1.0 wt% and slightly diverge at higher nanoplatelets content (Figure 4.35.a`). Meanwhile, a rather different scenario can be observed in the predicted mechanical response as the nanoplatelet aspect ratio is increased. Based on the predicted $D_{11}$ values (Figure 4.35.b`), the mechanical response for CP-8 panels reinforced with GNP, 4GNP, FGO, and GO is mostly insensitive to the increase in the nanoplatelet aspect ratio up to 100. A virtually identical reinforcing effect can be observed for the nanoplatelets with aspect ratio values less than 100. CP-8 panels reinforced with FGO or GO remain insensitive (very slight improvement in the predicted D_{11}) to the increase in the nanoplatelet aspect ratio up to 10^5. For CP-8 panels reinforced with GNP or 4GNP, however, rapid improvement in the predicted D_{11} as the nanoplatelet aspect ratio was increased up to 10^4, with CP-8 panels reinforced with GNP being slightly in the lead. However, the reinforcing effect of 4GNP slightly surpasses that of GNP at nanoplatelet aspect ratio values greater than 10^4 (Figure 4.35.b`). Similar trends can be observed for the predicted D_{11} values of AP-8 and AP-6 laminated hybrid composite panels shown in Figure 4.36 and Figure 4.37, respectively.

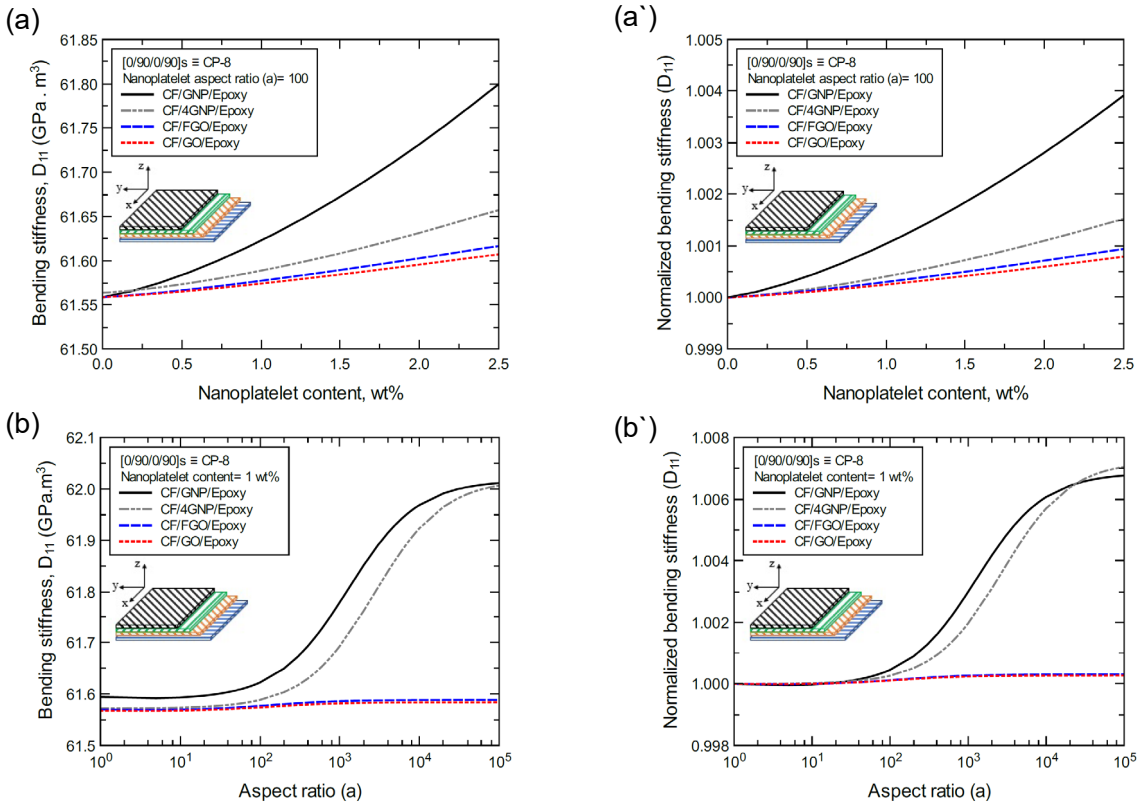

Figure 4.35: Comparison of the predicted bending stiffness (D_{11}) for [0/90/0/90]s ≡ CP-8 laminated composite panels based on the nanoplatelet type, content, and aspect ratio; (a) predicted D_{11} for various nanoplatelets content at 100 aspect ratio, and the normalized response is shown in (a`); (b) predicted $D_{11}$ for various aspect ratio values at 1.0 wt% of the nanoplatelets content, and the normalized response is shown in (b`). The volume fraction of CF is 56%.

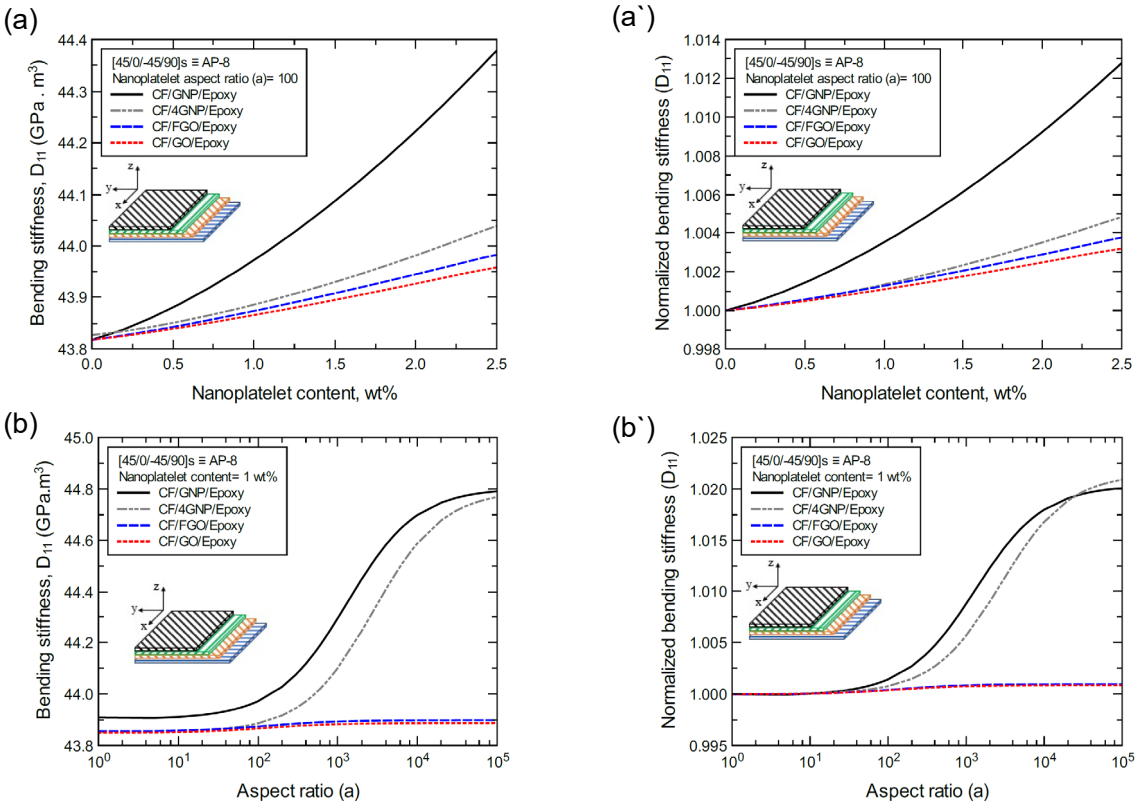

Figure 4.36: Comparison of the predicted bending stiffness (D_{11}) for [45/0/-45/90]s ≡ AP-8 laminated composite panels based on the nanoplatelet type, content, and aspect ratio; (a) predicted D_{11} for various nanoplatelets content at 100 aspect ratio, and the normalized response is shown in (a`); (b) predicted $D_{11}$ for various aspect ratio values at 1.0 wt% of the nanoplatelets content, and the normalized response is shown in (b`). The volume fraction of CF is 56%.

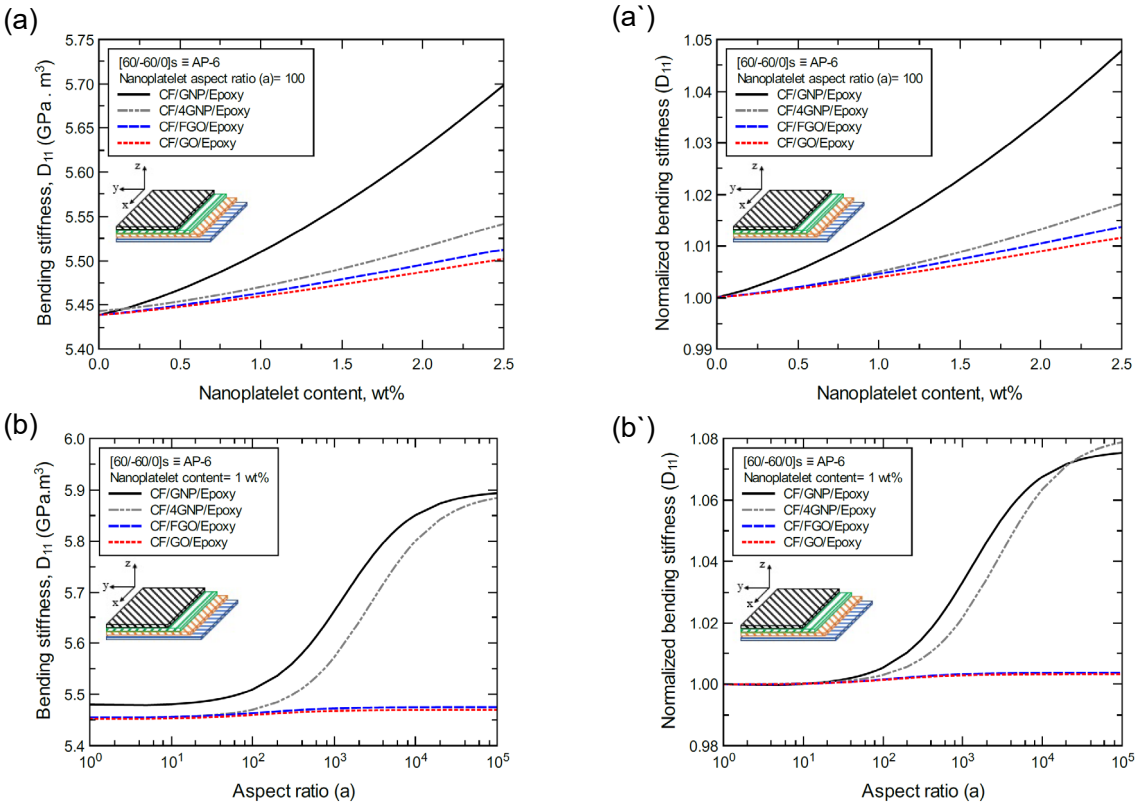

Figure 4.37: Comparison of the predicted bending stiffness (D_{11}) for [60/-60/0]s ≡ AP-6 laminated composite panels based on the nanoplatelet type, content, and aspect ratio; (a) predicted D_{11} for various nanoplatelets content at 100 aspect ratio, and the normalized response is shown in (a`); (b) predicted $D_{11}$ for various aspect ratio values at 1.0 wt% of the nanoplatelets content, and the normalized response is shown in (b`). The volume fraction of CF is 56%.

Figure 4.38.a shows the predicted elastic modulus (E_{xx}= E_{yy}) values of CP-8 laminated hybrid composite panel along with their normalized values shown in Figure 4.38.a`. The comparison between E_{xx} values is based on the nanoplatelet type whether being GNP, 4GNP, FGO, or GO with various nanoplatelets content and constant aspect ratio of 100. However, Figure 4.38.b shows the E_{xx} values for the same laminated hybrid composite panel along with their normalized values shown in Figure 4.38.b`, which are predicted for various nanoplatelet aspect ratio values and constant nanoplatelets content of 1.0 wt%. Once more, the CP-8 hybrid composite panel reinforced with GNP exhibits the highest improvement in E_{xx} with increasing the nanoplatelets content. Yet, hybrid composite panels reinforced with 4GNP, FGO, and GO exhibit lower improvement in the predicted E_{xx} values which shows nearly identical mechanical response at nanoplatelets content less than 1.0 wt% and slightly diverge at higher nanoplatelets content (Figure 4.38.a`). Meanwhile, a rather different scenario can be observed in the predicted mechanical response as the nanoplatelet aspect ratio is increased. Based on the predicted $E_{xx}$ values (Figure 4.38.b`), the mechanical response for CP-8 panels reinforced with GNP, 4GNP, FGO, and GO is mostly insensitive to the increase in the nanoplatelet aspect ratio up to 100. A virtually identical reinforcing effect can be observed for the nanoplatelets with aspect ratio values less than 100. CP-8 panels reinforced with FGO or GO remain insensitive (very slight improvement in the predicted E_{xx}) to the increase in the nanoplatelet aspect ratio up to 10^5. For CP-8 panels reinforced with GNP or 4GNP, however, rapid improvement in the predicted E_{xx} as the nanoplatelet aspect ratio was increased up to 10^4, with CP-8 panels reinforced with GNP being slightly in the lead. However, the reinforcing effect of 4GNP slightly surpasses that of GNP at nanoplatelet aspect ratio values greater than 10^4 (Figure 4.38.b`). Similar trends can be observed for the predicted E_{xx} values of AP-8 and AP-6 laminated hybrid composite panels shown in Figure 4.39 and Figure 4.40, respectively.

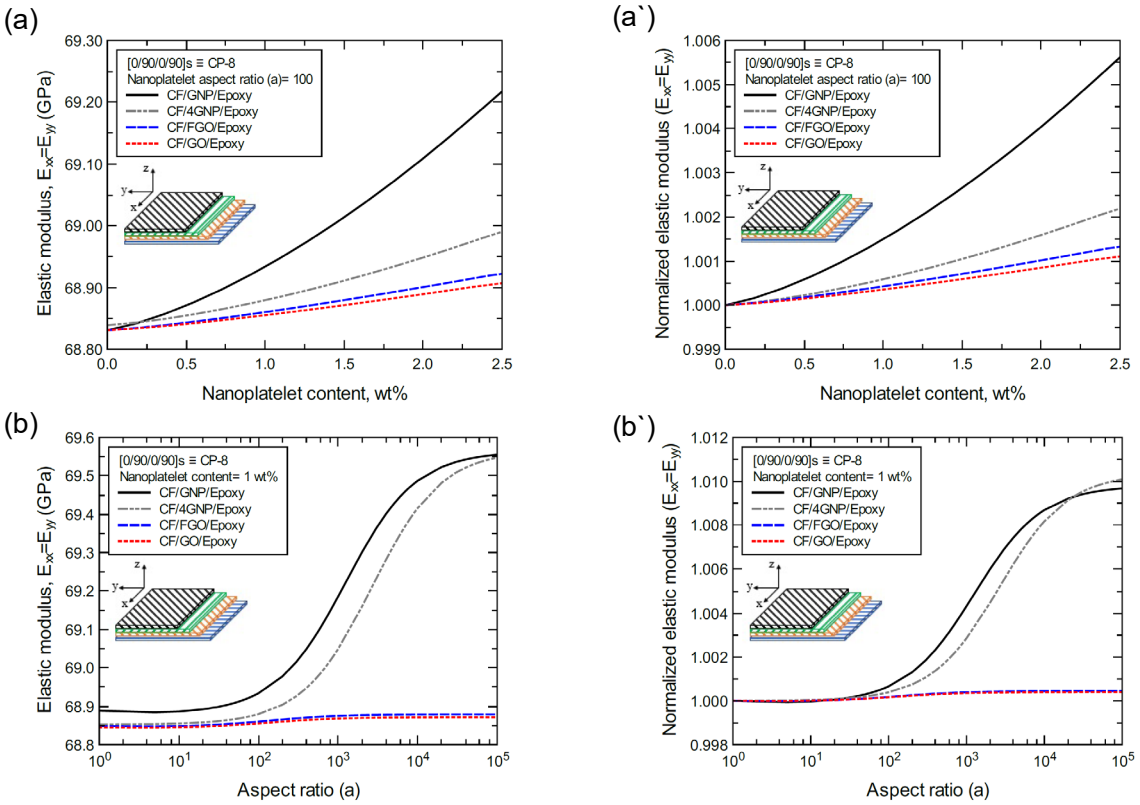

Figure 4.38: Comparison of the predicted in-plane elastic modulus (E_{xx}= E_{yy}) for [0/90/0/90]s ≡ CP-8 laminated composite panels based on the nanoplatelet type, content, and aspect ratio; (a) predicted E_{xx} for various nanoplatelets content at 100 aspect ratio, and the normalized response is shown in (a`); (b) predicted $E_{xx}$ for various aspect ratio values at 1.0 wt% of the nanoplatelets content, and the normalized response is shown in (b`). The volume fraction of CF is 56%.

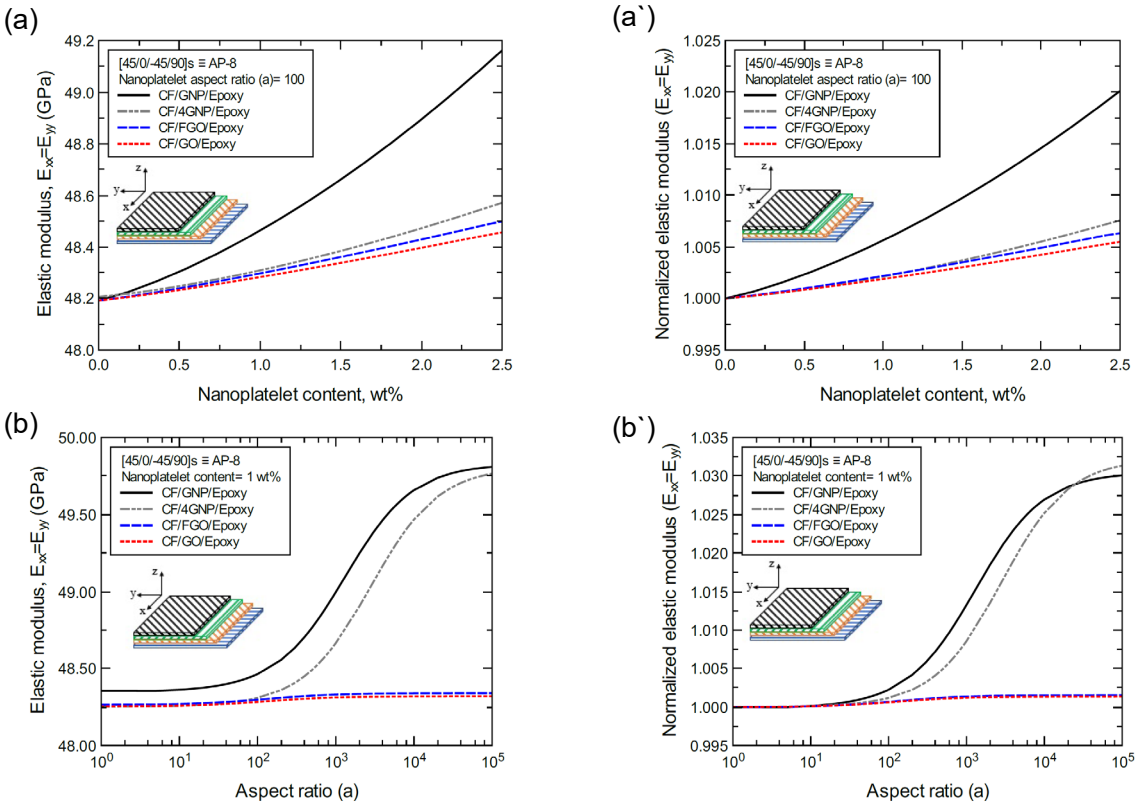

Figure 4.39: Comparison of the predicted in-plane elastic modulus (E_{xx}= E_{yy}) for [45/0/-45/90]s ≡ AP-8 laminated composite panels based on the nanoplatelet type, content, and aspect ratio; (a) predicted E_{xx} for various nanoplatelets content at 100 aspect ratio, and the normalized response is shown in (a`); (b) predicted $E_{xx}$ for various aspect ratio values at 1.0 wt% of the nanoplatelets content, and the normalized response is shown in (b`). The volume fraction of CF is 56%.

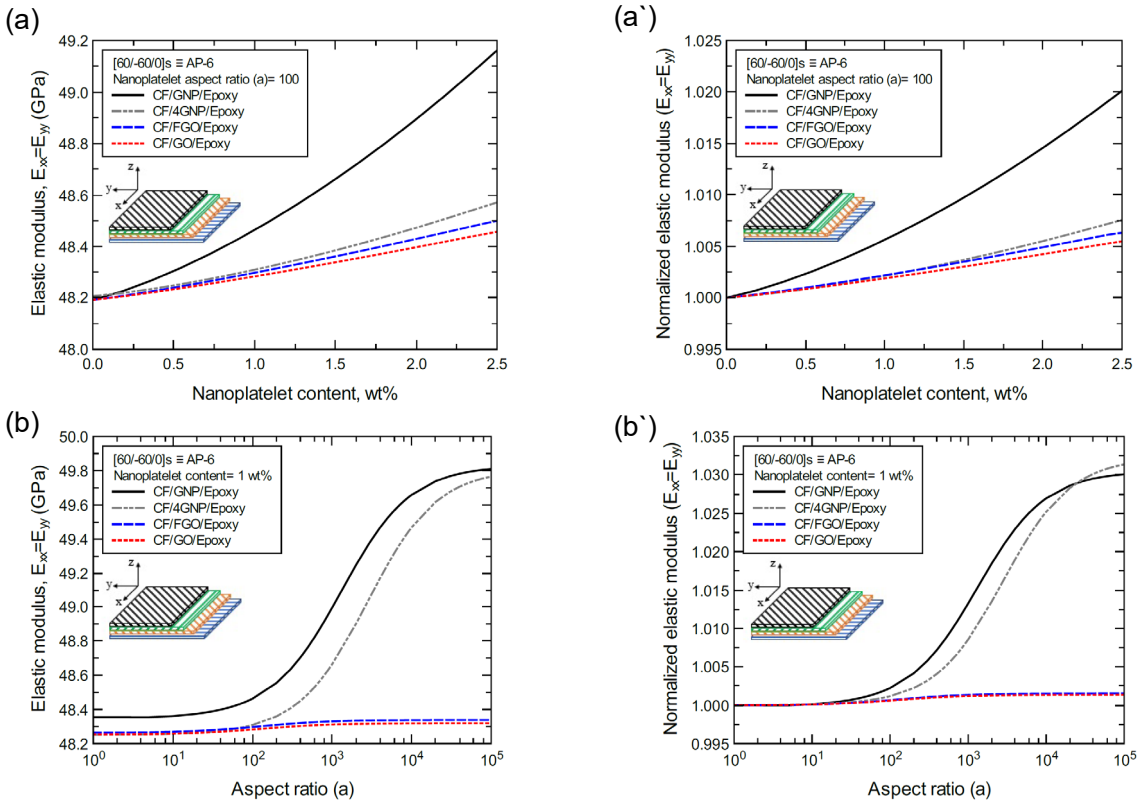

Figure 4.40: Comparison of the predicted in-plane elastic modulus (E_{xx}= E_{yy}) for [60/-60/0]s ≡ AP-6 laminated composite panels based on the nanoplatelet type, content, and aspect ratio; (a) predicted E_{xx} for various nanoplatelets content at 100 aspect ratio, and the normalized response is shown in (a`); (b) predicted $E_{xx}$ for various aspect ratio values at 1.0 wt% of the nanoplatelets content, and the normalized response is shown in (b`). The volume fraction of CF is 56%.

Figure 4.41.a shows the predicted shear modulus (G_{xy}) values of CP-8 laminated hybrid composite panel along with their normalized values shown in Figure 4.41.a`. The comparison between G_{xy} values is based on the nanoplatelet type whether being GNP, 4GNP, FGO, or GO with various nanoplatelets content and constant aspect ratio of 100. However, Figure 4.41.b shows the G_{xy} values for the same laminated hybrid composite panel along with their normalized values shown in Figure 4.41.b`, which are predicted for various nanoplatelet aspect ratio values and constant nanoplatelets content of 1.0 wt%. The CP-8 hybrid composite panel reinforced with GNP exhibits the highest improvement in G_{xy} with increasing the nanoplatelets content. Yet, hybrid composite panels reinforced with 4GNP, FGO, and GO exhibit lower improvement in the predicted G_{xy} values which shows nearly identical to close mechanical response with increasing the nanoplatelets content (Figure 4.41.a`). Meanwhile, a rather different scenario can be observed in the predicted mechanical response as the nanoplatelet aspect ratio is increased. Based on the predicted $G_{xy}$ values (Figure 4.41.b`), the mechanical response for CP-8 panels reinforced with GNP, 4GNP, FGO, and GO is mostly insensitive to the increase in the nanoplatelet aspect ratio up to 100. A virtually identical reinforcing effect can be observed for the nanoplatelets with aspect ratio values less than 100. CP-8 panels reinforced with FGO or GO remain insensitive (very slight improvement in the predicted G_{xy}) to the increase in the nanoplatelet aspect ratio up to 10^5. For CP-8 panels reinforced with GNP or 4GNP, however, rapid improvement in the predicted G_{xy} as the nanoplatelet aspect ratio was increased up to 10^4, with CP-8 panels reinforced with GNP being slightly in the lead. However, the reinforcing effect of 4GNP slightly surpasses that of GNP at nanoplatelet aspect ratio values greater than 10^4 (Figure 4.41.b`). Similar trend can be observed for the predicted G_{xy} values of AP-8 and AP-6 laminated hybrid composite panels shown in Figure 4.42 and Figure 4.43, respectively.

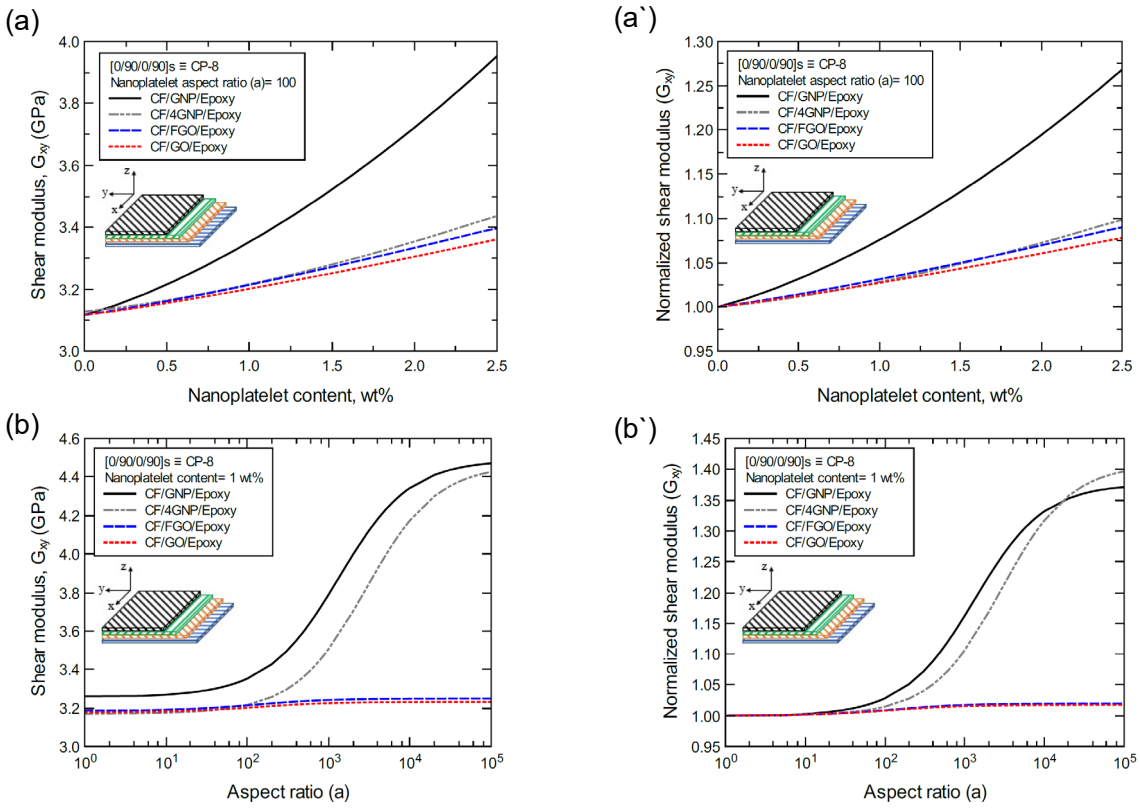

Figure 4.41: Comparison of the predicted in-plane shear modulus (G_{xy}) for [0/90/0/90]s ≡ CP-8 laminated composite panels based on the nanoplatelet type, content, and aspect ratio; (a) predicted G_{xy} for various nanoplatelets content at 100 aspect ratio, and the normalized response is shown in (a`); (b) predicted $G_{xy}$ for various aspect ratio values at 1.0 wt% of the nanoplatelets content, and the normalized response is shown in (b`). The volume fraction of CF is 56%.

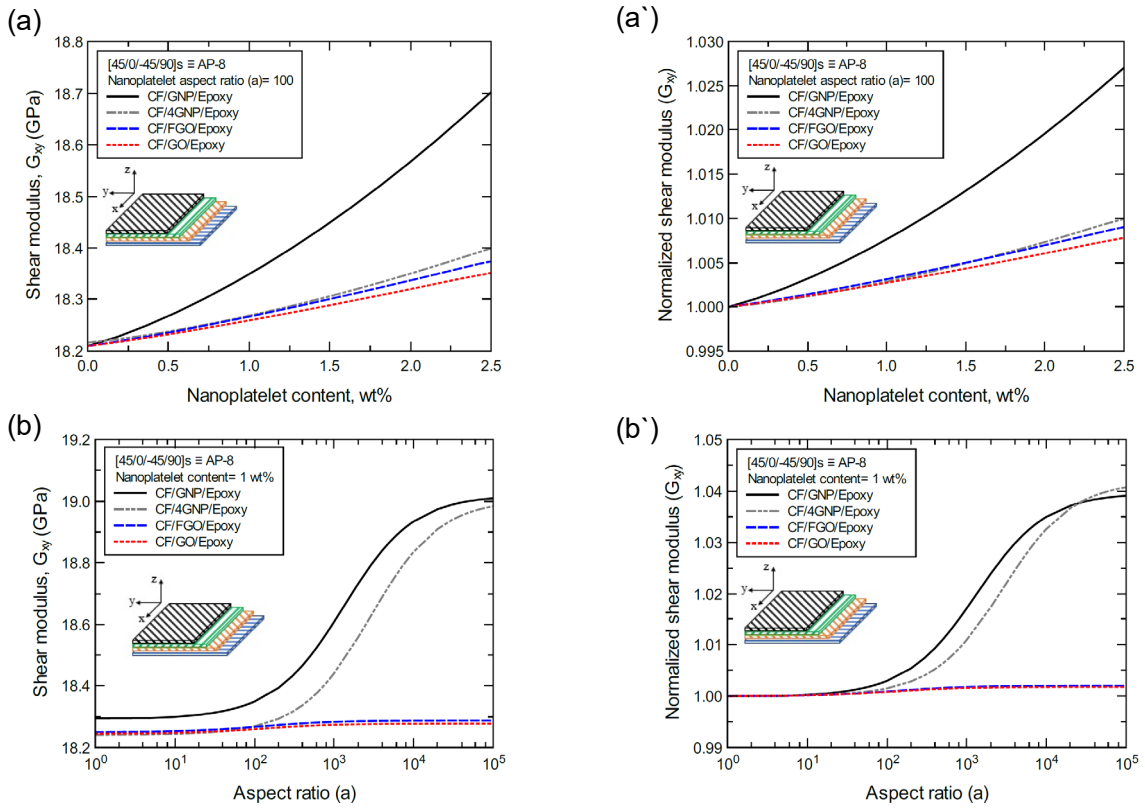

Figure 4.42: Comparison of the predicted in-plane shear modulus (G_{xy}) for [45/0/-45/90]s ≡ AP-8 laminated composite panels based on the nanoplatelet type, content, and aspect ratio; (a) predicted G_{xy} for various nanoplatelets content at 100 aspect ratio, and the normalized response is shown in (a`); (b) predicted $G_{xy}$ for various aspect ratio values at 1.0 wt% of the nanoplatelets content, and the normalized response is shown in (b`). The volume fraction of CF is 56%.

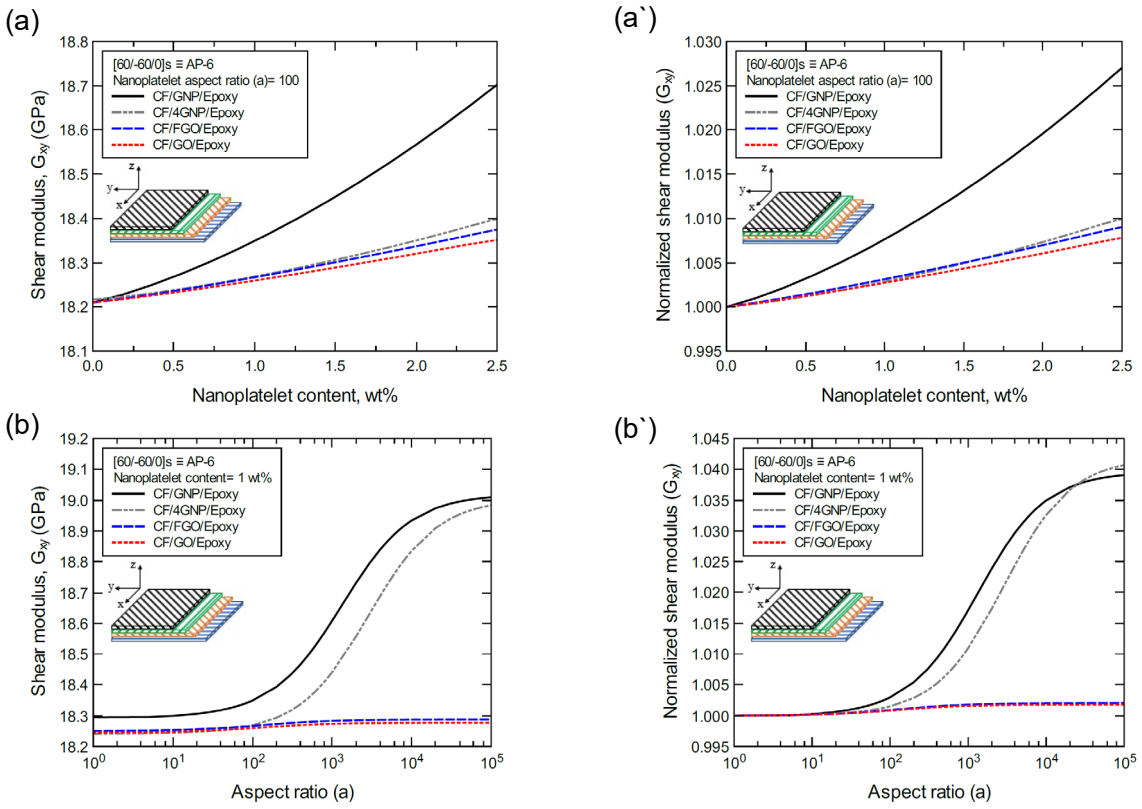

Figure 4.43: Comparison of the predicted in-plane shear modulus (G_{xy}) for [60/-60/0]s ≡ AP-6 laminated composite panels based on the nanoplatelet type, content, and aspect ratio; (a) predicted G_{xy} for various nanoplatelets content at 100 aspect ratio, and the normalized response is shown in (a`); (b) predicted $G_{xy}$ for various aspect ratio values at 1.0 wt% of the nanoplatelets content, and the normalized response is shown in (b`). The volume fraction of CF is 56%.

Figure 4.44.a shows the predicted Poisson's ratio (ν_{xy}) values of CP-8 laminated hybrid composite panel along with their normalized values shown in Figure 4.44.a`. The comparison between ν_{xy} values is based on the nanoplatelet type whether being GNP, 4GNP, FGO, or GO with various nanoplatelets content and constant aspect ratio of 100. Increasing the GNP and 4GNP content produces an increase in the predicted ν_{xy} with CP-8 panel reinforced with GNP being in the lead. However, a slight drop in the predicted ν_{xy} values can be observed as the FGO and GO nanoplatelets content increased. Note that CP-8 panels reinforced with FGO and GO exhibit nearly identical lateral contractions. To some extent, a similar trend can be observed in the predicted ν_{xy} with increasing the nanoplatelet aspect ratio. Figure 4.44.b shows the ν_{xy} values for the same laminated hybrid composite panel along with their normalized values shown in Figure 4.44.b`, which are predicted for various nanoplatelet aspect ratio values and constant nanoplatelets content of 1.0 wt%. The Poisson contraction in all CP-8 hybrid composite panels is insensitive to the increase in the nanoplatelet aspect ratio up to 100. For CP-8 panels reinforced with FGO or GO, the predicted ν_{xy} values remain insensitive to the increase in the nanoplatelet aspect ratio up to 10^5. For CP-8 panels reinforced with GNP or 4GNP, however, rapid increase in the predicted ν_{xy} as the nanoplatelet aspect ratio was increased up to 10^4, with CP-8 panels reinforced with GNP being slightly in the lead. However, the lateral contraction in CP-8 panel reinforced with 4GNP becomes slightly higher than that of GNP reinforced panel at nanoplatelet aspect ratio values greater than 10^4.

The Poisson lateral contraction response of AP-8 and AP-6 are shown in Figure 4.45 and Figure 4.46, respectively. Generally, all hybrid composite panels exhibit a decrease in the predicted ν_{xy} as the nanoplatelet content and its aspect ratio were increased. For nanoplatelets with 100 constant aspect ratio (Figures 4.45.a,a` and Figures 4.46.a,a`), AP-8 and AP-6 panels reinforced with GNP show the largest decrease in the predicted ν_{xy} as the nanoplatelets content increased. However, AP-8 and AP-6 panels reinforced with 4GNP, FGO, and GO exhibit nearly identical and moderate decrease in the predicted ν_{xy} as the nanoplatelets content increased. For 1.0 wt% of nanoplatelets content (Figures 4.45.b,b` and Figures 4.46.b.b`), the Poisson contraction in all hybrid composite panels is insensitive to the increase in the nanoplatelet aspect ratio up to 100. At larger nanoplatelet aspect ratio, the Poisson contraction in AP-8 and AP-6 panels reinforced with FGO and GO remains rather insensitive to the increase in the nanoplatelet aspect ratio up to 10^5. In contrast, the Poisson contraction in AP-8 and AP-6 panels reinforced with GNP and 4GNP is more sensitive to the increase in the nanoplatelet aspect ratio where a rapid decrease in the predicted ν_{xy} values can be observed. More specifically, the predicted ν_{xy} values for composite panels reinforced with GNP exhibit a larger decrease trend with increasing the aspect ratio up to 10^4. At aspect ratio values greater than 10^4, however, composite panels reinforced with 4GNP become slightly more sensitive to the increase in the aspect ratio as larger decrease in the predicted ν_{xy} can be observed.

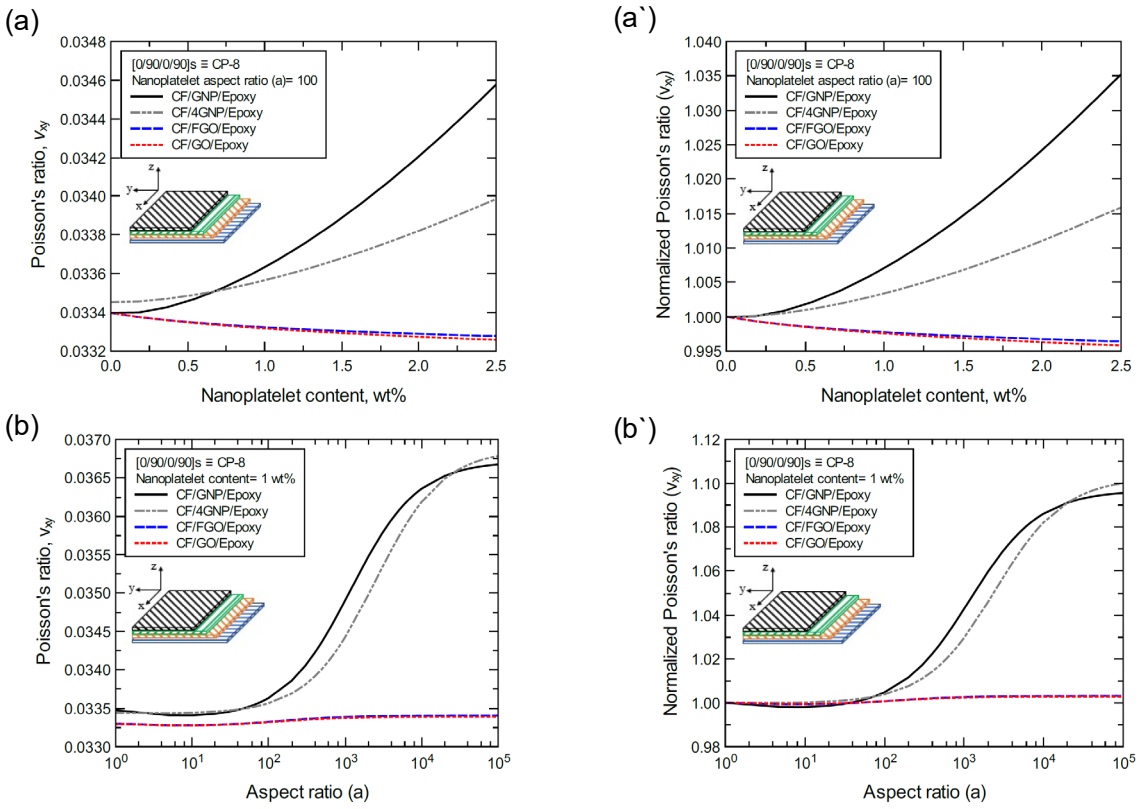

Figure 4.44: Comparison of the predicted in-plane Poisson's ratio (ν_{xy}) for [0/90/0/90]s ≡ CP-8 laminated composite panels based on the nanoplatelet type, content, and aspect ratio; (a) predicted ν_{xy} for various nanoplatelets content at 100 aspect ratio, and the normalized response is shown in (a`); (b) predicted $\nu_{xy}$ for various aspect ratio values at 1.0 wt% of the nanoplatelets content, and the normalized response is shown in (b`). The volume fraction of CF is 56%.

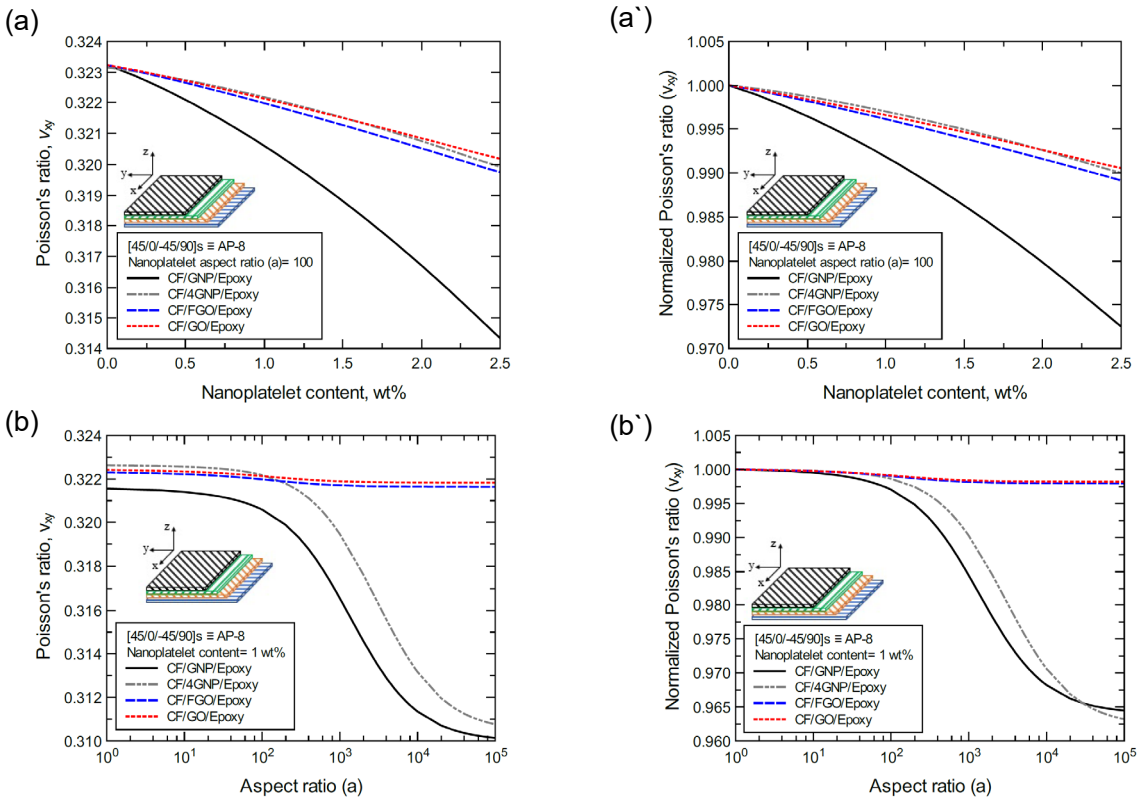

Figure 4.45: Comparison of the predicted in-plane Poisson's ratio (ν_{xy}) for [45/0/-45/90]s ≡ AP-8 laminated composite panels based on the nanoplatelet type, content, and aspect ratio; (a) predicted ν_{xy} for various nanoplatelets content at 100 aspect ratio, and the normalized response is shown in (a`); (b) predicted $\nu_{xy}$ for various aspect ratio values at 1.0 wt% of the nanoplatelets content, and the normalized response is shown in (b`). The volume fraction of CF is 56%.

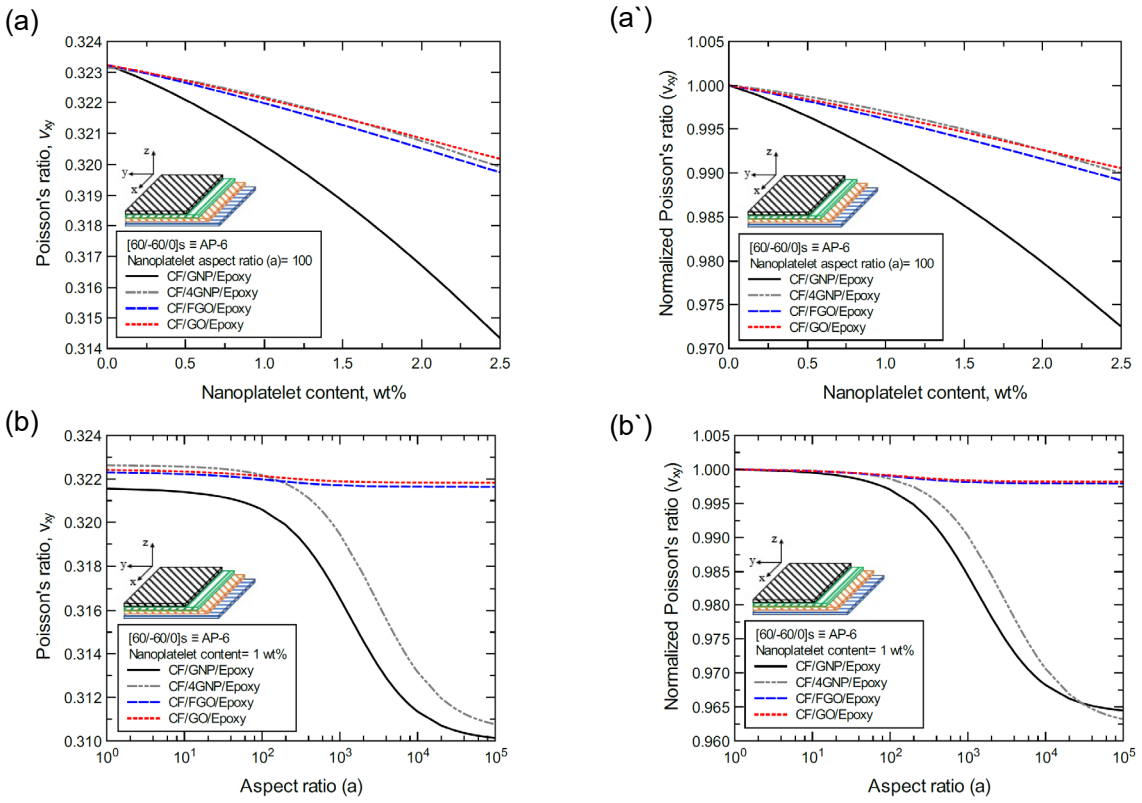

Figure 4.46: Comparison of the predicted in-plane Poisson's ratio (ν_{xy}) for [60/-60/0]s ≡ AP-6 laminated composite panels based on the nanoplatelet type, content, and aspect ratio; (a) predicted ν_{xy} for various nanoplatelets content at 100 aspect ratio, and the normalized response is shown in (a`); (b) predicted $\nu_{xy}$ for various aspect ratio values at 1.0 wt% of the nanoplatelets content, and the normalized response is shown in (b`). The volume fraction of CF is 56%.

4.4 Summary and Conclusions

Considering the reinforcing effect of the four nanoplatelet types (GNP, 4GNP, GO, FGO) modeled and analyzed in this work, the mechanical response of CF/nanoplatelet/epoxy laminated hybrid composites was extensively investigated using micromechanics analysis. The nanoplatelet/epoxy mechanical properties were imposed as the matrix, which was reinforced with CF. The unidirectional CF/nanoplatelet/epoxy hybrid composites were first modeled to address the reinforcing effect of CF and the proposed nanoplatelets on the composite mechanical response. The predicted mechanical properties indicate that the axial mechanical response is dominated by the CF, which is directly dependent on the CF content. However, there is an improvement in the transverse mechanical response owing to the nanoplatelets reinforcing effect. The improvement degree varies according to the nanoplatelet dispersion level, functionality, content, and its aspect ratio. It can be generalized that the reinforcing effect of the nanoplatelets follows the order GNP > 4GNP > FGO ≥ GO.

For the laminated composite panel models, the observed improvement in the mechanical properties of unidirectional CF/nanoplatelet/epoxy hybrid composite plates was utilized in building larger laminated hybrid composite structures. Generally, the reinforcing effect of the nanoplatelets was found to improve the overall mechanical properties of the laminated hybrid composite. Even though the improvement is limited along the CF direction in each lamina, it is crucial in the transverse direction of the lamina. The different orientation, or stacking order, of the laminates in the composite panel helped to redistribute the reinforcing effect of the nanoplatelets. Accordingly, improved transversely isotropic mechanical properties were obtained for the proposed laminated hybrid composite structures. In effect, the nanoplatelets inclusion can also improve the out-of-plane elastic and shear moduli of the laminated composite panel. They can also improve the interlaminar, intralaminar, and translaminar toughening mechanisms in the laminated structure.

The comparison studies performed in this work can provide the options for designing or fabricating laminated composite panels based on the engineering application and the mechanical function of the structural component. These studies can be utilized to optimize the mechanical behavior of the laminated hybrid composite by controlling the variables (key processing parameters) that affect the mechanical response. These controlling variables can be adjusted according to the component function within the structure. Specifically, the CF angle/direction in each lamina and the number of laminas and their stacking order are fundamental to determine the mechanical response of the constructed laminated composite panel.

Chapter 5

RECOMMENDATIONS FOR FUTURE WORK

Micromechanics analysis using MAC/GMC 4.0 based on the nanoscale predictions of MD modeling with ReaxFF using LAMMPS has shown the potential to model, predict, and optimize the mechanical response of advanced polymer-based hybrid composite materials. These computational tools can also be used to resolve, address, and analyze many other structural issues of such composite materials. The current work can be extended to undertake the following topics which are recommended for future work.

5.1 The Reinforcing Effect of Reduced Graphene Oxide (rGO)

The poor mechanical performance of the highly concentrated GO nanoplatelets resulted in a weak reinforcing effect when integrated into the epoxy matrix. Hence, this work can be extended to study the reinforcing effect of reduced graphene oxide nanoplatelets (rGO) on the mechanical response of the hosting matrix. Such a study can help to specify the required amount of oxygen additives that satisfies the optimum rGO stiffness/strength and interfacial interaction/adhesion between rGO and the hosting matrix. Note that using different concentrations of oxygen can produce variable wrinkling/waviness degree in the rGO structure. This would provide information about the wrinkling effect of rGO on the predicted mechanical response.

5.2 Interfacial Failure

The nanocomposite MD models simulated in this work can be used to study the interfacial failure between the nanoplatelets and hosting matrix. Typically, GNP surface functionalization can lead to a fundamental change in the GNP lattice structure such as its morphology and stiffness. The presence of functional groups on the GNP surface was also found to greatly affect the molecular structure at the interphase region in addition to the improved interfacial interaction. These observations bring to the mind the question of how GNP surface functionalization would affect the interfacial shear strength, tribology, and delamination failure. Performing such a study would provide additional essential information regarding the nanocomposite structural integrity. The study outcome can be optimized using different types and amounts of GNP surface functionalization. In addition, speculating the effect of using a different hosting matrix is another factor that can be considered for such a study.

5.3 Thermo-Mechanical Properties

All the MD and micromechanics modeling and predictions in this work were performed at room temperature. However, this is not the case in real life. Polymer-based composite structures are expected to serve in different environmental conditions. For example, most

aircraft structures are designed considering an operating temperature range between +40 and -50 ºC [6]. Because of their low glass transition temperature (T_g), polymer-based composite materials can only be used for structural and engine components that are exposed to low-temperature. Accordingly, it is of great importance to determine the thermo-mechanical response of the proposed composite materials considering the expected range of service temperature. Both LAMMPS and MAC/GMC 4.0 has the capability to analyze and predict the mechanical response of the composites considering temperature effect at nanoscale and microscale, respectively. Consequently, the effective coefficients of thermal expansion (CTE) and the effective thermal conductivity (κ) of the composite can also be investigated at both modeling levels.

5.4 Fatigue Damage and failure Analysis

In the aerospace industry, fatigue life and fatigue strength of composites can be determined using S-N curves. Fast fatigue damage or failure in composites is governed by fiber breakage which is mostly predominant at high-stress regimes. Under these circumstances, composite materials would experience an early structural failure. That is, short fatigue life is expected for the composite structure at high-stress fatigue loading. For intermediate stress levels, however, the fatigue process in composite structures would include different types of fatigue damage. Fatigue damages such as matrix cracking, fiber-matrix debonding, and delamination cracking are most likely to occur at intermediate fatigue loading. A slow process of fiber breakage can also occur under intermediate fatigue loading. That is, prolonged fatigue life is expected for the composite structures at intermediate stress levels. For very low fatigue stress loading, low possibility of fatigue damage with very long fatigue life (could be infinite) is expected for composite structures. Under these circumstances, the fatigue limit of the polymer matrix is used to determine the fatigue endurance limit of the composite [6]. Fortunately, MAC/GMC 4.0 provides the capability for efficiently analyzing fiber-matrix debonding, fiber breakage, and fatigue damage/failure. These failure or damage concepts are essential for assessing the mechanical performance and fatigue life of composite structures under loading.

REFERENCES

1. C. Soutis, "Fibre reinforced composites in aircraft construction," *Progress in Aerospace Sciences,* vol. 41, no. 2, pp. 143-151, 2005.
2. E. C. Botelho, R. A. Silva, L. C. Pardini, and M. C. Rezende, "A review on the development and properties of continuous fiber/epoxy/aluminum hybrid composites for aircraft structures," *Materials Research,* vol. 9, no. 3, pp. 247-256, 2006.
3. Y. Xu and S. Van Hoa, "Mechanical properties of carbon fiber reinforced epoxy/clay nanocomposites," *Composites Science and Technology,* vol. 68, no. 3, pp. 854-861, 2008.
4. S. Sprenger, M. H. Kothmann, and V. Altstaedt, "Carbon fiber-reinforced composites using an epoxy resin matrix modified with reactive liquid rubber and silica nanoparticles," *Composites Science and Technology,* vol. 105, pp. 86-95, 2014.
5. E. Phil and C. Soutis, *Polymer composites in the aerospace industry* (no. 50). Elsevier, 2014.
6. A. P. Mouritz, *Introduction to aerospace materials*. Elsevier, 2012.
7. I. Zaman, T. T. Phan, H.-C. Kuan, Q. Meng, L. T. B. La, L. Luong, O. Youssf, and J. Ma, "Epoxy/graphene platelets nanocomposites with two levels of interface strength," *Polymer,* vol. 52, no. 7, pp. 1603-1611, 2011.
8. C. Hadden, B. Jensen, A. Bandyopadhyay, G. Odegard, A. Koo, and R. Liang, "Molecular modeling of EPON-862/graphite composites: interfacial characteristics for multiple crosslink densities," *Composites Science and Technology,* vol. 76, pp. 92-99, 2013.
9. M. Radue and G. Odegard, "Multiscale modeling of carbon fiber/carbon nanotube/epoxy hybrid composites: Comparison of epoxy matrices," *Composites Science and Technology,* vol. 166, pp. 20-26, 2018.
10. G. M. Odegard, B. D. Jensen, S. Gowtham, J. Wu, J. He, and Z. Zhang, "Predicting mechanical response of crosslinked epoxy using ReaxFF," *Chemical Physics Letters,* vol. 591, pp. 175-178, 2014.
11. R. F. Gibson, "A review of recent research on mechanics of multifunctional composite materials and structures," *Composite structures,* vol. 92, no. 12, pp. 2793-2810, 2010.
12. I. M. De Rosa, F. Sarasini, M. S. Sarto, and A. Tamburrano, "EMC impact of advanced carbon fiber/carbon nanotube reinforced composites for next-generation aerospace applications," *IEEE Transactions on Electromagnetic Compatibility,* vol. 50, no. 3, pp. 556-563, 2008.
13. M. Bhattacharya, "Polymer nanocomposites—a comparison between carbon nanotubes, graphene, and clay as nanofillers," *Materials,* vol. 9, no. 4, p. 262, 2016.
14. D. R. Bortz, E. G. Heras, and I. Martin-Gullon, "Impressive fatigue life and fracture toughness improvements in graphene oxide/epoxy composites," *Macromolecules,* vol. 45, no. 1, pp. 238-245, 2011.
15. S. A. Sydlik, J.-H. Lee, J. J. Walish, E. L. Thomas, and T. M. Swager, "Epoxy functionalized multi-walled carbon nanotubes for improved adhesives," *Carbon,* vol. 59, pp. 109-120, 2013.
16. V. Singh, D. Joung, L. Zhai, S. Das, S. I. Khondaker, and S. Seal, "Graphene based materials: past, present and future," *Progress in materials science,* vol. 56, no. 8, pp. 1178-1271, 2011.
17. P.-C. Ma, N. A. Siddiqui, G. Marom, and J.-K. Kim, "Dispersion and functionalization of carbon nanotubes for polymer-based nanocomposites: a review," *Composites Part A: Applied Science and Manufacturing,* vol. 41, no. 10, pp. 1345-1367, 2010.
18. A. Hinchliffe, *Molecular modelling for beginners*. John Wiley & Sons, 2005.
19. S. Plimpton, "Fast parallel algorithms for short-range molecular dynamics," *Journal of computational physics,* vol. 117, no. 1, pp. 1-19, 1995.
20. H. M. Aktulga, J. C. Fogarty, S. A. Pandit, and A. Y. Grama, "Parallel reactive molecular dynamics: Numerical methods and algorithmic techniques," *Parallel Computing,* vol. 38, no. 4, pp. 245-259, 2012.
21. B. D. Jensen, G. M. Odegard, J.-W. Kim, G. Sauti, E. J. Siochi, and K. E. Wise, "Simulating the effects of carbon nanotube continuity and interfacial bonding on composite strength and stiffness," *Composites Science and Technology,* 2018.
22. S. Chinkanjanarot, M. S. Radue, S. Gowtham, J. M. Tomasi, D. R. Klimek-McDonald, J. A. King, and G. M. Odegard, "Multiscale thermal modeling of cured cycloaliphatic epoxy/carbon fiber composites," *Journal of Applied Polymer Science,* vol. 135, no. 25, p. 46371, 2018.

23. M. S. Radue, B. D. Jensen, S. Gowtham, D. R. Klimek-McDonald, J. A. King, and G. M. Odegard, "Comparing the mechanical response of di-, tri-, and tetra-functional resin epoxies with reactive molecular dynamics," *Journal of Polymer Science Part B: Polymer Physics,* vol. 56, no. 3, pp. 255-264, 2018.
24. W. L. Jorgensen, D. S. Maxwell, and J. Tirado-Rives, "Development and testing of the OPLS all-atom force field on conformational energetics and properties of organic liquids," *J. Am. Chem. Soc,* vol. 118, no. 45, pp. 11225-11236, 1996.
25. E. K. Watkins and W. L. Jorgensen, "Perfluoroalkanes: Conformational analysis and liquid-state properties from ab initio and Monte Carlo calculations," *The Journal of Physical Chemistry A,* vol. 105, no. 16, pp. 4118-4125, 2001.
26. L. Liu, Y. Liu, S. V. Zybin, H. Sun, and W. A. Goddard III, "ReaxFF-lg: Correction of the ReaxFF reactive force field for London dispersion, with applications to the equations of state for energetic materials," *The Journal of Physical Chemistry A,* vol. 115, no. 40, pp. 11016-11022, 2011.
27. D. C. Rapaport and D. C. R. Rapaport, *The art of molecular dynamics simulation*. Cambridge university press, 2004.
28. M. P. Allen and D. J. Tildesley, *Computer simulation of liquids*. Oxford university press, 2017.
29. J. Aboudi, "Micromechanical analysis of composites by the method of cells," *Applied Mechanics Reviews,* vol. 42, no. 7, pp. 193-221, 1989.
30. M. Paley and J. Aboudi, "Micromechanical analysis of composites by the generalized cells model," *Mechanics of materials,* vol. 14, no. 2, pp. 127-139, 1992.
31. J. Aboudi, M.-J. Pindera, and S. M. Arnold, "High-fidelity generalization method of cells for inelastic periodic multiphase materials," 2002.
32. J. Aboudi, S. M. Arnold, and B. A. Bednarcyk, *Micromechanics of composite materials: a generalized multiscale analysis approach*. Butterworth-Heinemann, 2012.
33. B. A. Bednarcyk and S. M. Arnold, "MAC/GMC 4.0 User's Manual: Keywords Manual. Volume 2," 2002.
34. B. A. Bednarcyk and S. M. Arnold, "MAC/GMC 4.0 User's Manual: Example Problem Manual. Volume 3," 2002.
35. K. S. Novoselov, A. K. Geim, S. V. Morozov, D. Jiang, Y. Zhang, S. V. Dubonos, I. V. Grigorieva, and A. A. Firsov, "Electric field effect in atomically thin carbon films," *science,* vol. 306, no. 5696, pp. 666-669, 2004.
36. C. Lee, X. Wei, J. W. Kysar, and J. Hone, "Measurement of the elastic properties and intrinsic strength of monolayer graphene," *science,* vol. 321, no. 5887, pp. 385-388, 2008.
37. S. Stankovich, D. A. Dikin, G. H. Dommett, K. M. Kohlhaas, E. J. Zimney, E. A. Stach, R. D. Piner, S. T. Nguyen, and R. S. Ruoff, "Graphene-based composite materials," *nature,* vol. 442, no. 7100, p. 282, 2006.
38. T. Ramanathan, A. Abdala, S. Stankovich, D. Dikin, M. Herrera-Alonso, R. Piner, D. Adamson, H. Schniepp, X. Chen, and R. Ruoff, "Functionalized graphene sheets for polymer nanocomposites," *Nature nanotechnology,* vol. 3, no. 6, p. 327, 2008.
39. X.-J. Shen, Y. Liu, H.-M. Xiao, Q.-P. Feng, Z.-Z. Yu, and S.-Y. Fu, "The reinforcing effect of graphene nanosheets on the cryogenic mechanical properties of epoxy resins," *Composites Science and Technology,* vol. 72, no. 13, pp. 1581-1587, 2012.
40. J. A. King, D. R. Klimek, I. Miskioglu, and G. M. Odegard, "Mechanical properties of graphene nanoplatelet/epoxy composites," *Journal of Applied Polymer Science,* vol. 128, no. 6, pp. 4217-4223, 2013.
41. M. A. Rafiee, J. Rafiee, Z. Wang, H. Song, Z.-Z. Yu, and N. Koratkar, "Enhanced mechanical properties of nanocomposites at low graphene content," *ACS nano,* vol. 3, no. 12, pp. 3884-3890, 2009.
42. X. Zhang, X. Fan, C. Yan, H. Li, Y. Zhu, X. Li, and L. Yu, "Interfacial microstructure and properties of carbon fiber composites modified with graphene oxide," *ACS applied materials & interfaces,* vol. 4, no. 3, pp. 1543-1552, 2012.
43. A. K. Pathak, M. Borah, A. Gupta, T. Yokozeki, and S. R. Dhakate, "Improved mechanical properties of carbon fiber/graphene oxide-epoxy hybrid composites," *Composites Science and Technology,* vol. 135, pp. 28-38, 2016.

44. Y. Liu, D. He, A.-L. Hamon, B. Fan, P. Haghi-Ashtiani, T. Reiss, and J. Bai, "Comparison of different surface treatments of carbon fibers used as reinforcements in epoxy composites: Interfacial strength measurements by in-situ scanning electron microscope tensile tests," *Composites Science and Technology,* vol. 167, pp. 331-338, 2018.
45. S.-C. Shiu and J.-L. Tsai, "Characterizing thermal and mechanical properties of graphene/epoxy nanocomposites," *Composites Part B: Engineering,* vol. 56, pp. 691-697, 2014.
46. C. M. Hadden, D. R. Klimek-McDonald, E. J. Pineda, J. A. King, A. M. Reichanadter, I. Miskioglu, S. Gowtham, and G. M. Odegard, "Mechanical properties of graphene nanoplatelet/carbon fiber/epoxy hybrid composites: Multiscale modeling and experiments," *Carbon,* vol. 95, pp. 100-112, 2015.
47. W. A. Pisani, M. S. Radue, S. Chinkanjanarot, B. A. Bednarcyk, E. J. Pineda, K. Waters, R. Pandey, J. A. King, and G. M. Odegard, "Multiscale modeling of PEEK using reactive molecular dynamics modeling and micromechanics," *Polymer,* vol. 163, pp. 96-105, 2019.
48. M. Shokrieh, Z. Shokrieh, and S. Hashemianzadeh, "A novel combined molecular dynamics–micromechanics method for modeling of stiffness of graphene/epoxy nanocomposites with randomly distributed graphene," *Materials & Design,* vol. 64, pp. 96-101, 2014.
49. J. Bieniaś, H. Dębski, B. Surowska, and T. Sadowski, "Analysis of microstructure damage in carbon/epoxy composites using FEM," *Computational Materials Science,* vol. 64, pp. 168-172, 2012.
50. J. Tomasi, W. A. Pisani, S. Chinkanjanarot, A. S. Krieg, D. Jaszczak, E. J. Pineda, B. A. Bednarcyk, S. Miller, J. A. King, and I. Miskioglu, "Modeling-Driven Damage Tolerant Design of Graphene Nanoplatelet/Carbon Fiber/Epoxy Hybrid Composite Panels for Full-Scale Aerospace Structures," in *AIAA Scitech 2019 Forum*, 2019, p. 1273.
51. H. Al Mahmud, M. Radue, S. Chinkanjanarot, W. Pisani, S. Gowtham, and G. Odegard, "Predicting the Effective Mechanical Properties of Graphene Nanoplatelet-Carbon Fiber-Epoxy Hybrid Composites Using ReaxFF: A Multiscale Modeling," in *ASCE Earth and Space conference*, Cleveland, Ohio, USA, April 9-12 2018, pp. 556-569.
52. H. Al Mahmud, M. S. Radue, S. Chinkanjanarot, W. A. Pisani, S. Gowtham, and G. M. Odegard, "Multiscale modeling of carbon fiber-graphene nanoplatelet-epoxy hybrid composites using a reactive force field," *Composites Part B: Engineering,* vol. 172, pp. 628-635, 2019.
53. A. C. van Duin, S. Dasgupta, F. Lorant, and W. A. Goddard, "ReaxFF: a reactive force field for hydrocarbons," *The Journal of Physical Chemistry A,* vol. 105, no. 41, pp. 9396-9409, 2001.
54. A. Stukowski, "Visualization and analysis of atomistic simulation data with OVITO–the Open Visualization Tool," *Modelling and Simulation in Materials Science and Engineering,* vol. 18, no. 1, p. 015012, 2010.
55. V. Varshney, S. S. Patnaik, A. K. Roy, and B. L. Farmer, "A molecular dynamics study of epoxy-based networks: cross-linking procedure and prediction of molecular and material properties," *Macromolecules,* vol. 41, no. 18, pp. 6837-6842, 2008.
56. A. Bandyopadhyay, P. K. Valavala, T. C. Clancy, K. E. Wise, and G. M. Odegard, "Molecular modeling of crosslinked epoxy polymers: The effect of crosslink density on thermomechanical properties," *Polymer,* vol. 52, no. 11, pp. 2445-2452, 2011.
57. S. Chinkanjanarot, J. M. Tomasi, J. A. King, and G. M. Odegard, "Thermal conductivity of graphene nanoplatelet/cycloaliphatic epoxy composites: Multiscale modeling," *Carbon,* vol. 140, pp. 653-663, 2018.
58. D. Gray, A. McCaughan, and B. Mookerji, "Crystal structure of graphite, graphene and silicon," *Physics for solid state applications. WVU, Boston,* 2009.
59. B. Shen, W. Zhai, C. Chen, D. Lu, J. Wang, and W. Zheng, "Melt blending in situ enhances the interaction between polystyrene and graphene through π–π stacking," *ACS applied materials & interfaces,* vol. 3, no. 8, pp. 3103-3109, 2011.
60. D. W. Steuerman, A. Star, R. Narizzano, H. Choi, R. S. Ries, C. Nicolini, J. F. Stoddart, and J. R. Heath, "Interactions between conjugated polymers and single-walled carbon nanotubes," *The Journal of Physical Chemistry B,* vol. 106, no. 12, pp. 3124-3130, 2002.
61. M. Yang, V. Koutsos, and M. Zaiser, "Interactions between polymers and carbon nanotubes: a molecular dynamics study," *The Journal of Physical Chemistry B,* vol. 109, no. 20, pp. 10009-10014, 2005.

62. K. Matsushita, H. Matsukawa, and N. Sasaki, "Atomic scale friction between clean graphite surfaces," *Solid state communications,* vol. 136, no. 1, pp. 51-55, 2005.
63. B. D. Jensen, K. E. Wise, and G. M. Odegard, "The effect of time step, thermostat, and strain rate on ReaxFF simulations of mechanical failure in diamond, graphene, and carbon nanotube," *Journal of computational chemistry,* vol. 36, no. 21, pp. 1587-1596, 2015.
64. R. Christensen and F. Waals, "Effective stiffness of randomly oriented fibre composites," *Journal of Composite Materials,* vol. 6, no. 4, pp. 518-532, 1972.
65. O. Blakslee, D. Proctor, E. Seldin, G. Spence, and T. Weng, "Elastic constants of compression-annealed pyrolytic graphite," *Journal of Applied Physics,* vol. 41, no. 8, pp. 3373-3382, 1970.
66. I. M. Daniel and O. Ishai, *Engineering mechanics of composite materials*, 2 ed. Oxford university press New York, 2006.
67. H. Al Mahmud, M. S. Radue, S. Chinkanjanarot, and G. M. Odegard, "MD Modeling of Epoxy-Based Nanocomposites Reinforced with Functionalized Graphene Nanoplatelets," in *Proceedings of the American Society for Composites, Thirty-Fourth Technical Conference*, Atlanta, Georgia, USA, September 23─25 2019: DEStech Publications, Inc., Lancaster, PA, USA, 2019, pp. 89-105.
68. M. R. Zakaria, M. H. A. Kudus, H. M. Akil, and M. Z. M. Thirmizir, "Comparative study of graphene nanoparticle and multiwall carbon nanotube filled epoxy nanocomposites based on mechanical, thermal and dielectric properties," *Composites Part B: Engineering,* vol. 119, pp. 57-66, 2017.
69. Y. Geng, S. J. Wang, and J.-K. Kim, "Preparation of graphite nanoplatelets and graphene sheets," *Journal of colloid and interface science,* vol. 336, no. 2, pp. 592-598, 2009.
70. T. Kuilla, S. Bhadra, D. Yao, N. H. Kim, S. Bose, and J. H. Lee, "Recent advances in graphene based polymer composites," *Progress in polymer science,* vol. 35, no. 11, pp. 1350-1375, 2010.
71. R. K. Layek and A. K. Nandi, "A review on synthesis and properties of polymer functionalized graphene," *Polymer,* vol. 54, no. 19, pp. 5087-5103, 2013.
72. L.-C. Tang, Y.-J. Wan, D. Yan, Y.-B. Pei, L. Zhao, Y.-B. Li, L.-B. Wu, J.-X. Jiang, and G.-Q. Lai, "The effect of graphene dispersion on the mechanical properties of graphene/epoxy composites," *Carbon,* vol. 60, pp. 16-27, 2013.
73. J. Cha, W. Kyoung, K. Song, S. Park, T. Lim, J. Lee, and H. Kang, "Quantitative evaluation of the dispersion of graphene sheets with and without functional groups using molecular dynamics simulations," *Nanoscale research letters,* vol. 11, no. 1, p. 136, 2016.
74. K. Karatasos and G. Kritikos, "Characterization of a graphene oxide/poly (acrylic acid) nanocomposite by means of molecular dynamics simulations," *RSC Advances,* vol. 6, no. 111, pp. 109267-109277, 2016.
75. W. S. Hummers Jr and R. E. Offeman, "Preparation of graphitic oxide," *Journal of the american chemical society,* vol. 80, no. 6, pp. 1339-1339, 1958.
76. H. Kim, A. A. Abdala, and C. W. Macosko, "Graphene/polymer nanocomposites," *Macromolecules,* vol. 43, no. 16, pp. 6515-6530, 2010.
77. M. Fang, Z. Zhang, J. Li, H. Zhang, H. Lu, and Y. Yang, "Constructing hierarchically structured interphases for strong and tough epoxy nanocomposites by amine-rich graphene surfaces," *Journal of Materials Chemistry,* vol. 20, no. 43, pp. 9635-9643, 2010.
78. Z. Su, H. Wang, K. Tian, F. Xu, W. Huang, and X. Tian, "Simultaneous reduction and surface functionalization of graphene oxide with wrinkled structure by diethylenetriamine (DETA) and their reinforcing effects in the flexible poly (2-ethylhexyl acrylate)(P2EHA) films," *Composites Part A: Applied Science and Manufacturing,* vol. 84, pp. 64-75, 2016.
79. L. Lai, L. Chen, D. Zhan, L. Sun, J. Liu, S. H. Lim, C. K. Poh, Z. Shen, and J. Lin, "One-step synthesis of NH2-graphene from in situ graphene-oxide reduction and its improved electrochemical properties," *Carbon,* vol. 49, no. 10, pp. 3250-3257, 2011.
80. W. Xiao, P. Zhao, S. Deng, and N. Zhang, "Anchoring H 3 PW 12 O 40 on 3-aminopropyltriethoxysilane modified graphene oxide: enhanced adsorption capacity and photocatalytic activity toward methyl orange," *New Journal of Chemistry,* vol. 39, no. 5, pp. 3719-3727, 2015.
81. A. Navaee and A. Salimi, "Efficient amine functionalization of graphene oxide through the Bucherer reaction: an extraordinary metal-free electrocatalyst for the oxygen reduction reaction," *RSC Advances,* vol. 5, no. 74, pp. 59874-59880, 2015.

82. M. Naebe, J. Wang, A. Amini, H. Khayyam, N. Hameed, L. H. Li, Y. Chen, and B. Fox, "Mechanical property and structure of covalent functionalised graphene/epoxy nanocomposites," *Scientific reports,* vol. 4, p. 4375, 2014.
83. M.-S. Park, S. Lee, and Y.-S. Lee, "Mechanical properties of epoxy composites reinforced with ammonia-treated graphene oxides," *Carbon letters,* vol. 21, pp. 1-7, 2017.
84. Q. Pei, Y. Zhang, and V. Shenoy, "A molecular dynamics study of the mechanical properties of hydrogen functionalized graphene," *Carbon,* vol. 48, no. 3, pp. 898-904, 2010.
85. H. Chong, S. Hinder, and A. Taylor, "Graphene nanoplatelet-modified epoxy: effect of aspect ratio and surface functionality on mechanical properties and toughening mechanisms," *Journal of materials science,* vol. 51, no. 19, pp. 8764-8790, 2016.
86. M. Karevan, R. V. Pucha, M. A. Bhuiyan, and K. Kalaitzidou, "Effect of interphase modulus and nanofiller agglomeration on the tensile modulus of graphite nanoplatelets and carbon nanotube reinforced polypropylene nanocomposites," *Carbon letters,* vol. 11, no. 4, pp. 325-331, 2010.
87. H. He, J. Klinowski, M. Forster, and A. Lerf, "A new structural model for graphite oxide," *Chemical physics letters,* vol. 287, no. 1-2, pp. 53-56, 1998.
88. Y. Jin, F. Duan, and X. Mu, "Functionalization enhancement on interfacial shear strength between graphene and polyethylene," *Applied Surface Science,* vol. 387, pp. 1100-1109, 2016.
89. C. Lv, Q. Xue, D. Xia, and M. Ma, "Effect of chemisorption structure on the interfacial bonding characteristics of graphene–polymer composites," *Applied Surface Science,* vol. 258, no. 6, pp. 2077-2082, 2012.
90. B. P. Vinayan, "Heteroatom-Doped Graphene-Based Hybrid Materials for Hydrogen Energy Conversion," in *Recent Advances in Graphene Research*: InTech, 2016.
91. X.-F. Li, K.-Y. Lian, L. Liu, Y. Wu, Q. Qiu, J. Jiang, M. Deng, and Y. Luo, "Unraveling the formation mechanism of graphitic nitrogen-doping in thermally treated graphene with ammonia," *Scientific reports,* vol. 6, p. 23495, 2016.
92. A. Buchsteiner, A. Lerf, and J. Pieper, "Water dynamics in graphite oxide investigated with neutron scattering," *The Journal of Physical Chemistry B,* vol. 110, no. 45, pp. 22328-22338, 2006.
93. K. Chu, W.-s. Li, and H. Dong, "Role of graphene waviness on the thermal conductivity of graphene composites," *Applied Physics A,* vol. 111, no. 1, pp. 221-225, 2013.
94. H. Kim and C. W. Macosko, "Processing-property relationships of polycarbonate/graphene composites," *Polymer,* vol. 50, no. 15, pp. 3797-3809, 2009.
95. G. Voronoi, "Nouvelles applications des paramètres continus à la théorie des formes quadratiques. Premier mémoire. Sur quelques propriétés des formes quadratiques positives parfaites," *Journal für die reine und angewandte Mathematik,* vol. 133, pp. 97-178, 1908.
96. C. Rycroft, "Voro++: A three-dimensional Voronoi cell library in C++," *Lawrence Berkeley National Laboratory,* 2009. [Online]. Available: https://escholarship.org/uc/item/8sf4t5x8.
97. B. Qi, Q. Zhang, M. Bannister, and Y.-W. Mai, "Investigation of the mechanical properties of DGEBA-based epoxy resin with nanoclay additives," *Composite structures,* vol. 75, no. 1-4, pp. 514-519, 2006.
98. J. Cho, J. Luo, and I. Daniel, "Mechanical characterization of graphite/epoxy nanocomposites by multi-scale analysis," *Composites science and technology,* vol. 67, no. 11-12, pp. 2399-2407, 2007.
99. K. N. Shivakumar, G. Swaminathan, and M. Sharpe, "Carbon/vinyl ester composites for enhanced performance in marine applications," *Journal of Reinforced Plastics and Composites,* vol. 25, no. 10, pp. 1101-1116, 2006.
100. H. Rahmani, S. H. M. Najaf, A. Ashori, and M. Golriz, "Elastic Properties of Carbon Fibre-Reinforced Epoxy Composites," *Polymers and Polymer Composites,* vol. 23, no. 7, pp. 475-482, 2015.

Appendix A: High-Performance Computing

A.1 HPC Resources and Specifications

All MD simulations in this work were performed using SUPERIOR. SUPERIOR is a high-performance computing infrastructure that is available to all researchers at Michigan Technological University. The specifications of the computing infrastructure and storage components of SUPERIOR are listed below:

Generation		Specification	
Generation 1.0, acquired between June-2013 and October-2015	a	Number of compute nodes	92
		Number of CPU cores/node	16
		CPU	Intel Xeon E5-2670
		CPU speed	2.60 GHz
		RAM per node	64 GB
		TFLOPS	30
	b	Number of compute nodes	4
		Number of CPU cores/node	24
		CPU	Intel Xeon E4-2680
		CPU speed	2.50 GHz
		RAM per node	256 GB
		TFLOPS	2
	c	Number of compute nodes	5 GPU
		Number of CPU cores/node	16
		CPU	Intel Xeon E5-2670
		CPU speed	2.60 GHz
		RAM per node	64 GB
		NVIDIA Tesla M2090 GPUs	4
		TFLOPS	13
		3 Storage nodes	96 TB
Generation 2.0, acquired between June-2017 and August-2018	-	Number of compute nodes	85
		Number of CPU cores/node	32
		CPU	Intel Xeon E5-2683
		CPU speed	2.10 GHz
		RAM per node	256 GB
		TFLOPS	91

For more information about HPC infrastructure at Michigan Tech, please visit https://hpc.mtu.edu/.

A.2 Computational Cost of MD Simulations

The total number of the MD simulations performed in this work using SUPERIOR with the corresponding total computational time is:

- Number of Completed MD Simulations: 2239
- Wall Time in (h:mm:ss): 121829:32:46
- CPU Time in (h:mm:ss): 7982535:24:03

The following tables include a representative computational cost of the MD simulation steps for the given nanocomposite MD samples:

A.2.1 For the 4-layer GNP/epoxy MD model with 6048 atoms

Simulation Description	Force Field	Simulation Time (ns)	No. of CPUs	CPU Time (hr)
Combine and densify monomers	OPLS	2.5	8	34
Crosslinking epoxy monomers	OPLS	1.0	8	110
Equilibrate the MD model	OPLS	1.0	16	140
Import into ReaxFF	ReaxFF	1.0	32	10488
Equilibrate the MD model	ReaxFF	1.0	32	9171
Normal strain	ReaxFF	0.5	32	6105
Shear strain	ReaxFF	0.5	32	6092

A.2.2 For the GNP/epoxy MD model with 7028 atoms

Simulation Description	Force Field	Simulation Time (ns)	No. of CPUs	CPU Time (hr)
Combine and densify monomers	OPLS	3.2	8	75
Crosslinking epoxy monomers	OPLS	1.0	8	153
Equilibrate the MD model	OPLS	1.0	16	200
Import into ReaxFF	ReaxFF	1.0	32	9937
Equilibrate the MD model	ReaxFF	1.0	32	9528
Normal strain	ReaxFF	0.5	32	5023
Shear strain	ReaxFF	0.5	32	4950

A.2.3 For the GO/epoxy MD model with 7841 atoms

Simulation Description	Force Field	Simulation Time (ns)	No. of CPUs	CPU Time (hr)
Combine and densify monomers	OPLS	3.2	8	88
Crosslinking epoxy monomers	OPLS	1.0	8	160
Equilibrate the MD model	OPLS	1.0	16	198
Import into ReaxFF	ReaxFF	1.0	32	10222
Equilibrate the MD model	ReaxFF	1.0	32	9637
Normal strain	ReaxFF	0.5	32	6590
Shear strain	ReaxFF	0.5	32	5671

A.2.4 For the FGO/epoxy MD model with 7811 atoms

Simulation Description	Force Field	Simulation Time (ns)	No. of CPUs	CPU Time (hr)
Combine and densify monomers	OPLS	3.2	8	86
Crosslinking epoxy monomers	OPLS	1.0	8	167
Equilibrate the MD model	OPLS	1.0	16	190
Import into ReaxFF	ReaxFF	1.0	32	11012
Equilibrate the MD model	ReaxFF	1.0	32	10649
Normal strain	ReaxFF	0.5	32	6139
Shear strain	ReaxFF	0.5	32	5668

Appendix B: Modeling Sample Scripts

The modeling processes in this computational work involved writing many scripts and codes toward achieving the ultimate objectives. Please consider visiting the following GitHub repository to look at some of the LAMMPS, BASH, Python, and MAC/GMC 4.0 scripts used in this work: https://github.com/hnalmahm/PhD

The following table includes a brief description of some of these modeling scripts and computational codes:

Script/Code/Package	Type	Usage
fixdens_script.lmp	LAMMPS	To densify the epoxy monomers in the GNP/epoxy MD model
Cross_Linking_Package	BASH, LAMMPS, Python	LAMMPS and Python scripts were written to perform the crosslinking process of epoxy monomers. The BASH script controls the iterative running of LAMMPS and Python scripts until reaching the targeted crosslinking density
relax_npt_OPLS_script.lmp	LAMMPS	To equilibrate the MD model in OPLS and relieve the residual stresses produced after crosslinking process
import_into_reaxff_script_lmp	LAMMPS	To import or transmit the relaxed MD model from OPLS into ReaxFF
relax_npt_ReaxFF_script.lmp	LAMMPS	To further equilibrate the MD model in ReaxFF and relieve the residual stresses produced after the transition from OPLS to ReaxFF
normal_strain_script.lmp	LAMMPS	Applying a normal strain on the MD model to acquire its mechanical response: $E_{xx}, E_{yy}, E_{zz}, \nu_{xy}, \nu_{zx}, \nu_{zy}$
shear_strain_script.lmp	LAMMPS	Applying a shear strain on the MD model to acquire its mechanical response: $G_{xy}, G_{\mathrm{xz}}, G_{\mathrm{yz}}$
ruc_vf_asp_gnp_epo.mac	MAC/GMC	To generate and predict the mechanical properties of GNP/epoxy RUC
uni_dir_CF_hybrid.mac	MAC/GMC	To generate and predict the mechanical properties of CF/GNP/epoxy hybrid composite
laminate_hybrid_composite.mac	MAC/GMC	To generate and predict the mechanical properties of CF/GNP/epoxy laminated hybrid composites

There are many other intermediate and post-processing scripts and codes that were written to perform all the calculations, plotting, and analyzing the results. In the link provided above, there is also a complete timeline of the research work activity and MD simulations that were performed in SUPERIOR. The research work timeline was generated using Gource (https://gource.io/), a software that can be used to display activity from repositories using a video visualization. The screenshots shown below were taken from the research work activity timeline to show the progress between February-2016 and October-2019.

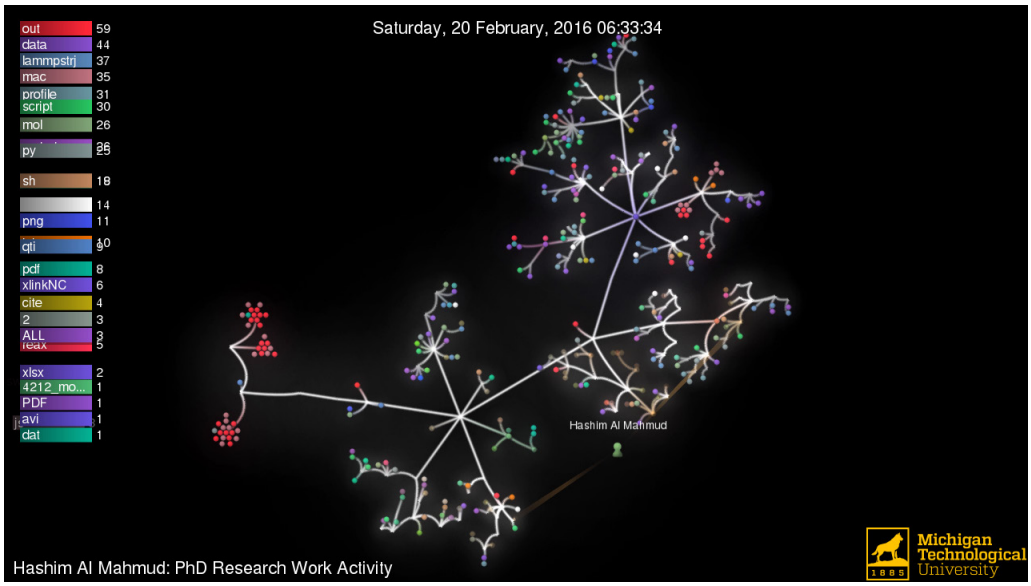

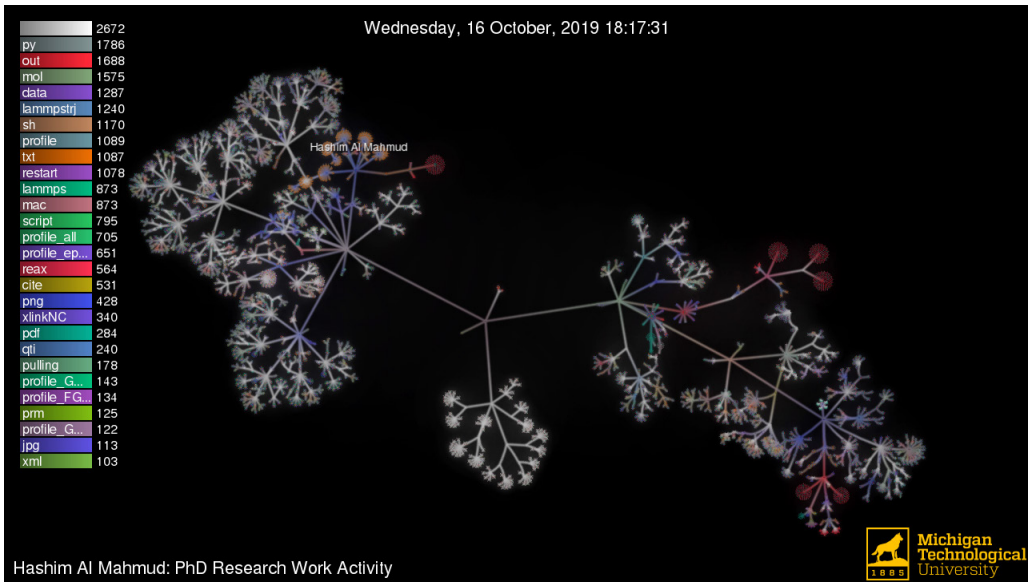

Appendix C: Copyright Agreements

This section includes the copyright clearance documentation for previously published work reused in this dissertation as part of the author's rights.

C.1 Copyright Clearance for Figure 1.1

Michigan Tech

Hashim Al Mahmud <hnalmahm@mtu.edu>

Permission to use a picture in my dissertation

2 messages

Hashim Al Mahmud <hnalmahm@mtu.edu> Wed, Oct 30, 2019 at 11:40 AM
To: JohnH@electroimpact.com

Hello Sir,

This is Hashim Al Mahmud, a PhD student at Michigan Technological University. I am in the process of writing my dissertation and I would like to use the attached picture which shows "Automated Fiber Placement (AFP) Technology; Fuselage Composite Panel".
May I have permission to include it in my dissertation?

Yours respectfully,
Hashim

https://www.electroimpact.com/Products/Composites/Overview.aspx

John Hartmann <johnh@electroimpact.com> Wed, Oct 30, 2019 at 2:37 PM
To: Hashim Al Mahmud <hnalmahm@mtu.edu>

Sure no problem. Good luck.

John Hartmann, Vice President
JohnH@electroimpact.com
Electroimpact, Inc.

Corporate Headquarters
Phone: (425) 348-8090
Fax: (425) 348-0716

Business Office
4413 Chennault Beach Rd
Mukilteo, WA 98275

C.2 Copyright Clearance for Ref [51]

H. Al Mahmud, M. Radue, S. Chinkanjanarot, W. Pisani, S. Gowtham, and G. Odegard, "Predicting the Effective Mechanical Properties of Graphene Nanoplatelet-Carbon Fiber-Epoxy Hybrid Composites Using ReaxFF: A Multiscale Modeling," in *ASCE Earth and Space conference*, Cleveland, Ohio, USA, April 9-12, 2018, pp. 556-569.

Michigan Tech

Hashim Al Mahmud <hnalmahm@mtu.edu>

Permission to include my published work in my dissertation

2 messages

Hashim Al Mahmud <hnalmahm@mtu.edu> Mon, Oct 28, 2019 at 1:49 PM
To: pubsful@asce.org

Hello,

This is Hashim Al Mahmud, a PhD student at Michigan Technological University. I am in the process of writing my dissertation, part of which was previously published in the ASCE Earth & Space Conference 2018. I am writing this email to request permission for reusing my work in my dissertation as I am required to include it in the copyright agreements section.

The publication details:

Title:
Predicting the Effective Mechanical Properties of Graphene Nanoplatelet-Carbon Fiber-Epoxy Hybrid Composites Using ReaxFF: A Multiscale Modeling

Authors:
H. Al Mahmud; M. S. Radue; S. Chinkanjanarot; W. A. Pisani; S. Gowtham; and G. M. Odegard

DOI:
https://doi.org/10.1061/9780784481899.053
Published online: November 15, 2018

ASCE Subject Headings:
Nanomechanics, Epoxy, Hybrid methods, Fiber reinforced composites, Carbon fibers, Composite materials, Mechanical properties, Strength of materials

Conference Information:
16th Biennial International Conference on Engineering, Science, Construction, and Operations in Challenging Environments
April 9–12, 2018 | Cleveland, Ohio

Yours respectfully,
Hashim

--
Hashim Al Mahmud, Ph.D. candidate,
Computational Mechanics & Materials Research Lab.,
Department of Mechanical Engineering-Engineering Mechanics,
Michigan Technological University
1400 Townsend Drive
Houghton, MI 49931

Michigan Tech

Hashim Al Mahmud <hnalmahm@mtu.edu>

Permission to include my published work in my dissertation

2 messages

PERMISSIONS <permissions@asce.org> Tue, Oct 29, 2019 at 8:56 AM
To: "hnalmahm@mtu.edu" <hnalmahm@mtu.edu>
Cc: Pubsful <pubsful@asce.org>

Dear Hashim,

Thank you for your inquiry. As an original author of an ASCE journal article or proceedings paper, you are permitted to reuse your own content (including figures and tables) for another ASCE or non-ASCE publication (including your dissertation), provided it does not account for more than 25% of the new work. This email serves as permission to reuse your work, *Predicting the Effective Mechanical Properties of Graphene Nanoplatelet-Carbon Fiber-Epoxy Hybrid Composites Using ReaxFF: A Multiscale Modeling* from Earth and Space 2018 Proceedings, https://doi.org/10.1061/9780784481899.053.

A full credit line must be added to the material being reprinted. For reuse in non-ASCE publications, add the words "With permission from ASCE" to your source citation. For Intranet posting, add the following additional notice: "This material may be downloaded for personal use only. Any other use requires prior permission of the American Society of Civil Engineers. This material may be found at [URL/link of abstract in the ASCE Library or Civil Engineering Database]."

Each license is unique, covering only the terms and conditions specified in it. Even if you have obtained a license for certain ASCE copyrighted content, you will need to obtain another license if you plan to reuse that content outside the terms of the existing license. For example: If you already have a license to reuse a figure in a journal, you still need a new license to use the same figure in a magazine. You need a separate license for each edition.

For more information on how an author may reuse their own material, please view: http://ascelibrary.org/page/informationforasceauthorsreusingyourownmaterial

Sincerely,

Leslie Connelly

Manager, Publications Marketing

American Society of Civil Engineers

1801 Alexander Bell Drive

Reston, VA 20191

PERMISSIONS@asce.org

C.3 Copyright Clearance for Ref [52]

H. Al Mahmud, M. S. Radue, S. Chinkanjanarot, W. A. Pisani, S. Gowtham, and G. M. Odegard, "Multiscale modeling of carbon fiber-graphene nanoplatelet-epoxy hybrid composites using a reactive force field," *Composites Part B: Engineering,* vol. 172, pp. 628-635, 2019.

Elsevier grants a number of rights to its journal authors as outlined here:

- https://www.elsevier.com/about/our-business/policies/copyright#Author-rights
- https://www.elsevier.com/__data/assets/pdf_file/0007/55654/AuthorUserRights.pdf

C.4 Copyright Clearance of Ref [67]

H. Al Mahmud, M. S. Radue, S. Chinkanjanarot, and G. M. Odegard, "MD Modeling of Epoxy-Based Nanocomposites Reinforced with Functionalized Graphene Nanoplatelets," in *Proceedings of the American Society for Composites, Thirty-Fourth Technical Conference*, Atlanta, Georgia, USA, September 23─25, 2019: DEStech Publications, Inc., Lancaster, PA, USA, 2019, pp. 89-105.

Michigan Tech

Hashim Al Mahmud <hnalmahm@mtu.edu>

Permission to include my published work in my dissertation

2 messages

Hashim Al Mahmud <hnalmahm@mtu.edu> Wed, Oct 23, 2019 at 10:19 AM
To: info@destechpub.com

Hello,

This is Hashim Al Mahmud, a PhD student at Michigan Technological University. I am in the process of writing my dissertation, part of which was previously published in the ASC Conference 2019. I am writing this email to request permission for reusing my work in my dissertation as I am required to include it in the copyright agreements section.

The publication details:

Title:
MD MODELING OF EPOXY-BASE NANOCOMPOSITES REINFORCED WITH FUNCTIONALIZED GRAPHENE NANOPLATELETS

Authors:
HASHIM AL MAHMUD, MATTHEW S. RADUE, SORAYOT CHINKANJANAROT, GREGORY M. ODEGARD

DOI:
10.12783/asc34/31377

Conference Information:
Proceedings of the American Society for Composites, Thirty-Fourth Technical Conference, Lancaster, PA, USA: DEStech Publications, Inc., Atlanta, Georgia, USA.

Yours respectfully,
Hashim

--
Hashim Al Mahmud, Ph.D. candidate,
Computational Mechanics & Materials Research Lab.,
Department of Mechanical Engineering-Engineering Mechanics,
Michigan Technological University
1400 Townsend Drive
Houghton, MI 49931

Michigan Tech

Hashim Al Mahmud <hnalmahm@mtu.edu>

Permission to include my published work in my dissertation

2 messages

Tony Deraco <aderaco@destechpub.com> Wed, Oct 23, 2019 at 10:32 AM

To: Hashim Al Mahmud <hnalmahm@mtu.edu>

Dear Hashim:

We grant you permission to use the material you requested for your dissertation and ask that you list credit with the paper used from the Proceedings. The wording should include:

This article appeared in the *Proceedings of the American Society for Composites: Thirty-fourth Technical Conference,* 2019. Lancaster, PA: DEStech Publications, Inc.

Best Regards,

Anthony A. Deraco

President

DEStech Publications, Inc.

439 North Duke Street

Lancaster, PA 17602-4967

Toll Free: 877-500-4337

Tel: 717-290-1660

Fax: 717-509-6100

E-Mail: aderaco@destechpub.com

Website: www.destechpub.com